

# ***SOLID AND GASEOUS CARBONIC ACID***

by  
**Jürgen Bernard**

A Doctoral Thesis (Dissertation) submitted in Conformity with the Requirements for Acquisition of the Degree of Doctor of Science (Dr.rer.nat) at the Faculty of Chemistry and Pharmacy of the University of Innsbruck.

Advisor:  
Assoc.-Prof. Dr. Thomas Loerting  
Institute of Physical Chemistry

Innsbruck, January 2014

---



## ***Acknowledgement***

Herzlich bedanken möchte ich mich bei Thomas Lörting für die interessante Themenstellung, die ausgezeichnete Betreuung, die stete Diskussionsbereitschaft, die ansteckende Begeisterung für neue Ergebnisse und die freundliche Unterstützung während meiner Doktorarbeit.

Weiters bedanke ich mich bei der gesamten Arbeitsgruppe bei Anatoli Bogdan, Violeta Fuentes Landete, Stephan Fuhrmann, Karl Handle, Philip Handle, Christian Mitterdorfer, Guadalupe Ruiz, Markus Seidl, Josef Stern, Katrin Amann-Winkel und Michael Elsaesser für die gute Zusammenarbeit, die vielen Diskussionen und das ausgezeichnete Arbeitsklima. Besonders bei Marion Bauer möchte ich mich für die vielen Diskussionen beim ausgezeichneten Frühstückskaffee bedanken.

Die Kooperationspartner waren eine große Unterstützung. Danke an Prof. Hinrich Grothe von der TU Wien für die zur Verfügung Stellung der Matrixanlage und die zahlreichen Diskussionen. Danke auch an Prof. Klaus Liedl und Mag. Roland Gruber von der Universität Innsbruck für die Vielzahl an theoretischen Berechnungen.

Danken möchte ich allen vom Institut für Physikalische Chemie für das ausgezeichnete Arbeitsklima und den super Institutsskitouren.

Meinen Eltern danke ich von ganzem Herzen, für die liebevolle Unterstützung und Aufmunterung. Ein besonderer Dank geht an meine Brüder und Freunde für die schönen Wochenenden und Abende.

Schlussendlich gilt ein besonders großer Dank meiner Freundin Petra für ihre Liebe, Freundschaft, Hilfe und Geduld in den letzten Jahren.

---



# Table of Contents

---

<b>1</b>	<b>ABSTRACT</b> .....	<b>1</b>
<b>2</b>	<b>CARBONIC ACID (H<sub>2</sub>CO<sub>3</sub>)</b> .....	<b>3</b>
<b>3</b>	<b>EXPERIMENTAL METHODS</b> .....	<b>7</b>
<b>3.1</b>	<b>Matrix isolation (MI)</b> .....	<b>7</b>
3.1.1	Matrix isolation: Principle.....	7
3.1.2	Properties of matrix materials.....	9
3.1.3	Matrix isolation: Setup in Vienna .....	10
3.1.4	Matrix isolation: Equipment .....	11
3.1.5	Steps of H <sub>2</sub> CO <sub>3</sub> isolation.....	12
<b>3.2</b>	<b>Preparation of starting material (H<sub>2</sub>CO<sub>3</sub>)</b> .....	<b>14</b>
<b>3.3</b>	<b><i>Ab initio</i> quantum mechanical calculations</b> .....	<b>17</b>
<b>4</b>	<b>PEER-REVIEWED PUBLICATIONS</b> .....	<b>19</b>
<b>4.1</b>	<b>General conclusions of the publications</b> .....	<b>20</b>
<b>4.2</b>	<b>Spectroscopic Observation of Matrix-Isolated Carbonic Acid Trapped from the Gas Phase</b> .....	<b>23</b>
<b>4.3</b>	<b>Matrix isolation studies of carbonic acid – the vapour phase above the β-polymorph</b> .....	<b>31</b>
<b>4.4</b>	<b>Formation and Stability of Bulk Carbonic Acid (H<sub>2</sub>CO<sub>3</sub>) by Protonation of Tropospheric Calcite</b> .....	<b>39</b>
<b>4.5</b>	<b>Aqueous carbonic acid (H<sub>2</sub>CO<sub>3</sub>)</b> .....	<b>47</b>
<b>4.6</b>	<b>Local structural order in carbonic acid polymorphs: Raman and FT-IR spectroscopy</b> .....	<b>55</b>
<b>5</b>	<b>POLYMORPHISM OF CARBONIC ACID</b> .....	<b>65</b>
<b>5.1</b>	<b>Solid state / liquid state reaction</b> .....	<b>67</b>
5.1.1	Reaction of KHCO <sub>3(s)</sub> from H <sub>2</sub> O with HCl in CH <sub>3</sub> OH .....	67
5.1.2	Reaction of KHCO <sub>3(s)</sub> from CH <sub>3</sub> OH with HCl in H <sub>2</sub> O .....	70
5.1.3	Reaction of KHCO <sub>3(s)</sub> from C <sub>2</sub> H <sub>5</sub> OH with HCl in C <sub>2</sub> H <sub>5</sub> OH .....	74
5.1.4	Reaction of KHCO <sub>3(s)</sub> from CD <sub>3</sub> OH with HCl in CH <sub>3</sub> OH.....	78
<b>5.2</b>	<b>Discussion</b> .....	<b>80</b>
<b>6</b>	<b>MATRIX ISOLATION: NEW INTERPRETATION</b> .....	<b>86</b>
<b>6.1</b>	<b>The vapor molecules over α-H<sub>2</sub>CO<sub>3</sub></b> .....	<b>87</b>

---

6.1.1	Monomethyl carbonic acid .....	87
6.1.2	New interpretation of the $\alpha$ -H <sub>2</sub> CO <sub>3</sub> /Ar-matrix.....	93
6.1.3	UV irradiation.....	96
<b>6.2</b>	<b>The vapour over the new specie (<math>\gamma</math>- and <math>\delta</math>-H<sub>2</sub>CO<sub>3</sub>) .....</b>	<b>103</b>
<b>6.3</b>	<b>Discussion .....</b>	<b>106</b>
<b>7</b>	<b>CARBONIC ACID HYDRATE .....</b>	<b>109</b>
7.1	Interaction of $\beta$ -H <sub>2</sub> CO <sub>3</sub> with water vapour.....	109
7.2	Reaction in concentrated solutions .....	112
7.3	Discussion .....	116
<b>8</b>	<b>APPENDIX.....</b>	<b>119</b>
8.1	Submitted Publication.....	119
8.2	References .....	149
8.3	List of Figure.....	151
8.4	List of Table.....	155
<b>9</b>	<b>CURRICULUM VITAE .....</b>	<b>157</b>

---

# 1 Abstract

---

This work focuses on the IR-spectroscopic characterization of solid polymorphs and gaseous carbonic acid ( $\text{H}_2\text{CO}_3$ ) trapped in inert matrices in the context of astrochemistry and atmospheric chemistry.

It was known before that by reaction of  $\text{KHCO}_3$  and  $\text{HCl}$   $\alpha\text{-H}_2\text{CO}_3$  crystallizes from methanolic solution, whereas  $\beta\text{-H}_2\text{CO}_3$  crystallizes from aqueous solution. Here, a new polymorph was found by protonation of  $\text{KHCO}_3$  dissolved in ethanol which we called  $\gamma\text{-H}_2\text{CO}_3$ . Investigations of  $\text{KHCO}_3$  dissolved in different solvents (water, methanol and ethanol), shows that in alcoholic solution the  $\text{HCO}_3^-$  reacts with  $\text{RO}^-$  to the carbonate ester ( $\text{ROCO}_2^-$ ). In acidic solution the carbonate ester may either be protonated, forming monoalkyl carbonic acid  $\text{HOCO}_2\text{R}$ , or hydrolyzed, forming  $\text{H}_2\text{CO}_3$ . Isotope substitution experiments suggest that the former may be the preferred pathway, in contrast to the view in literature. Further studies are necessary to clarify whether what was regarded as  $\alpha\text{-H}_2\text{CO}_3$  in literature may be in fact be  $\text{HOCO}_2\text{CH}_3$ .

Investigation of solid  $\beta\text{-H}_2\text{CO}_3$  interacting with solid water has revealed the formation of a new species, which converts upon heating ( $T = 230\text{ K}$ ) to  $\beta\text{-H}_2\text{CO}_3$ . This unknown species appears in the presence of relative humidities with respect to ice ( $\text{RH}_{\text{ice}}$ ) in excess of 100 %. It is also formed at  $\approx 200\text{ K}$  by reaction of  $\text{HCO}_3^-$  and  $\text{H}^+$  in concentrated aqueous solutions. One possible interpretation would be a reaction of ice with solid carbonic acid resulting in the incorporation of water molecules into the crystal structure of  $\text{H}_2\text{CO}_3$ , thereby, forming a  $\text{H}_2\text{CO}_3$ -hydrate.

By sublimation of  $\alpha$ - and  $\beta$ -polymorphs it was possible to trap the mainly undecomposed vapor-phase in solid noble gas matrices. IR-spectroscopic investigation of the matrix suggests two monomer conformers (cis-cis, cis-trans) and a cyclic dimer do be present in the gas phase. However, there are subtle differences between the vapors sublimated from the  $\alpha$ - and  $\beta$ -polymorph. As a consequence of this, also the polymorph that crystallizes after removal of the matrix is different:  $\alpha\text{-H}_2\text{CO}_3$  crystallizes from sublimed  $\alpha\text{-H}_2\text{CO}_3$ , while  $\beta\text{-H}_2\text{CO}_3$  crystallizes from sublimed  $\beta\text{-H}_2\text{CO}_3$ . This difference in the gas phase may be attributed to different sublimation temperatures of  $\alpha\text{-H}_2\text{CO}_3$  ( $> 210\text{ K}$ ) and  $\beta\text{-H}_2\text{CO}_3$  ( $> 230\text{ K}$ ). However, the above mentioned results suggest that monomethyl carbonic acid may be present as a species in the  $\alpha\text{-H}_2\text{CO}_3$  matrix isolation spectra. Both  $\text{H}_2\text{CO}_3$  and  $\text{HOCO}_2\text{CH}_3$  allow for a good fit between measured and calculated spectra. Here isotope substitution prefers the latter.

Experiments, at atmospheric conditions at altitudes of up to 5 km, show formation and stability of carbonic acid up to 260 K by protonation of mineral dust ( $\text{CaCO}_3$ ) particles with  $\text{HCl}$  droplets. This suggests existence in our atmosphere, especially in ice clouds. At

200 K aqueous/amorphous  $\text{H}_2\text{CO}_3$  is produced and crystallizes to  $\beta\text{-H}_2\text{CO}_3$  at higher temperatures under low humidity conditions and does not decompose readily even at 250 K in a humid atmosphere. These results render  $\text{H}_2\text{CO}_3$  as well as  $\text{H}_2\text{CO}_3$ -hydrate important in the atmosphere, where it could contribute to the acidity in the troposphere.

## 2 Carbonic acid (H<sub>2</sub>CO<sub>3</sub>)

Carbonic acid (H<sub>2</sub>CO<sub>3</sub>) is the short-lived intermediate in the CO<sub>2</sub>/HCO<sub>3</sub><sup>-</sup>/CO<sub>3</sub><sup>2-</sup> equilibrium. <sup>[1-6]</sup> In biological and geochemical carbonate containing systems H<sub>2</sub>CO<sub>3</sub> plays an important role. For a long time it was the opinion that H<sub>2</sub>CO<sub>3</sub> is a short lived intermediate which cannot be isolated. Under the conditions on Earth at a temperature of around 298 K, a base pressure of 1015 mbar and atmospheric humidity H<sub>2</sub>CO<sub>3</sub> cannot exist in pure form. Theoretical calculations about the stability of H<sub>2</sub>CO<sub>3</sub> show under dry conditions a very slow decomposition rate of 1.2 x 10<sup>-13</sup> s<sup>-1</sup> at 300 K. <sup>[4]</sup> A single water molecule, however, increases the rate of decomposition by a factor of 10<sup>7</sup> – 10<sup>9</sup>. <sup>[4]</sup> The half-life of H<sub>2</sub>CO<sub>3</sub> at dry conditions at 300 K amounts to 0.18 million years, but one water molecule reduces the half-life to 10 h. <sup>[4]</sup> H<sub>2</sub>CO<sub>3</sub> dissolved in water dissociates rapidly into CO<sub>2</sub> and H<sub>2</sub>O.

H<sub>2</sub>CO<sub>3</sub> is less stable than CO<sub>2</sub> + H<sub>2</sub>O and, thus its formation is an endothermic reaction with a calculated energy difference of 43.4 kJ/mol. <sup>[5]</sup> Figure 1.1 shows the energy level and reaction scheme for the formation of H<sub>2</sub>CO<sub>3</sub>, including the aqueous solvation of CO<sub>2</sub> as well as protolysis. In pure water the formation of H<sub>2</sub>CO<sub>3</sub> from aqueous solvation of CO<sub>2</sub> is followed by deprotonation to HCO<sub>3</sub><sup>-</sup> and CO<sub>3</sub><sup>2-</sup>. <sup>[6]</sup> The energy barriers of the forward and reverse pathway are calculated to be 217.2 and 173.8 kJ/mol. <sup>[5]</sup> The rate constant of hydration of CO<sub>2</sub> in aqueous solution k<sub>32</sub> is 15.1 s<sup>-1</sup>, but the dehydration rate k<sub>23</sub> is 0.043 s<sup>-1</sup>. <sup>[7]</sup> The protolysis is a fast diffusion process with k<sub>12</sub> ≈ 5 x 10<sup>10</sup> M<sup>-1</sup> s<sup>-1</sup>. <sup>[7]</sup> The rate-constants for direct way 1-3 followed directly from measured data are k<sub>13</sub> = 5.6 x 10<sup>4</sup> M<sup>-1</sup> s<sup>-1</sup> and k<sub>31</sub> = 0.043 s<sup>-1</sup>. <sup>[7]</sup>

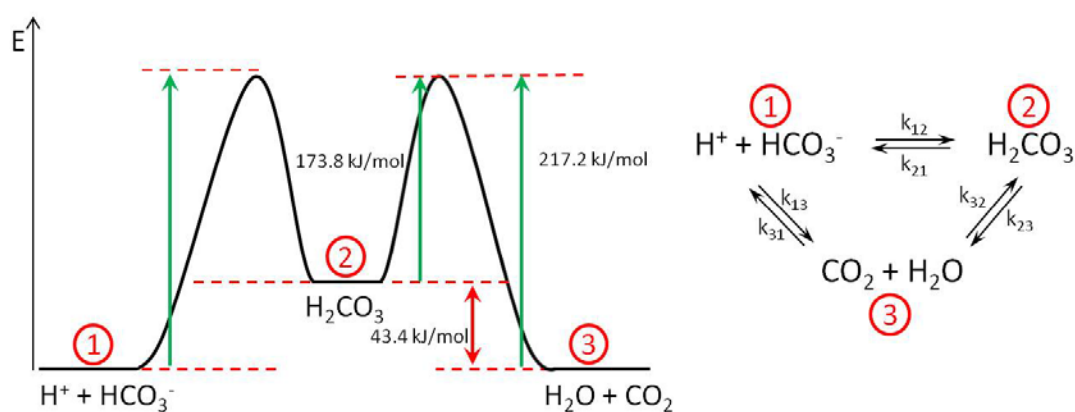


**Figure 1.1** The energy level and reaction scheme for the formation of H<sub>2</sub>CO<sub>3</sub>.

In 1990 Falcke and Eberle recorded Raman spectra from NaHCO<sub>3</sub> solutions after rapid acidification with HCl to pH 0-1 in a continuous flow apparatus. The spectra show two bands at 1382 and 1280 cm<sup>-1</sup> caused by CO<sub>2</sub>, and an intensive peak at 1017 cm<sup>-1</sup> assumed to be caused by the C-OH stretching vibration of carbonic acid (H<sub>2</sub>CO<sub>3</sub>). <sup>[8]</sup> The research group of Erik Nibbering observed in 2009 the formation of H<sub>2</sub>CO<sub>3</sub> in aqueous

solution, using time-resolved femtosecond infrared spectroscopy by ultrafast protonation of bicarbonate. [6] They obtained an acidity constant, a measure of the strength of an acid in solution, of  $pK_a = 3.45$  [6].

Pure  $H_2CO_3$  could not be synthesized and isolated for a long time, because it decomposes on the time scale of seconds in aqueous solutions. The first successful isolation of solid  $H_2CO_3$  was achieved in the 1990's.

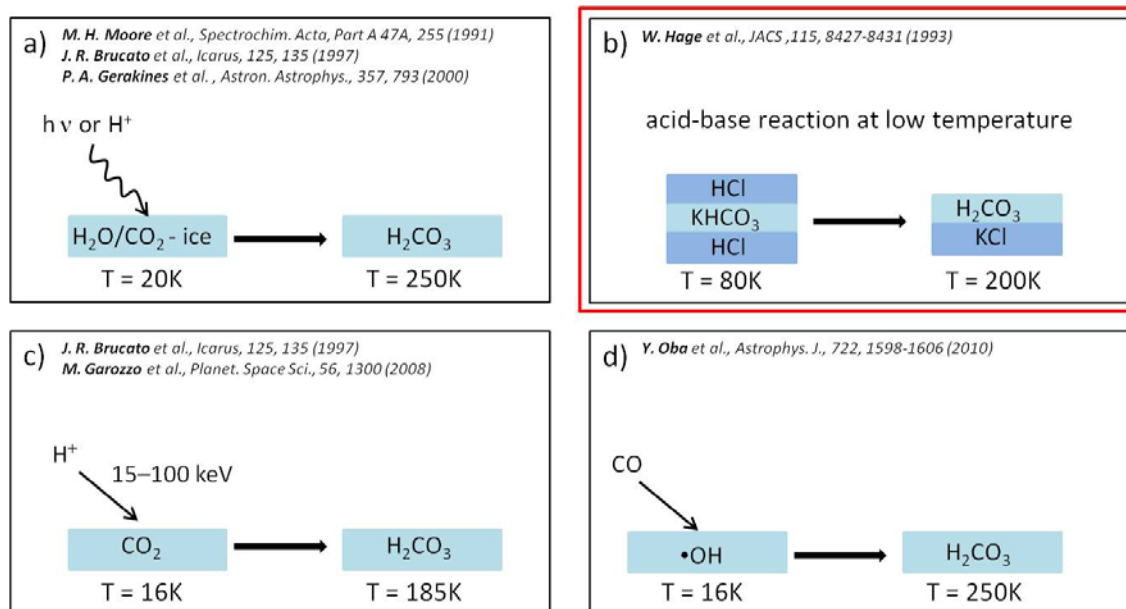


**Figure 1.2 Pathways to form  $H_2CO_3$ . a) by high energy and proton irradiation of  $H_2O/CO_2$ -ice, b) by acid base reaction at low temperature, c) by proton implantation in  $CO_2$ -ice and d) by surface reactions of  $CO$  molecules with non-energetic hydroxyl radicals ( $OH\bullet$ ).**

Under extreme conditions at low temperatures ( $T = 180 - 240 K$ ) and in *vacuo* ( $p = 10^{-5}$  mbar)  $H_2CO_3$  can be synthesised and isolated. These conditions are found in outer space, for example, in the atmosphere of Mars or Venus and in trails of comets.

The literature reports four different ways for producing and isolating  $H_2CO_3$ . In 1991 Moore and Khanna investigated the effects of proton irradiation on mixed  $H_2O:CO_2$  (1:1) ices at 20 K. The mixtures were irradiated with 700 keV protons. [9] With infrared and mass spectroscopy they identified radicals ( $HCO\bullet$ ,  $CO_3\bullet$ ) and molecular ( $CO$ ) species, and a new species which evolved into a residual film at 215 – 250 K and has been assigned to  $H_2CO_3$ . [9] In 2000 Gerakines et al. investigated the formation of  $H_2CO_3$  by exposing  $H_2O:CO_2$  ice mixtures to either UV photons ( $10 \text{ eV photon}^{-1}$ ) or high-energy protons ( $0.8 \text{ MeV protons, } p^+$ ) [10] (Figure 1.2a). The results showed that  $H_2CO_3$  was formed by  $p^+$  bombardment. The formation via UV photolysis is limited by the penetration of the UV photons. [10]

In 1997 Brucato et al. and then in 2008 Garozzo et al. showed also that  $H_2CO_3$  is formed after bombardment of  $CO_2$ -ice with hydrogen ions. The implanted ions are incorporated

into the target, break molecular bonds and form new ones. A new species is formed <sup>[11-12]</sup> (Figure 1.2c).

These results have a possible astrophysical relevance, because they show that  $H_2CO_3$  can be formed in bodies of our solar system.  $H_2O$  and  $CO_2$  are two of the most abundant molecules identified in icy grain mantles in the interstellar medium. <sup>[13]</sup> They are detected also in comets like Hale-Bopp <sup>[14]</sup> and in icy Galilean satellites Europa, Ganymede, and Callisto. <sup>[15-16]</sup> Also on the surface of Mars  $CO_2$  and  $H_2O$  molecules have been identified. <sup>[17-18]</sup>

In 1993 Hage et al. chose a more chemical pathway. They isolated  $H_2CO_3$  via an acid-base reaction at low temperatures (Figure 1.2b). With a new cryogenic method (see chapter 3) glassy solutions of  $KHCO_3$ , with an excess of  $HBr$  or  $HCl$  were deposited at 78 K in form of droplets on a cryoplate and their reaction was studied by FTIR spectroscopy from 78 – 300 K. <sup>[1-2, 19-23]</sup>

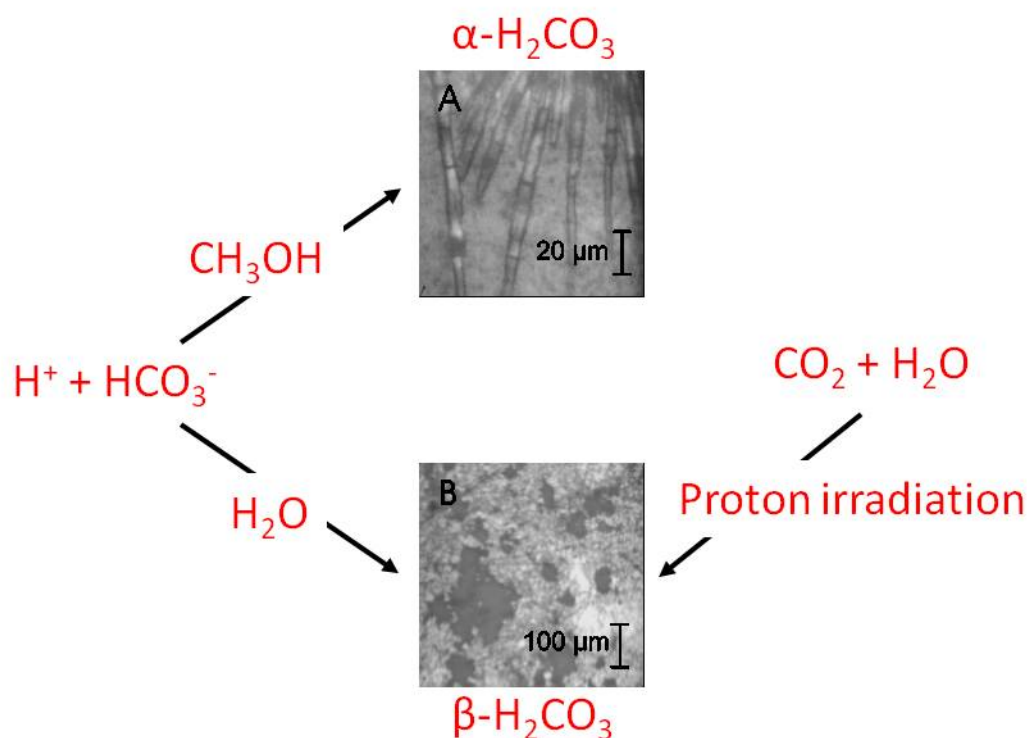


**Figure 1.3** Two polymorphs of carbonic acid. By reaction in methanolic solutions the  $\alpha$ -polymorph is obtained (the needles in the microscopic picture A). By reaction in aqueous solution and by proton irradiation the  $\beta$ -polymorph of carbonic acid is obtained (the black area in the microscopic picture B).

They found two different polymorphs of  $H_2CO_3$ . The reaction in water solutions formed the  $\beta$ -polymorph; in methanolic solutions the  $\alpha$ -polymorph of  $H_2CO_3$  was obtained. It is very interesting that by high energy irradiation of  $H_2O/CO_2$ -ice and by proton implantation into  $CO_2$ -ice the  $H_2CO_3$   $\beta$ -polymorph is formed (Figure 1.3). The  $\alpha$ -polymorph grows as crystal needles (microscopic picture A in Figure 1.3), in the microscopic picture B in Figure 1.3 the  $\beta$ -polymorph is marked by the black areas.

In 2010 Oba et al. formed carbonic acid by a new path of synthesis. They presented the formation of carbonic acid ( $\text{H}_2\text{CO}_3$ ) by surface reactions of CO molecules with non-energetic hydroxyl (OH) radicals at 10 – 40 K. With IR spectra and thermally programmed desorption mass spectra they clearly identified the formation of  $\text{H}_2\text{CO}_3$ .<sup>[24]</sup> The structure of  $\text{H}_2\text{CO}_3$  obtained in this way differs from the ones formed by energetic processes such as UV irradiation and ion irradiation of  $\text{H}_2\text{O}/\text{CO}_2$  binary ices.<sup>[24]</sup>

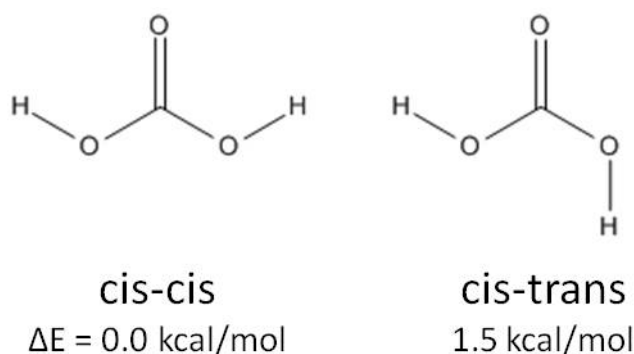


**Figure 1.4** The two  $\text{H}_2\text{CO}_3$  monomers, which were identified in experiment by Fourier-transform microwave spectroscopy.<sup>[25-26]</sup>

Observation of gaseous  $\text{H}_2\text{CO}_3$  was first reported by Terlouw et al. 1987 after the thermolysis of  $(\text{NH}_4)\text{HCO}_3$ . In the results of an electron ionization mass spectrometry experiment they attributed a weak signal at  $m/z = 62$  to gas-phase  $\text{H}_2\text{CO}_3$ .<sup>[27]</sup> In the gas-phase three possible conformers of the  $\text{H}_2\text{CO}_3$  monomer are possible. Two of them, the cis-cis and cis-trans monomer (Figure 1.4), were identified experimentally by Fourier-transform microwave spectroscopy.<sup>[25-26]</sup> The monomers were generated in a supersonic jet within a discharge nozzle by applying a pulsed high voltage of 1.8 kV on a  $\text{H}_2\text{O}/\text{CO}_2$  gas mixture.<sup>[25-26]</sup> In 1998 Hage et al. showed that  $\text{H}_2\text{CO}_3$  can be sublimed and recondensed without decomposition to  $\text{CO}_2$  and  $\text{H}_2\text{O}$ .<sup>[23, 28]</sup> In this thesis, the isolation of  $\alpha$ - and  $\beta$ - $\text{H}_2\text{CO}_3$  vapor in inert gas matrices after sublimation from their crystalline forms is shown (**Paper I & II; chapter 4**).

# 3 Experimental Methods

---

## 3.1 Matrix isolation (MI)

The main experimental technique in my thesis is matrix isolation. I carried out these experiments in the institute of materials chemistry, Vienna University of Technology, in the research group of Prof. Dr. Hinrich Grothe. A short overview of theory and setup is given in the paper "Spectroscopic Observation of Matrix-Isolated Carbonic Acid Trapped from the Gas Phase" [29].

In this chapter I outline in more detail the theory of the matrix isolation method and the setup used in Vienna.

### 3.1.1 Matrix isolation: Principle

Matrix isolation (MI) is a technique which permits spectroscopic study of highly reactive molecules. These molecules would be transient or non-existent under ambient conditions. [30] The molecules are trapped and isolated in an inert solid (i.e. the matrix) at low temperature. Under such conditions the life-time of the trapped molecules greatly increases. [30] The matrix cage inhibits bimolecular collisions, molecule rotation and consecutive reaction. [30] Metaphorically, the concept of matrix isolation resembles a raisins cake (Figure 2.1), where the raisins represent the trapped molecules (in our case carbonic acid) and the cake dough the inert solid (noble gas).

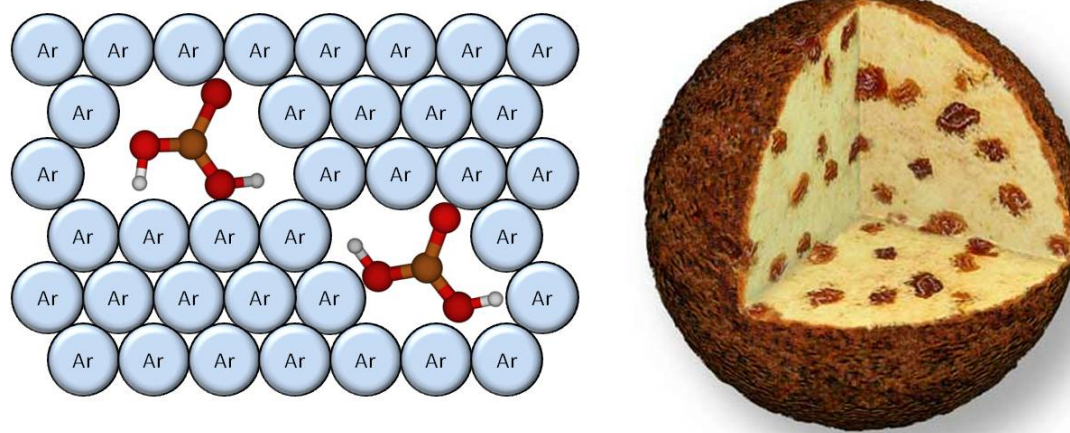


**Figure 2.1** The concept of matrix isolation resembles a raisins cake, where the raisins represent the trapped molecules (our case  $H_2CO_3$ ) and the cake mixture the inert solid (noble gas). (The picture of the raisins cake was taken from [http://scientific-multimedia.com/index.php5?chap=5\\_1&gid=581&..](http://scientific-multimedia.com/index.php5?chap=5_1&gid=581&..))

The most significant analytical method for the study of low temperature matrices is IR-spectroscopy. The spectrum of a molecule trapped in an inert matrix closely resembles that of the gas phase molecule. Spectra of vaporized molecules are extremely complex

to interpret. The spectra contain many hot bands, due to population of rotational and low-lying vibrational levels (Figure 2.2a).<sup>[30]</sup> Matrix spectra do not show rotational transitions, but instead represent vibrational spectra of non-rotating molecules. The bands appear at the center of the Q-branch (change of rotational quantum number  $\Delta J = 0$ ) (Figure 2.2b). Figure 2.2a shows the gas phase spectrum of H<sub>2</sub>O between 2000 – 1300 cm<sup>-1</sup>. We can see many rotational transitions of the H<sub>2</sub>O-molecules. Figure 2.2b shows the IR matrix spectrum of the H<sub>2</sub>O-molecules isolated in an Argon (Ar) matrix. It depicts the pure vibrational spectrum of the non-rotating H<sub>2</sub>O-molecule. The different bands in the matrix spectrum can be assigned to different species of H<sub>2</sub>O-molecule monomers, dimers and oligomers, which are isolated in the matrix.

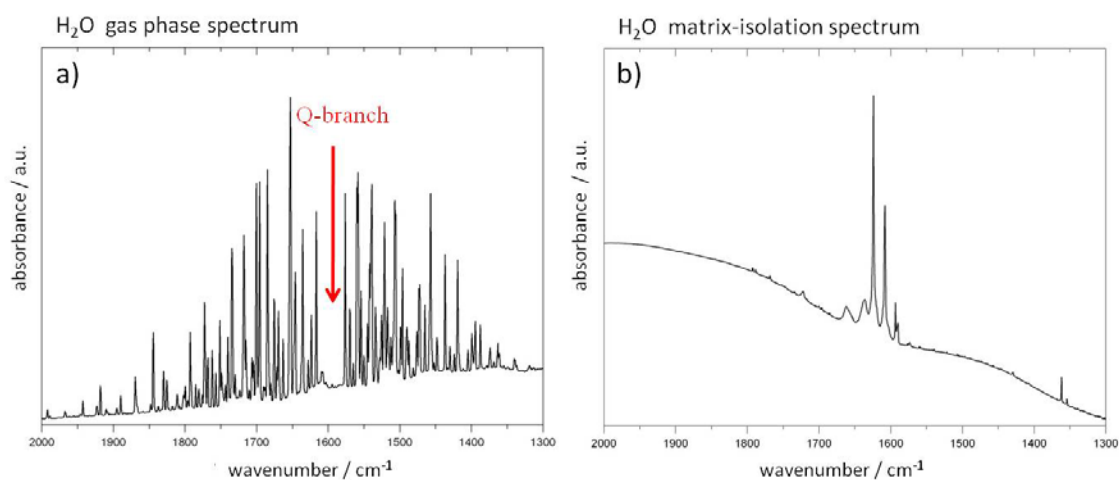


**Figure 2.2** Difference between H<sub>2</sub>O gas phase (a) and H<sub>2</sub>O matrix isolation (b) spectrum. The gas phase spectrum depicts rotational vibrational transitions (Q-branch region with  $\Delta J = 0$ ). The matrix spectrum shows the pure vibrational spectrum of the non-rotating H<sub>2</sub>O-molecule. The different bands in the matrix spectrum can be assigned to different species of H<sub>2</sub>O-molecule monomers, dimers and oligomers, which are isolated in the matrix.

The resolution of matrix spectra is high and permits the separation of narrowly spaced bands. This is important for the measurement of isotope effects, in our case to separate the bands which involve vibration of <sup>13</sup>C and <sup>12</sup>C. For H<sub>2</sub>CO<sub>3</sub>, the full width of the C=O stretching vibration band at half maximum (FWHM) is approximately 50 cm<sup>-1</sup> in the spectrum obtained from the crystalline solid (Figure 2.3 red curve) and 2 cm<sup>-1</sup> in the spectrum obtained in Ar-matrix (Figure 2.3 black curve). The high resolution of the matrix spectrum allows the clear differentiation and identification of bands separated approximately 2 cm<sup>-1</sup>.

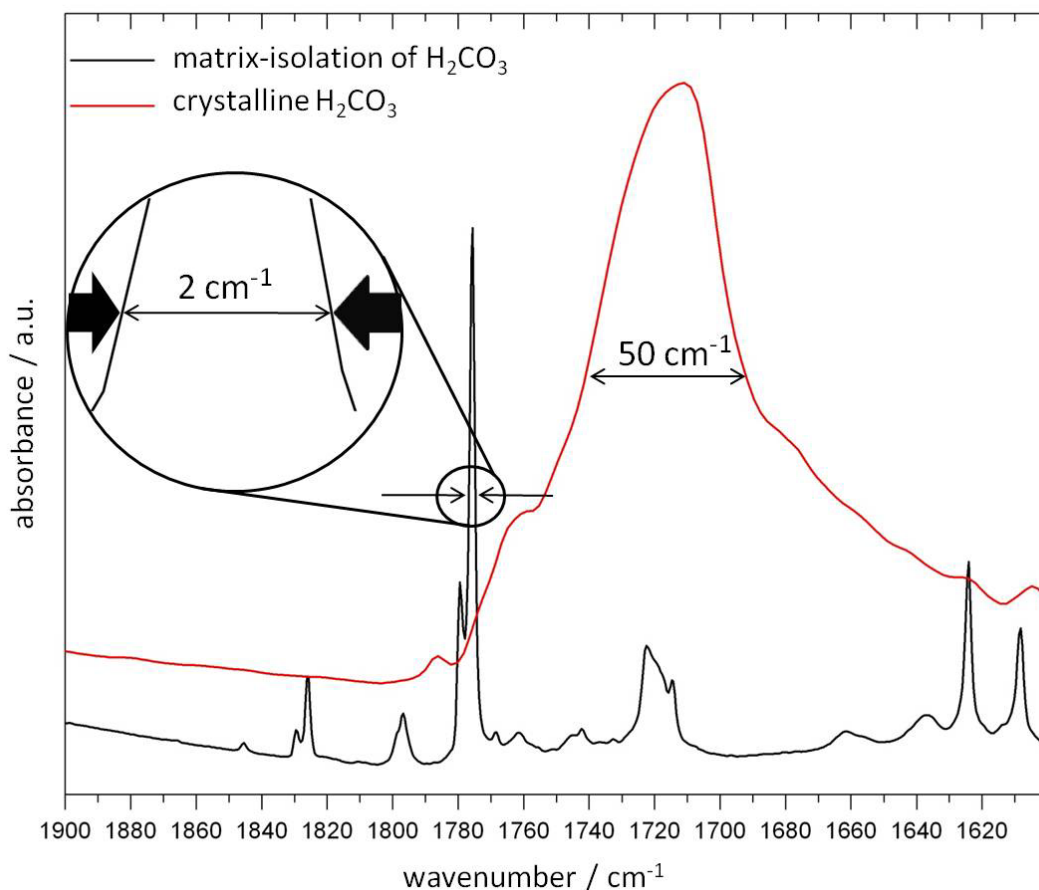


**Figure 2.3** Full width at half maximum (FWHM) of  $\nu(\text{C}=\text{O})$  for  $\text{H}_2\text{CO}_3$  in the crystalline solid state (red) and in matrix-isolation (black).

### 3.1.2 Properties of matrix materials

The choice of matrix material in the experiment depends on its properties, as well as the experimental setup. The matrix material should possess a high degree of purity to obtain reproducible spectra. Many materials show IR absorption, but for measuring IR-spectra of trapped molecules no IR absorption of the matrix is wanted. Otherwise the matrix material could mask regions where bands of interest may be located. The matrix must also be inert to prevent reaction with the solute. An important requirement to study isolated species is rigidity of the matrix. In rigid matrices diffusion of the solute molecules within the matrix does not occur and recombination of free radicals or formation of multimeric species is prevented. The rigidity of a matrix is characterized by the temperature at which diffusion in the matrix takes place. The diffusion temperature  $T_d$  is dependent on the melting point  $T_m$  of the matrix. For salts, oxides, etc.  $T_d \approx 0.57 T_m$ , for covalent compounds  $T_d \approx 0.90 T_m$ .<sup>[30-31]</sup> Usually the matrix material and the solute are mixed in the gas phase before the mixture is frozen out on the cold plate of the cryostat. A sufficiently high vapor pressure at room temperature of the solute in its liquid or solid state is required, in order to reach good mixing ratios with the matrix.<sup>[30]</sup>

During the condensation of the gases to form a matrix it is important to remove the heat of condensation from the support area. The latent heat of fusion  $L_f$  is a measure of the amount of heat which is removed. When the gas mixture hits the cold plate of the cryostat (typically at  $T = 6$  K), a lattice is formed. The lattice energy  $U_0$  represents the energy which is required to form a lattice at 0 K as well as to remove a molecule from its place in the lattice. <sup>[30]</sup> The last important thermal property is the thermal conductivity  $\lambda$  of the matrix material. Gas at a temperature of 295 K should be condensing on the 6 K cold plate. As the matrix layer grows, the heat of the newly condensing gas must be carried away through this layer. If the thermal conductivity  $\lambda$  of the matrix is poor, local heating will occur and results in diffusion of solute. Monomers and radicals get lost due to multimerization or recombination. <sup>[30]</sup>

For our MI experiments we used three different noble gases, Neon (Ne), Argon (Ar) and Krypton (Kr), as matrix. The thermal properties of the gases are shown in Table 2.1.

**Table 2.1 Thermal properties of matrix materials according to H. E. Hallam (Hrsg.), *Vibrational Spectroscopy of Trapped Species* (1973). <sup>[30]</sup>**

	$T_d / \text{K}$	m.p. / K	b.p. / K	$L_f / \text{Jmol}^{-1}$	$-U_0 / \text{Jmol}^{-1}$	$\lambda_{(20\text{K})} / \text{Wm}^{-1} \text{K}^{-1}$
Ne	10	24.6	27.1	335	1874	0.4
Ar	35	83.3	87.3	1190	7724	1.3
Kr	50	115.8	119.8	1640	11155	1.2

### 3.1.3 Matrix isolation: Setup in Vienna

Generally, MI studies are done by mixing matrix gas and reactants at room temperature and condensing both on the cold plate. The reactants are usually substances with a high vapor pressure.

The isolation of carbonic acid, is more difficult. We know from chapter 1 that carbonic acid is not stable at room temperature. For the isolation of carbonic acid we need temperatures from 180 – 260 K, which are below room temperature (298 K). Calculation of the vapor pressure from the rate of sublimation for  $\alpha\text{-H}_2\text{CO}_3$  at 200 K by Hage et al. shows the saturation vapor pressure ( $p_s$ ) to be  $4 \cdot 10^{-7}$  mbar for the  $\text{H}_2\text{CO}_3$  monomer and  $3 \cdot 10^{-7}$  mbar for the dimer in the gas phase. <sup>[23]</sup> Peeters et al. measured the vapor pressure of  $\beta\text{-H}_2\text{CO}_3$  to be about  $0.290 \cdot 10^{-9} - 2.33 \cdot 10^{-9}$  mbar at 240 – 255 K. <sup>[32]</sup> Besides of the low vapor pressure, a further obstacle to the matrix isolation of  $\text{H}_2\text{CO}_3$  is the thin film nature of the solid. We work with carbonic acid layers with a thickness of a few micrometers, which we deposit on a Si-window ( $\varnothing$  25 mm).

In spite of these challenges and the anticipated low mixing ratios of  $\text{H}_2\text{CO}_3$  in the matrix I have attempted the MI in close collaboration with Prof. Dr. Hinrich Grothe from the Institute of Materials Chemistry, Vienna University of Technology, Austria. The project

has required rebuilding their MI equipment so that we could work at low temperatures, with low vapor pressure and small amount of solid  $\text{H}_2\text{CO}_3$ .

### 3.1.4 Matrix isolation: Equipment

The MI equipment consists of a high vacuum (HV) and an ultra high vacuum (UHV) chamber (Figure 2.4). The two chambers are separated through a valve. Using a high-performance rotary vane pump (Pfeiffer Vacuum DUO 10 M) and a turbomolecular drag pump (Pfeiffer Vacuum TMH 520), the HV-chamber was pumped to a base pressure of  $10^{-5}$  mbar. The UHV-chamber, pumped to a base pressure of  $10^{-9}$  mbar was pumped by another high-performance rotary vane pump (Pfeiffer Vacuum DUO 10 M) and a turbomolecular drag pump (Pfeiffer Vacuum TMU 520).

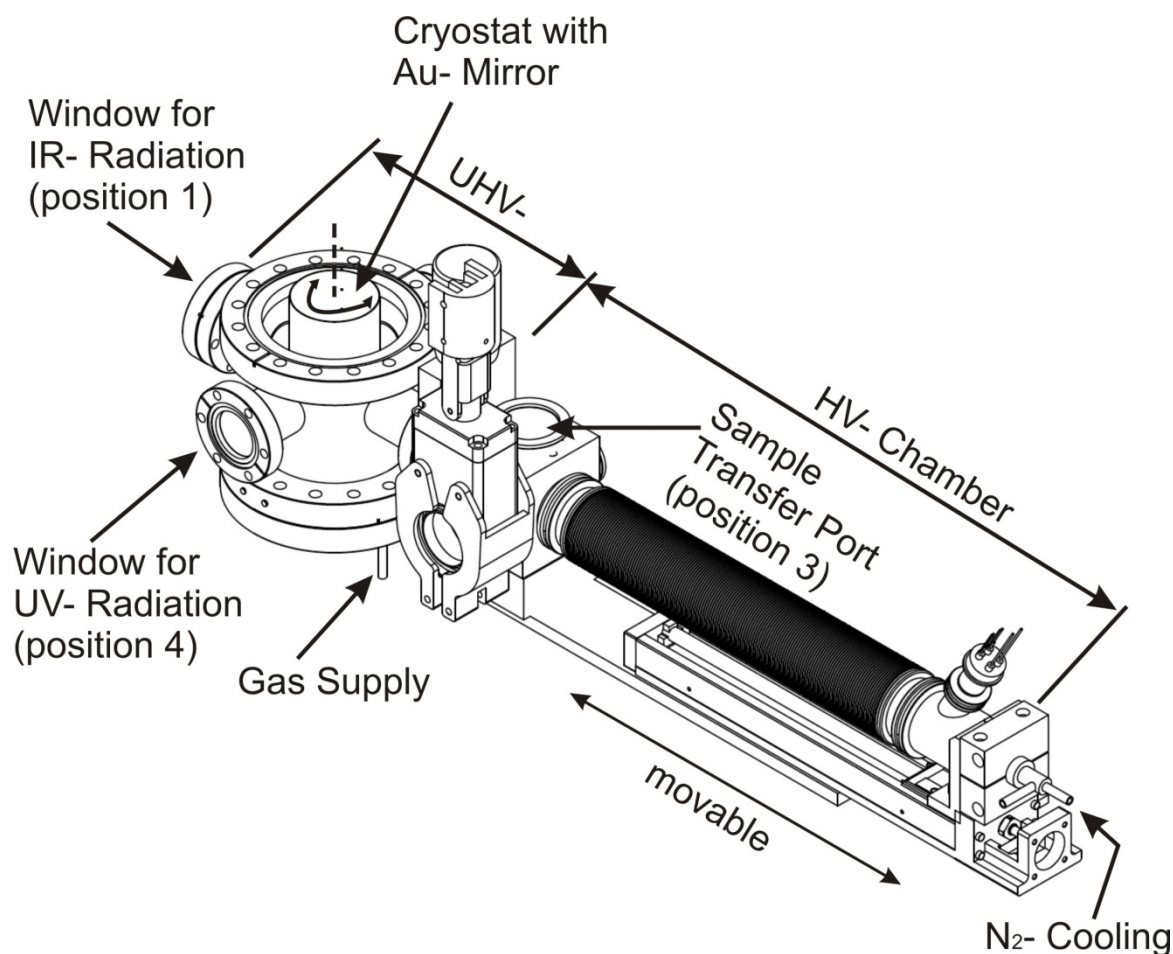


**Figure 2.4** Sketch of the matrix isolation equipment.

The sample holder (SH) is localized in the HV-chamber and can be moved between the two chambers with an electromotor. The temperature of the SH can be regulated from 180 – 260 K. The temperature is reached by blowing nitrogen gas ( $\text{N}_{2(g)}$ ) through a tube and liquid  $\text{N}_{2(l)}$  to the SH. A Pt-100 is mounted directly on the SH to read out the temperature.

The cold plate connected to a He-cryostat (Leybold-cryostat RDK 6-320; temperature range 1st stage: 28 K - 320 K; temperature range 2nd stage: 6 – 320 K) is localized in the UHV-chamber. The cold plate is coated with gold (Au). The Au-mirror is surrounded with a radiation-protection-shield, protecting the mirror from external rays of heat. This arrangement is necessary to reach temperatures down to 6 K. The cryostat with the Au-mirror can be rotated around its axis. There are four different angle positions which are important throughout the work:

- Position 1: 90° for IR measurement
- Position 2: 140° radiation-protection-shield is located between mirror and SH
- Position 3: 270° for vapor deposition
- Position 4: 0° for UV irradiation

The Bruker optics VERTEX 80 FTIR spectrometer is located at position 1. FTIR spectra are recorded with a liquid N<sub>2</sub> cooled narrow band MCT detector, applying a spectral resolution of 0.5 cm<sup>-1</sup> and adding 512 scans, using a Ge-coated KBr beam splitter. The optical path of the spectrometer was evacuated down to 2 mbar, minimizing interferences from CO<sub>2</sub> and H<sub>2</sub>O absorption from the ambient atmosphere. A window of potassium bromide (KBr) which is transparent for IR radiation is mounted on the UHV-chamber. To start the vapor deposition the cryostat had to be rotated by 180°. In this position the mirror faces in the direction where HV-chamber and SH are localized (position 3). Before we opened the valve between the two chambers, the cryostat is moved in position 2. In this position, the radiation-protection-shield is located between mirror and SH. Due to the pressure difference between the chambers impurities of water are accelerated into the UHV-chamber. Consequently, position 2 prevents condensation of particles from the HV-chamber onto the Au-mirror. After orienting the Au-mirror into position 3 we moved the SH into the UHV-chamber and started the vapor deposition. A suprasil quartz window is mounted on position 4, which is transparent for UV-radiation. In this position the matrix can be treated with UV radiation, using a Xenon (Xe) lamp from Lot Oriel. The UV-lamp consists of a 300 W Xe arc light and power supplies for 300 W Xe lamps with variable output current. The lamp works ozone free and covers the spectral range from about 250 to 2500 nm. (Figure 2.4)

### 3.1.5 Steps of H<sub>2</sub>CO<sub>3</sub> isolation

Before H<sub>2</sub>CO<sub>3</sub> could be isolated, the thin film of H<sub>2</sub>CO<sub>3</sub> on the Si-windows was stored in liquid N<sub>2</sub>, and the sample holder in the HV-chamber was precooled to 180 K. Next, an overpressure of Ar was applied when opening the HV-chamber. The sample on the Si-window was then placed onto the sample holder in a constant stream of Ar to avoid excessive take-up of humidity. Subsequently, the valve was closed and the chamber evacuated. By decreasing the cold N<sub>2</sub> gas flow the SH was heated slowly to 200 K, and the window was cleaned from water condensed during the transfer. After this step the sample was ready for the isolation.

We disconnected the HV-chamber from the vacuum pumps and opened the valve to the UHV-chamber. When opening the valve, the cryostat has to be in position 2 so that the radiation-protection-shield is located between mirror and SH. Sublimated water then recondenses on the shield rather than the Au-mirror. Then the cryostat was switched to position 3 and the SH moved into the UHV-chamber. We made the setup in such a way that the sample can be brought to a distance of 2 cm to the mirror. The short distance reduces decomposition of  $\text{H}_2\text{CO}_3$  after sublimation to a minimum. The matrix gas was regulated with a mass flow controller (MKS M-330, flow about 1.68 mmol/h). The SH was heated to 210 K ( $\alpha\text{-H}_2\text{CO}_3$ ) or 240 K ( $\beta\text{-H}_2\text{CO}_3$ ), which results in sublimation of the thin film, and the isolation then took place within an hour. After the vapor deposition, the SH was moved out of the UHV-chamber and the two chambers were disconnected. In position 1 the IR spectrum of the isolated species was recorded subsequently. (Figure 2.5)

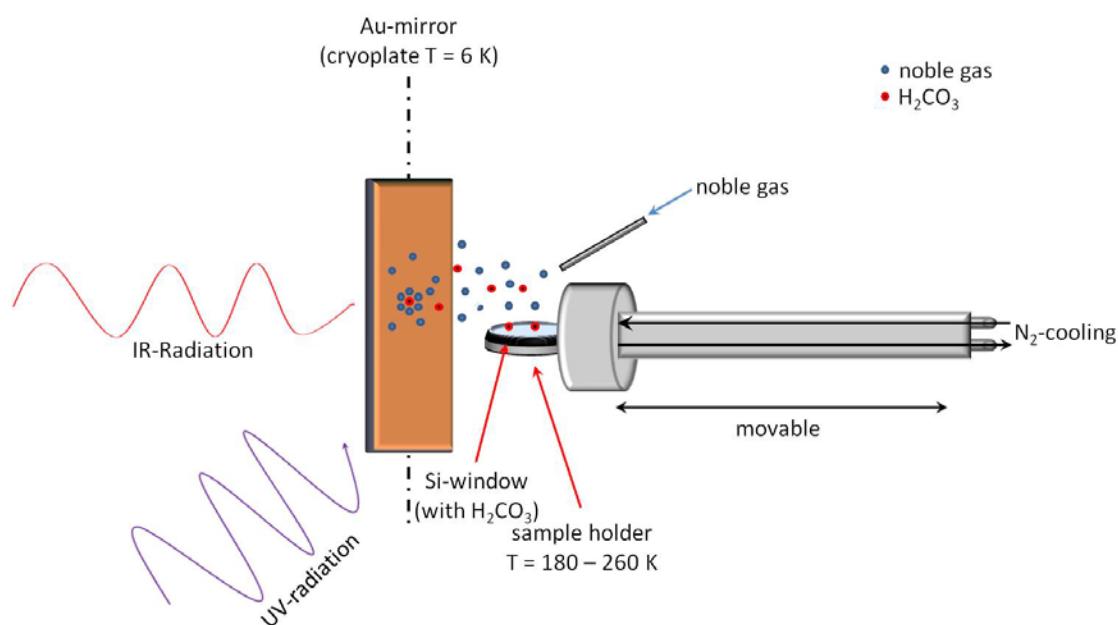


**Figure 2.5** Schema of the matrix isolation of  $\text{H}_2\text{CO}_3$ .

## 3.2 Preparation of starting material ( $\text{H}_2\text{CO}_3$ )

The preparation of the starting material ( $\text{H}_2\text{CO}_3$ ) was done by hyperquenching<sup>[33-34]</sup> of solutions in the laboratory of the Institute of Physical Chemistry University of Innsbruck. The technique<sup>[33-34]</sup> was applied for the first time in the eighties, and in the nineties  $\text{H}_2\text{CO}_3$  was synthesized from hyperquenched deposits<sup>[21-22]</sup>.

Layers of glassy solutions were deposited on a cryoplate at liquid nitrogen temperature ( $T = 78 \text{ K}$ ) in form of droplets (Figure 3.1). The solution was nebulized in  $\text{N}_2$  carrier gas (droplets of  $\approx 3 \mu\text{m}$ ) by means of an air brush pistol (Harder & Steenbeck; model grafo or infinity) and introduced into a vacuum chamber ( $\approx 10^{-7} \text{ mbar}$ ) through an aperture ( $500 \mu\text{m}$ ). The solution droplets are immobilized almost instantaneously to form glassy layers at  $78 \text{ K}$  (cooling rates up to  $10^7 \text{ K/s}$ ) when they hit the IR transparent window (cesium iodide, CsI, or silicon, Si, windows).<sup>[2, 21-22]</sup>

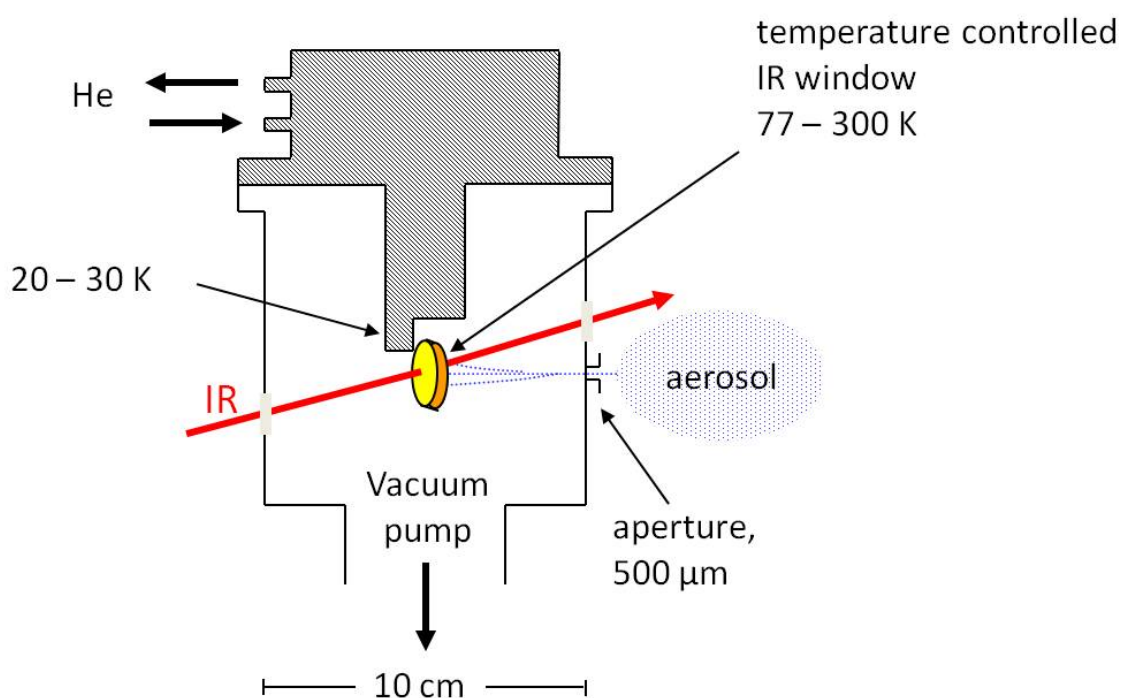


**Figure 3.6 Hyperquenching setup.** A solution is nebulized (droplets of  $\approx 3 \mu\text{m}$ ) and introduced into a vacuum chamber ( $\approx 10^{-7} \text{ mbar}$ ) through an aperture. The solution droplets are immobilized almost instantaneously and form glassy layers at  $78 \text{ K}$  (cooling rates up to  $10^7 \text{ K/s}$ ) when they hit the IR transparent window.

Layers of acids ( $\text{HX}$ ,  $\text{X} = \text{Cl}, \text{Br}$ ) and hydrogen carbonates ( $\text{MHCO}_3$ ;  $\text{M} = \text{K}$ ) or carbonates ( $\text{M}_2\text{CO}_3$ ;  $\text{M} = \text{K}$ ) were deposited on the window. Below the glass transition temperature ( $T_g$ ) of the solvent long range diffusion and reaction are inhibited. At about  $20 \text{ K}$  above  $T_g$  coalescence of the droplets begins. At  $40 \text{ K}$  above  $T_g$  diffusion of reactants and protonation of  $\text{HCO}_3^-/\text{CO}_3^{2-}$  starts. To achieve complete protonation of  $\text{HCO}_3^-/\text{CO}_3^{2-}$  an excess of acid was used. After protonating the solvent, excess of acid and residual water

had to be pumped off ( $T \gg T_g$ ). Amorphous carbonic acid is formed and by further increasing temperature, the amorphous form transformed to crystalline carbonic acid (Figure 3.2).<sup>[35]</sup>

To prepare  $\alpha$ -H<sub>2</sub>CO<sub>3</sub> we used methanolic solutions (Sigma Aldrich; methanol CHROMASOLV<sup>®</sup>, for HPLC,  $\geq 99.9\%$ ) of hydrochloric acid,  $c = 1.5$  M, (Supelco methanolic HCl 3 N) and KHCO<sub>3</sub> (Sigma Aldrich, potassium bicarbonate, minimum 99.5%),  $c = 0.4$  M. The glass transition ( $T_g$ ) of methanol is at 103 K. Coalescence begins at about 120 K and protonation starts at 140 K. The separation of  $\alpha$ -H<sub>2</sub>CO<sub>3</sub> from the solvent was achieved by heating in *vacuo* up to  $\approx 180$  K. First methanol and excess HCl and then residual water are pumped off. For the study of isotope effects we used K<sub>2</sub><sup>13</sup>CO<sub>3</sub> (Cambridge Isotope Laboratories, Inc., potassium carbonate <sup>13</sup>C, 99%) which was dissolved in methanol (Sigma Aldrich; CHROMASOLV<sup>®</sup>, for HPLC,  $\geq 99.9\%$ ), and for the deuteration K<sub>2</sub>CO<sub>3</sub> (Fluka, potassium carbonate anhydrous, purum p. a.  $> 99.0\%$ ) in CH<sub>3</sub>OD (Sigma Aldrich, methyl alcohol-OD) and DBr (Cambridge Isotope Laboratories, Inc., DBr 48 % in D<sub>2</sub>O) dissolved in CH<sub>3</sub>OD.

Layers of glassy solutions are deposited at a cryoplate at  $T = 78$  K in the form of droplets.

Below the glass transition temperature  $T_g$  of the solvent, long-range diffusion and reaction are inhibited.

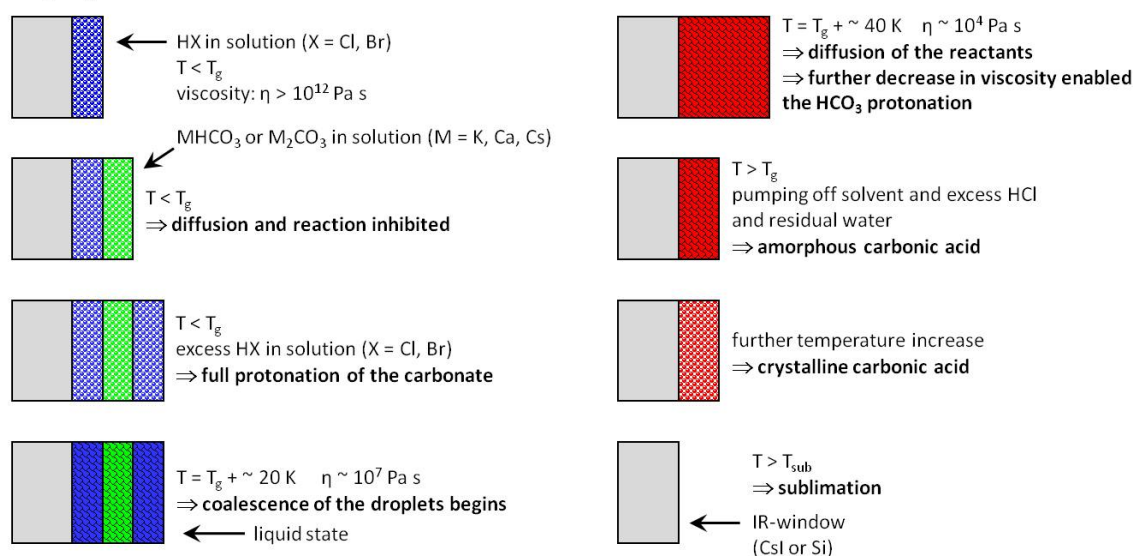


**Figure 3.7 Preparation and formation of crystalline H<sub>2</sub>CO<sub>3</sub> upon heating the IR-windows.**

$\beta$ -H<sub>2</sub>CO<sub>3</sub> was prepared by reaction of excess HBr (Fluka, Hydrobromic acid 48%),  $c = 2$  M, with KHCO<sub>3</sub> (Sigma Aldrich, potassium bicarbonate, minimum 99.5%) in aqueous solutions,  $c = 1$  M. In the case of water as solvent, protonation of HCO<sub>3</sub><sup>-</sup>/CO<sub>3</sub><sup>2-</sup> apparently occurs in the freeze-concentrated state. About 15 K above water's  $T_g \approx 136$  K the layers crystallize to cubic ice and a residual freeze-concentrated solution (Figure 3.3).<sup>[2, 20]</sup> For the isotope substitution we used K<sub>2</sub><sup>13</sup>CO<sub>3</sub> (Cambridge Isotope Laboratories, Inc., potassium carbonate <sup>13</sup>C, 99%) and for the deuteration, K<sub>2</sub>CO<sub>3</sub> (Fluka, potassium

carbonate anhydrous, purum p. a. > 99.0%) and DBr (Cambridge Isotope Laboratories, Inc., DBr 48 % in D<sub>2</sub>O) in D<sub>2</sub>O (Euriso-top deuterium oxide 100 %).

Instead of water itself becoming sufficiently fluid for coalescence, the freeze concentrated solution transports protons to the carbonate anion. Possibly crystalline hexahydrate of HBr acts as a proton donor, producing H<sub>2</sub>CO<sub>3</sub> in solution. When pumping off the solvent at  $T \approx 210$  K also in this case first amorphous H<sub>2</sub>CO<sub>3</sub> is formed, which crystallizes at  $T \approx 230$  K to  $\beta$ -H<sub>2</sub>CO<sub>3</sub>.

The preparation of the polymorph of H<sub>2</sub>CO<sub>3</sub> was monitored *in situ* by FTIR-spectra using a Varian Excalibur 3100 FTIR-spectrometer. Through two 49 mm diameter optical discs (KBr) the beam of light can pass into the vacuum chamber and the sample. The FTIR spectra were recorded with a resolution of 4 cm<sup>-1</sup> and by accumulating 100 scans. The hyperquenching chamber was pumped to a base pressure of 10<sup>-7</sup> mbar, using an oil-free scroll pump (Varian Triscroll) and a turbomolecular pump (Leybold Turbovac 361). To keep the base pressure after the injection of the solutions in nitrogen as carrier gas low a cryo-pump (Leybold RW 6000 compressor unit and RGD 1245 cold head) is located inside the vacuum chamber and kept at 11 K. At this temperature the carrier gas condenses as a solid on the cryopump.

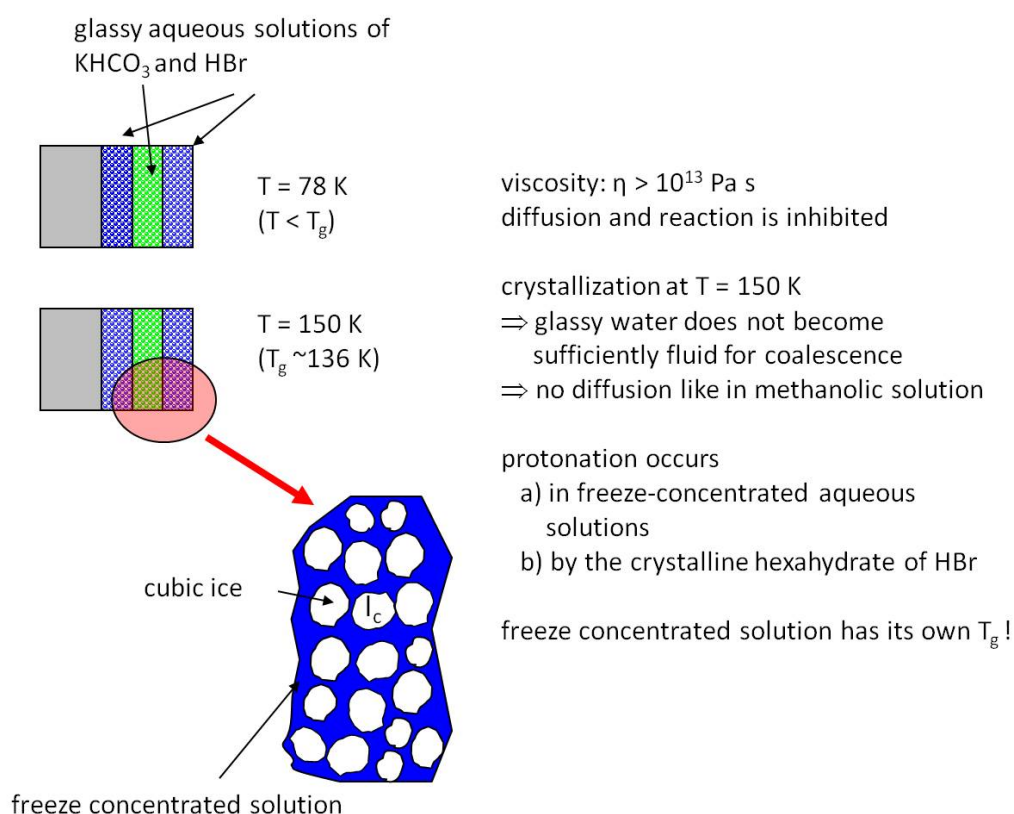


**Figure 3.8 Protonation of  $\text{HCO}_3^-/\text{CO}_3^{2-}$  apparently occurs in freeze-concentrated state, after crystallization of glassy water to cubic ice, when water is used as a solvent.**

### 3.3 *Ab initio* quantum mechanical calculations

*Ab-initio* quantum mechanical calculations of carbonic acid in various isotope configurations were performed to obtain reference frequencies for annotating measured spectra. The calculations were done by Prof. DDr. Klaus R. Liedl and Mag. Roland Huber from the Institute of General, Inorganic and Theoretical Chemistry, University of Innsbruck, Austria. All calculations were performed using the Gaussian 09 package <sup>[36]</sup>. Both the  $C_{2v}$  and  $C_s$  conformations were employed for geometry optimization, where the former is the energetically most favorable conformation. <sup>[5, 37]</sup> Calculations were performed using second-order Møller-Plesset perturbation theory (MP2) with the augmented correlation consistent basis sets of Dunning and co-workers. <sup>[38-40]</sup> Initial optimization was done at the MP2/aug-cc-pVDZ level of theory requiring “verytight” convergence on displacement and forces. Starting from the resulting geometry, further optimization at the MP2/aug-cc-pVTZ level of theory using “verytight” convergence criteria yielded an energy minimum for frequency calculations. Subsequently, IR and Raman modes were determined at this minimum geometry using MP2/aug-cc-pVTZ. Isotope shifts were calculated by performing frequency calculations at the same minimum for either all  $^2\text{H}$  or  $^{13}\text{C}$ -labeled carbonic acid. Calculated frequencies and isotope shifts were then used to identify the various signals observed in the experimentally obtained spectra.



## 4 Peer-Reviewed Publications

---

**Juergen Bernard**, Markus Seidl, Ingrid Kohl, Klaus R. Liedl, Erwin Mayer, Óscar Gálvez, Hinrich Grothe, Thomas Loerting;

*“Spectroscopic Observation of Matrix-Isolated Carbonic Acid Trapped from the Gas Phase.”*

*Angew. Chem. Int. Ed. 50 (2011) 1939–1943*

**Juergen Bernard**, Roland. G. Huber, Klaus R. Liedl, Hinrich Grothe, Thomas Loerting;

*“Matrix isolation studies of carbonic acid – the vapour phase above the  $\beta$ -polymorph.”*

*J. Am. Chem. Soc. (2013) 7732-7737*

**Juergen Bernard**, Markus Seidl, Erwin Mayer, Thomas Loerting;

*“Formation and Stability of Bulk Carbonic Acid ( $H_2CO_3$ ) by Protonation of Tropospheric Calcite.”*

*Chem. Phys. Chem. 13 (2012) 3087–3091*

Thomas Loerting, **Juergen Bernard**;

*“Aqueous carbonic acid ( $H_2CO_3$ ).”*

*Chem. Phys. Chem. 11 (2010) 2305–2309.*

Christian Mitterdorfer, **Juergen Bernard**, Frederik Klauser, Katrin Winkel, Ingrid Kohl, Klaus R. Liedl, Hinrich Grothe, Erwin Mayer, Thomas Loerting;

*“Local structural order in carbonic acid polymorphs: Raman and FT-IR spectroscopy.”*

*J. Raman Spectrosc. 43 (2012) 108–115*

## 4.1 General conclusions of the publications

Low temperature experiments combined with spectroscopic methods are important to characterize metastable molecules. Carbonic acid ( $\text{H}_2\text{CO}_3$ ) as the C1 diprotic acid has received a lot of interest for many years in basic research as well as in astrochemistry and atmospheric chemistry. Combining both – basic research and astrochemistry and atmospheric chemistry – is not an easy task. Nevertheless, this was attempted for this thesis. Huber et al. <sup>[41]</sup> have emphasized that the sublimation temperature of  $\text{H}_2\text{CO}_3$  of up to 260 K matches conditions met in the troposphere and might allow for  $\text{H}_2\text{CO}_3$  to exist in Earth's atmosphere. The stability of gas-phase  $\text{H}_2\text{CO}_3$  also has relevance in thin atmospheres of astrophysical objects. E.g., on the Mars surface the temperature is known to vary between 140 K and 300 K. In this environment  $\text{H}_2\text{CO}_3$  may undergo sublimation and recondensation cycles and reach a steady-state concentration near the polar caps. It would be a challenge to discover  $\text{H}_2\text{CO}_3$  in the Earth's atmosphere as well as in the outer space. Contactless techniques, e. g. infrared and Raman spectroscopy can help to detect carbonic acid in our atmosphere and in astrophysical objects by field studies. Our IR and Raman data can help to identify this exclusive molecule, both in the gas phase and in the solid state.

### ***Paper I and II***

Carbonic acid is important in a lot of systems. Since  $\text{H}_2\text{O}$  and  $\text{CO}_2$  coexist in various astrophysical environments, for example at the polar caps of Mars or in the tail of comets such as Hale Bopp, formation of solid or gaseous carbonic acid by high-energy irradiation becomes highly significant in astrophysical terms. The science of spectroscopic characterization of this molecule can help to identify  $\text{H}_2\text{CO}_3$  in outer space. Spectroscopic characterization of the solid state has been done in the nineties. In my work I show for the first time IR-spectroscopic data of vapor molecules, which sublime from the  $\alpha$ - and  $\beta$ -polymorph of  $\text{H}_2\text{CO}_3$  by trapping the molecules in inert matrices. The experiments allow to identify monomers with symmetry of  $\text{C}_{2v}$  as well as  $\text{C}_s$  and a dimer with symmetry of  $\text{C}_{2h}$  in the vapor of  $\alpha$ - $\text{H}_2\text{CO}_3$ . However, no dimers, but only monomers with symmetry of  $\text{C}_{2v}$  as well as  $\text{C}_s$  are identified from sublimed  $\beta$ - $\text{H}_2\text{CO}_3$ . The molar ratio of about 1:10 for the two monomers suggests that the  $\text{C}_{2v}$  monomer is the stable one and that, the  $\text{C}_s$  monomer is less stable by about  $4 \text{ kJ mol}^{-1}$ . The UV irradiation of the  $\text{H}_2\text{CO}_3/\text{Ar}$  matrix leads to the formation of the energetically disfavoured monomer  $\text{C}_s$  at the expense of the  $\text{C}_{2v}$  monomer. As a consequence of the difference in gas phase composition, also the polymorph that crystallizes after removal of the matrix is different:  $\alpha$ - $\text{H}_2\text{CO}_3$  crystallizes from sublimed  $\alpha$ - $\text{H}_2\text{CO}_3$ , while  $\beta$ - $\text{H}_2\text{CO}_3$  crystallizes from sublimed  $\beta$ - $\text{H}_2\text{CO}_3$ . We attribute the difference in the gas phase to the change of sublimation temperature of  $\alpha$ - $\text{H}_2\text{CO}_3$  ( $> 210 \text{ K}$ ) and  $\beta$ - $\text{H}_2\text{CO}_3$  ( $> 230 \text{ K}$ ). This suggests that two monomers are entropically favored at the sublimation temperature of 250 K for  $\beta$ - $\text{H}_2\text{CO}_3$ , whereas they are not at the sublimation temperature of 210 K for  $\alpha$ - $\text{H}_2\text{CO}_3$ . The

sublimation and recondensation cycles of  $\text{H}_2\text{CO}_3$  add new aspects to the chemistry of carbonic acid in astrophysical environments. With this new data, not only solid  $\text{H}_2\text{CO}_3$  can be detected in the outer space but also its vapor molecules. That can be achieved from a distance with spectrometers installed on satellites (e.g. ISO or Herschel space telescope) or in situ by Mars missions (e.g. "Mars-Microbeam Raman Spectrometer"). Our spectroscopic data are important for NASA and ESA, for a possible detection of this molecule in the outer space.

### ***Paper III***

Solid carbonic acid is supposed to exist in our atmosphere, especially in ice clouds. Mineral dust acts as the nucleus for the formation of ice particles in ice clouds. Calcium carbonate ( $\text{CaCO}_3$ ) is the major component in the mineral dust. The research group of Vicky Grassian has studied surface chemistry of  $\text{CaCO}_3$  in the presence of several trace atmospheric acids ( $\text{HNO}_3$ ,  $\text{SO}_2$ ,  $\text{HCOOH}$  and  $\text{CH}_3\text{COOH}$ ).<sup>[42-43]</sup> They have found that carbonic acid plays an important role in the surface chemistry of calcium carbonate and that  $\text{H}_2\text{CO}_3$  is stable on the surface in the absence of water at a temperature of up to 298 K.<sup>[42-43]</sup> In our work we firstly have shown in experiment that under conditions existing in the atmosphere at an altitude of 5000 m bulk carbonic acid can be produced and is stable up to 260 K. We propose a new mechanism how bulk carbonic acid is formed under conditions relevant to our atmosphere. The mechanism involves the protonation of  $\text{CaCO}_3$  particles with HCl droplets. At 200 K aqueous/amorphous  $\text{H}_2\text{CO}_3$  is produced on a time scale of hours in a humid atmosphere and crystallizes to  $\beta\text{-H}_2\text{CO}_3$  at higher temperatures under low humidity conditions. We demonstrate furthermore, that  $\text{H}_2\text{CO}_3$  does not decompose readily even at 250 K in a humid atmosphere. The stability of  $\text{H}_2\text{CO}_3$  at conditions relevant to the troposphere renders  $\text{H}_2\text{CO}_3$  important in the atmosphere, where it could contribute to the acidity in the troposphere.

### ***Paper IV***

Carbonic acid is responsible for the acid-base balance in our blood and for the  $\text{CO}_2$  transfer between body tissue and blood capillary. Carbonic acid changes the  $pH$  value of the seas, which has grave consequences for the natural environment.  $\text{CO}_2$  is easily soluble in  $\text{H}_2\text{O}$  and with higher  $\text{CO}_2$ -concentration in the atmosphere the amount of  $\text{CO}_2$  in the seas increases. Part of the dissolved  $\text{CO}_2$  reacts with  $\text{H}_2\text{O}$  to  $\text{H}_2\text{CO}_3$ , and thus decreases the  $pH$  value of the seas. The insoluble salt  $\text{CaCO}_3$  transforms to the salt with higher solubility,  $\text{Ca}(\text{HCO}_3)_2$ . Corals and shells of crustaceans which are made of  $\text{CaCO}_3$  are destroyed and so such species are no longer able to exist. In this paper the current knowledge related to aqueous carbonic acid is highlighted with a particular emphasis on the novel results by Adamczyk et al.<sup>[6]</sup> Using time-resolved femtosecond infrared spectroscopy Adamczyk et al. observed the protonation of  $\text{DCO}_3^-$  via a photoacid (e.g. 8-hydroxypyrene-1,2,6-trisulfonate, HPTS). The formation of  $\text{D}_2\text{CO}_3$  is complete after a few hundred picoseconds. During this time no decomposition to  $\text{CO}_2$  is observed. The

ionization constant is determined to be  $pK_a \approx 3.45$ .<sup>[44]</sup> This renders  $\text{H}_2\text{CO}_3$  a stronger acid than acetic acid ( $pK_a \approx 4.7$ ) and cannot be ignored in discussions of oceanic acidification.<sup>[28]</sup>

### **Paper V**

The investigation of the crystal structure of  $\text{H}_2\text{CO}_3$  remains a work for the future. For the crystal structure a  $\text{H}_2\text{CO}_3$  single crystal is needed. It is difficult to grow and handle a single crystal and no group has yet succeeded in growing millimeter (mm) sized single crystals. In Innsbruck it was possible in the past to grow crystal-needles of  $\alpha\text{-H}_2\text{CO}_3$ , which are about 80  $\mu\text{m}$  long and 10  $\mu\text{m}$  broad (see microscopy images Fig. 3 in ref.<sup>[45]</sup>). Our spectroscopic observations in the solid and gaseous state give the best reference points for the molecular structure. IR and Raman data of solid  $\text{H}_2\text{CO}_3$  show the basic motif in the crystal structure.  $\alpha\text{-H}_2\text{CO}_3$  shows Raman and IR bands at similar position over the entire accessible range.  $\beta\text{-H}_2\text{CO}_3$  obeys the rule of mutual exclusion, i.e., if a band is Raman active then it is not IR active, and *vice versa*. The principle of mutual exclusion requires a local center of inversion to be present in the crystal. This suggests the cyclic carbonic acid dimer, which contains a center of inversion in the case of  $\beta\text{-H}_2\text{CO}_3$  and a catemar chain or a sheet like structure, based on a carbonic acid dimer without center of inversion for  $\alpha\text{-H}_2\text{CO}_3$  as basic crystal building block.<sup>[45]</sup> Research of the gas phase of  $\text{H}_2\text{CO}_3$  shows monomers as main components, which underlines the results of the solid state investigations<sup>[29]</sup> and gives new information about the structure. So in the near future the crystal structure of the two  $\text{H}_2\text{CO}_3$  polymorphs might be resolved.

## 4.2 Spectroscopic Observation of Matrix-Isolated Carbonic Acid Trapped from the Gas Phase





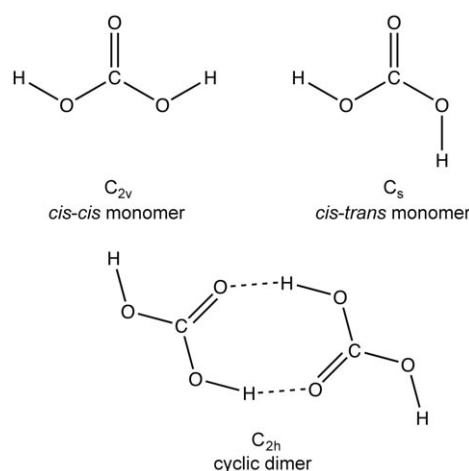
# Spectroscopic Observation of Matrix-Isolated Carbonic Acid Trapped from the Gas Phase\*\*

Jürgen Bernard, Markus Seidl, Ingrid Kohl, Klaus R. Liedl, Erwin Mayer, Óscar Gálvez, Hinrich Grothe,\* and Thomas Loerting\*

Carbonic acid ( $\text{H}_2\text{CO}_3$ ) is of fundamental importance, for example, for regulation of blood pH, in the acidification of the oceans, and in the dissolution of carbonates. This six-atom molecule commonly found in carbonated drinks in submicromolar concentrations has so far eluded most attempts at isolation and direct detection. Despite the widespread belief that it is a highly unstable molecule, the pure solid could be prepared previously,<sup>[1–5]</sup> and it is thought that solid carbonic acid exists in cirrus clouds on Earth and in astrophysical environments.<sup>[6–11]</sup> Gas-phase carbonic acid was long thought to immediately decompose to water and carbon dioxide, and therefore to be nonexistent or detectable only as a trace component.<sup>[12]</sup>

We show herein that gas-phase carbonic acid is stable at temperatures above 200 K and describe the trapping of carbonic acid vapor in an inert matrix at 6 K. Spectroscopic analysis of this matrix reveals that carbonic acid vapor is composed of at least three species (Scheme 1): two monomeric conformers and the cyclic dimer ( $\text{H}_2\text{CO}_3$ )<sub>2</sub>; carbon dioxide and water are minor components. The molar ratio of the two monomers suggests that the *cis-cis* monomer is the most stable one, and the *cis-trans* monomer is less stable by about 4 kJ mol<sup>-1</sup>, in accordance with theoretical predictions.<sup>[13,14]</sup> The stability of gas-phase carbonic acid at temper-

atures above 200 K suggests that carbonic acid may sublime in astrophysical environments without decomposition, for example, on the poles of Mars or in the coma of comets such as Hale-Bopp, and, therefore, our infrared spectra represent a benchmark for possible identification of naturally occurring carbonic acid vapor.



**Scheme 1.** Carbonic acid species identified in the current study.

Carbonic acid easily decomposes to carbon dioxide and water at ambient conditions, and even more so in the presence of water.<sup>[15]</sup> In aqueous solution detection of its formation and/or decomposition is feasible only by use of fast<sup>[16]</sup> or ultrafast spectroscopic techniques.<sup>[17]</sup> However, at the temperature of many extraterrestrial environments, its decomposition is hindered. Formation of solid carbonic acid was achieved in laboratory experiments by acid–base chemistry at low temperatures<sup>[2]</sup> and also under conditions akin to those encountered in space. For example, solid carbonic acid is formed from 1:1 mixtures of solid  $\text{CO}_2$  and  $\text{H}_2\text{O}$  ice by proton irradiation<sup>[1,3,4]</sup> or UV photolysis<sup>[4]</sup> from the reaction of CO with OH radicals,<sup>[11]</sup> and in the absence of water from solid  $\text{CO}_2$  ice by H implantation.<sup>[3,5]</sup> It has thus been suggested that solid carbonic acid may be found on the Martian surface, on interstellar grains, on comets, especially in the Oort cloud, and on Jupiter's icy satellites Europa, Ganymede, and Callisto.<sup>[6–10]</sup>

The  $\alpha$  polymorph (spectrum shown in Figure 1 a) is stable up to at least 200 K. Above this temperature it sublimates slowly in vacuo, and it was believed to decompose upon sublimation. Even more thrilling, though, carbonic acid vapor can be recondensed on cold substrates.<sup>[8]</sup> Hudson recently

[\*] Prof. Dr. H. Grothe

Institut für Materialchemie, Technische Universität Wien  
 Getreidemarkt 9/BC/01, 1060 Wien (Austria)

Fax: (+43) 1-58801-165122

E-mail: grothe@tuwien.ac.at

Homepage: <http://www.imc.tuwien.ac.at>

J. Bernard, M. Seidl, Prof. Dr. T. Loerting

Institut für Physikalische Chemie, Universität Innsbruck  
 Innrain 52a, 6020 Innsbruck (Austria)

Fax: (+43) 512-507-2925

E-mail: thomas.loerting@uibk.ac.at

Homepage: <http://homepage.uibk.ac.at/~c724117/>

J. Bernard, Dr. I. Kohl, Prof. Dr. K. R. Liedl, Prof. Dr. E. Mayer  
 Institut für Allgemeine, Anorganische und Theoretische Chemie  
 Universität Innsbruck (Austria)

Dr. Ó. Gálvez

Instituto de Estructura de la Materia, CSIC Madrid (Spain)

[\*\*] We are grateful to P. Ehrenfreund and R. Hudson for comments and to the Austrian Science Fund (P18187), the European Research Council (SULIWA), the Austrian Academy of Sciences (DOC fellowship for M.S.), the TU Wien Materials Research Cluster, and the Austrian Exchange Service for financial support. We thank J. Frank, A. Zoerner, and M. Schitter for the design and construction of the cryostat.



Supporting information for this article is available on the WWW under <http://dx.doi.org/10.1002/anie.201004729>.

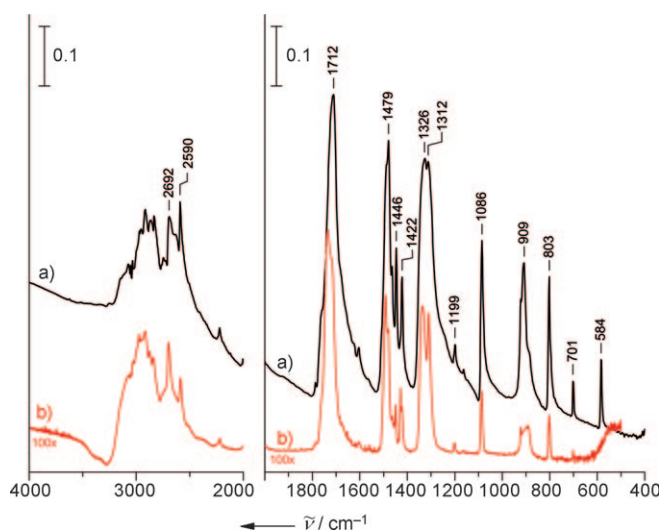


**Figure 1.** a) IR spectrum of a thin film of crystalline  $\alpha$ - $\text{H}_2\text{CO}_3$  as prepared by protonation of  $\text{KHCO}_3$  with  $\text{HCl}$  in methanolic solution at cryogenic temperatures (80–210 K) and removal of solvent in vacuum. b) IR spectrum of crystalline  $\alpha$ - $\text{H}_2\text{CO}_3$  obtained after sublimation of the thin film of crystalline  $\alpha$ - $\text{H}_2\text{CO}_3$  at 210 K, isolation of carbonic acid vapor in an argon matrix at 6 K, and removal of argon in vacuum by heating to 180 K. The good match of the two spectra proves first that carbonic acid has sublimed without decomposition to carbon dioxide at 210 K, and second that the same crystalline polymorph crystallizes from a supercooled methanolic solution and from solid argon. Spectra are shifted vertically for clarity.

emphasized that “this gives cause to hope that gas-phase interstellar  $\text{H}_2\text{CO}_3$  may one day be detected, adding this elusive species to the other interstellar molecules” and that this exciting challenge is “awaiting the next generation of scientists”.<sup>[18]</sup>

In order to bear this challenge it is necessary to measure laboratory spectra of gaseous carbonic acid. This task has proven to be so difficult that no one has succeeded so far. The only pieces of evidence that gaseous carbonic acid even exists were provided by Terlouw et al.,<sup>[12]</sup> who obtained a weak mass spectrometric signal at  $m/z$  62, by Mori et al., who obtained microwave spectra of *cis-trans* carbonic acid,<sup>[14]</sup> and by Hage et al., who recondensed solid  $\text{H}_2\text{CO}_3$  from the gas phase.<sup>[8]</sup> The extremely low sublimation rates of  $10^{-8} \text{ g cm}^{-2} \text{ s}^{-1}$  at 200 K estimated by Hage et al.<sup>[8]</sup> and the vapor pressure of  $10^{-7}$  mbar at 250 K estimated by Moore et al.<sup>[19]</sup> are quite discouraging for the prospect of measuring laboratory spectra of gaseous carbonic acid. For comparison, typical matrix-isolation experiments of gas-phase species are done with volatile liquids, which have vapor pressures on the order of mbar at room temperature. Defying these odds, we here report infrared

spectra of gaseous carbonic acid trapped in a solid matrix of either argon or neon.

Selected regions of the spectra of the matrix-isolated material on a gold mirror recorded at 6 K are depicted in Figure 2. The spectra contain bands assignable to water monomers, dimers, and trimers,<sup>[24]</sup> carbon dioxide,<sup>[25]</sup> and traces of methanol trapped in argon;<sup>[26]</sup> however, water adducts of  $\text{CO}_2$  and  $\text{CH}_3\text{OH}$  are absent.<sup>[27]</sup> These matrix-trapped species can be assigned unequivocally because the band positions typically agree with literature data to within  $\pm 0.1 \text{ cm}^{-1}$ .

The most intense bands depicted in Figure 2, however, cannot be explained by any of the known matrix-isolated species. We argue below that these bands arise from two conformers of the matrix-isolated carbonic acid monomer and the cyclic  $(\text{H}_2\text{CO}_3)_2$  dimer ( $C_{2h}$  point group symmetry). The assignments of the bands have been confirmed by selective changes of the experimental conditions: a)  $^{12}\text{C}/^{13}\text{C}$  and H/D isotope shifts, b) changes of the matrix/absorber ratio for identification of dimer bands, c) photolysis of the matrix with UV/Vis light, and d) annealing of the matrix at 20 K and 30 K for monitoring transitions between different conformers. Every trapped species exhibits bands having constant relative intensities, which allows identification in successive experiments. In addition the assignments of monomer versus dimer bands were double-checked by comparison to the spectra of trapped monocarboxylic acid monomers and dimers. Finally, the experimental assignment was validated by comparing the experimental isotope shifts with calculated isotope shifts.

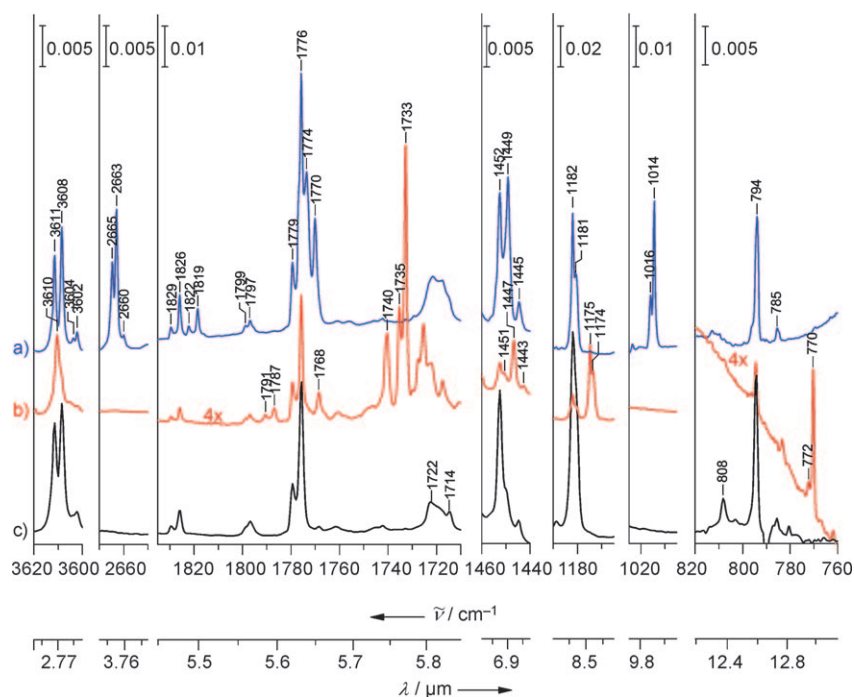


**Figure 2.** IR spectra of carbonic acid vapor and isotopologues after sublimation of crystalline  $\alpha$ - $\text{H}_2\text{CO}_3$  at 210 K and isolation in argon matrix at 6 K. The matrix to absorber ratio is estimated to be approximately 1000:1, which is in coincidence with the half-bandwidth of similar isolated molecules. a)  $\text{D}_2\text{CO}_3$  (50%), b)  $\text{H}_2^{13}\text{CO}_3$  (65%), c)  $\text{H}_2\text{CO}_3$ . Spectra are shifted for clarity. Assignment of bands is given in Table 1.

**Table 1:** Assignment of bands (all values in  $\text{cm}^{-1}$ ; weak bands are denoted with a “w”). For more details see the Experimental Section.

$\text{H}_2^{12}\text{CO}_3$		$\text{H}_2^{13}\text{CO}_3$	$^{12}\text{C}/^{13}\text{C}$ shift		$\text{D}_2^{12}\text{CO}_3$		H/D shift		Normal mode	Assign.	Molec. symmetry
in Ne	in Ar	theor.	in Ar	expt.	theor.	in Ar	expt.	theor.			
3634	3611	3790	3610	1	0.2	2665	946	1031	$\nu(\text{A}_1)/\nu(\text{A}')$	$\nu_s(\text{OH})$	$\text{C}_{2v}/\text{C}_s$
3630	3608	3788	3607	1	0.1	2663	945	1033	$\nu(\text{B}_2)$	$\nu_{as}(\text{OH})$	$\text{C}_{2v}$
3628	3604w	3785	3603w	1	0.2	2660w	944	1030	$\nu(\text{A}')$	$\nu_{as}(\text{OH})$	$\text{C}_s$
3623	3602w	3783	3601w	1	0.2	2660w	942	1030	$\nu(\text{A}_g)/\nu(\text{B}_u)$	$\nu(\text{OH})$	$\text{C}_{2h}$
1836	1829/1826	1860	1791/1787	38/39	47	1822/1819	7	14	$\nu(\text{A}')$	$\nu(\text{C}=\text{O})$	$\text{C}_s$
1799	1799/1797	1780	1768/1740	31/57	45				$\nu(\text{B}_u)$	$\nu(\text{C}=\text{O})$	$\text{C}_{2h}$
1727	1722/1714	1716							$\nu(\text{A}_g)$	$\nu(\text{C}=\text{O})$	$\text{C}_{2h}$
1783	1779/1776	1815	1735/1733	44/43	46	1774/1770	6/5	13	$\nu(\text{A}_1)$	$\nu(\text{C}=\text{O})$	$\text{C}_{2v}$
1565		1554							$\nu(\text{A}_g)$	$\nu_{as}(\text{C}(\text{OH})_2)$	$\text{C}_{2h}$
1515		1520							$\nu(\text{B}_u)$	$\nu_{as}(\text{C}(\text{OH})_2)$	$\text{C}_{2h}$
1456	1452/1451	1453			32			75	$\nu(\text{B}_2)$	$\nu_{as}(\text{C}(\text{OH})_2)$	$\text{C}_{2v}$
1427		1401							$\nu(\text{A}')$	$\nu_{as}(\text{C}(\text{OH})_2)$	$\text{C}_s$
1274w	ca. 1270w	1234							$\nu(\text{B}_u)$	$\delta_{ip}(\text{COH})$	$\text{C}_{2h}$
1184w	ca. 1175w	1155							$\nu(\text{A}')$	$\delta_{ip}(\text{COH})$	$\text{C}_s$
1187	1182/1181	1166	1175/1174	7	8	1016	167/166	203	$\nu(\text{B}_2)$	$\delta_{ip}(\text{COH})$	$\text{C}_{2v}$
811	808	801/800	784 sh	24	25/25			-5/-1	$\nu(\text{A}_u)/\nu(\text{B}_g)$	$\delta_{oop}(\text{CO}_3)$	$\text{C}_{2h}$
798	794	789	772/770	24	25	794	0	1	$\nu(\text{B}_1)$	$\delta_{oop}(\text{CO}_3)$	$\text{C}_{2v}$
784	785	777	762	23	24	785	0	1	$\nu(\text{A}')$	$\delta_{oop}(\text{CO}_3)$	$\text{C}_s$

Ab initio calculations of the band positions of  $\text{H}_2\text{CO}_3$ ,  $\text{D}_2\text{CO}_3$ , and  $\text{H}_2\text{CO}_3\cdot\text{H}_2\text{O}$  have been reported before.<sup>[13]</sup> Since a comparison with the experimental data of the isotopically substituted compounds reported in Figure 2 necessitates also availability of data on  $\text{H}_2^{13}\text{CO}_3$  and on other monomer conformers, we repeated the geometry optimization and frequency calculations at the MP2/aug-cc-pVDZ level of theory. The relevant frequencies and isotope shifts are reported in Table 1. According to ab initio calculations three conformations of monomeric carbonic acid are possible,<sup>[13]</sup> which can be interconverted by rotating around the two OCO–H dihedral angles. The three rotamers representing local potential minima are called *cis-cis* ( $\text{C}_{2v}$  symmetry), *cis-trans* ( $\text{C}_s$  symmetry), and *trans-trans*. The  $\text{C}_{2v}$  monomer is predicted to be the dominant gas-phase species since it is the most stable (because of two weak internal hydrogen bonds). The  $\text{C}_s$  monomer is predicted to be less stable by about 4–8  $\text{kJ mol}^{-1}$  and to be a possible gas-phase species, whereas the *trans-trans* conformation is less stable by more than  $\approx 40 \text{ kJ mol}^{-1}$  and is not expected to appear in experiments.<sup>[13,14]</sup> The cyclic dimer ( $\text{H}_2\text{CO}_3$ )<sub>2</sub> is stabilized by two strong hydrogen bonds, and the enthalpy of decomposition to carbon dioxide and water is astonishingly close to zero.<sup>[28]</sup> By contrast, the monomers show a negative enthalpy of decomposition; in other words, they are kinetically stable, but thermodynamically they should decompose. For this reason, an appreciable fraction of the cyclic dimer ( $\text{H}_2\text{CO}_3$ )<sub>2</sub> possibly forms and persists in the gas phase. Higher oligomers such as ( $\text{H}_2\text{CO}_3$ )<sub>3</sub> are thermodynamically even more stable in the gas phase,<sup>[29]</sup> but are not thought to occur because an encounter of three or more carbonic acid molecules in the gas phase is extremely unlikely.

In the OH-stretching region there is a triplet at 3611/3608/3602  $\text{cm}^{-1}$ , which shows an intensity ratio of 8:10:1, that is,

two intense bands and one weak band. A carbonic acid sample, in which roughly 50% of all H atoms have been replaced by D atoms, shows a similar triplet with a similar intensity ratio at 2665/2663/2660  $\text{cm}^{-1}$  in the OD-stretching region. In some spectra, the weak band is resolved as two weak bands of roughly the same intensity. In the calculations it is predicted that a mixture of the  $\text{C}_{2v}$  monomer,  $\text{C}_s$  monomer, and  $\text{C}_{2h}$  dimer shows four bands at 3790/3788/3785/3783  $\text{cm}^{-1}$ , which show an H/D isotope shift of roughly 1000  $\text{cm}^{-1}$ , but no  $^{12}\text{C}/^{13}\text{C}$  isotope shift, which is in agreement with the experimental data. The two weak bands can be attributed to the  $\text{C}_{2h}$  dimer and  $\text{C}_s$  monomer, whereas the most intense band can be attributed to the  $\text{C}_{2v}$  monomer according to the calculations.

Assuming identical cross-sections, the intensity pattern suggests an abundance ratio of 10:1:1; in other words, the  $\text{C}_{2v}$  monomer is indeed the most abundant molecule in the matrix. A ratio of 10:1 translates in thermodynamic equilibrium at 210 K to a difference in Gibbs energies  $\Delta G(\text{C}_{2v} \rightarrow \text{C}_s)$  of 4.0  $\text{kJ mol}^{-1}$ , which is in excellent agreement with the calculations.<sup>[13,14]</sup> While we observe mainly the  $\text{C}_{2v}$  monomer, Mori et al. observed exclusively the less stable  $\text{C}_s$  monomer.<sup>[14]</sup> We believe this is so because an isomerization to the thermodynamically less stable takes place under the influence of the high voltages applied by Mori et al.<sup>[14]</sup> Similarly, we observe an isomerization from  $\text{C}_{2v}$  to  $\text{C}_s$  under the influence of UV/Vis radiation (see Figure 2 in the Supporting Information).

This picture of almost 90%  $\text{C}_{2v}$  monomers and the presence of some  $\text{C}_s$  monomers and  $\text{C}_{2h}$  dimers is corroborated also in the other spectral regions shown in Figure 2. In the C=O stretching region at ca. 1700–1850  $\text{cm}^{-1}$  the most intense band is located at 1776  $\text{cm}^{-1}$  and shows a matrix splitting of 3  $\text{cm}^{-1}$ . These bands are attributed to the  $\text{C}_{2v}$

monomer. The intense  $\nu(\text{C}=\text{O})$  is observed at very similar positions in small argon-isolated monocarboxylic acids such as formic acid ( $1767\text{ cm}^{-1}$ ), acetic acid ( $1779\text{ cm}^{-1}$ ), and propionic acid ( $1777\text{ cm}^{-1}$ ).<sup>[30]</sup> Bands at  $1826\text{ cm}^{-1}$ ,  $1797\text{ cm}^{-1}$ , and  $1714\text{ cm}^{-1}$  show an intensity of about one-tenth of the most intense band at  $1776\text{ cm}^{-1}$ . A predicted shift between the  $C_{2v}$  and  $C_s$  modes of  $+45\text{ cm}^{-1}$  compared to the observed  $+50\text{ cm}^{-1}$  suggests an assignment of the  $1826\text{ cm}^{-1}$  band as  $\nu(\text{C}=\text{O})$  of the  $C_s$  monomer. In acetic acid the most stable cyclic dimer shows a band at  $1720\text{ cm}^{-1}$ ,<sup>[31]</sup> very close to the band at  $1722\text{ cm}^{-1}$ , which we have assigned to the cyclic carbonic acid dimer in Table 1. After assignment of the species  $C_{2h}$ ,  $C_s$ , and  $C_{2v}$ , some very weak features ( $<1\%$  of the intensity of the  $C_{2v}$  absorptions) remain unexplained; they may, for example, arise from traces of an open dimer<sup>[32]</sup> or an  $\text{H}_2\text{CO}_3\cdot\text{H}_2\text{O}$  adduct. Such species were also observed in matrix-isolated mixtures of water and carboxylic acids.<sup>[30,31]</sup> The spectral region at  $1000\text{--}1500\text{ cm}^{-1}$  is the most difficult to interpret since in this region three fundamental modes, namely asymmetric and symmetric C–(OH) stretching and in-plane deformation modes, overlap, and since some of these modes are only weakly IR active. In the spectral region at roughly  $750\text{--}820\text{ cm}^{-1}$  again this intensity ratio of 1:10:1 is observed for the bands at  $808/794/785\text{ cm}^{-1}$ , which are assigned to the out-of-plane deformation of carbonic acid in the  $C_{2h}/C_{2v}/C_s$  conformations, respectively. This represents, to the best of our knowledge, the first experimental proof for the existence of dimeric carbonic acid in the gas phase, and also for the existence of more than one monomer conformation.

An important piece of evidence for the success of the isolation of carbonic acid from the gas phase is provided by checking what remains on the gold mirror after removal of the matrix. Heating matrix-isolated carbonic acid to  $180\text{ K}$  results in desorption of argon, and to some extent carbonic acid is dragged away from the surface along with argon. However, some carbonic acid molecules remain on the surface even after removal of argon. The spectrum of the sample remaining after evaporation of the matrix is shown in Figure 1b. This spectrum exhibits a remarkable similarity to the spectrum of the as-produced thin film of carbonic acid shown in Figure 1a. There is only one band missing in Figure 1b (at  $584\text{ cm}^{-1}$ ), which is explained by the fact that the available detector in Vienna had no sensitivity below  $600\text{ cm}^{-1}$ . This spectrum can be clearly attributed to crystalline carbonic acid. That is, the isolated carbonic acid molecules form larger aggregates upon removal of argon and finally arrange themselves to produce the same polymorph produced also after removal of the solvent methanol from dissolved carbonic acid.<sup>[2,22,23]</sup> The main difference between the two spectra is that the absorbance is roughly a factor 100 lower in Figure 1b, which corresponds to the reduced thickness of the film. The morphology and the texture of the respective crystallites and clusters are in turn responsible for the additional differences in the two spectra.

The matrix data allow firm assignment of the gas-phase bands at  $(3608 \pm 30)\text{ cm}^{-1}$  [ $(2.77 \pm 0.02)\text{ }\mu\text{m}$ ],  $(1776 \pm 7)\text{ cm}^{-1}$  [ $(5.63 \pm 0.03)\text{ }\mu\text{m}$ ],  $(1452 \pm 4)\text{ cm}^{-1}$  [ $(6.89 \pm 0.02)\text{ }\mu\text{m}$ ],  $(1182 \pm 5)\text{ cm}^{-1}$  [ $(8.46 \pm 0.03)\text{ }\mu\text{m}$ ], and  $(794 \pm 4)\text{ cm}^{-1}$  [ $(12.59 \pm 0.06)\text{ }\mu\text{m}$ ] to the  $C_{2v}$  monomer. The band positions

for the  $C_s$  monomer and the  $C_{2h}$  dimer are found in Table 1. These appear at a fraction of roughly 10% here, but may be the main components under different conditions in nature. These are the positions to be employed for the search of carbonic acid in astrophysical environments.

We emphasize that our spectra do not show the rotational transitions observable in high-resolution infrared spectra recorded in astrophysical environments, for instance, by the Infrared Space Observatory (ISO), because rotation is prevented in the matrix cages. Nevertheless, the spectra indicate the exact position of the Q branch and the respective center of the zero gap. Unidentified bands may be attributable to carbonic acid fundamentals on the basis of our data. We, thus, suggest including our data in spectroscopy databases for molecules of astrophysical or atmospheric interest, for example, the Cologne Database for Molecular Spectroscopy (CDMS).<sup>[33]</sup> In many astrophysical environments solid carbonic acid may form from  $\text{CO}_2$  and  $\text{H}_2\text{O}$  upon irradiation and then undergo many sublimation and recondensation cycles without decomposition. We expect gaseous carbonic acid to be present, for example, in the atmosphere of Mars or Venus and in cometary comae or tails once the comet reaches a position sufficiently close to the sun, where the temperature rises beyond  $200\text{ K}$ . In principle, one or the other of these four modes may also be caused by other species; the C=O stretching mode of monocarboxylic acids such as formic acid, for instance, is also found at  $5.6\text{ }\mu\text{m}$ .<sup>[34]</sup> However, these do not show any intense bands in the vicinity of  $6.9\text{ }\mu\text{m}$ ,  $8.6\text{ }\mu\text{m}$ , and  $12.7\text{ }\mu\text{m}$ , and so the presence of carbonic acid can be distinguished from the presence of monocarboxylic acids by employing the set of four monomer marker bands in high-resolution IR spectra.

### Experimental Section

Matrix-isolation spectroscopy is a technique aimed at obtaining pure vibrational spectra of nonrotating molecules by trapping them in an inert and transparent matrix of argon or neon. In the ideal case there is no interaction between the matrix material and the trapped species. In reality, there is a weak interaction resulting in a slight blueshift of individual absorptions. In addition, there may be different geometrical types of cages, resulting in matrix-induced band splittings. These shifts are typically on the order of a few wavenumbers compared to the gas-phase spectrum. Spectra obtained in neon matrices are considered to most closely resemble gas-phase spectra. Similarly, the probably most common matrix material, argon, is known to result in only a small deviation from gas-phase spectra. Comparison between argon and neon matrix reveals the particular impact of the matrix and explains the respective splitting of some bands. Our matrix-isolation study was done in the ultrahigh-vacuum chamber in Vienna (see Figure 1 in the Supporting Information), which was previously employed for successfully isolating reactive species such as halogen oxides.<sup>[20,21]</sup> Solid carbonic acid was produced for the purpose of matrix isolation as a micrometer-thin film on IR-transparent windows, typically CsI, in Innsbruck using the low-temperature technique developed in the 1990s in this laboratory.<sup>[2,22,23]</sup> The IR spectrum depicted in Figure 1a was recorded on the carbonic acid sample after production and coincides with the literature spectrum,<sup>[2,22,23]</sup> which implies that the thin film is crystalline. The sample was then transported immersed in liquid nitrogen to Vienna, and the matrix-isolation procedure was performed as described in the Supporting Information by subliming solid carbonic

acid at 210 K. Gaseous carbonic acid together with argon was deposited at a gold mirror placed a distance of six centimeters from the sample window.

The experimental data in Table 1 ("expt.") are taken from Figure 2 for the argon matrix and from Figure 3 in the Supporting Information for neon matrix. Calculated data ("theor.") were obtained at the MP2/aug-cc-pVDZ level of theory from harmonic frequency calculations of optimized geometries. Three carbonic acid species are considered, namely the *cis-cis* monomer ( $C_{2v}$ ), the *cis-trans* monomer ( $C_s$ ), and the cyclic dimer ( $C_{2h}$ ). Please note that frequencies calculated using MP2 ab initio methods are known to deviate from experimentally observed gas-phase results typically by factors between 0.95 and 1.05. These scaling factors differ for low-frequency and high-frequency modes.<sup>[35]</sup> Deviations of up to  $50\text{ cm}^{-1}$  for modes at  $<2000\text{ cm}^{-1}$  and up to  $200\text{ cm}^{-1}$  for OH-stretching modes are to be expected. Thus, agreement of absolute frequencies is not the basis for assignment of vibrational modes, but rather the shift incurred upon isotopic substitution.

Received: July 30, 2010

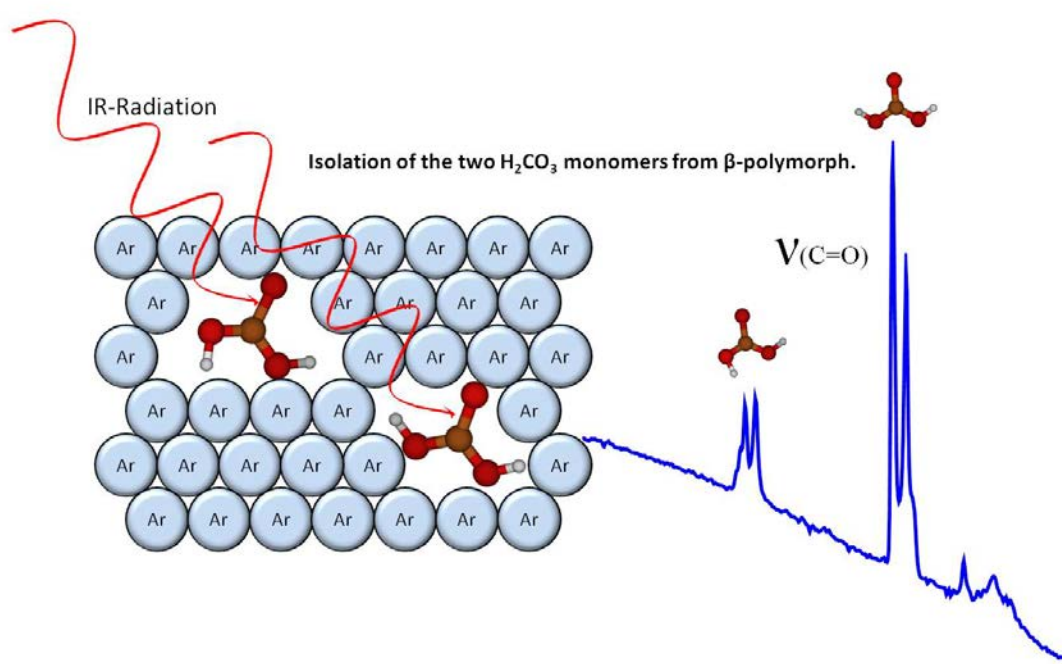
Published online: December 22, 2010

**Keywords:** carbonic acid · IR spectroscopy · matrix isolation

- [1] M. H. Moore, R. H. Khanna, *Spectrochim. Acta Part A* **1991**, *47*, 255–262.
- [2] W. Hage, A. Hallbrucker, E. Mayer, *J. Am. Chem. Soc.* **1993**, *115*, 8427–8431.
- [3] J. R. Brucato, M. E. Palumbo, G. Strazzulla, *Icarus* **1997**, *125*, 135–144.
- [4] P. A. Gerakines, M. H. Moore, R. L. Hudson, *Astron. Astrophys.* **2000**, *357*, 793–800.
- [5] M. Garozzo, D. Fulvio, O. Gomis, M. E. Palumbo, G. Strazzulla, *Planet. Space Sci.* **2008**, *56*, 1300–1308.
- [6] N. DelloRusso, R. K. Khanna, M. H. Moore, *J. Geophys. Res.* **1993**, *E 98*, 5505–5510.
- [7] G. Strazzulla, J. R. Brucato, G. Cimino, M. E. Palumbo, *Planet. Space Sci.* **1996**, *44*, 1447–1450.
- [8] W. Hage, K. R. Liedl, A. Hallbrucker, E. Mayer, *Science* **1998**, *279*, 1332–1335.
- [9] M. L. Delitsky, A. L. Lane, *J. Geophys. Res.* **1998**, *103*, 31391–31403.
- [10] I. Kohl, K. Winkel, M. Bauer, K. R. Liedl, T. Loerting, E. Mayer, *Angew. Chem.* **2009**, *121*, 2728–2732; *Angew. Chem. Int. Ed.* **2009**, *48*, 2690–2694.
- [11] Y. Oba, N. Watanabe, A. Kouchi, T. Hama, V. Pirronello, *Astrophys. J.* **2010**, *722*, 1598–1606.
- [12] J. K. Terlouw, C. B. Lebrilla, H. Schwarz, *Angew. Chem.* **1987**, *99*, 352–353; *Angew. Chem. Int. Ed. Engl.* **1987**, *26*, 354–355.
- [13] C. A. Wight, A. I. Boldyrev, *J. Phys. Chem.* **1995**, *99*, 12125–12130.
- [14] T. Mori, K. Suma, Y. Sumiyoshi, Y. Endo, *J. Chem. Phys.* **2009**, *130*, 204308.
- [15] T. Loerting, C. Tautermann, R. T. Kroemer, I. Kohl, A. Hallbrucker, E. Mayer, K. R. Liedl, *Angew. Chem.* **2000**, *112*, 919–922; *Angew. Chem. Int. Ed.* **2000**, *39*, 891–894.
- [16] H. Falcke, S. H. Eberle, *Water Res.* **1990**, *24*, 685–688.
- [17] K. Adamczyk, M. Premont-Schwarz, D. Pines, E. Pines, E. T. J. Nibbering, *Science* **2009**, *326*, 1690–1694.
- [18] R. L. Hudson, *J. Chem. Educ.* **2006**, *83*, 1611–1616.
- [19] M. H. Moore, R. L. Hudson, P. A. Gerakines, *Spectrochim. Acta Part A* **2001**, *57*, 843–858.
- [20] H. Grothe, H. Willner, *Angew. Chem.* **1994**, *106*, 1581–1583; *Angew. Chem. Int. Ed. Engl.* **1994**, *33*, 1482–1484.
- [21] O. Gálvez, A. Zoermer, A. Loewenschuss, H. Grothe, *J. Phys. Chem. A* **2006**, *110*, 6472–6481.
- [22] W. Hage, A. Hallbrucker, E. Mayer, *J. Chem. Soc. Faraday Trans.* **1996**, *92*, 3183–3195.
- [23] W. Hage, A. Hallbrucker, E. Mayer, *J. Mol. Struct.* **1997**, *408–409*, 527–531.
- [24] A. Givan, L. A. Larsen, A. Loewenschuss, C. J. Nielsen, *J. Chem. Soc. Faraday Trans.* **1998**, *94*, 827–835.
- [25] A. Schriver, L. Schriver-Mazzuoli, A. A. Vigin, *Vib. Spectrosc.* **2000**, *23*, 83–94.
- [26] A. J. Barnes, H. E. Hallam, *Trans. Farad. Soc.* **1970**, *66*, 1920–1931.
- [27] A. Givan, H. Grothe, A. Loewenschuss, C. J. Nielsen, *Phys. Chem. Chem. Phys.* **2002**, *4*, 255–263.
- [28] K. R. Liedl, S. Sekusak, E. Mayer, *J. Am. Chem. Soc.* **1997**, *119*, 3782–3784.
- [29] J. A. Tossell, *Inorg. Chem.* **2006**, *45*, 5961–5970.
- [30] J. Čeponkus, D. Leščiūte, D. Čepulinskaite, M. Pučetaitė, V. Šablinskas, *Lith. J. Phys.* **2009**, *49*, 53–62.
- [31] W. Sander, M. Gantenberg, *Spectrochim. Acta Part A* **2005**, *62*, 902–909.
- [32] J. Murillo, J. David, A. Restrepo, *Phys. Chem. Chem. Phys.* **2010**, *12*, 10963–10970.
- [33] H. S. P. Müller, F. Schlöder, J. Stutzki, G. Winnewisser, *J. Mol. Struct.* **2005**, *742*, 215–227.
- [34] I. D. Reva, A. M. Plokhotnichenko, E. D. Radchenko, G. G. Sheina, Y. P. Blagoi, *Spectrochim. Acta Part A* **1994**, *50*, 1107–1111.
- [35] J. P. Merrick, D. Moran, L. Radom, *J. Phys. Chem. A* **2007**, *111*, 11683–11700.



### 4.3 Matrix isolation studies of carbonic acid – the vapour phase above the $\beta$ -polymorph





# Matrix Isolation Studies of Carbonic Acid—The Vapor Phase above the $\beta$ -Polymorph

Jürgen Bernard,<sup>†</sup> Roland G. Huber,<sup>‡</sup> Klaus R. Liedl,<sup>‡</sup> Hinrich Grothe,<sup>\*,§</sup> and Thomas Loerting<sup>\*,†</sup>

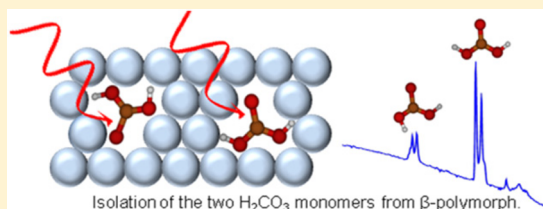
<sup>†</sup>Institute of Physical Chemistry, University of Innsbruck, A-6020 Innsbruck, Austria

<sup>‡</sup>Institute of General, Inorganic, and Theoretical Chemistry, University Innsbruck, A-6020 Innsbruck, Austria

<sup>§</sup>Institute of Materials Chemistry, Vienna University of Technology, A-1060 Vienna, Austria

## Supporting Information

**ABSTRACT:** Twenty years ago two different polymorphs of carbonic acid,  $\alpha$ - and  $\beta$ - $\text{H}_2\text{CO}_3$ , were isolated as thin, crystalline films. They were characterized by infrared and, of late, by Raman spectroscopy. Determination of the crystal structure of these two polymorphs, using cryopowder and thin film X-ray diffraction techniques, has failed so far. Recently, we succeeded in sublimating  $\alpha$ - $\text{H}_2\text{CO}_3$  and trapping the vapor phase in a noble gas matrix, which was analyzed by infrared spectroscopy. In the same way we have now investigated the  $\beta$ -polymorph. Unlike  $\alpha$ - $\text{H}_2\text{CO}_3$ ,  $\beta$ - $\text{H}_2\text{CO}_3$  was regarded to decompose upon sublimation. Still, we have succeeded in isolation of undecomposed carbonic acid in the matrix and recondensation after removal of the matrix here. This possibility of sublimation and recondensation cycles of  $\beta$ - $\text{H}_2\text{CO}_3$  adds a new aspect to the chemistry of carbonic acid in astrophysical environments, especially because there is a direct way of  $\beta$ - $\text{H}_2\text{CO}_3$  formation in space, but none for  $\alpha$ - $\text{H}_2\text{CO}_3$ . Assignments of the FTIR spectra of the isolated molecules unambiguously reveal two different carbonic acid monomer conformers ( $C_{2v}$  and  $C_s$ ). In contrast to the earlier study on  $\alpha$ - $\text{H}_2\text{CO}_3$ , we do not find evidence for centrosymmetric ( $C_{2h}$ ) carbonic acid dimers here. This suggests that two monomers are entropically favored at the sublimation temperature of 250 K for  $\beta$ - $\text{H}_2\text{CO}_3$ , whereas they are not at the sublimation temperature of 210 K for  $\alpha$ - $\text{H}_2\text{CO}_3$ .



## INTRODUCTION

Carbonic acid,  $\text{H}_2\text{CO}_3$ , plays an important role in many fields<sup>1</sup> of chemistry and physics, including astrophysics,<sup>2–6</sup> and biological and geochemical carbonate containing systems. This six-atom molecule commonly found in carbonated drinks at submicromolar concentration has so far eluded most attempts of isolation in its pure form and direct detection. This is mainly because it easily decomposes to carbon dioxide and water under ambient conditions and even more so in the presence of water.<sup>7</sup> In aqueous solution, detection of its formation and/or decomposition is only feasible by use of fast<sup>8</sup> or ultrafast spectroscopic techniques.<sup>9</sup> However, at the temperature of many extraterrestrial environments, its decomposition is hindered. Formation of two distinct solid carbonic acid polymorphs,  $\alpha$  and  $\beta$ , was achieved in laboratory experiments by acid–base chemistry at cryotemperatures.<sup>10</sup>  $\beta$ - $\text{H}_2\text{CO}_3$  is also formed under conditions akin to those encountered in space. For example, it is formed from 1:1 mixtures of solid carbon dioxide ( $\text{CO}_2$ ) and water ( $\text{H}_2\text{O}$ ) ice by proton-irradiation,<sup>2,3,11</sup> electron irradiation,<sup>12</sup> or UV-photolysis.<sup>11,13</sup> In the absence of water it may form from solid  $\text{CO}_2$  ice by H-implantation<sup>3,14</sup> or from carbon monoxide ( $\text{CO}$ ) by reaction with hydroxyl radicals ( $\text{OH}\cdot$ ).<sup>15</sup> It has thus been suggested that  $\beta$ -carbonic acid may be found on the Martian surface, on interstellar grains, on comets, especially in the Oort cloud, or on Jupiter's icy satellites Europa, Ganymede, and Callisto.<sup>4,16–19</sup>

The crystal structures of both carbonic acid polymorphs still remain unsolved. Powder X-ray diffraction cryotechniques were recently employed by us to observe two amorphous forms of carbonic acid, which then crystallize to the two polymorphs.<sup>20</sup> So far our attempts of indexing and refining the Bragg reflections after crystallization were unsuccessful, though. For this reason, FTIR and Raman studies of the solid polymorphs remain to date the only available data providing clues about symmetry and short-range order. The mutual exclusion of Raman and IR bands in the case of  $\beta$ - $\text{H}_2\text{CO}_3$  suggests a centrosymmetric building block, whereas mutual exclusion and a local inversion center were not found for  $\alpha$ - $\text{H}_2\text{CO}_3$ .<sup>19,20</sup> Examples for possible building blocks of the two polymorphs are depicted in Figure 1, which can merely be regarded as working hypotheses in lieu of refined crystal structures.

First indications for the possible existence of carbonic acid in the gas phase were provided by mass spectrometric observation of the vapor phase produced after ammonium bicarbonate ( $\text{NH}_4\text{HCO}_3$ ) thermolysis.<sup>21</sup> Later, two  $\text{H}_2\text{CO}_3$  conformers with symmetry  $C_{2v}$  (denoted cis–cis, see Figure 1) and  $C_s$  (denoted cis–trans) were produced by using a pulsed supersonic jet discharge nozzle and studied using microwave spectroscopy.<sup>22,23</sup> We have studied the vapor phase above  $\alpha$ - $\text{H}_2\text{CO}_3$  by slowly sublimating the crystalline thin film at 210 K in vacuo.

Received: February 27, 2013

Published: April 30, 2013

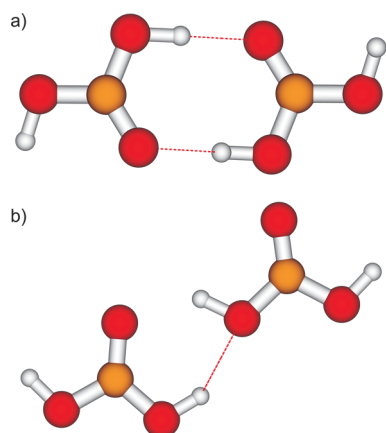


**Figure 1.** Possible basic building blocks in the solid state for (a)  $\beta$ - $\text{H}_2\text{CO}_3$ , which is studied in this work, and (b)  $\alpha$ - $\text{H}_2\text{CO}_3$ , which was studied in our previous work.<sup>24</sup> The local symmetries of these polymorphs were inferred by testing the validity of the mutual exclusion principle from Raman and IR spectroscopic data.<sup>19</sup> The monomers are arbitrarily depicted in the cis–cis conformation ( $C_{2v}$ ). In the crystal field of each of the two polymorphs also the cis–trans conformation ( $C_s$ ) could be the more stable one. Counterintuitively, the centrosymmetric dimer can only be detected in the gas phase above  $\alpha$ - $\text{H}_2\text{CO}_3$ , but not in the gas phase above  $\beta$ - $\text{H}_2\text{CO}_3$ . We attribute this to the lower temperature of the gas-phase above  $\alpha$ - $\text{H}_2\text{CO}_3$  (210 K vs 250 K), which favors dimerization in the gas phase.

Thrillingly, the vapor phase above  $\alpha$ - $\text{H}_2\text{CO}_3$  can be recondensed as  $\alpha$ - $\text{H}_2\text{CO}_3$  on cold substrates at a different location,<sup>17</sup> which demonstrates that carbonic acid sublimates at least partly without decomposition to carbon dioxide and water. Previously, we succeeded in isolating the vapor phase above  $\alpha$ - $\text{H}_2\text{CO}_3$  in a range of noble gas matrices and analyzed these matrices by infrared spectroscopy.<sup>24</sup> We have interpreted these infrared spectra in terms of the presence of the  $C_{2v}$  and  $C_s$  monomers at a ratio of 10:1, a small fraction of centrosymmetric ( $C_{2h}$ ) carbonic acid dimers, and some carbon dioxide and water mono- and oligomers. After removal of the matrix, the isolated gas-phase molecules rebuild a hydrogen-bonded network and condense to a crystalline polymorph. Interestingly, it is again the  $\alpha$ -polymorph that is observed after sublimation of the  $\alpha$ -polymorph, matrix isolation, and removal of the matrix.

In the present paper, we show the isolation of the  $\beta$ -polymorph in a solid rare gas matrix. The vapor phase above the  $\beta$ -polymorph is harder to isolate because the vapor pressure and sublimation rate of this polymorph are even lower than for the  $\alpha$ -polymorph, so higher sublimation temperatures are required.<sup>17</sup> Calculation of the vapor pressure for  $\alpha$ - $\text{H}_2\text{CO}_3$  at 200 K by Hage et al. shows the saturation vapor pressure ( $p_s$ ) of  $4 \times 10^{-7}$  mbar for the  $\text{H}_2\text{CO}_3$  monomer and  $3 \times 10^{-7}$  mbar for the dimer in the gas phase.<sup>17</sup> Peeters et al. measure the vapor pressure of  $\beta$ - $\text{H}_2\text{CO}_3$  of about  $(0.29\text{--}2.33) \times 10^{-9}$  mbar at 240–255 K.<sup>6</sup>

## EXPERIMENTAL SECTION

Matrix isolation spectroscopy is a technique aimed at obtaining pure vibrational spectra at low temperatures that isolates nonrotating single molecules by trapping them in a solid matrix of, for example, neon, argon, or krypton, which are optically transparent in the mid infrared and are chemically inert. Our matrix isolation study was done in the ultrahigh-vacuum chamber in Vienna (see Supp.-Figure 1 in ref 24), which was previously employed for successfully isolating reactive species such as halogen oxides<sup>25</sup> or the sublimation product of the  $\alpha$ -

polymorph of  $\text{H}_2\text{CO}_3$ .<sup>24</sup> The preparation of the starting material ( $\beta$ - $\text{H}_2\text{CO}_3$ ) was done in Innsbruck as described in refs 5, 10, and 26 by layer-by-layer spray deposition of glassy aqueous solutions of acid (2 M HBr) and base (1 M  $\text{KHCO}_3$ ) on optical windows kept at 80 K. Subsequently, this acid–base “sandwich” is heated slowly to 180 K in order to trigger translational diffusion and acid–base chemistry. Finally, ice is removed in the high-vacuum chamber by heating to 210 K, which results in the formation of first an amorphous thin film of carbonic acid, which finally crystallizes to  $\beta$ - $\text{H}_2\text{CO}_3$ . The preparation process of the thin film of carbonic acid is monitored in situ by FTIR spectra recorded on the Varian Excalibur spectrometer in Innsbruck. Figure 2a shows the typical FTIR spectrum (recorded at 80 K) of a

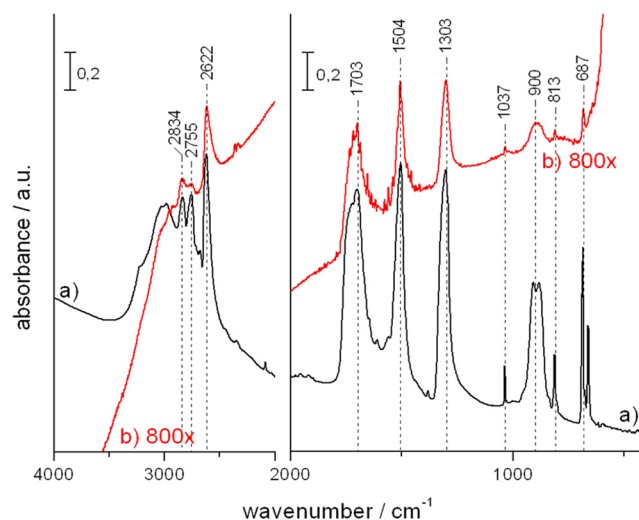


**Figure 2.** (a) IR spectrum of a thin film of crystalline  $\beta$ - $\text{H}_2\text{CO}_3$  at 80 K, as prepared by protonation of  $\text{KHCO}_3$  with HBr in aqueous solution and removal of the solvent in vacuum at 230 K. (b) IR spectrum of crystalline  $\beta$ - $\text{H}_2\text{CO}_3$  that re-forms after removal of the argon matrix containing trapped carbonic acid molecules. Only a small fraction of carbonic acid re-forms, so the intensity of this spectrum has to be multiplied by 800 to obtain comparable intensities. Spectra are shifted vertically for clarity.

thin film of crystalline  $\beta$ - $\text{H}_2\text{CO}_3$  prepared using this procedure on a Si window. The vertical lines indicate the position of the absorption bands of crystalline  $\beta$ - $\text{H}_2\text{CO}_3$ .<sup>26</sup> These thin films on the optical windows were then stored in liquid nitrogen and transferred to the matrix isolation chamber in Vienna. In this chamber the ice that has condensed during the transfer of the window at 77 K from ambient air was first removed and then the thin film was sublimated. The vapor above the thin film was then mixed with noble gas (argon or krypton) and recondensed on a cold mirror as a solid mixture of sublimation products and noble gas, typically at a ratio of 1:1000. The details of the matrix isolation procedure can be found in ref 24. FTIR spectra of the matrix were recorded by a Vertex 80v (Bruker Optic GmbH, Karlsruhe, Germany) equipped with a liquid  $\text{N}_2$  cooled narrow band MCT detector applying a spectral resolution of  $0.5 \text{ cm}^{-1}$ , adding 512 scans, and using a Ge-coated KBr beamsplitter. The optical path of the spectrometer was evacuated down to 2 mbar, which minimizes interferences from  $\text{CO}_2$  and  $\text{H}_2\text{O}$  absorptions of the ambient atmosphere. Such a sensitive setup is particularly important when measuring a substance like carbonic acid, which is a very weak absorber in especially these spectral regions.

Ab initio quantum mechanical calculations of carbonic acid in various isotope configurations were performed to obtain reference frequencies for annotating measured spectra. All calculations were performed using the Gaussian 09 package.<sup>27</sup> Both the  $C_{2v}$  and  $C_s$  conformations were employed for geometry optimization, where the former is the energetically most favorable conformation.<sup>28,29</sup> Calculations were performed using second-order Møller–Plesset

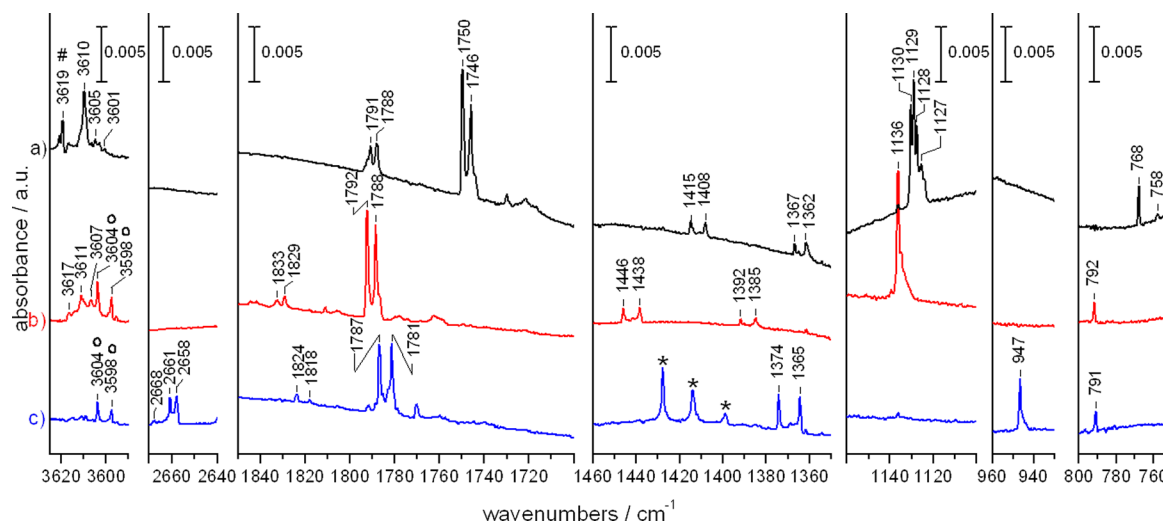


**Figure 3.** Selected regions of the IR spectra of carbonic acid vapor and isotopologues after sublimation of crystalline  $\beta$ - $\text{H}_2\text{CO}_3$  at 230–260 K and isolation in solid argon at 6 K: (a)  $\text{H}_2^{13}\text{CO}_3$ , (b)  $\text{H}_2\text{CO}_3$ , (c)  $\text{D}_2\text{CO}_3$ . Spectra are shifted for clarity. Bands marked by  $\star$  arise from the  $\nu_2$  bend of the HDO monomer and dimer, by  $\#$  from combination bands of  $^{13}\text{CO}_2$ , and by  $o$  from combination band of  $\text{CO}_2$ .

**Table 1.** Band Positions Assigned to Carbonic Acid Monomers and Isotope Shifts (both in  $\text{cm}^{-1}$ )<sup>a</sup>

$\text{H}_2^{12}\text{CO}_3$			$^{12}\text{C}/^{13}\text{C}$ shift		H/D shift		norm. mode	assign.	molec sym
Ar	Kr	theor	Ar	theor	Ar	theor			
3617/3614		3805					$\nu(\text{A}')$	$\nu_s(\text{OH})$	$\text{C}_s$
3611/3607		3801	1/−3	0	950/949	1037	$\nu(\text{B}_2)$	$\nu_{as}(\text{OH})$	$\text{C}_{2v}$
1833/1829	1828	1880	42/41	48	9/11	13	$\nu(\text{A}')$	$\nu(\text{C}=\text{O})$	$\text{C}_s$
1792/1788	1787	1834	42	46	5/7	12	$\nu(\text{A}_1)$	$\nu(\text{C}=\text{O})$	$\text{C}_{2v}$
1446/1438	1443	1467	31/30	34	72/73	68	$\nu(\text{B}_2)$	$\nu_{as}(\text{C}(\text{OH})_2)$	$\text{C}_{2v}$
1392/1385	1390	1409	25/23	27			$\nu(\text{A}')$	$\nu_{as}(\text{C}(\text{OH})_2)$	$\text{C}_s$
1255	1254	1289			189	212	$\nu(\text{A}_1)$	$\delta_{ip}(\text{COH})$	$\text{C}_{2v}$
1228	1226	1270					$\nu(\text{A}')$	$\delta_{ip}(\text{COH})$	$\text{C}_s$
1136	1134	1166	6	6	189	204	$\nu(\text{B}_2)$	$\delta_{ip}(\text{COH})$	$\text{C}_{2v}$
792	791	802	24	25	1	1	$\nu(\text{B}_1)$	$\delta_{oop}(\text{CO}_3)$	$\text{C}_{2v}$
782	781	790	24	23			$\nu(\text{A}'')$	$\delta_{oop}(\text{CO}_3)$	$\text{C}_s$

<sup>a</sup>Data taken from Figure 2 and Figure S2 (Supporting Information). Values in columns labeled “theor” are calculated at the MP2/aug-cc-pVTZ level of theory. Normal modes are assigned on the basis of these calculations. Two distinct monomer geometries, namely, in the cis–cis ( $\text{C}_{2v}$  point group symmetry) and the cis–trans conformation ( $\text{C}_s$  point group symmetry), are necessary to explain the spectra.

perturbation theory (MP2) with the augmented correlation consistent basis sets of Dunning and co-workers.<sup>30–32</sup> Initial optimization was done at the MP2/aug-cc-pVDZ level of theory requiring “very tight” convergence on displacement and forces. Starting from the resulting geometry, further optimization at the MP2/aug-cc-pVTZ level of theory using very tight convergence criteria yielded an energy minimum for frequency calculations. Subsequently, IR modes were determined at this minimum geometry using MP2/aug-cc-pVTZ. Isotope shifts were calculated by performing frequency calculations at the same minimum for either all  $^2\text{H}$ - or  $^{13}\text{C}$ -labeled carbonic acid. Calculated frequencies and isotope shifts were then used to identify the various signals observed in the experimentally obtained spectra.

## RESULTS

For  $\beta$ - $\text{H}_2\text{CO}_3$ , the same procedure of sublimation and trapping in solid matrices (Ar or Kr) was applied as for  $\alpha$ - $\text{H}_2\text{CO}_3$ , with the exception that higher sublimation temperatures are required. The  $\beta$ -polymorph (spectrum shown in Figure 2a) is stable up to at least 230 K. Above this temperature it sublimates slowly in vacuum. So far it was believed to decompose under such conditions. Indeed, we do observe the decomposition products carbon dioxide and water in the spectra (see Figure S1, Supporting Information). Besides carbon dioxide and the

water monomer, also higher water oligomers are found in the matrix. The bands near  $3750\text{ cm}^{-1}$  correlate with the rotation and nonrotation mode of  $\text{H}_2\text{O}$  monomer and dimer,<sup>33,34</sup> and the bands near  $1600\text{ cm}^{-1}$  with the bending mode of  $\text{H}_2\text{O}$  monomer and dimer.<sup>33,34</sup> The most intensive bands near  $2300\text{ cm}^{-1}$  and the band around  $680\text{ cm}^{-1}$  appertain to  $\text{CO}_2$  (with  $^{12}\text{C}$  or  $^{13}\text{C}$ ) molecules.<sup>35</sup>

During the transfer of the Si window from the liquid  $\text{N}_2$  to the high vacuum chamber some air moisture condenses on the window, which we tried to remove before the matrix isolation by pumping it off in the vacuum at 210–220 K. During the matrix production, some ambient water can also be isolated. A differentiation between water molecules stemming from moisture or from the decomposition of  $\text{H}_2\text{CO}_3$  is shown in the spectrum of matrix isolated  $\text{D}_2\text{CO}_3$  (Figure S1c, Supporting Information). The band system at 2783, 2771, 2746, 2724, and  $2678\text{ cm}^{-1}$  belongs to the absorption bands of the  $\text{D}_2\text{O}$  monomer and polymer.<sup>33,36</sup> Unambiguously, this band can only result from the decomposition of  $\text{D}_2\text{CO}_3$ . In the spectrum of  $\text{H}_2^{13}\text{CO}_3$  (Figure S1a, Supporting Information), the decomposition is clearly evident in the strong  $^{13}\text{CO}_2$  bands at 2280, 2275, and  $2274\text{ cm}^{-1}$ .<sup>35</sup> These bands are unequivocally assigned

because the band positions typically agree with literature data to within  $\pm 0.5 \text{ cm}^{-1}$ .

However, additional bands that cannot be assigned to carbon dioxide or water are apparent in the spectrum, which we assign to carbonic acid as outlined below. The intensity of the  $\nu(\text{C}=\text{O})$  mode in carbonic acid amounts to about 10% of the intensity of the most intense  $\nu(\text{O}-\text{H})$  mode in the water monomer and to about 5% of asymmetric stretching mode  $\nu_3$  in carbon dioxide. Thus, above 230 K a part of  $\beta\text{-H}_2\text{CO}_3$  sublimates with decomposition, whereas another part does not decompose.

Figure 3 shows the spectral regions that cannot be explained using  $\text{CO}_2$  or  $\text{H}_2\text{O}$  mono- or oligomers, which we assign to  $\text{H}_2\text{CO}_3$  and its isotopologues after sublimation of crystalline  $\beta\text{-H}_2\text{CO}_3$  at 230–260 K and isolation in solid argon at 6 K. We assign all these bands to two conformers of the carbonic acid monomer (symmetries  $C_{2v}$  and  $C_s$ ; see Scheme 1 in ref 24) on the basis of selective changes of the experimental conditions: (a)  $^{12}\text{C}/^{13}\text{C}$  and H/D isotope shifts, (b) UV radiation of the matrix, and (c) change of the matrix material (Ar or Kr). Also theoretical prediction concerning band positions and shifts between the symmetry of the isotopologues support our interpretation.

Our band assignment is exemplarily explained here on the CO-stretching region at  $1850\text{--}1700 \text{ cm}^{-1}$ , which contains two doublets (see Figure 3b). They appear as doublets because of a splitting induced by different Ar matrix cages. By contrast, in Kr matrix two single bands appear at a similar position (see Figure S2, Supporting Information). This immediately suggests the presence of two distinct gas-phase carbonic acid species. These doublets are red-shifted by  $5\text{--}11 \text{ cm}^{-1}$  for  $\text{D}_2\text{CO}_3/\text{Ar}$  (Figure 3c) and by  $42 \text{ cm}^{-1}$  for  $\text{H}_2^{13}\text{CO}_3/\text{Ar}$ . These isotope shifts are in excellent agreement with the theoretical prediction of isotope shifts for  $\nu_s(\text{C}=\text{O})$  of the  $\text{H}_2\text{CO}_3$  monomers (see Table 1). The assignment of the two carbonic acid species is immediately evident when looking at the calculated separation of the  $\nu_s(\text{C}=\text{O})$  between the cis–cis monomer of  $C_{2v}$  symmetry and the cis–trans monomer of  $C_s$  symmetry. This amounts to  $46 \text{ cm}^{-1}$  at the MP2/aug-cc-pVTZ level of theory ( $1880$  vs  $1834 \text{ cm}^{-1}$ ; see column labeled 'theor' in Table 1) employed here and is almost the same also at other levels of theory.<sup>37–39</sup> In the matrix spectrum the two bands are separated by  $41 \text{ cm}^{-1}$  ( $1828$  vs  $1787 \text{ cm}^{-1}$ ; see Table 1), which is an excellent match and allows an unambiguous assignment of the bands.

Upon UV irradiation of the  $\text{H}_2\text{CO}_3/\text{Ar}$  matrix one of the two doublets increases with time at the cost of the other doublet (see difference spectra in Figure S3, Supporting Information). According to the assignment this implies that the  $C_s$  isomer grows at the expense of the  $C_{2v}$  isomer. That is, the isomer that is calculated to be slightly energetically disfavored is formed from the favored one upon UV irradiation. Most likely this shift of the equilibrium takes place by a rotation of one H-atom around the C–O bond from the cis-position to the trans-position. The ratio of the intensities of  $C_{2v}$  and  $C_s$  bands before UV irradiation varies between 5:1 (Figure 3a) and 10:1 (Figure 3c), which is in accordance with the theoretical predictions of the higher stability of the  $C_{2v}$  monomer. The presence of the two weak internal hydrogen bonds in the  $C_{2v}$  monomer compared to the single internal hydrogen bond in the  $C_s$  monomer results in an increased stability of about  $4\text{--}8 \text{ kJ/mol}$ .<sup>22,28,29,38–41</sup> This interpretation of the presence of these two monomers at these ratios can also be deduced from all

other spectral ranges shown in Figure 3 and is demonstrated in the Supporting Information.

After having assigned these bands, all the bands observed in the whole spectral range are explained. Other possible species, such as complexes of water with carbonic acid or carbonic acid dimers, trimers, or higher oligomers, are not present or are at most trace components producing bands near the noise level of the spectrum.

In order to hedge our assignments, we have evaporated the solid noble gas matrices at the end of the spectroscopic characterization by carefully heating the matrix and checking for the component remaining on the sample holder. The spectrum after sublimation of  $\beta\text{-H}_2\text{CO}_3$ , matrix isolation of gas-phase carbonic acid in argon at 6 K, and removal of the argon matrix by heating to 220 K is shown in Figure 2b. This spectrum is highly similar to the spectrum of  $\beta\text{-H}_2\text{CO}_3$  before sublimation, albeit with intensities that are about a factor of 1000 lower. That is, the isolated carbonic acid monomers start to hydrogen bond upon removal of the argon and finally produce crystalline  $\beta\text{-H}_2\text{CO}_3$ . For comparison, after isolation of the gas-phase above  $\alpha\text{-H}_2\text{CO}_3$  in argon and removal of argon,  $\alpha\text{-H}_2\text{CO}_3$  is finally observed.<sup>24</sup>

## CONCLUSIONS AND IMPLICATIONS FOR CARBONIC ACID DETECTION

In the past we were successful in the isolation of the  $\alpha$ -polymorph of carbonic acid ( $\alpha\text{-H}_2\text{CO}_3$ ) in a solid matrix.<sup>24</sup> Now we show the isolation of the  $\beta$ -polymorph ( $\beta\text{-H}_2\text{CO}_3$ ) in a solid noble gas matrix and present our band assignment. The  $\beta$ -polymorph has a lower vapor pressure and lower sublimation rates than the  $\alpha$ -polymorph at the same temperature. In order to reach a significant vapor pressure above the  $\beta$ -polymorph, it is necessary to sublime the  $\beta$ -polymorph at 230–260 K, as compared to 210 K for the  $\alpha$ -polymorph. Similar to our former experiment, we also find the  $C_{2v}$  monomer to be the dominating species in the gas phase. The ratio between  $C_{2v}$  and  $C_s$  of the  $\beta$ -polymorph at 230–260 K is similar to that of the  $\alpha$ -polymorph at 210 K<sup>24</sup> and to the calculations of Schwerdtfeger et al.<sup>42</sup> Both polymorphs show the  $C_s$  monomer as the minor species, which occurs at a ratio from about 1:5 to 1:10. In contrast to our earlier matrix isolation study, we now do not find evidence for the presence of a centrosymmetric dimer. We attribute this difference to the higher sublimation temperature, which favors two monomers over the dimer because of the entropy term. That is, the results suggest that the enthalpy gain incurred because of hydrogen bond formation in the dimer is sufficient for the observation of the dimer at a sublimation temperature of 210 K,<sup>24</sup> but not at sublimation temperatures of 230–260 K used here. There is furthermore no indication for the presence of a linear oligomer<sup>43</sup> in the gas phase. As a consequence of this difference in the composition of the gas phase, also the polymorph that crystallizes upon removal of the matrix is different:  $\alpha\text{-H}_2\text{CO}_3$  crystallizes from sublimed  $\alpha\text{-H}_2\text{CO}_3$ , and  $\beta\text{-H}_2\text{CO}_3$  crystallizes from sublimed  $\beta\text{-H}_2\text{CO}_3$ .

The finding here that not only  $\alpha\text{-H}_2\text{CO}_3$  can sublime and recondense as  $\alpha\text{-H}_2\text{CO}_3$  but also  $\beta\text{-H}_2\text{CO}_3$  can sublime and recondense as  $\beta\text{-H}_2\text{CO}_3$  is novel and of atmospheric and astrophysical relevance, especially because it was previously thought that  $\beta\text{-H}_2\text{CO}_3$  decomposes entirely upon sublimation.<sup>2,6,11,12,14–16</sup>

In our atmosphere some solid-state carbonic acid may be present in cirrus clouds or on mineral dust. This possibility was

conjectured 15 years ago,<sup>17</sup> but only very recently it could be shown that indeed  $\beta$ -H<sub>2</sub>CO<sub>3</sub> may form as a bulk species on mineral dust in the presence of acids and remain stable in the troposphere even in the presence of high relative humidities up to 260 K.<sup>44</sup> Huber et al.<sup>39</sup> have emphasized that the sublimation temperature of  $\alpha$ -H<sub>2</sub>CO<sub>3</sub> of 210 K<sup>17,24</sup> is too low for a possible existence of gas-phase carbonic acid in Earth's atmosphere. This is because such low temperatures are only found in the stratosphere, where cirrus clouds cannot be observed. However, the sublimation temperature of  $\beta$ -H<sub>2</sub>CO<sub>3</sub> of up to 260 K reported in this work is of relevance in the troposphere, where  $\beta$ -H<sub>2</sub>CO<sub>3</sub> is presumed to exist and may sublime and recondense without decomposition. That is, some gas-phase carbonic acid may indeed be present in the troposphere, albeit at very low mixing ratios: the vapor pressure of  $\beta$ -H<sub>2</sub>CO<sub>3</sub> at 260 K is on the order of 10<sup>-8</sup>–10<sup>-9</sup> mbar, and the atmospheric pressure is about 200–400 mbar at the relevant altitudes of 5–10 km. These low mixing ratios will make it very challenging to detect gas-phase carbonic acid in Earth's troposphere.

Our findings presented here increase the chance for detection of gas-phase carbonic acid in astrophysical environments. First, direct routes for the formation of  $\beta$ -H<sub>2</sub>CO<sub>3</sub> in astrophysical environments are known,<sup>2,3,11,12</sup> whereas no direct route for the formation of  $\alpha$ -H<sub>2</sub>CO<sub>3</sub> is known. Typically,  $\beta$ -H<sub>2</sub>CO<sub>3</sub> is considered in environments containing both H<sub>2</sub>O and CO<sub>2</sub> ices, which are exposed to radiation, e.g., solar photons or cosmic rays. This is the case for the icy satellites of Jupiter and Saturn and also for the polar caps of Mars. The stability of gas-phase carbonic acid up to 260 K presented here might then result in a release and accumulation of carbonic acid in these thin atmospheres. For example, on the Mars surface it is known that the temperatures may change between 140 and 300 K, so carbonic acid may experience sublimation and recondensation cycles and reach a steady-state concentration near the icy caps. However, even with next-generation telescopes, the remote detection of carbonic acid in the thin atmospheres of such bodies seems very challenging, as explained by Huber et al.<sup>39</sup> Because of the high angular resolution required we might need to wait for the European Extremely Large Telescope (E-ELT), which is planned to be operative in the early 2020s.<sup>39</sup> It might, therefore, be useful to investigate the gas phase there in the future using microwave<sup>22,23</sup> or infrared absorption spectroscopy, e.g., by the METIS instrument on the E-ELT. Judging from the present and our earlier work,<sup>24</sup> the most intense and characteristic bands suitable for detection of the most abundant C<sub>2v</sub> carbonic acid monomers are the bands at 3608 ± 30 cm<sup>-1</sup> (2.77 μm), 1780 ± 10 cm<sup>-1</sup> (5.62 μm), 1445 ± 10 cm<sup>-1</sup> (6.92 μm), and 794 ± 4 cm<sup>-1</sup> (12.6 μm). A distinction between C<sub>2v</sub> C<sub>s</sub> monomers and C<sub>2h</sub> dimers will always be very hard. However, the ν(C=O) band seems most promising for this purpose, because it has the best separation (see Figure S4, Supporting Information): 1830 ± 5 cm<sup>-1</sup> (5.46 μm, C<sub>s</sub>), 1780 ± 10 cm<sup>-1</sup> (5.62 μm, C<sub>2v</sub>), and 1720 ± 10 cm<sup>-1</sup> (5.81 μm, C<sub>2h</sub>).<sup>24</sup>

In addition to remote detection, the possibility of on-site detection might be feasible in the future: for instance, a mid-infrared spectrometer on a Mars lander might provide the possibility to locate carbonic acid, both in the solid state on icy soil and also in the atmosphere. In this context, the detection of (bi)carbonate anions in soil excavated near the Martian pole in the Wet Chemistry Laboratory on the Phoenix Mars Lander seems very promising for the future endeavor of carbonic acid detection.<sup>45,46</sup> Also lander missions to other bodies, such as the

attempt of Philae to land on the comet 67P/Churyumov–Gerasimenko at the end of 2014 (ESA's Rosetta mission) or the plan of an ESA spacecraft visiting the icy Jovian moons ("Jupiter Icy Moon Explorer"), hold promise for the detection of carbonic acid.

## ■ ASSOCIATED CONTENT

### 📄 Supporting Information

Additional spectra and more details about band assignments. This material is available free of charge via the Internet at <http://pubs.acs.org>.

## ■ AUTHOR INFORMATION

### Corresponding Author

grothe@tuwien.ac.at; thomas.loerting@uibk.ac.at

### Notes

The authors declare no competing financial interest.

## ■ ACKNOWLEDGMENTS

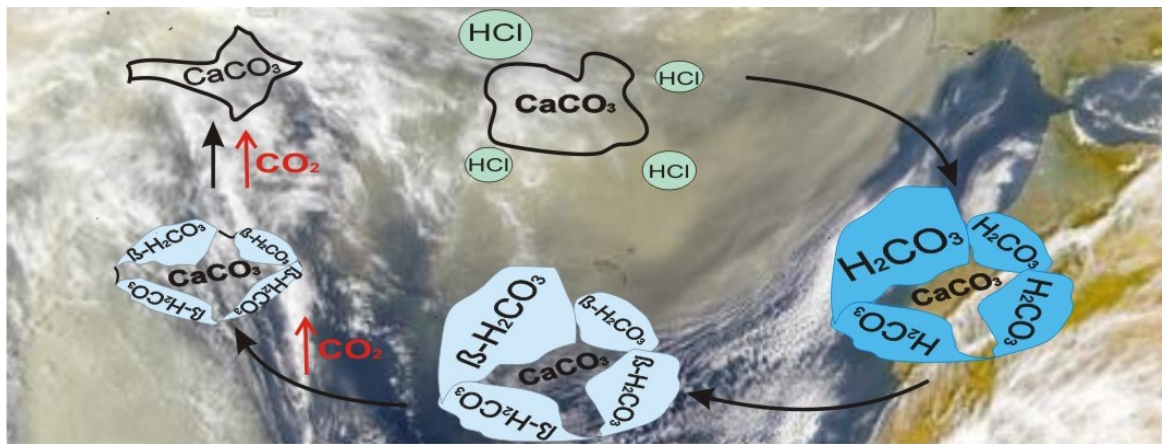
We are grateful to the Austrian Science Fund (FWF, projects P18187 and P23027) and the European Research Council (ERC Starting Grant SULIWA) for financial support. H.G. acknowledges travel support by the Österreichische Forschungsgemeinschaft (ÖFG).

## ■ REFERENCES

- (1) Loerting, T.; Bernard, J. *ChemPhysChem* **2010**, *11*, 2305–2309.
- (2) Moore, M. H.; Khanna, R. K. *Spectrochim. Acta, Part A* **1991**, *47A*, 255–262.
- (3) Brucato, J. R.; Palumbo, M. E.; Strazzulla, G. *Icarus* **1997**, *125*, 135–144.
- (4) DelloRusso, N.; Khanna, R. K.; Moore, M. H. *J. Geophys. Res. E* **1993**, *98*, 5505–5510.
- (5) Hage, W.; Hallbrucker, A.; Mayer, E. *J. Chem. Soc., Farad. Trans.* **1995**, *91*, 2823–2826.
- (6) Peeters, Z.; Hudson, R. L.; Moore, M. H.; Lewis, A. *Icarus* **2010**, *210*, 480–487.
- (7) Loerting, T.; Tautermann, C.; Kroemer, R. T.; Kohl, I.; Hallbrucker, A.; Mayer, E.; Liedl, K. R. *Angew. Chem., Int. Ed.* **2000**, *39*, 892–894.
- (8) Falcke, H.; Eberle, S. H. *Water Res.* **1990**, *24*, 685–688.
- (9) Adamczyk, K.; Premont-Schwarz, M.; Pines, D.; Pines, E.; Nibbering, E. T. *J. Science* **2009**, *326*, 1690–1694.
- (10) Hage, W.; Hallbrucker, A.; Mayer, E. *J. Am. Chem. Soc.* **1993**, *115*, 8427–8431.
- (11) Gerakines, P. A.; Moore, M. H.; Hudson, R. L. *Astron. Astrophys.* **2000**, *357*, 793–800.
- (12) Zheng, W.; Kaiser, R. I. *Chem. Phys. Lett.* **2007**, *450*, 55–60.
- (13) Wu, C. Y. R.; Judge, D. L.; Cheng, B.-M.; Yih, T.-S.; Lee, C. S.; Ip, W. H. *J. Geophys. Res.: Planets* **2003**, *108*, 5032.
- (14) Garozzo, M.; Fulvio, D.; Gomis, O.; Palumbo, M. E.; Strazzulla, G. *Planet. Space Sci.* **2008**, *56*, 1300–1308.
- (15) Oba, Y.; Watanabe, N.; Kouchi, A.; Hama, T.; Pirronello, V. *Astrophys. J.* **2010**, *722*, 1598–1606.
- (16) Strazzulla, G.; Brucato, J. R.; Cimino, G.; Palumbo, M. E. *Planet. Space Sci.* **1996**, *44*, 1447–1450.
- (17) Hage, W.; Liedl, K. R.; Hallbrucker, A.; Mayer, E. *Science* **1998**, *279*, 1332–1335.
- (18) Delitsky, M. L.; Lane, A. L. *J. Geophys. Res.: Planets* **1998**, *103*, 31391–31403.
- (19) (a) Kohl, I.; Winkel, K.; Bauer, M.; Liedl, K. R.; Loerting, T.; Mayer, E. *Angew. Chem., Int. Ed.* **2009**, *48*, 2690–2694. (b) Mitterdorfer, C.; Bernard, J.; Klauser, F.; Winkel, K.; Kohl, I.; Liedl, K. R.; Grothe, H.; Mayer, E.; Loerting, T. *J. Raman Spectrosc.* **2012**, *43*, 108–115.

- (20) Winkel, K.; Hage, W.; Loerting, T.; Price, S. L.; Mayer, E. *J. Am. Chem. Soc.* **2007**, *129*, 13863–13871.
- (21) Terlouw, J. K.; Lebrilla, C. B.; Schwarz, H. *Angew. Chem.* **1987**, *99*, 352–353.
- (22) Mori, T.; Suma, K.; Sumiyoshi, Y.; Endo, Y. *J. Chem. Phys.* **2009**, *130*, 204308.
- (23) Mori, T.; Suma, K.; Sumiyoshi, Y.; Endo, Y. *J. Chem. Phys.* **2011**, *134*, 044319.
- (24) Bernard, J.; Seidl, M.; Kohl, I.; Mayer, E.; Liedl, K. R.; Galvez, O.; Grothe, H.; Loerting, T. *Angew. Chem., Int. Ed.* **2011**, *50*, 1939–1943.
- (25) Galvez, O.; Zoerner, A.; Loewenschuss, A.; Grothe, H. *J. Phys. Chem. A* **2006**, *110*, 6472–6481.
- (26) Hage, W.; Hallbrucker, A.; Mayer, E. *J. Chem. Soc., Farad. Trans.* **1996**, *92*, 3197–3209.
- (27) Frisch, M. J.; et al. *Gaussian 09*; Gaussian Inc.: Wallingford, CT, 2009.
- (28) Janoschek, R.; Csizmadia, I. G. *J. Mol. Struct.* **1993**, *300*, 637–645.
- (29) Wight, C. A.; Boldyrev, A. I. *J. Phys. Chem.* **1995**, *99*, 12125–12130.
- (30) Dunning, T. H. *J. Chem. Phys.* **1989**, *90*, 1007–1023.
- (31) Kendall, R. A.; Dunning, T. H.; Harrison, R. J. *J. Chem. Phys.* **1992**, *96*, 6796–6806.
- (32) Woon, D. E.; Dunning, T. H. *J. Chem. Phys.* **1995**, *103*, 4572–4585.
- (33) Ayers, G. P.; Pullin, A. D. E. *Spectrochim. Acta Part A* **1976**, *32*, 1629–1639.
- (34) Givan, A.; Larsen, L. A.; Loewenschuss, A.; Nielsen, C. J. *J. Chem. Soc., Faraday Trans.* **1998**, *94*, 827–835.
- (35) Schriver, A.; Schriver-Mazzuoli, L.; Vigasin, A. A. *Vib. Spectrosc.* **2000**, *23*, 83–94.
- (36) Givan, A.; Larsen, L. A.; Loewenschuss, A.; Nielsen, C. J. *J. Mol. Struct.* **1999**, *509*, 35–47.
- (37) Parra, R. D.; Arena, A.; Sankisa, S. *THEOCHEM* **2007**, *815*, 31–40.
- (38) Wu, Y.-J.; Wu, C. Y. R.; Liang, M.-C. *Icarus* **2011**, *214*, 228–235.
- (39) Huber, S. E.; Dalnodar, S.; Kausch, W.; Kimeswenger, S.; Probst, M. *AIP Adv.* **2012**, *2*, 032180.
- (40) Tossell, J. A. *Inorg. Chem.* **2006**, *45*, 5961–5970.
- (41) Kumar, P. P.; Kalinichev, A. G.; Kirkpatrick, R. J. *J. Chem. Phys.* **2007**, *126*, 204315.
- (42) Schwerdtfeger, C. A.; Mazziotti, D. A. *J. Phys. Chem. A* **2011**, *115*, 12011–12016.
- (43) Reddy, S. K.; Kulkarni, C. H.; Balasubramanian, S. *J. Phys. Chem. A* **2012**, *116*, 1638–1647.
- (44) Bernard, J.; Seidl, M.; Mayer, E.; Loerting, T. *ChemPhysChem* **2012**, *13*, 3087–3091.
- (45) Boynton, W. V.; et al. *Science* **2009**, *325*, 61–64.
- (46) Hecht, M. H.; et al. *Science* **2009**, *325*, 64–67.

#### 4.4 Formation and Stability of Bulk Carbonic Acid ( $\text{H}_2\text{CO}_3$ ) by Protonation of Tropospheric Calcite





## Formation and Stability of Bulk Carbonic Acid (H<sub>2</sub>CO<sub>3</sub>) by Protonation of Tropospheric Calcite

Juergen Bernard,<sup>[a]</sup> Markus Seidl,<sup>[a]</sup> Erwin Mayer,<sup>[b]</sup> and Thomas Loerting\*<sup>[a]</sup>

Organic acids play an important role in the acidification of our atmosphere. These weak acids can contribute up to 60% of the free airborne acidity. By far the most abundant organic acids are the C1 and C2 monocarboxylic acids, formic acid (HCOOH) and acetic acid (CH<sub>3</sub>COOH), which show mixing ratios in the gas phase ranging up to 20 ppb over land<sup>[1,2]</sup> and down to 0.2 ppb in the remote oceanic boundary layer or troposphere.<sup>[3,4]</sup> These acids are partitioned between the gas phase and the particulate phase, where roughly one half to two thirds can be found in particulate matter (PM<sub>2.5</sub>).<sup>[2]</sup> The most important removal mechanism is dry deposition, which accounts for more than 90% of the total organic acid deposition budget. The remaining fraction is removed by rain as particulate-phase acids, whereas removal by chemical reactions is negligible.<sup>[1,5]</sup> In addition to the two most important organic acids, C3–C10 aliphatic monocarboxylic acids<sup>[1]</sup> and C2–C11 aliphatic dicarboxylic acids<sup>[1,2,6–11]</sup> as well as aromatic carboxylic acids<sup>[1]</sup> have also been observed in air. The water-soluble fraction of organic carbon can on average consist of 35% mono- and dicarboxylic acids.<sup>[12]</sup> While the C2-dicarboxylic acid, oxalic acid (COOH)<sub>2</sub>, is commonly observed in all field studies, the C1-dicarboxylic acid, carbonic acid (H<sub>2</sub>CO<sub>3</sub>), has barely received any attention, mainly because it is thought that it immediately decomposes to water and carbon dioxide. However, it has previously been shown that gaseous, water-free carbonic acid is surprisingly stable,<sup>[13]</sup> that amorphous and crystalline solids of pure carbonic acid can be produced and stored without decomposition at temperatures up to 230 K even in the presence of water<sup>[14]</sup> and that this solid can be sublimed at, for example, 220 K and recondensed in vacuo at surfaces of lower temperature.<sup>[15]</sup>

Formation of bulk carbonic acid in the laboratory has so far been achieved 1) by high-energy irradiation of CO<sub>2</sub> or CO<sub>2</sub>/H<sub>2</sub>O mixtures,<sup>[16–20]</sup> 2) through surface reactions of CO molecules with hydroxyl (OH) radicals at 10–40 K<sup>[21]</sup> and 3) by protonation of aqueous or methanolic solutions of KHCO<sub>3</sub> or K<sub>2</sub>CO<sub>3</sub> at low temperatures of ~140–180 K.<sup>[22–25]</sup> Mechanism (1) is believed to

be of astrophysical relevance, and carbonic acid is hence supposed to be present, for example, on comets, the Galilean satellites, on Venus and on the Martian surface.<sup>[15,18,26–33]</sup> For mechanisms (2) and (3) no relevance in nature, and in particular in the Earth's atmosphere, is envisioned because in the case of (2) temperatures are too low and in case of (3) aqueous/methanolic solutions of potassium(b)carbonate are not present in the atmosphere at  $T < 180$  K. A possible mechanism (4) of carbonic acid formation in nature was outlined by Grassian et al., who studied the interaction of gas-phase acids such as formic acid, acetic acid, sulphur dioxide and nitric acid with calcium carbonate particles (CaCO<sub>3</sub>) at ambient temperature. Under dry conditions of <1% relative humidity these acids react with the Ca(OH)(CO<sub>3</sub>H) surface layer of calcium carbonate and produce *surface-adsorbed* carbonic acid, which is stable even at 296 K under dry vacuum conditions, but decomposes at higher relative humidities.<sup>[34–36]</sup> According to this mechanism, carbonic acid is an important, but short-lived intermediate in the surface chemistry of calcium carbonate even at room temperature.

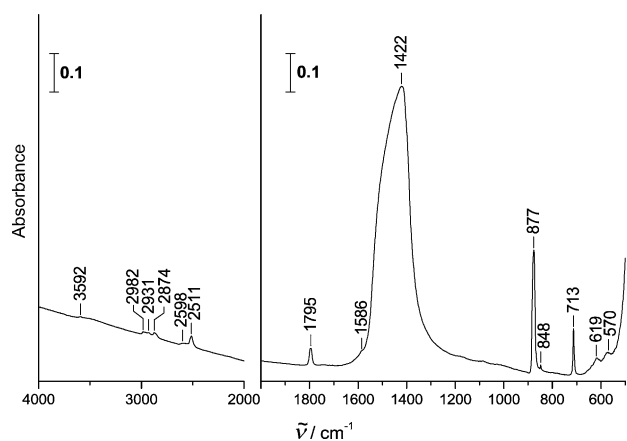
Here, we propose a novel mechanism (5), which produces *bulk* carbonic acid under conditions relevant to our atmosphere. This mechanism involves protonation of mineral dust particles, such as CaCO<sub>3</sub>, in the troposphere by acids, for example droplets containing HCl, at  $\geq 200$  K. Using FT-IR spectroscopy we demonstrate that high-surface-area CaCO<sub>3</sub> particles are consumed on a time scale of hours at 200 K in a humid atmosphere, while a non-volatile component, possibly Ca(HCO<sub>3</sub>)<sub>2</sub>, and aqueous/amorphous H<sub>2</sub>CO<sub>3</sub> (that crystallizes at 220 K to the  $\beta$ -polymorph of carbonic acid) are produced. By contrast, as shown by Santschi et al.,<sup>[37]</sup> reaction of CaCO<sub>3</sub> with HCl at 300 K involves Ca(OH)(HCO<sub>3</sub>) and presumably CaCl<sub>2</sub>·2H<sub>2</sub>O, but not carbonic acid and not Ca(HCO<sub>3</sub>)<sub>2</sub>. Furthermore, we show that H<sub>2</sub>CO<sub>3</sub> does not decompose readily even at 250 K in a humid atmosphere (0.6–0.8 mbar water vapour pressure,  $\approx 60$ –100% relative humidity,  $\approx 100$ –450 mbar total pressure). At higher temperatures H<sub>2</sub>CO<sub>3</sub> sublimates and/or decomposes. We therefore suggest that some of the CaCO<sub>3</sub> and also the MgCO<sub>3</sub> fraction of mineral dust, such as Saharan or Asian dust, is converted in the mid- and high troposphere at 200–250 K to aqueous/amorphous H<sub>2</sub>CO<sub>3</sub> and may even crystallize and exist as H<sub>2</sub>CO<sub>3</sub>, more precisely as the  $\beta$ -polymorph.<sup>[22–25]</sup> Because of the long-term stability of H<sub>2</sub>CO<sub>3</sub> at conditions relevant to the troposphere we suggest that carbonic acid contributes to the acidity in the troposphere.

Figure 1 depicts the IR spectrum of the CaCO<sub>3</sub> powder in the optical window of the range of 4000–500 cm<sup>-1</sup>. The spectrum clearly shows calcite bands, in particular  $\nu_4(E)$  at 713 cm<sup>-1</sup>,  $\nu_2(A_2'')$  at 877 cm<sup>-1</sup> and the broad and strong  $\nu_3(E)$

[a] J. Bernard, M. Seidl, Prof. Dr. T. Loerting  
Institute of Physical Chemistry  
University of Innsbruck  
Innrain 52a, 6020 Innsbruck (Austria)  
Fax: (+43) 512 507 2925  
E-mail: thomas.loerting@uibk.ac.at  
Homepage: <http://homepage.uibk.ac.at/~c724117/>

[b] Prof. Dr. E. Mayer  
Institute of General, Inorganic and Theoretical Chemistry  
University of Innsbruck (Austria)

Re-use of this article is permitted in accordance with the Terms and Conditions set out at [http://onlinelibrary.wiley.com/journal/10.1002/\(ISSN\)1439-7641/homepage/2267\\_onlineopen.html](http://onlinelibrary.wiley.com/journal/10.1002/(ISSN)1439-7641/homepage/2267_onlineopen.html).



**Figure 1.** FT-IR spectrum of  $\approx 1$  mg high-surface-area calcite ( $\text{CaCO}_3$ ) particles of equivalent spherical diameter of  $600 \text{ nm}^{[38]}$  on a  $25 \times 4 \text{ mm}$  ZnSe optical disc.

centred at  $1422 \text{ cm}^{-1}$ . This agrees well with literature data.<sup>[38,39]</sup> In addition, smaller absorptions, including overtones and combination bands, can be seen, for example at  $1795 \text{ cm}^{-1}$ ,  $2511 \text{ cm}^{-1}$  and  $2874 \text{ cm}^{-1}$ . The sloping baseline between  $4000$  and  $2000 \text{ cm}^{-1}$  is characteristic of wavelength-dependent scattering of small particles.<sup>[38]</sup> No ethanol bands can be discerned in Figure 1, which indicates that the calcite sample is dry after the procedure of transferring the powder onto the ZnSe window.

Figure 2a shows FT-IR spectra after treatment with aqueous HBr at 82 K, introduction of a 10.7 mbar inert atmosphere, heating to 200 K and remaining at 200 K for 60 min. Spectrum (1) was recorded immediately before pumping off the atmosphere, spectrum (2) immediately after pumping off the atmosphere. While calcite absorptions can still be seen in this spectrum (e.g.  $1791/1417/875$ ), new bands clearly appear at  $1722 \text{ cm}^{-1}$ ,  $1630 \text{ cm}^{-1}$ ,  $1471 \text{ cm}^{-1}$ ,  $\sim 1300 \text{ cm}^{-1}$  and  $801 \text{ cm}^{-1}$ . The new bands agree well with the band positions reported for amorphous carbonic acid ( $1721/1476/1306/803$ ) in ref. [14] [Figure 1, spectrum (1) therein]. All strong absorptions reported by Winkel et al.<sup>[14]</sup> also appear here and so we conclude that amorphous carbonic acid was formed. In addition, we attribute the band at  $1630 \text{ cm}^{-1}$  to the hexahydrate of HBr.<sup>[40–43]</sup> Spectra (3) and (4) show that calcite disappears within 71 min at 200 K, that is, the absorptions at  $1791/1417/875$  disappear slowly and simultaneously. After 71 min all the calcite bands are very weak, indicating that most of the calcite has disappeared. In addition some peaks also sharpen. In particular, a sharp band at  $1634 \text{ cm}^{-1}$  develops from the broader one at  $1630 \text{ cm}^{-1}$ . We attribute this to crystallization of the HBr hexahydrate from the amorphous phase. Water is pumped off only to a small extent at 200 K within 71 min, as indicated by the broad OH stretching band centered at  $\sim 3300 \text{ cm}^{-1}$ , which remains largely unaffected.

This broad band disappears, however, after 70 min at 220 K and 12 min at 230 K [see spectrum (1) of Figure 2b], which mimics the evaporation of water at low humidity in the troposphere. At the same time the amorphous carbonic acid crystal-

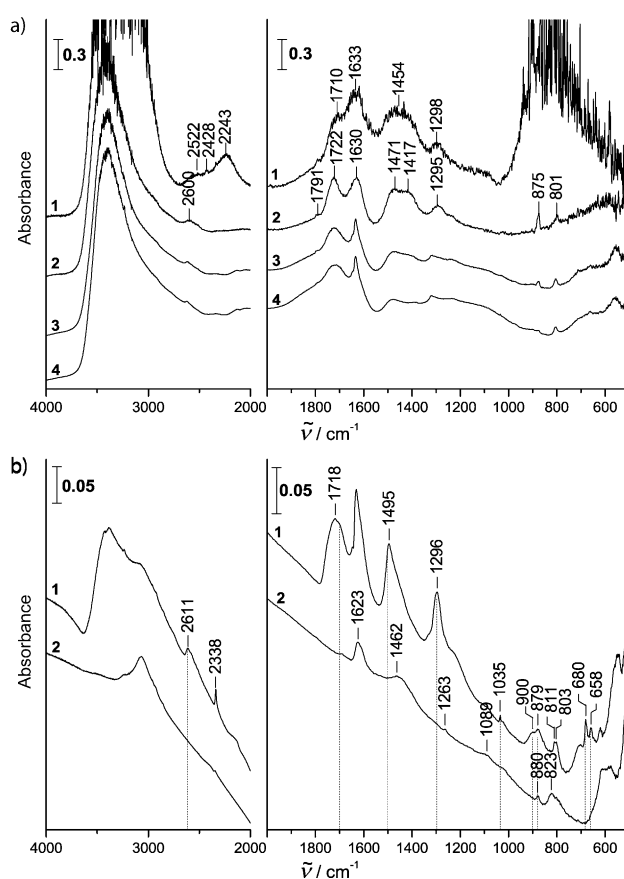


**Figure 2.** a) FT-IR spectra indicating formation of reaction products (amorphous  $\text{H}_2\text{CO}_3$  and  $\text{HBr}\cdot 6\text{H}_2\text{O}$ ) after spraying a layer of 4 M HBr at 82 K onto the calcite sample in a vacuum chamber and heating the sample to 200 K and annealing for 60 min at 200 K in a helium atmosphere of 11 mbar (1), after pumping off the helium atmosphere to  $1 \times 10^{-3}$  mbar (2), after 16 min at 200 K (3) and after 71 min at 200 K (4). b) FT-IR spectra indicating crystalline  $\beta\text{-H}_2\text{CO}_3$  in the product mixture after 70 min at 220 K and 12 min at 230 K (1) and non-volatile component remaining after removal of  $\beta\text{-H}_2\text{CO}_3$  by keeping the sample overnight in vacuo at 300 K (2).

lizes to the  $\beta$ -polymorph. Winkel et al. have established the following criteria indicating the crystallization of  $\beta\text{-H}_2\text{CO}_3$  (see Figure 1 in ref. [14]): 1) growth of a doublet at  $661 \text{ cm}^{-1}$  and  $683 \text{ cm}^{-1}$  at the cost of a broad band at  $649 \text{ cm}^{-1}$ ; 2) appearance of a broad band with a double-maximum at  $880 \text{ cm}^{-1}/900 \text{ cm}^{-1}$ ; 3) growth of a sharp band at  $1035 \text{ cm}^{-1}$  from a broad band at  $1020 \text{ cm}^{-1}$ ; 4) appearance of a single band at  $1297 \text{ cm}^{-1}$  from a structured band with a maximum at  $1267 \text{ cm}^{-1}$ ; 5) shift and sharpening of a broad band from  $1476 \text{ cm}^{-1}$  to  $1501 \text{ cm}^{-1}$ ; 6) changes in a structured band at  $1721 \text{ cm}^{-1}$  to a differently structured band at  $1700 \text{ cm}^{-1}$  and 7) shift and sharpening of a broad band from  $2555 \text{ cm}^{-1}$  to  $2616 \text{ cm}^{-1}$ . All these criteria, except maybe for the shift in  $\nu(\text{C}=\text{O})$ , are clearly evident in spectrum (1) in Figure 2b and are marked by vertical lines. That is, we infer crystallization to  $\beta\text{-H}_2\text{CO}_3$  at 220 K. In addition, the crystalline hexahydrate of HBr is still present in the sample. Some additional features of the spectrum can be discerned. The sharp band at  $2338 \text{ cm}^{-1}$  is attributed to trapped  $\text{CO}_2$ . The asymmetric shape of the HBr hex-

ahydrate band at  $1634\text{ cm}^{-1}$  and of the carbonic acid bands at  $1495$  and  $1296\text{ cm}^{-1}$  indicate the presence of a trace of an additional, unidentified species. This species can be separated from carbonic acid and the HBr hexahydrate, because, in contrast to them, it is a non-volatile species. After heating to  $300\text{ K}$  and leaving the sample in vacuo overnight,  $\text{CO}_2$ , carbonic acid and the HBr hexahydrate are pumped off, and the non-volatile species remains. The spectrum of this species with bands at  $1623/1462/1263/1089/880/823$  is shown as trace 2 in Figure 2b. The  $\nu(\text{C}=\text{O})$  at  $1623$  and the  $\pi(\text{CO}_3)$  at  $832$  is close to the  $\nu(\text{C}=\text{O})$  and  $\pi(\text{CO}_3)$  observed in  $\text{KHCO}_3$  ( $1618/832$ ).<sup>[44]</sup> However, other bands are shifted:  $1462$  vs  $1405$ ,  $1089$  vs  $1001$ ,  $610$  vs  $690$ . We speculate that the species remaining in the window is  $\text{Ca}(\text{HCO}_3)_2$ , which crystallizes as an alkaline-earth bicarbonate in a space group different from the one known for alkali bicarbonates such as  $\text{KHCO}_3$ . That is, calcite dust is converted by freeze-concentrated aqueous acid droplets to amorphous carbonic acid after an hour at  $200\text{ K}$ , and crystallization of carbonic acid may occur at slightly higher temperatures in low-humidity conditions. Incomplete conversion results in the formation of what we regard to be  $\text{Ca}(\text{HCO}_3)_2$ .

Furthermore, we tested the stability of  $\beta\text{-H}_2\text{CO}_3$  at tropospheric conditions. We produced some  $\beta\text{-H}_2\text{CO}_3$  by reaction of concentrated HCl ( $12\text{ M}$ ) with an excess of  $\text{CaCO}_3$  at  $200\text{ K}$  at  $\sim 100\text{ mbar}$  pressure. We identify excess  $\text{CaCO}_3$ ,  $\text{CaCl}_2\cdot 2\text{H}_2\text{O}$  and  $\beta\text{-H}_2\text{CO}_3$  as the products of this reaction.  $\text{CaCl}_2\cdot 2\text{H}_2\text{O}$  bands are observed at  $\sim 3500/1629/1614$ . Figure 3a shows the spectra collected after having reached  $260\text{ K}$  (1), after 17 min at  $260\text{ K}$  (2) and after an hour at  $260\text{ K}$  (3). Bands assigned to  $\beta\text{-H}_2\text{CO}_3$ ,  $\text{CaCO}_3$  and  $\text{CaCl}_2\cdot 2\text{H}_2\text{O}$  are marked by arrows, stars and open circles, respectively. While the spectra are unchanged after a few hours at  $200\text{--}250\text{ K}$ , the decomposition of  $\beta\text{-H}_2\text{CO}_3$  is evident on a time scale of one hour at  $260\text{ K}$  and  $50\text{--}70\%$  relative humidity. After having been kept for prolonged periods at lower temperatures at  $50\text{--}70\%$  relative humidity, it is clear that carbonic acid is still present initially at  $260\text{ K}$ , from the presence of the bands marked by the arrows in Figure 3a, spectrum (1). The difference spectrum between spectra (3) and (1) from Figure 3a is shown as spectrum (1) in Figure 3b. This difference spectrum is compared to spectrum (2) in Figure 3b of crystalline  $\beta$ -carbonic acid (identical to spectrum 4 in Figure 1 of ref. [14]). The agreement between these two spectra is excellent, which leads us to conclude that  $\beta\text{-H}_2\text{CO}_3$  slowly disappears at  $260\text{ K}$  and  $50\text{--}70\%$  relative humidity, whereas the other components in the mixture ( $\text{CaCl}_2\cdot 2\text{H}_2\text{O}$  and  $\text{CaCO}_3$ ) remain unaffected. After an hour at  $260\text{ K}$  only a minor fraction of the carbonic acid band intensities remains [see spectrum (3) of Figure 3a), so that the half-life can be estimated to be about 30 min at these conditions. For comparison, two of us calculated the half-life of carbonic acid in the presence of two water molecules to be about 40 minutes at  $260\text{ K}$  and about 20 years at  $200\text{ K}$  (Figure 2 in ref. [13a]). The agreement between these calculations and the experimental findings reported herein suggests that the decomposition mechanism involving carbonic acid and water at a 1:2 ratio is suitable for describing decomposition kinetics at  $60\%$  relative humidity. Independent experiments on the stability of pure crystalline  $\beta$ -car-

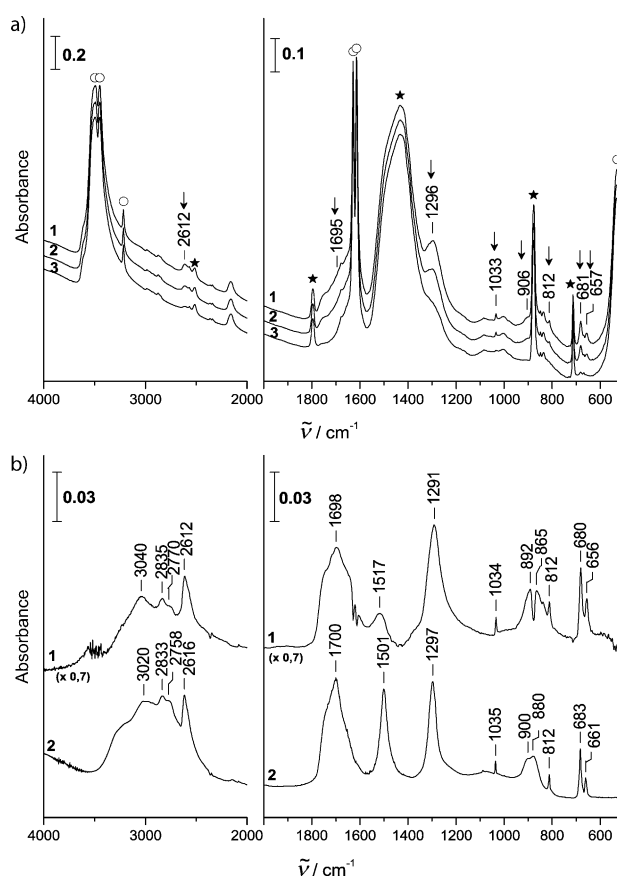


**Figure 3.** Thermal stability of  $\beta\text{-H}_2\text{CO}_3$  in the product mixture at  $260\text{ K}$ ,  $\sim 400\text{ mbar}$  helium and  $\sim 60\%$  relative humidity. The product mixture was obtained by protonation of high-surface area calcite with  $\sim 12\text{ M}$  HCl at  $200\text{ K}$  for 60 min in  $\sim 100\text{ mbar}$  helium at relative humidities exceeding  $100\%$ , i.e., in the presence of condensed ice. The sample was kept for  $\sim 5\text{ h}$  at  $200\text{--}250\text{ K}$  before heating to  $260\text{ K}$ . a) Spectra recorded at  $260\text{ K}$ ,  $\sim 400\text{ mbar}$  helium and  $\sim 60\%$  relative humidity. 0 min at  $260\text{ K}$  (1), 17 min at  $260\text{ K}$  (2) and one hour at  $260\text{ K}$  (3). Arrows:  $\beta\text{-H}_2\text{CO}_3$ , stars:  $\text{CaCO}_3$ , circles:  $\text{CaCl}_2\cdot 2\text{H}_2\text{O}$  b) Comparison of the spectrum of the disappearing species [calculated as difference spectrum of spectra (3) and (1) of (a)] with the spectrum of crystalline  $\beta$ -carbonic acid (corresponds to spectrum (4) in Figure 1 from ref. [14]).

bonic acid have confirmed this result of slow decomposition at  $260\text{ K}$  and  $50\text{--}70\%$  relative humidity, but of no significant decomposition at lower temperature. That is, at  $240\text{ K}$  and high relative humidity, carbonic acid, once formed from mineral dust, may persist over many hours. At lower humidities and/or temperatures we even expect stability for many days without any significant decomposition.

Figure 4 summarizes the experiments reported herein schematically in the context of atmospheric chemistry. The encounter of a mineral dust particle of  $\sim 600\text{ nm}$  diameter, namely  $\text{CaCO}_3$ , with concentrated aqueous HCl droplets constitutes step (1). At temperatures and pressures relevant in the troposphere the reaction progresses within about an hour. Some  $\text{CaCO}_3$  remains, while  $\text{CaCl}_2\cdot 2\text{H}_2\text{O}$ , possibly some  $\text{Ca}(\text{HCO}_3)_2$ , and amorphous carbonic acid form. At somewhat higher temperatures ( $\sim 220\text{--}240\text{ K}$ ) amorphous carbonic acid crystallizes to  $\beta\text{-H}_2\text{CO}_3$ . We emphasize that treatment of particulate calcite with acids as shown here above  $200\text{ K}$  results in the same poly-

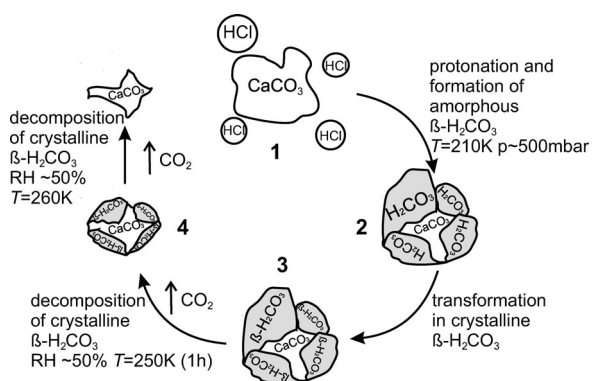


**Figure 4.** Carbonic acid formation in the atmosphere. Processing of mineral dust particles ( $\text{CaCO}_3$ ) by highly concentrated aqueous HCl droplets (1). Amorphous carbonic acid forms at  $T=200\text{ K}$  and  $p\sim 450\text{ mbar}$  (2), and crystallizes at higher temperatures to  $\beta$ - $\text{H}_2\text{CO}_3$  (3). Decomposition of  $\beta$ - $\text{H}_2\text{CO}_3$  does not take place at  $220\text{ K}$ , a few hundred millibars total pressure and  $>50\%$  relative humidity, but takes place with a half-life of 30 min at  $260\text{ K}$  and  $50\text{--}70\%$  (4).

morph obtained previously by high-energy irradiation of  $\text{CO}_2$  or  $\text{CO}_2/\text{H}_2\text{O}$  ice mixtures<sup>[16–20]</sup> and by reaction of water-soluble (b)carbonates with acids in aqueous solution above  $160\text{ K}$ ,<sup>[14, 15, 23, 25, 27]</sup> whereas other methods involving solvents other than water<sup>[22, 24]</sup> or no solvents<sup>[21]</sup> produce different polymorphs.  $\beta$ - $\text{H}_2\text{CO}_3$  remains stable over prolonged periods below  $240\text{ K}$  even at relative humidities of  $50\text{--}70\%$ . We notice slow disappearance of  $\beta$ - $\text{H}_2\text{CO}_3$  only at  $260\text{ K}$ , where the half-life is of the order of 30 min at  $50\text{--}70\%$  relative humidity, presumably due to decomposition to  $\text{CO}_2$  and  $\text{H}_2\text{O}$ . In total,  $\text{CaCO}_3$  is consumed by HCl, producing  $\text{CO}_2$ ,  $\text{H}_2\text{O}$  and  $\text{CaCl}_2\cdot 2\text{H}_2\text{O}$ . However, at tropospheric temperatures of  $200\text{--}240\text{ K}$  bulk (amorphous and/or crystalline) solid carbonic acid may exist over prolonged periods of time. We therefore suggest that amorphous and crystalline  $\beta$ - $\text{H}_2\text{CO}_3$  exists as bulk species in the troposphere containing mineral dust. A proof of this hypothesis would be equivalent to the discovery of this elusive species outside scientific laboratories as bulk species in the environment of the Earth. In order to possibly detect carbonic acid in air samples by field studies, we suggest using contactless techniques, for example, infrared spectroscopy, or alternatively sampling techniques not involving bringing the collected sample to ambient temperature and not involving dissolution of the sample in water in order to avoid decomposition of carbonic acid. By contrast to other organic acids in the atmosphere, carbonic acid decomposes at ambient temperature and in aqueous solution. However, it is surprisingly stable over prolonged periods even in the presence of water vapour at tropospherically relevant temperatures.

## Experimental Section

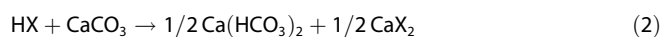
Commercial  $\text{CaCO}_3$  powder (OMYACarb, UF) provided by the group of Vicki Grassian with a manufacturer specified spherical diameter of  $600\text{ nm}$  was used in this study. The BET surface area of this powder was found to be  $10.1\pm 0.3\text{ m}^2\text{ g}^{-1}$  using  $\text{N}_2$  gas.<sup>[38]</sup> Approximately  $1\text{ mg}$  of this powder was immersed in two droplets of

ethanol and distributed evenly on a  $25\text{ mm}$  diameter optical disc (ZnSe or CsI). After evaporation of ethanol the powder sticks to the optical disc and is mounted in a cryo-sample holder inside a vacuum chamber. The vacuum chamber, pumped to a base pressure of  $5\times 10^{-7}\text{ mbar}$  using an oil-free scroll pump (Varian Triscroll 300) and a turbomolecular pump (Leybold Turbovac 361) is equipped with a hygro-thermometer (Qhygo-Temp80) and two  $49\text{ mm}$  diameter optical discs (KBr) so that a beam of light can pass through the vacuum chamber and the sample. FT-IR measurements are done using a VARIAN Excalibur 3100 spectrometer at  $4\text{ cm}^{-1}$  resolution. Figure 1 shows the FT-IR spectrum of the calcite powder on the optical disc. Two sets of experiments related to possible protonation of calcite are reported herein. The first set (results depicted in Figure 2) deals with the formation of carbonic acid from calcite at  $200\text{--}220\text{ K}$ . The second set deals with the question of the stability of carbonic acid in a humid environment up to  $260\text{ K}$  (Figure 3).

After cooling the cryo-sample holder to  $82\text{ K}$ , an airbrush (Harder&Steenbeck Infinity) is used to spray micron-sized droplets of a concentrated aqueous solution of HX ( $4\text{ M HBr}$  or  $12\text{ M HCl}$ ) through an orifice ( $500\text{ }\mu\text{m}$  diameter) into the pumped vacuum chamber, which produces a directed, supersonic beam of droplets onto the sample. This process mimics the encounter of micron-sized acid droplets and calcium carbonate particles in mineral dust in the troposphere. A temperature of  $82\text{ K}$  is used for droplet deposition because diffusion and chemical reaction are inhibited, and so droplets and solid particles coexist without reaction<sup>[22–24]</sup>. In order to stress the relevance of this experiment in the context of the chemical processing of mineral dust in the upper troposphere we then disconnected the pumps from the vacuum chamber and introduced an inert atmosphere of  $10.7\pm 0.5\text{ mbar}$  into the chamber. The sample temperature was next kept in this atmosphere for an hour at  $200\text{ K}$ . The acid droplets are in a semi-frozen, freeze-concentrated state under such conditions, similar to the situation in the troposphere. At this temperature there is significant diffusion, dissolution of calcium carbonate in the droplets and chemical reaction, which is monitored by FT-IR spectroscopy. After processing the calcite particles with acid droplets for one hour the atmosphere was pumped off in order to improve the signal-to-noise ratio of spectra. Please note that direct deposition of the droplets in vacuo at  $200\text{ K}$  produces similar spectra, whereas a directed beam of droplets to the sample is not possible in the presence of an atmosphere. In previous publications we reported the formation of  $\beta$ -carbonic acid of water-soluble carbonates ( $\text{K}_2\text{CO}_3$ ,  $\text{Cs}_2\text{CO}_3$ ) and bicarbonates ( $\text{KHCO}_3$ ) with aqueous acids (HCl, HBr)<sup>[14, 15, 23, 25, 27]</sup> at temperatures of  $160\text{--}240\text{ K}$  in vacuo. That is, we reported reaction between (freeze-concentrated) aqueous solutions of carbonate with (freeze-concentrated) acidic solutions. Here, we study for the first time whether or not reaction also takes place between solid particulate matter, namely a carbonate insoluble in water ( $\text{CaCO}_3$ ), and (freeze-concentrated) acidic droplets at  $200\text{--}220\text{ K}$  (Figure 2). In order to obtain quantitative conversion to carbonic acid, a molar ratio  $\text{HX}:\text{CaCO}_3$  of 2:1 is necessary according to Equation (1):



A lower ratio results in incomplete protonation and appearance of the intermediate calcium bicarbonate, which is not known to exist as a solid, but merely in solution. As an example the situation involving a ratio of 1:1 is shown in Equation (2):



The second set of experiments is aiming at the question whether or not carbonic acid ( $\text{H}_2\text{CO}_3$ ), once formed by processing of mineral dust in the atmosphere, remains stable without decomposition for a sufficiently long time in the humid troposphere. To this end we studied the reaction of concentrated HCl (12 M) with an excess of  $\text{CaCO}_3$  at 200 K, and the stability of the resulting  $\beta\text{-H}_2\text{CO}_3$  in the mixture of products up to 260 K and 50–70% relative humidity (Figure 3). The humidity was measured to be  $\approx 1.0\text{--}1.3$  mbar using a hygrometer sitting 20 cm above the cryo-sample holder. The temperature was increased in steps to 260 K within about four hours during which the sample was monitored using FT-IR spectroscopy.

## Acknowledgements

We thank Vicki Grassian and Courtney Hatch for providing us with the OMYACarb- $\text{CaCO}_3$ . We gratefully acknowledge support by the Austrian Science Fund FWF (project P18187), the Austrian Academy of Sciences ÖAW (DOC-fellowship to M.S.) and the European Research Council ERC (Starting Grant SULIWA to T.L.).

**Keywords:** atmospheric chemistry · carbonic acid · gas-phase chemistry · IR spectroscopy · mineral dust

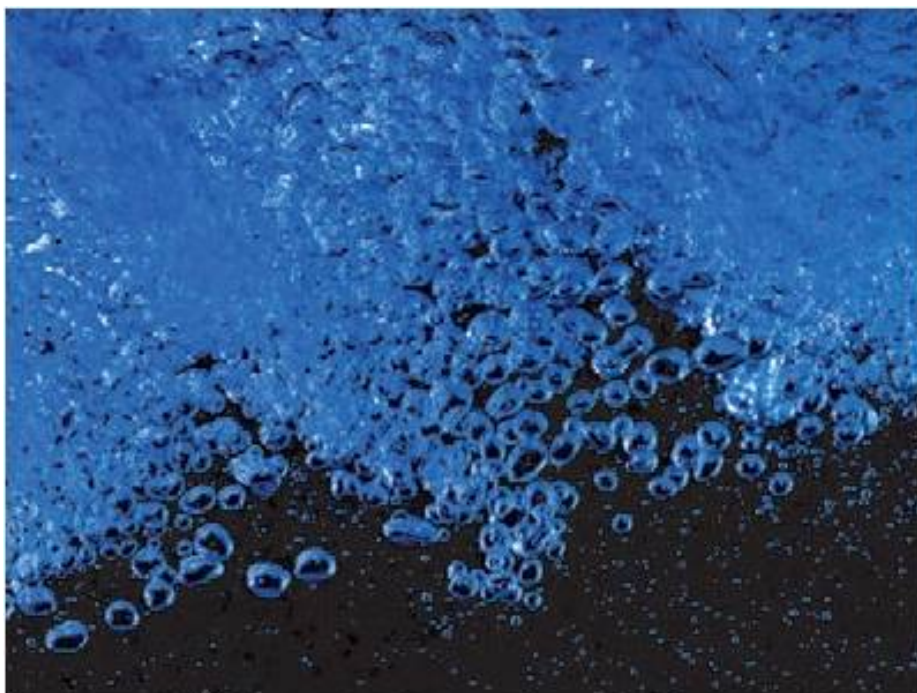
- [1] D. Grosjean, *Environ. Sci. Technol.* **1989**, *23*, 1506.
- [2] M. T. Limon-Sanchez, J. L. Arriaga-Colina, S. Escalona-Segura, L. G. Ruiz-Suarez, *Sci. Total Environ.* **2002**, *287*, 203.
- [3] D. W. Arlander, D. R. Cronn, J. C. Farmer, F. A. Menzia, H. H. Westberg, *J. Geophys. Res. [Atmos.]* **1990**, *95*, 16391.
- [4] E. D. Baboukas, M. Kanakidou, N. Mihalopoulos, *J. Geophys. Res. [Atmos.]* **2000**, *105*, 14459.
- [5] D. Grosjean, *Atmos. Environ. Part A* **1992**, *26*, 3279.
- [6] M. Mochida, A. Kawabata, K. Kawamura, H. Hatsushika, K. Yamazaki, *J. Geophys. Res. [Atmos.]* **2003**, *108*, A4193/1.
- [7] C. P. Rinsland, E. Mahieu, R. Zander, A. Goldman, S. Wood, L. Chiou, *J. Geophys. Res. [Atmos.]* **2004**, *109*, D18308/1.
- [8] M. Legrand, S. Preunkert, C. Galy-Lacaux, C. Liousse, D. Wagenbach, *J. Geophys. Res. [Atmos.]* **2005**, *110*, D13302/1.
- [9] A. Limbeck, Y. Kraxner, H. Puxbaum, *J. Aerosol Sci.* **2005**, *36*, 991.
- [10] A. Römpf, R. Winterhalter, G. K. Moortgat, *Atmos. Environ.* **2006**, *40*, 6846.
- [11] H. Wang, K. Kawamura, K. Yamazaki, *J. Atmos. Chem.* **2006**, *53*, 43.
- [12] M. Kanakidou, J. H. Seinfeld, S. N. Pandis, I. Barnes, F. J. Dentener, M. C. Facchini, R. Van Dingenen, B. Ervens, A. Nenes, C. J. Nielsen, E. Swietlicki, J. P. Putaud, Y. Balkanski, S. Fuzzi, J. Horth, G. K. Moortgat, R. Winterhalter, C. E. L. Myhre, K. Tsigaridis, E. Vignati, E. G. Stephanou, J. Wilson, *Atmos. Chem. Phys.* **2005**, *5*, 1053.
- [13] T. Loerting, C. Tautermann, R. T. Kroemer, I. Kohl, A. Hallbrucker, E. Mayer, K. R. Liedl, *Angew. Chem.* **2000**, *112*, 919; *Angew. Chem. Int. Ed.* **2000**, *39*, 891.
- [14] K. Winkel, W. Hage, T. Loerting, S. L. Price, E. Mayer, *J. Am. Chem. Soc.* **2007**, *129*, 13863.
- [15] W. Hage, K. R. Liedl, A. Hallbrucker, E. Mayer, *Science* **1998**, *279*, 1332.
- [16] M. H. Moore, R. K. Khanna, *Spectrochim. Acta, Part A* **1991**, *47*, 255.
- [17] N. DelloRusso, R. K. Khanna, M. H. Moore, *J. Geophys. Res. [Planets]* **1993**, *98*, E5505.
- [18] J. R. Brucato, M. E. Palumbo, G. Strazzulla, *Icarus* **1997**, *125*, 135.
- [19] P. A. Gerakines, M. H. Moore, R. L. Hudson, *Astron. Astrophys.* **2000**, *357*, 793.
- [20] S. Pilling, E. Seperuelo Duarte, A. Domaracka, H. Rothard, P. Boduch, E. F. da Silveira, *Astron. Astrophys.* **2010**, *523*, A77.
- [21] Y. Oba, N. Watanabe, A. Kouchi, T. Hama, V. Pirronello, *Astrophys. J.* **2010**, *722*, 1598.
- [22] W. Hage, A. Hallbrucker, E. Mayer, *J. Am. Chem. Soc.* **1993**, *115*, 8427.
- [23] W. Hage, A. Hallbrucker, E. Mayer, *J. Chem. Soc. Faraday Trans.* **1996**, *92*, 3197.
- [24] W. Hage, A. Hallbrucker, E. Mayer, *J. Chem. Soc. Faraday Trans.* **1996**, *92*, 3183.
- [25] W. Hage, A. Hallbrucker, E. Mayer, *J. Mol. Struct.* **1997**, *408–409*, 527.
- [26] R. K. Khanna, J. A. Tossell, K. Fox, *Icarus* **1994**, *112*, 541.
- [27] W. Hage, A. Hallbrucker, E. Mayer, *J. Chem. Soc. Faraday Trans.* **1995**, *91*, 2823.
- [28] G. Strazzulla, J. R. Brucato, G. Cimino, M. E. Palumbo, *Planet. Space Sci.* **1996**, *44*, 1447.
- [29] T. B. McCord, R. W. Carlson, W. D. Smythe, G. B. Hansen, R. N. Clark, C. A. Hibbitts, F. P. Fanale, J. C. Granahan, M. Segura, D. L. Matson, T. V. Johnson, P. D. Martin, *Science* **1997**, *278*, 271.
- [30] D. C. B. Whittet, P. A. Gerakines, A. G. G. M. Tielens, A. J. Adamson, A. C. A. Boogert, J. E. Chiar, T. de Graauw, P. Ehrenfreund, T. Prusti, W. A. Schutte, B. Vandenbussche, E. F. van Dishoeck, *Astrophys. J.* **1998**, *498*, L159.
- [31] W. Zheng, R. I. Kaiser, *Chem. Phys. Lett.* **2007**, *450*, 55.
- [32] I. Kohl, K. Winkel, M. Bauer, K. R. Liedl, T. Loerting, E. Mayer, *Angew. Chem.* **2009**, *121*, 2728; *Angew. Chem. Int. Ed.* **2009**, *48*, 2690.
- [33] Z. Peeters, R. L. Hudson, M. H. Moore, A. Lewis, *Icarus* **2010**, *210*, 480.
- [34] H. A. Al-Hosney, V. H. Grassian, *J. Am. Chem. Soc.* **2004**, *126*, 8068.
- [35] H. A. Al-Hosney, V. H. Grassian, *Phys. Chem. Chem. Phys.* **2005**, *7*, 1266.
- [36] H. A. Al-Hosney, S. Carlos-Cuellar, J. Baltrusaitis, V. H. Grassian, *Phys. Chem. Chem. Phys.* **2005**, *7*, 3587.
- [37] C. Santschi, M. J. Rossi, *J. Phys. Chem. A* **2006**, *110*, 6789.
- [38] A. Preszler Prince, V. H. Grassian, P. Kleiber, M. A. Young, *Phys. Chem. Chem. Phys.* **2007**, *9*, 622.
- [39] K. Nakamoto, *Infrared and Raman Spectra of Inorganic and Coordination Compounds, 4th ed.*, Wiley, New York, **1986**, p. 124.
- [40] A. S. Gilbert, N. Sheppard, *J. Chem. Soc. Faraday Trans. 2* **1973**, *69*, 1628.
- [41] G. Ritzhaupt, J. P. Devlin, *J. Phys. Chem.* **1991**, *95*, 90.
- [42] L. Delzeit, B. Rowland, J. P. Devlin, *J. Phys. Chem.* **1993**, *97*, 10312.
- [43] I. K. Ortega, R. Escibano, D. Fernandez-Torre, V. J. Herrero, B. Mate, M. A. Moreno, *Chem. Phys. Lett.* **2004**, *396*, 335.
- [44] K. Nakamoto, Y. A. Sarma, H. Ogoshi, *J. Chem. Phys.* **1965**, *43*, 1177.

Received: May 25, 2012

Published online on June 15, 2012



## 4.5 Aqueous carbonic acid ( $\text{H}_2\text{CO}_3$ )

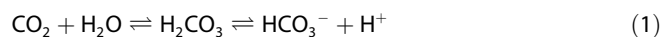




## Aqueous Carbonic Acid (H<sub>2</sub>CO<sub>3</sub>)

Thomas Loerting\* and Juergen Bernard<sup>[a]</sup>

Carbonic acid (H<sub>2</sub>CO<sub>3</sub>) is a molecule right at the interface between organic and inorganic chemistry. In fact, according to some definitions it is an organic molecule, while according to others it is an inorganic molecule. Its exceptionality can also be recognized from the fact that it formally belongs neither to the mono- nor dicarboxylic acids, even though it is a C1 diprotic acid. The diprotic nature, that is, the ability to react to its conjugate base bicarbonate (HCO<sub>3</sub><sup>-</sup>) and to carbonate (CO<sub>3</sub><sup>2-</sup>), provides a link to geology and mineralogy. Carbonate minerals such as calcite, dolomite or siderite are ubiquitous in sedimentary rock. In addition to the acid–base equilibrium, carbonic acid is in equilibrium with carbon dioxide and water. Both equilibria can be summarized as Equation (1):



In mineralogy, it has long been known that carbonate minerals kept in acidic environments dissolve and release carbon dioxide.<sup>[1,2]</sup> This process of weathering impedes efforts to preserve buildings made from carbonates.<sup>[3]</sup> Only recently was it recognized that carbonic acid may be a relatively stable intermediate as a surface-adsorbed species in the presence of acidic gases, but only in case of dry conditions near 0% relative humidity.<sup>[4–6]</sup> Once the humidity increases to up to 5%, the surface-adsorbed H<sub>2</sub>CO<sub>3</sub> immediately decomposes to carbon dioxide, leaving behind a Ca(OH)(CO<sub>3</sub>H) surface. In marine science, this link between carbon dioxide and acidic behaviour is of importance in understanding ocean acidification and dissolution of carbonate minerals induced by uptake of anthropogenic carbon dioxide from the atmosphere.<sup>[7–9]</sup> In physiology, the kidneys and lungs work together to maintain a blood pH of 7.40 ± 0.05 by balancing carbon dioxide and bicarbonate levels in the bloodstream. In case this balance is disturbed, acidosis (pH < 7.35) or alkalosis (pH > 7.45) can result. For example, when one hyperventilates, carbon dioxide is lost, which shifts the equilibrium to the left (“alkalosis”). The process of converting these species into each other has to be so efficient in all living organisms that one of the enzymes that accelerate the reaction is one of the fastest known by biochemists. This enzyme belongs to the family of carbonic anhydrases and shows turnover rates of up to 10<sup>6</sup> reactions per second.

Because of the two equilibria in Equation (1), a solution of carbon dioxide in water reacts as an acid. However, the neutralization of carbon dioxide is a slow process compared with

other weak acids.<sup>[10]</sup> In 1912 McBain showed in a simple and memorable experiment that the neutralization process of basic solutions with solutions saturated with carbon dioxide progresses rather slowly. He coloured the basic solution with the pH indicator phenolphthalein in pink, and this colour fades away slowly within fifteen seconds, after which neutralization is complete.<sup>[11,12]</sup> By contrast the neutralization with, for example, formic acid takes place suddenly at the moment of mixing. The reason for the delay is that only much less than 1% of the solution exists as H<sub>2</sub>CO<sub>3</sub>. Eigen et al. have even asked the question whether H<sub>2</sub>CO<sub>3</sub> is a short-lived intermediate, as implicitly assumed in Equation (1), or rather a transition state, which can not be isolated at all.<sup>[13]</sup> The slow kinetics of the first step together with the much faster second step of deprotonation prevent a significant build-up of transient H<sub>2</sub>CO<sub>3</sub>. This makes observation of carbonic acid in aqueous solution a real challenge, and all researchers failed to observe carbonic acid when walking down the route of hydration of carbon dioxide.

The acid dissociation constant  $K'_a$  in the temperature range between 0 °C and 50 °C was determined by a few researchers in the first half of the 20th century.<sup>[14–19]</sup> All data are in quite good agreement and show  $\text{p}K'_a(\text{CO}_2 \text{ in } \text{H}_2\text{O}, 25^\circ\text{C}) \approx 6.4 \pm 0.1$ . This was referred to as the acid dissociation constant of “carbonic acid”, but in fact involves both equilibria, that is, hydrated carbon dioxide is also present in equilibrium. It is, therefore, more appropriate to regard this number as the “apparent” dissociation constant of carbonic acid. We use the notion  $K'_a$  in order to indicate that more than one process is involved. The “true” dissociation constant of carbonic acid (defined as  $K_a = [\text{H}^+][\text{HCO}_3^-]/[\text{H}_2\text{CO}_3]$ ) remained unclear due to the presence of carbon dioxide in the equilibrium. Determining  $K_a$  would require dissolving H<sub>2</sub>CO<sub>3</sub> in water and measuring the pH or bicarbonate equilibrium concentration. This remained a gedankenexperiment simply because pure H<sub>2</sub>CO<sub>3</sub> could not be synthesized and isolated for a long time, and also because it decomposes on the time scale of seconds in aqueous solutions.<sup>[20–22]</sup> In some contemporary chemistry textbooks H<sub>2</sub>CO<sub>3</sub> is described as an instable species decomposing rapidly to carbon dioxide and water, which can not be isolated in its pure form.<sup>[23]</sup> This is no longer correct. Evidence that carbonic acid has enough thermal stability to allow for its characterization using standard techniques accreted in the late 1980s and 1990s, both in the solid phase and in the gas phase.

In 1993 the Innsbruck group succeeded not only in isolating micrometer-thick films of pure H<sub>2</sub>CO<sub>3</sub>, but also in characterizing this species by FTIR spectroscopy.<sup>[24]</sup> This was possible by means of a cryo-technique for isolation of short-lived intermediates in acid–base reactions, in this case the protonation of bicarbonates studied at temperatures ranging from 77 K to

[a] Prof. Dr. T. Loerting, J. Bernard  
Institute of Physical Chemistry  
University of Innsbruck  
Innrain 52a, A-6020 Innsbruck (Austria)  
E-mail: thomas.loerting@uibk.ac.at

240 K. The first isolation was performed in methanolic solution,<sup>[24]</sup> later on in aqueous solution as well, or, more precisely, in an ice matrix.<sup>[25]</sup> In both cases the IR spectra, after removal of the solvent, can be clearly attributed to crystalline H<sub>2</sub>CO<sub>3</sub> because of the position and sharpness of the bands as well as several band splittings. Still, the spectra obtained from the two different solvents show some bands at clearly different wavelengths, with different intensities and different band splitting. This implies that carbonic acid crystallizes in (at least) two different polymorphs called  $\alpha$ -H<sub>2</sub>CO<sub>3</sub> (from the methanolic solution) and  $\beta$ -H<sub>2</sub>CO<sub>3</sub> (from the aqueous solution). The unambiguous assignment of the bands was possible by IR characterization of the D and <sup>13</sup>C isotopic forms crystallized both from methanolic<sup>[26]</sup> and aqueous solutions.<sup>[27]</sup> Lately, it was recognized that immediately after removal of the solvent, two amorphous solids of carbonic acid can be characterized, which develop into crystalline solids upon heating. This transition takes place within hours at ~200 K and within minutes at ~220 K and was followed by Raman<sup>[28]</sup> and IR spectroscopy and powder X-ray diffraction.<sup>[29]</sup> The basic structural motif found in the two polymorphs of carbonic acid has already developed in the two amorphous forms. From spectroscopic considerations the building block in the  $\beta$ -polymorph and in the amorphous precursor is a centrosymmetric unit such as the cyclic carbonic acid dimer.<sup>[28]</sup> The crystal structure of the two polymorphs is not yet known, though. In a vacuum chamber (~10<sup>-7</sup> mbar) the two polymorphs are stable up to ~210 K ( $\alpha$ ) and ~230 K ( $\beta$ ). At these temperatures desorption rates are so high that the sample is pumped off.

In 1991, after irradiation of a 1:1 mixture of solid carbon dioxide and H<sub>2</sub>O-ice with 700 keV protons at 20 K, Moore and Khanna obtained a mixture of several radical and molecular product species, and after heating to 215–250 K they observed an unknown species by FT-IR spectroscopy, which they tentatively (and correctly) assigned to crystalline carbonic acid.<sup>[30–32]</sup> Besides proton irradiation, UV bombardment<sup>[33]</sup> and ion implantation<sup>[34]</sup> also have the potential to convert carbon dioxide water ices to carbonic acid, even though this is limited to the near surface area. For instance, 4:1 mixtures of water and carbon dioxide are converted to carbonic acid under high-flux UV radiation at the wavelength of prominent solar lines.<sup>[35]</sup> This implies that in outer space cryogenic CO<sub>2</sub>-H<sub>2</sub>O deposits will possibly be converted to  $\beta$ -H<sub>2</sub>CO<sub>3</sub> after irradiation.<sup>[36]</sup> Indeed, the 2.4–5.0  $\mu$ m spectral region of comet Halley shows several bands consistent with the IR-bands found in the laboratory.<sup>[37]</sup> The infrared spectra of the Martian surface and of the Galilean satellites of Jupiter<sup>[38–40]</sup> are also at wavelengths very similar to that of carbonic acid. Lately, solid carbonic acid has also been discussed as a surface compound on Edgeworth–Kuiper–Belt bodies.<sup>[41]</sup> In these environments carbonic acid can occur either as the crystalline  $\beta$ -polymorph or as an amorphous solid.

Observation of carbonic acid in the gas-phase was first claimed by Terlouw et al. after thermolysis of (NH<sub>4</sub>)HCO<sub>3</sub>.<sup>[42]</sup> They succeeded in observing a weak signal at  $m/z=62$  by electron-ionization mass spectroscopy, which they attributed to gas-phase H<sub>2</sub>CO<sub>3</sub>.<sup>[42]</sup> The intensity of the signal was less than 1% of the signal arising from the decomposition product

carbon dioxide, but could still be selected as parent ion for fragmentation studies. In the gas-phase three possible conformations of carbonic acid are possible, which can be interconverted by rotating around the angles  $\Phi_1$  and  $\Phi_2$  (see Figure 1).

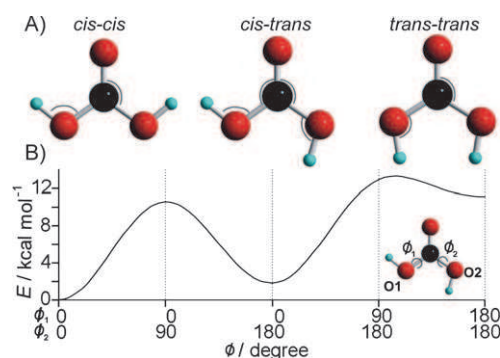


**Figure 1.** A) Conformational isomerism of the carbonic acid monomer. The isomers can be interconverted by changing either one of the two dihedral angles  $\Phi_1$  or  $\Phi_2$  (inset). B) Calculated potential energy curve showing that there are two low-energy minima (*cis-cis*, *cis-trans*) and one high-energy minimum (*trans-trans*) in the gas-phase. The curve was obtained from ab initio calculations of the gas-phase molecule at the CCSD(T)/cc-pVQZ level of theory. The potential energy curve for conformational isomerism in aqueous solution is unknown at present. The figure is adapted from ref. [44], with permission.

The three rotamers representing local potential minima are called *cis-cis*, *cis-trans* and *trans-trans*. According to calculations the *cis-cis* conformation is the most stable, mostly because both hydrogen atoms form a weak internal hydrogen bond. The *cis-trans* conformation is less stable by ~1–2 kcal mol<sup>-1</sup>,<sup>[43,44]</sup> that is, in equilibrium at 200 K one would expect the *cis-cis* rotamer to be the main conformer, whereas less than 10% of *cis-trans* monomers are expected. The *trans-trans* conformation is less stable by more than 10 kcal mol<sup>-1</sup> and is not supposed to appear in experiments (see Figure 1). In some calculations it is even an unstable transition state rather than a metastable equilibrium state. By contrast, the cyclic dimer (H<sub>2</sub>CO<sub>3</sub>)<sub>2</sub> is stabilized by two strong hydrogen bonds and, therefore, the enthalpy of decomposition to carbon dioxide and water is astonishingly close to zero.<sup>[45]</sup> For this reason, an appreciable fraction of the cyclic dimer (H<sub>2</sub>CO<sub>3</sub>)<sub>2</sub> is thought to be present in the gas phase. Higher oligomers such as (H<sub>2</sub>CO<sub>3</sub>)<sub>3</sub> are thermodynamically even more stable in the gas phase,<sup>[46]</sup> but are not thought to occur because an encounter of three or more carbonic acid molecules in the gas phase is extremely unlikely. On this basis, Tossell has even suggested a strategy for capturing and sequestration of carbon dioxide in the form of solid carbonic acid.<sup>[47]</sup>

While *cis-trans* H<sub>2</sub>CO<sub>3</sub> could be positively identified in experiments,<sup>[44]</sup> a clear spectroscopic proof for the presence of *cis-cis* H<sub>2</sub>CO<sub>3</sub> and cyclic (H<sub>2</sub>CO<sub>3</sub>)<sub>2</sub> is currently missing. *Cis-trans* H<sub>2</sub>CO<sub>3</sub> and three deuterated isotopologues were generated in a supersonic jet within a discharge nozzle by applying a pulsed high voltage of 1.8 kV on a gas mixture saturated with water vapour and containing 5% carbon dioxide and identified from the observation of pure rotational transitions by Fourier-

transform microwave spectroscopy.<sup>[44]</sup> It remains unclear why in this experiment the thermodynamically most stable rotamer is not observed, but a metastable one instead. Hage et al. showed that crystalline  $\text{H}_2\text{CO}_3$  can be sublimed and recondensed without decomposition to  $\text{CO}_2$  and  $\text{H}_2\text{O}$ .<sup>[37]</sup> After desorption at  $\sim 220$  K and flying for a few centimetres through the gas phase, roughly 50% of the initial amount recondensed as  $\alpha\text{-H}_2\text{CO}_3$  on a window kept at  $\sim 10$  K. This is consistent with a high kinetic stability of water-free carbonic acid as inferred from transition state theory considerations.<sup>[48]</sup> Once water is present, the half-life with respect to decomposition to carbon dioxide is greatly reduced from 180 000 years (water-free) to roughly a minute in a 1:3 complex of water with carbonic acid.<sup>[49]</sup> When hydrated with water carbonic acid decays via thermally easily accessible transition states by a proton-relay mechanism rather than via a highly strained four-membered transition state.<sup>[48,50,51]</sup> Kinetic isotope effects and rate constants are in rather good agreement with experiments, which suggests that any attempt of detecting carbonic acid in aqueous solution has to be done on timescales faster than a second.

Some fast techniques were developed more than 50 years ago in order to cope with this challenge, such as rapid mixing or stopped-flow techniques followed by a time-dependent readout of fast high-field conductance,<sup>[52]</sup> temperature<sup>[20]</sup> or pH.<sup>[53]</sup> Using such techniques, the “true ionization constant” was determined to be  $\text{p}K_{\text{a}} \approx 3.8$  in the temperature range  $5\text{--}45$  °C at zero ionic strength<sup>[54]</sup> and later refined to  $\text{p}K_{\text{a}} \approx 3.45 \pm 0.05$ .<sup>[53]</sup> This renders carbonic acid a stronger acid than for example, acetic acid ( $\text{p}K_{\text{a}} \approx 4.7$ ) and comparable to formic acid ( $\text{p}K_{\text{a}} \approx 3.8$ ). It should therefore not be ignored in discussions of ocean acidification, especially in view of increasing atmospheric  $\text{CO}_2$  mixing ratios.

Spectroscopic identification of carbonic acid has remained elusive for quite a long time. The first report in solution was possible by means of a fast technique, namely rapid acquisition of Raman spectra in a continuous flow apparatus.<sup>[55]</sup> Rather than walking down the route of carbon dioxide hydration, Falcke and Eberle took the reverse pathway of protonation of bicarbonates, which provides the possibility of a significant buildup of intermediary carbonic acid as a slow second step (decomposition) follows a rapid first step (protonation). After rapid acidification of 1 M  $\text{NaHCO}_3$  with 3 M HCl to  $\text{pH} \approx 0\text{--}1$  they succeeded to observe a marker band of carbonic acid, namely the C–OH stretching vibration at  $1017\text{ cm}^{-1}$ , and followed its time-dependent decay caused by decomposition to carbon dioxide (observed at  $1280\text{ cm}^{-1}$  and  $1382\text{ cm}^{-1}$ ).<sup>[55]</sup> The analysis of the kinetics of decomposition has proven to be difficult because bicarbonate in aqueous solution shows a band at  $1017\text{ cm}^{-1}$  overlapping with the marker band of carbonic acid.<sup>[56]</sup> The rate of decomposition to carbon dioxide by Falcke and Eberle is slightly higher than the earlier literature data.<sup>[20]</sup> In the very recent work by Adamczyk et al. the C=O stretching vibration was used for spectroscopic observation of aqueous  $\text{H}_2\text{CO}_3$ .<sup>[57]</sup> The C=O mode has the advantage that there is no overlap between carbonic acid (C=O double bond), bicarbonate (C–O 3/2 bond) or carbonate (C–O 4/3 bond)

[Figure 2]. This mode can be observed only with difficulty by using Raman spectroscopy, but easily using infrared spectroscopy. The work by Adamczyk et al.<sup>[57]</sup> goes far beyond what

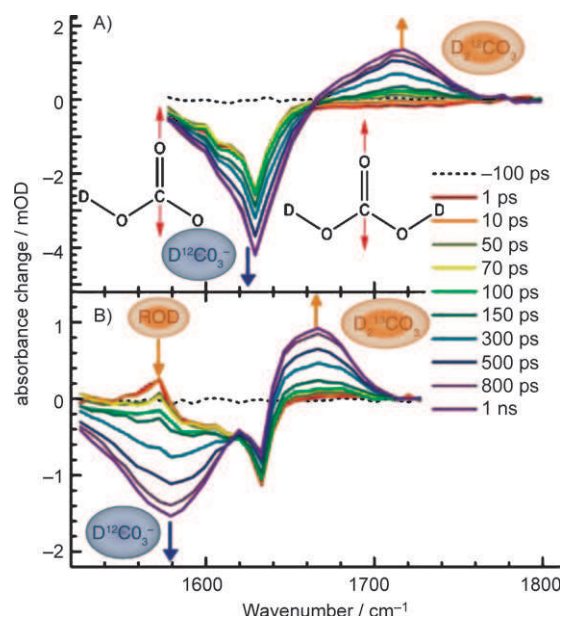


**Figure 2.** Time-resolved infrared spectra in the  $\nu(\text{C}=\text{O})$  range  $1520\text{--}1800\text{ cm}^{-1}$ . A) The deuteration of aqueous  $\text{D}^{12}\text{CO}_3^-$  producing aqueous  $\text{D}_2^{12}\text{CO}_3$  is followed. B) The deuteration of aqueous  $\text{D}^{13}\text{CO}_3^-$  producing aqueous  $\text{D}_2^{13}\text{CO}_3$  is followed. For both C-isotopes a correlated decrease of the bicarbonate marker mode (arrows pointing down) and the rise of the carbonic acid C=O stretching marker band (arrows pointing up) is observed. In case of  $^{13}\text{C}$  the bicarbonate mode overlaps with a mode of the photoacid, which triggers the deuteron transfer event at the time of 0 ps. A simplified normal-mode depiction is shown in the inset. The figure is adapted from ref. [57], with permission.

Falcke and Eberle achieved. They used time-resolved femtosecond infrared spectroscopy and even succeeded to monitor the buildup of  $\text{D}_2\text{CO}_3$  also by walking down the lane of ultrafast protonation of bicarbonate. In a system buffered at  $\text{pD} = 8$  they observe the protonation of  $\text{NaDCO}_3$  at relatively high ionic strengths (0.1–0.8 M solutions) on the fly, which is highly non-trivial because this event takes place within one nanosecond. The most elegant aspect of this study is that the proton transfer reaction can be triggered by a short pulse of light. The source of the proton is a “photoacid”. Typical photoacids suitable for studying proton transfer reactions in aqueous solutions are pyranine (8-hydroxypyrene-1,3,6-trisulfonate, HPTS) or 2-naphthol-6,8-disulfonate (2N-6,8S). For the latter, the dissociation constant in the ground state  $\text{p}K_{\text{a}}(\text{S}_0) \approx 9.3 \pm 0.1$ , while in the excited state  $\text{p}K_{\text{a}}(\text{S}_1) \approx 1.2 \pm 0.2$ . That is, the proton is not donated to water in the ground state, but in the excited state. Thus, the short pulse of light at 330 nm excites the photoacid, weakens its OH-bond and triggers proton transfer. The events following the proton transfer can be followed on a femtosecond time resolution, for example by infrared spectroscopy, which provides the basis for observations of microscopic details of proton transfer events with unprecedented resolution.<sup>[58]</sup> For instance, the traditional Eigen–Weller picture of

neutralization reactions between an acid and a base in water has been shown by Rini et al. to need refinement to a three-stage model using this technique.<sup>[59]</sup> Also, proton exchange between an acid and a base in aqueous solution has been shown to proceed by a sequential von Grothuss-type proton-hopping mechanism through water bridges involving intermediary  $\text{H}_3\text{O}^+$  ions stabilized in the Eigen configuration.<sup>[60]</sup>

In the case of proton transfer to bicarbonate, or more precisely, deuteron transfer to  $\text{DCO}_3^-$ , the question to be answered was whether or not carbonic acid  $\text{D}_2\text{CO}_3$  would form as a transient species, and this can be clearly positively answered now when inspecting the data collected by Adamczyk et al., which is reproduced in Figure 2, where it is shown that the C=O stretching vibration shifts from  $1628\text{ cm}^{-1}$ , which is characteristic of  $\text{DCO}_3^-$ , to  $1720\text{ cm}^{-1}$ , which is characteristic of carbonic acid. The process occurs simultaneously, as can be seen from the fact that the increase in peak area below the  $1720\text{ cm}^{-1}$  marker band is proportional to the loss below the  $1628\text{ cm}^{-1}$  marker mode. The assignment of this band to the C=O stretching band is ascertained by observing the expected  $^{12}\text{C}/^{13}\text{C}$  isotope shift, namely to  $1579\text{ cm}^{-1}$  for  $\text{D}^{13}\text{CO}_3^-$  and to  $1666\text{ cm}^{-1}$  for  $\text{D}_2^{13}\text{CO}_3$ . The shifts of  $-49\text{ cm}^{-1}$  and  $-54\text{ cm}^{-1}$ , respectively, are in good agreement with the shifts observed for the C=O stretching mode in crystalline carbonic acid.<sup>[26,27]</sup> Together with the simultaneous build-up of the deprotonated photoacid (marker modes at  $1410\text{ cm}^{-1}$  and  $1510\text{ cm}^{-1}$ ) and the simultaneous loss of photoacid (marker mode at  $1472\text{ cm}^{-1}$ ) this observation eliminates any doubt about the formation of  $\text{D}_2\text{CO}_3$  in aqueous solution. The formation is complete after a few hundred picoseconds according to the data in Figure 2. On this time scale no decomposition to carbon dioxide is observable, which is monitored by the absence of the  $\text{CO}_2$  marker mode at  $2364\text{ cm}^{-1}$ . From the kinetic data an on-contact deuteron transfer time of 8 ps is extracted, and a deprotonation rate slower by roughly four orders of magnitude, 280 000 ps, is calculated. The deprotonation is still much faster than decomposition to carbon dioxide, which takes place in the order of seconds. Thus, the lifetime of  $\text{D}_2\text{CO}_3$  clearly exceeds a few nanoseconds. From a Marcus plot, Adamczyk et al. obtain an acidity constant of  $\text{p}K_a = 3.45$  for carbonic acid. Computational predictions on the basis of CBS-QB3 gas phase calculations and a continuous solvation model (CPCM) result in  $\text{p}K_a(\text{cis-cis}) = 3.8$ ,  $\text{p}K_a(\text{cis-trans}) = 3.6$  and  $\text{p}K_a(\text{trans-trans}) = 2.2$ .<sup>[61]</sup> Assuming an error of  $\pm 0.5$ , the comparison between experiment and calculation suggests that both *cis-cis* and *cis-trans* are species relevant in aqueous solution, but not *trans-trans*. What remains open from this study is whether water molecules act as shuttles to transfer the proton from the photoacid to bicarbonate (or, more unlikely, whether the protonation is direct). It also remains unanswered whether the decomposition reaction depends on specific conformations of the carbonic acid molecule. From theoretical calculations it seems that oligomers such as the dimer<sup>[45]</sup> and the most stable monomer conformer (*cis-cis*) have to pass through a high transition state, whereas the less stable *cis-trans* conformer can access a lower transition state, and may be hence of higher importance in understanding decomposition to carbon dioxide.<sup>[48,49]</sup> We

hope these issues will be addressed in future studies on much longer time scales than employed in the present meticulous work by Adamczyk et al.<sup>[57]</sup> In view of the astrophysical relevance of carbonic acid it would also be of interest to study the rates of protonation/deprotonation in glassy water or ice matrices at low temperatures rather than in aqueous solution.

## Acknowledgements

We wish to thank Erwin Mayer for introducing us to carbonic acid and to the sponsors of our own research on the topic (FWF project P18187, ERC Starting Grant SULIWA).

**Keywords:** acidity · carbonic acid · IR spectroscopy · metastable compounds · time-resolved spectroscopy

- [1] P. Glynn, *Rev. Mineral. Geochem.* **2000**, *40*, 481.
- [2] J. W. Morse, R. S. Arvidson, *Earth Sci. Rev.* **2002**, *58*, 51.
- [3] F. G. Bell, *Environ. Geol.* **1993**, *21*, 187.
- [4] H. A. Al-Hosney, V. H. Grassian, *J. Am. Chem. Soc.* **2004**, *126*, 8068.
- [5] H. A. Al-Hosney, S. Carlos-Cuellar, J. Baltrusaitis, V. H. Grassian, *Phys. Chem. Chem. Phys.* **2005**, *7*, 3587.
- [6] H. A. Al-Hosney, V. H. Grassian, *Phys. Chem. Chem. Phys.* **2005**, *7*, 1266.
- [7] R. A. Feely, C. L. Sabine, K. Lee, W. Berelson, J. Kleyvas, V. J. Fabry, F. J. Millero, *Science* **2004**, *305*, 362.
- [8] C. L. Sabine et al., *Science* **2004**, *305*, 367.
- [9] J. C. Orr et al., *Nature* **2005**, *437*, 681.
- [10] D. M. H. Kern, *J. Chem. Educ.* **1960**, *37*, 14.
- [11] J. W. McBain, *J. Chem. Soc. Trans.* **1912**, *101*, 814.
- [12] J. W. McBain, *Proc. Chem. Soc.* **1912**, *28*, 106.
- [13] M. Eigen, K. Kustin, G. Maass, *Z. Phys. Chem.* **1961**, *30*, 130.
- [14] J. Kendall, *J. Am. Chem. Soc.* **1916**, *38*, 1480.
- [15] A. C. Walker, U. B. Bray, J. Johnson, *J. Am. Chem. Soc.* **1927**, *49*, 1235.
- [16] D. A. MacInnes, D. Belcher, *J. Am. Chem. Soc.* **1933**, *55*, 2630.
- [17] D. A. MacInnes, D. Belcher, *J. Am. Chem. Soc.* **1935**, *57*, 1683.
- [18] T. Shedlovsky, D. A. MacInnes, *J. Am. Chem. Soc.* **1935**, *57*, 1705.
- [19] H. S. Harned, R. Davis, Jr., *J. Am. Chem. Soc.* **1943**, *65*, 2030.
- [20] F. J. W. Roughton, *J. Am. Chem. Soc.* **1941**, *63*, 2930.
- [21] J. Meier, G. Schwarzenbach, *Helv. Chim. Acta* **1957**, *40*, 907.
- [22] E. Magid, B. O. Turbeck, *Biochim. Biophys. Acta* **1968**, *165*, 515.
- [23] a) *Encyclopedia of Inorganic Chemistry, Vol.2* (Ed.: R. B. King) Wiley, Chichester, **1994**, b) T. L. Brown, H. E. Le May, Jr., B. E. Bursten, C. J. Murphy, *Chemistry—The Central Science, 11th Ed.*, Pearson Education, Inc., Upper Saddle River, **2009**, c) H. Beyer, W. Walter, *Lehrbuch der Organischen Chemie, 24th Ed.*, Hirzel-Verlag, Stuttgart, **2004**.
- [24] W. Hage, A. Hallbrucker, E. Mayer, *J. Am. Chem. Soc.* **1993**, *115*, 8427.
- [25] W. Hage, A. Hallbrucker, E. Mayer, *J. Chem. Soc. Faraday Trans.* **1995**, *91*, 2823.
- [26] W. Hage, A. Hallbrucker, E. Mayer, *J. Chem. Soc. Faraday Trans.* **1996**, *92*, 3183.
- [27] W. Hage, A. Hallbrucker, E. Mayer, *J. Chem. Soc. Faraday Trans.* **1996**, *92*, 3197.
- [28] I. Kohl, K. Winkel, M. Bauer, K. R. Liedl, T. Loerting, E. Mayer, *Angew. Chem.* **2009**, *121*, 2728; *Angew. Chem. Int. Ed.* **2009**, *48*, 2690.
- [29] K. Winkel, W. Hage, T. Loerting, S. L. Price, E. Mayer, *J. Am. Chem. Soc.* **2007**, *129*, 13863.
- [30] M. H. Moore, R. Khanna, B. Donn, *J. Geophys. Res.* **1991**, *96*, 17541.
- [31] M. H. Moore, R. K. Khanna, *Spectrochim. Acta A* **1991**, *47 A*, 255.
- [32] J. R. Brucato, M. E. Palumbo, G. Strazzulla, *Icarus* **1997**, *125*, 135.
- [33] P. A. Gerakines, M. H. Moore, R. L. Hudson, *Astron. Astrophys.* **2000**, *357*, 793.
- [34] G. Strazzulla, G. A. Baratta, M. E. Palumbo, M. A. Satorre, *Nucl. Instrum. Methods Phys. Res. B* **2000**, *166–167*, 13.
- [35] C. Y. R. Wu, D. L. Judge, B.-M. Cheng, T.-S. Yih, C. S. Lee, W. H. Ip, *J. Geophys. Res.* **2003**, *108*, 5032.

- [36] M. H. Moore, R. L. Hudson, P. A. Gerakines, *Spectrochim. Acta A* **2001**, *57*, 843.
- [37] W. Hage, K. R. Liedl, A. Hallbrucker, E. Mayer, *Science* **1998**, *279*, 1332.
- [38] G. Strazzulla, J. R. Brucato, G. Cimino, M. E. Palumbo, *Planet. Space Sci.* **1996**, *44*, 1447.
- [39] M. L. Delitsky, A. L. Lane, *J. Geophys. Res.* **1998**, *103*, 31391.
- [40] G. Strazzulla, *Planet. Space Sci.* **1999**, *47*, 1371.
- [41] M. H. Moore, R. L. Hudson, R. F. Ferrante, *Earth Moon Planets* **2003**, *92*, 291.
- [42] J. K. Terlouw, C. B. Lebrilla, H. Schwarz, *Angew. Chem. Angewandte Chemie* **1987**, *99*, 352.
- [43] C. A. Wight, A. I. Boldyrev, *J. Phys. Chem.* **1995**, *99*, 12125.
- [44] T. Mori, K. Suma, Y. Sumiyoshi, Y. Endo, *J. Chem. Phys.* **2009**, *130*, 204308.
- [45] K. R. Liedl, S. Sekusak, E. Mayer, *J. Am. Chem. Soc.* **1997**, *119*, 3782.
- [46] J. A. Tossell, *Inorg. Chem.* **2006**, *45*, 5961.
- [47] J. A. Tossell, *Environ. Sci. Technol.* **2009**, *43*, 2575.
- [48] T. Loerting, C. Tautermann, R. T. Kroemer, I. Kohl, A. Hallbrucker, E. Mayer, K. R. Liedl, *Angew. Chem. Int. Ed.* **2000**, *39*, 892; *Angew. Chem.* **2000**, *112*, 919.
- [49] C. S. Tautermann, A. F. Voegelé, T. Loerting, I. Kohl, A. Hallbrucker, E. Mayer, K. R. Liedl, *Chem. Eur. J.* **2002**, *8*, 66.
- [50] B. Jonsson, G. Karlstrom, H. Wennerstrom, S. Forsen, B. Roos, J. Almlöf, *J. Am. Chem. Soc.* **1977**, *99*, 4628.
- [51] M. T. Nguyen, T. K. Ha, *J. Am. Chem. Soc.* **1984**, *106*, 599.
- [52] D. Berg, A. Patterson, Jr., *J. Am. Chem. Soc.* **1953**, *75*, 5197.
- [53] A. L. Soli, R. H. Byrne, *Mar. Chem.* **2002**, *78*, 65.
- [54] K. F. Wissbrun, D. M. French, A. Patterson, Jr., *J. Phys. Chem.* **1954**, *58*, 693.
- [55] H. Falcke, S. H. Eberle, *Water Res.* **1990**, *24*, 685.
- [56] B. G. Oliver, A. R. Davis, *Can. J. Chem.* **1973**, *51*, 698.
- [57] K. Adamczyk, M. Premont-Schwarz, D. Pines, E. Pines, E. T. J. Nibbering, *Science* **2009**, *326*, 1690.
- [58] E. T. J. Nibbering, H. Fidder, E. Pines, *Annu. Rev. Phys. Chem.* **2005**, *56*, 337.
- [59] M. Rini, B.-Z. Magnes, E. Pines, E. T. J. Nibbering, *Science* **2003**, *301*, 349.
- [60] O. F. Mohammed, D. Pines, J. Dreyer, E. Pines, E. T. J. Nibbering, *Science* **2005**, *310*, 83.
- [61] J. A. Tossell, *Geochim. Cosmochim. Acta* **2005**, *69*, 5647.

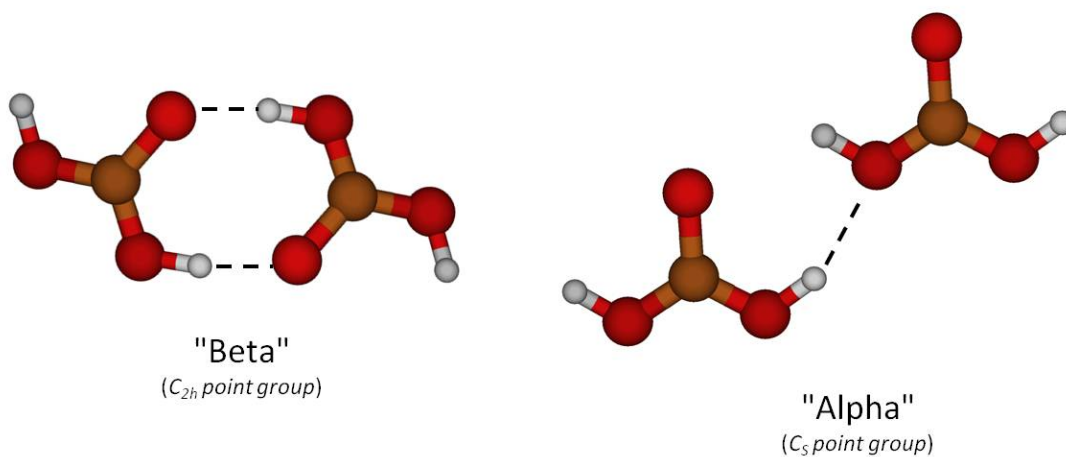
---

Received: March 17, 2010

Published online on April 15, 2010



## 4.6 Local structural order in carbonic acid polymorphs: Raman and FT-IR spectroscopy





# Local structural order in carbonic acid polymorphs: Raman and FT-IR spectroscopy

Christian Mitterdorfer,<sup>a</sup> Jürgen Bernard,<sup>a,b</sup> Frederik Klauser,<sup>a</sup> Katrin Winkel,<sup>a,b</sup> Ingrid Kohl,<sup>b</sup> Klaus R. Liedl,<sup>b</sup> Hinrich Grothe,<sup>c</sup> Erwin Mayer<sup>b</sup> and Thomas Loerting<sup>a\*</sup>

Two different polymorphs of carbonic acid,  $\alpha$ - and  $\beta$ -H<sub>2</sub>CO<sub>3</sub>, were identified and characterized using infrared spectroscopy (FT-IR) previously. Our attempts to determine the crystal structures of these two polymorphs using powder and thin-film X-ray diffraction techniques have failed so far. Here, we report the Raman spectrum of the  $\alpha$ -polymorph, compare it with its FT-IR spectrum and present band assignments in line with our work on the  $\beta$ -polymorph [*Angew. Chem. Int. Ed.* 48 (2009) 2690–2694]. The Raman spectra also contain information in the wavenumber range  $\sim 90$ – $400$  cm<sup>-1</sup>, which was not accessible by FT-IR spectroscopy in the previous work. While the  $\alpha$ -polymorph shows Raman and IR bands at similar positions over the whole accessible range, the rule of mutual exclusion is obeyed for the  $\beta$ -polymorph. This suggests that there is a center of inversion in the basic building block of  $\beta$ -H<sub>2</sub>CO<sub>3</sub> whereas there is none in  $\alpha$ -H<sub>2</sub>CO<sub>3</sub>. Thus, as the basic motif in the crystal structure we suggest the cyclic carbonic acid dimer containing a center of inversion in case of  $\beta$ -H<sub>2</sub>CO<sub>3</sub> and a catemer chain or a sheet-like structure based on carbonic acid dimers not containing a center of inversion in case of  $\alpha$ -H<sub>2</sub>CO<sub>3</sub>. This hypothesis is strengthened when comparing Raman active lattice modes at  $<400$  cm<sup>-1</sup> with the calculated Raman spectra for different dimers. In particular, the intense band at  $192$  cm<sup>-1</sup> in  $\beta$ -H<sub>2</sub>CO<sub>3</sub> can be explained by the inter-dimer stretching mode of the centrosymmetric RC(OHO)<sub>2</sub> CR entity with R=OH. The same entity can be found in gas-phase formic acid (R=H) and in  $\beta$ -oxalic acid (R=COOH) and produces an intense Raman active band at a very similar wavenumber. The absence of this band in  $\alpha$ -H<sub>2</sub>CO<sub>3</sub> confirms that the difference to  $\beta$ -H<sub>2</sub>CO<sub>3</sub> is found in the local coordination environment and/or monomer conformation rather than on the long range. Copyright © 2011 John Wiley & Sons, Ltd.

**Keywords:** carbonic acid; polymorphism; center of inversion; rule of mutual exclusion; crystal structure building blocks

## Introduction

Carbonic acid and its acid–base system CO<sub>2</sub>/H<sub>2</sub>O  $\rightleftharpoons$  H<sub>2</sub>CO<sub>3</sub>  $\rightleftharpoons$  HCO<sub>3</sub><sup>-</sup>/H<sup>+</sup> are of fundamental importance in many fields<sup>[1]</sup> including astrophysics,<sup>[2–15]</sup> medicine,<sup>[16–19]</sup> marine chemistry<sup>[20–22]</sup> and geochemistry.<sup>[23,24]</sup> Synthesis and characterization of the intermediate carbonic acid (H<sub>2</sub>CO<sub>3</sub>) was long believed to be impossible owing to the two decay channels to carbon dioxide and bicarbonate. In spite of that, different routes to solid and gaseous carbonic acid have been established in the last two decades.<sup>[1]</sup> Also, in aqueous solutions, trace amounts of H<sub>2</sub>CO<sub>3</sub> were detected and characterized using spectroscopic techniques.<sup>[25–27]</sup> Gas-phase carbonic acid was detected following the thermolysis of NH<sub>4</sub>HCO<sub>3</sub> by means of mass spectrometry,<sup>[28]</sup> following the application of a high-voltage pulse to wet CO<sub>2</sub> gas and supersonic jet expansion by means of FT-microwave spectroscopy<sup>[29,30]</sup> and very recently following the sublimation of pure solid H<sub>2</sub>CO<sub>3</sub> by means of matrix isolation FT-IR spectroscopy.<sup>[31]</sup> Pure solid H<sub>2</sub>CO<sub>3</sub> is accessible by five different techniques: (1) high-energy H or He irradiation of CO<sub>2</sub>/H<sub>2</sub>O ice mixtures,<sup>[3,32–35]</sup> (2) high-energy UV irradiation of CO<sub>2</sub>/H<sub>2</sub>O ice mixtures,<sup>[36]</sup> (3) H implantation in pure CO<sub>2</sub> ice,<sup>[34,37]</sup> (4) the reaction of non-energetic OH radicals with CO<sup>[38]</sup> and (5) acid–base chemistry in both (a) aqueous and (b) methanolic solution at cryo temperatures.<sup>[5,8,14,39–43]</sup> As a surface-adsorbed species, carbonic acid was also identified on carbonate minerals in acidic but dry atmosphere<sup>[44–46]</sup> and is a possible surface intermediate in the process of CO<sub>2</sub> adsorption on hydroxylated oxides, e.g. Fe<sub>2</sub>O<sub>3</sub> or Al<sub>2</sub>O<sub>3</sub>.<sup>[47,48]</sup>

The main analytical tool for the detection and characterization of solid carbonic acid has been infrared spectroscopy. Techniques (1), (2), (3)<sup>[3,32–37]</sup> and (5a)<sup>[5,8,40,42]</sup> (in aqueous environment) yield practically identical infrared spectra which are assigned to crystalline  $\beta$ -carbonic acid. By contrast, technique (5b) (in methanolic solution) results in a distinct spectrum assigned to crystalline  $\alpha$ -carbonic acid.<sup>[39,41,42]</sup> Other polymorphs of carbonic acid are not known at present, even though the infrared spectra obtained recently by Oba *et al.*<sup>[38]</sup> might be interpreted to be different from the spectra of the  $\alpha$ - and  $\beta$ -forms. The formation of these two crystalline polymorphs from solution is preceded by the formation of two distinct amorphous forms, in which the hydrogen-bond connectivity and conformational state are similar to the crystalline forms<sup>[43]</sup> – reflecting Ostwald's step rule. The process of crystallization from the amorphous forms

\* Correspondence to: Thomas Loerting, Institute of Physical Chemistry, University of Innsbruck, Innrain 52a, A-6020 Innsbruck, Austria.  
E-mail: Thomas.Loerting@uibk.ac.at

a Institute of Physical Chemistry, University of Innsbruck, A-6020 Innsbruck, Austria

b Institute of General, Inorganic and Theoretical Chemistry, University of Innsbruck, A-6020 Innsbruck, Austria

c Institute of Materials Chemistry, Vienna University of Technology, A-1060 Vienna, Austria

was also followed by powder X-ray diffraction.<sup>[43]</sup> However, the quality of the powder diffractograms in the crystalline state is currently not sufficient to solve the crystal structures of the two polymorphs using techniques such as Rietveld refinement. Thus, 'no information on either the local or long-range structure' of the carbonic acid polymorphs is known as pointed out by Tossell.<sup>[49]</sup>

Here, we report the Raman spectra of  $\alpha$ - and  $\beta$ -carbonic acid in the range  $\sim 90$ – $4000\text{ cm}^{-1}$ . This is a continuation of our recent Raman study on amorphous and  $\beta$ -carbonic acid, which aimed at the question whether amorphous and/or  $\beta$ -carbonic acid might be present on the icy parts of the Mars surface.<sup>[14]</sup> Raman spectra of  $\alpha$ -carbonic acid are presented here for the first time, and the Raman spectra of  $\beta$ -carbonic acid are extended to lower wavenumbers. Raman and IR spectra yield complementary information, as IR-forbidden transitions may be Raman active and vice versa. This is called 'The rule of mutual exclusion'<sup>[50–54]</sup> and obeyed strictly in case of  $\beta$ -carbonic acid. By contrast, we here find that bands are both Raman and IR active in case of  $\alpha$ -carbonic acid. This is suggestive of the centrosymmetric cyclic dimer as the local structural motif in  $\beta$ -carbonic acid and a non-centrosymmetric motif in  $\alpha$ -carbonic acid. Based on the observed band positions and on the observation of needle-like crystals under the light microscope, we suggest a chain-like catemer motif or a sheet-like motif for  $\alpha$ -carbonic acid. This finding is supported by normal mode analysis in dimeric carbonic acid units. Whereas we have focused on the  $400$ – $4000\text{ cm}^{-1}$  region in our earlier study, the comparison with theory focuses on the low wavenumber region at  $<400\text{ cm}^{-1}$  here. In addition, also a comparison with other carboxylic acids such as oxalic acid or malonic acid is presented.

## Experimental

Solid  $\text{H}_2\text{CO}_3$  was prepared via a cryogenic technique (5) by protonation of hydrogencarbonate anions. For details of the technique, see Refs [40,41], and for a schematic drawing of the apparatus see Ref. [55]. For the preparation of  $\alpha$ -carbonic acid (technique 5b) methanolic solutions of  $0.4\text{ M KHCO}_3$  and  $1.5\text{ M HCl}$  and for  $\beta$ -carbonic acid (technique 5a) aqueous solutions of  $0.1\text{ M KHCO}_3$  and  $1\text{ M HBr}$  were used [ $\text{KHCO}_3$  (Merck p. a.),  $\text{CH}_3\text{OH}$  (Aldrich, HPLC quality),  $\text{HBr}$  (Fluka, 48% p. a.),  $\text{HCl}$  (Supelco, 3 M in  $\text{CH}_3\text{OH}$ )]. Thin films ( $<4\text{ }\mu\text{m}$ ) of crystalline carbonic acid were prepared by alternately vitrifying droplets of the acidic and basic solutions on optical CsI windows ( $13 \times 2\text{ mm}$ ) held at  $77\text{ K}$ . By heating the films *in vacuo* ( $\sim 10^{-7}$  mbar) to  $200\text{ K}$  (methanolic solution) or  $220\text{ K}$  (aqueous solution), the protonation of  $\text{KHCO}_3$  takes place and the solvent and excess acid are removed from the window. To confirm the removal of the solvent and formation of crystalline carbonic acid, infrared spectra were recorded *in situ* in transmission. For this purpose, the beam passes through two KBr windows ( $49 \times 6\text{ mm}$ ) sealing the vacuum chamber and the sample on the CsI window inside the chamber. IR spectra were recorded on a Varian Excalibur FT-IR spectrometer at  $4\text{ cm}^{-1}$  resolution, by co-adding 100 scans.

After breaking the vacuum, the CsI window with the  $\text{H}_2\text{CO}_3$  film was transferred under liquid nitrogen to a precooled ( $\sim 80\text{ K}$ ) microscope cryostat (Microstat N, Oxford) in order to carry out Raman measurements, for which we employ a Labram-1B 10/78IM instrument from Dilor S.A. The excitation wavelength of  $632.8\text{ nm}$  is supplied by a  $20\text{ mW}$  He–Ne laser. The laser light is totally reflected by a dichroic mirror (Super Notch Plus filter) through a quartz window of the cryostat towards the sample

placed below an Olympus BX 40 microscope (using a LM Plan  $50\times$  NA 0.50 objective). The Raman scattered light is collected by the microscope and totally transmitted through the notch filter towards the confocal hole and the entrance slit of the spectrometer. Then a spectrum is formed on a CCD detector. A  $1800\text{ grooves mm}^{-1}$  grating with a resolution of  $\sim 2\text{ cm}^{-1}$  was used. The overall recording time for the spectra shown in Figs 1 and 2 was 7 min. The abscissa was calibrated with a silicon standard, and the sharp Raman shifts are accurate to  $\pm 2\text{ cm}^{-1}$  for the  $1800\text{ g mm}^{-1}$  grating. The relative intensities of the bands in different parts of the figures are not shown on the same scale. An Oxford Microstat was used as the cryostat. The temperature of the sample was controlled by a LakeShore CI330 autotuning temperature controller and remained constant to within  $\pm 0.2\text{ K}$ . For imaging of the surface, a TV camera is used.

Since the crystal structure is unknown, we do not attempt an assignment of the Raman bands to normal modes of a particular symmetry type. Therefore, the assignment can only be attempted by a qualitative description of the modes, similar to that of the IR spectra of  $\text{H}_2\text{CO}_3$  polymorphs,<sup>[3,5,32,33,36,40,41,43,56]</sup> and it is based on comparisons with assignments of other crystalline carboxylic acids and on our calculation of the harmonic wavenumbers in carbonic acid oligomers. We note that strong coupling between the various modes is often observed for carboxylic acid oligomers, which makes vibrational assignments in terms of distinct modes even less meaningful.<sup>[57–59]</sup> The vibrational spectra, including Raman and IR intensities, of carbonic acid oligomers were calculated using the Gaussian09 and Gaussian98 suite of programs. Carbonic acid dimers were calculated at a range of levels of theory, including MP2/aug-cc-pVDZ, B3LYP/6-31G(d), B3LYP/aug-cc-pVDZ and B3LYP/6-31+G(d). In this work, we pay particular attention to the Raman active modes in the range  $100$ – $500\text{ cm}^{-1}$ . In this range, variation of the basis set and/or method results in a shift of no more than  $\pm 5\text{ cm}^{-1}$ . This good performance of the hybrid density functional and the low computational cost of this method allowed us to examine also the spectra of two possible tetramer configurations.

## Results

Raman spectra of  $\alpha$ - $\text{H}_2\text{CO}_3$  (Fig. 1, bottom; and Fig. 2, bottom) were recorded by focusing the laser on the crystal needles (Fig. 3, top). The infrared spectrum (Fig. 1, top) was recorded directly before transferring the sample window to the Raman microstat. The vertical dashed lines are shown as a guide to the eye where the intensity is seen both in the Raman and IR in Fig. 1. Compared to the Raman spectrum of  $\beta$ - $\text{H}_2\text{CO}_3$  (reported in Ref. [14]), more bands are detected in case of  $\alpha$ - $\text{H}_2\text{CO}_3$  at  $500$ – $4000\text{ cm}^{-1}$ . This immediately suggests a lower symmetry of the latter. The assignment of Raman bands is presented in Table 1 and is based on the assignment of IR bands presented in Ref. [41] because of the appearance of the bands in the Raman spectrum at very similar positions as in the infrared spectrum. The assignment of IR bands in Ref. [41] is itself based on IR spectra of different carbonic acid isotopologues. In addition to this assignment, we also refer to the assignment of the acid I to acid VII fundamentals presented by Wolfs and Desseyn on the example of some dicarboxylic acids.<sup>[59]</sup> We wish to stress that the assignments made in Table 1 do not imply that we are dealing with uncoupled modes. Instead, most modes are coupled with other modes, as also found in other (di)carboxylic acids such as malonic acid,<sup>[57]</sup> and so the assignments represent only qualitative descriptions.

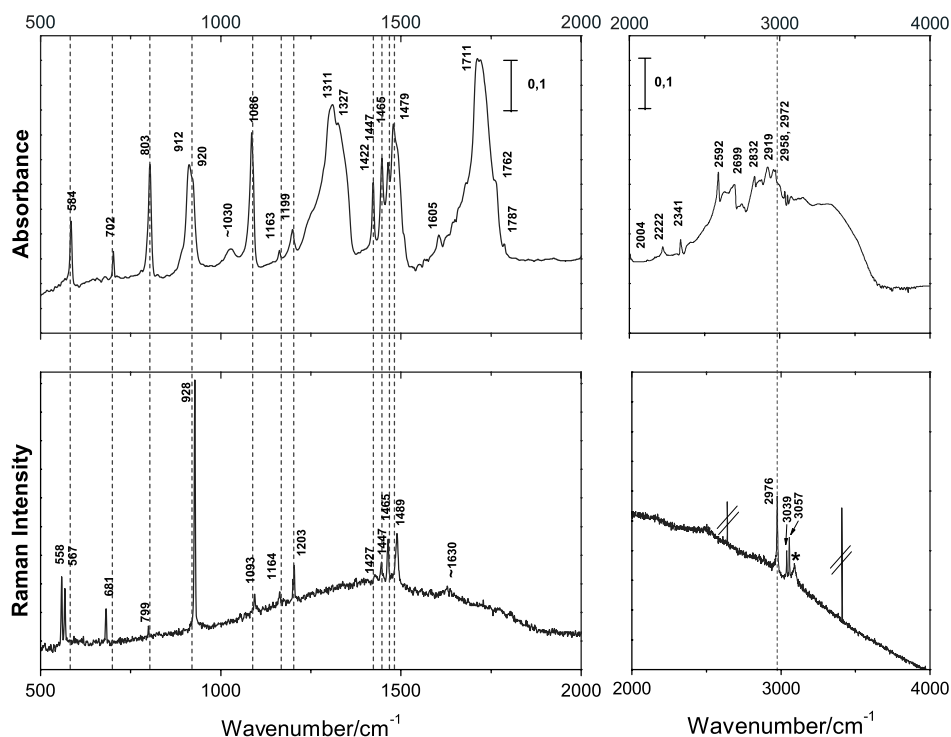


**Figure 1.** Comparison between FT-IR spectrum (top) and Raman spectrum (bottom) of  $\alpha$ -H<sub>2</sub>CO<sub>3</sub>. The comparison between FT-IR spectrum and Raman spectrum of  $\beta$ -H<sub>2</sub>CO<sub>3</sub> is published as Fig. 2 in Kohl et al., *Angew. Chem. Int. Ed.* **2009**, 48, 2690.

**Table 1.** Raman wavenumbers (cm<sup>-1</sup>) of  $\alpha$ -H<sub>2</sub>CO<sub>3</sub>, made by protonation of KHCO<sub>3</sub> in methanolic solution, and their assignment

$\nu$ (cm <sup>-1</sup> )	Raman intensity	Assignment	Di- and polycarboxylic acids, Raman at 20 °C, Refs [59,67]
3057, 3039	m, m	$\nu$ (O–H)	
2976	s	$\nu$ (O–H)	
1630	vw	$\nu$ (C=O), acid I	1647–1782
1489, 1465, 1447, 1427	m, m, w, vw	$\nu_{as}$ [C(OH) <sub>2</sub> ], acid II	1367–1437
1203	m	$\delta$ (COH), acid III	1219–1275
1164	w		
1093	w	$\nu_s$ [C(OH) <sub>2</sub> ]	
928	vs	$\pi$ (OH), $\delta_{oop}$ (COH· · O), acid IV	915–950 (IR)
799	w	$\delta_{oop}$ (CO <sub>3</sub> )	
681	m	$\delta$ (COO), acid V	641–684
567, 558	s, s	$\rho$ (COO), $\delta_{ip}$ (CO <sub>3</sub> ), acid VI	442–601
149			
134			
113			

Low wavenumber modes (<400 cm<sup>-1</sup>) are listed in Table 3. Spectra were recorded at ~80 K and ~10 mbar.

In the OH stretching region, we find two intense Raman bands at 3057 and at 3039 cm<sup>-1</sup> as well as a very strong band at 2976 cm<sup>-1</sup>, which we detect as weak bands in the IR. By contrast, we cannot find the IR overtones at 2701 and 2593 cm<sup>-1</sup> in the Raman spectrum.<sup>[41]</sup> The absence of overtones in the Raman spectrum was expected because only a very small fraction of photons is scattered inelastically in the Raman process. The absence of these bands, therefore, corroborates the earlier assignment of these IR bands to overtones and combination bands (see Table 1 in Ref. [41]). We attribute the Raman band centered in Fig. 1 at ~3090 cm<sup>-1</sup> to the O–H stretching vibration of hexagonal ice (ice *1h*)<sup>[60]</sup> that

had condensed onto the film during the transfer of the film and the disk from the IR apparatus to the Raman microstat. Also, the translational mode of ice *1h* centered at 225 cm<sup>-1</sup> is detected in this film (Fig. 2, bottom).<sup>[61,62]</sup> The band at ~3090 cm<sup>-1</sup> is also observable in the Raman spectra of D<sub>2</sub>CO<sub>3</sub> samples (not shown) and shows a significantly higher full width at half-maximum, which is consistent with our assignment of this band to ice *1h*. We note that the carboxylic acid OH stretching bands are generally weak in the Raman spectrum.<sup>[58]</sup> Whereas we were unable to detect it reliably in case of  $\beta$ -H<sub>2</sub>CO<sub>3</sub>,<sup>[14]</sup> we did detect (at least) three sharp bands in case of  $\alpha$ -H<sub>2</sub>CO<sub>3</sub>. We interpret these bands due

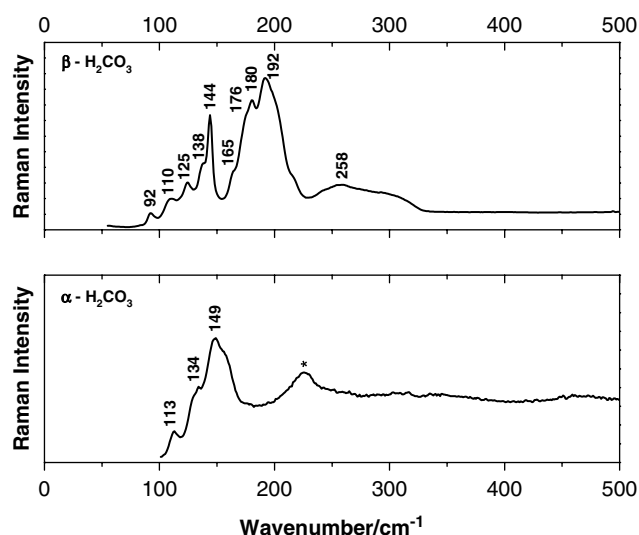


**Figure 2.** Low wavenumber Raman modes ( $<500\text{ cm}^{-1}$ ) in  $\beta\text{-H}_2\text{CO}_3$  (top) and  $\alpha\text{-H}_2\text{CO}_3$  (bottom).

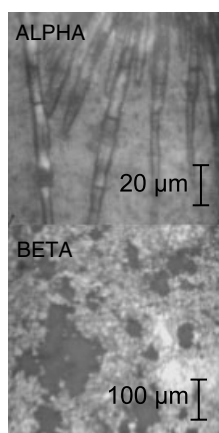


**Figure 3.** Microscopy images of  $\alpha\text{-H}_2\text{CO}_3$  (top) and  $\beta\text{-H}_2\text{CO}_3$  (bottom). The images were recorded at 80 K in the Raman microstat using the confocal Raman microscope equipped with a  $50\times$  ULWD objective. Raman spectra of  $\alpha$ -carbonic acid as depicted in Figs 1 and 2 were obtained only when focusing directly on the needles, whereas no bands at all were obtained when focusing slightly beneath the needles. Raman spectra of  $\beta$ -carbonic acid as shown in Fig. 2 and in Ref. [14] were obtained by focusing the laser on the dark sites.

to the OH groups in (at least) three different environments, two of which might be similar because of the very small wavenumber shift and one being inherently different. Tentatively, we assign two weakly intermolecular-bonded OH groups and one more strongly hydrogen-bonded OH group at lower wavenumbers. The picture of two weakly interacting catemer chains appears. Every chain has the same kind of intrachain hydrogen bonds and OH groups sticking out alternately to the left and right of the chain direction. These OH groups might loosely interact with the neighboring chains, thereby producing sheets of carbonic acid.

The intense and structured carbonyl stretching band in the IR spectrum of  $\alpha\text{-H}_2\text{CO}_3$  is centered at  $1711\text{ cm}^{-1}$ . The  $\text{C}=\text{O}$  stretching mode is observed typically in the  $1780\text{ cm}^{-1}$  region for isolated carboxylic acids and is shifted to  $1720\text{ cm}^{-1}$  on hydrogen-bond formation.<sup>[59]</sup> In the Raman spectrum, the  $\text{C}=\text{O}$  stretch is

typically observed at much lower intensity in most carboxylic acid polymorphs<sup>[59]</sup> and shifted to lower wavenumbers. The difference, which is also referred to as factor-group splitting, is typically on the order of  $30\text{--}50\text{ cm}^{-1}$ . In case of carbonic acid, we observe a very weak Raman band at  $\sim 1630\text{ cm}^{-1}$ , which implies a splitting  $\Delta\nu(\text{C}=\text{O})$  of  $\sim 80\text{ cm}^{-1}$ . The large splitting between the Raman  $\nu_3\text{C}=\text{O}$  mode and the IR  $\nu_{\text{as}}\text{C}=\text{O}$  mode is characteristic for carboxylic acid dimers<sup>[59]</sup> and has been examined theoretically for the formic acid dimer.<sup>[63,64]</sup> The  $\Delta\nu(\text{C}=\text{O})$  value  $\sim 80\text{ cm}^{-1}$  is consistent with splittings obtained in various calculations of the carbonic acid dimer.<sup>[14,65]</sup> If the carbonyl group in the acid were not hydrogen-bonded or formed only (an) internal hydrogen bond(s), then one would expect a band in the range  $1705\text{--}1760\text{ cm}^{-1}$  in both the IR and Raman spectra.<sup>[66,67]</sup> The absence of the Raman band in this region and the large splitting are strong indications for the presence of a dimer or a longer polymeric chain in  $\alpha\text{-H}_2\text{CO}_3$ . Different polymorphs of di- and polycarboxylic acids such as oxalic acid, malonic acid or citric acid show the Raman active antisymmetric stretch  $\nu(\text{C}=\text{O})$  at  $1647\text{--}1782\text{ cm}^{-1}$ .<sup>[59,67]</sup> As a consequence of the OH group directly connected to the carboxyl group rather than a carbon atom, both  $\alpha\text{-H}_2\text{CO}_3$  ( $1630\text{ cm}^{-1}$ ) and  $\beta\text{-H}_2\text{CO}_3$  ( $1608\text{ cm}^{-1}$ ) show weak Raman bands at even lower wavenumbers. We, therefore, assign this band as the acid I band in Table 1 and suggest a chainlike catemer motif for  $\alpha\text{-H}_2\text{CO}_3$ .

The simultaneous appearance of bands in the Raman and IR is best evidenced at  $500\text{--}1500\text{ cm}^{-1}$ . All bands observed in the Raman spectrum in this region can also be observed at very similar positions in the IR. These are marked by vertical dashed lines in Fig. 1. Bandsplitting is apparent in both IR and Raman spectra, especially in the COH deformation region between  $1430$  and  $1490\text{ cm}^{-1}$ , where four bands separated by approximately  $20\text{ cm}^{-1}$  are observed in both spectra. Also, this band system falls outside the range typically seen in other carboxylic or dicarboxylic acids, namely  $1367\text{--}1437\text{ cm}^{-1}$  (cf Table 1). This might again be explained in terms of the second OH group directly attached to the  $\text{C}=\text{O}$  group, and so we assign these bands as the acid II bands. Bands at  $1203$  and  $1164\text{ cm}^{-1}$  are intense in Raman but weak in the IR. The intense IR band at  $1087\text{ cm}^{-1}$  has a Raman counterpart at  $1093\text{ cm}^{-1}$ . The most intense Raman band at  $928\text{ cm}^{-1}$  can be attributed to the split band in the IR spectrum at  $912/920\text{ cm}^{-1}$ . The IR active band at  $803\text{ cm}^{-1}$  has its counterpart at  $799\text{ cm}^{-1}$  in the Raman. The Raman bands in the skeletal region at  $681\text{ cm}^{-1}$  and the doublet at  $567$  and  $558\text{ cm}^{-1}$  are shifted by *ca.*  $+20\text{ cm}^{-1}$  to  $702$  and  $584\text{ cm}^{-1}$ . The latter band is only resolved as a doublet in the Raman but not in the IR. All these coincidences between Raman and IR clearly show that the principle of mutual exclusion does not hold in case of  $\alpha\text{-H}_2\text{CO}_3$ , in contrast to the situation in  $\beta\text{-H}_2\text{CO}_3$ .<sup>[14]</sup> A local center of inversion and the cyclic centrosymmetric dimer of carbonic acid (depicted in Fig. 4(a)) can clearly be ruled out to be the building block of  $\alpha\text{-H}_2\text{CO}_3$ , whereas we suggest this dimer to be the building block of  $\beta\text{-H}_2\text{CO}_3$ .<sup>[14]</sup> The large factor-group splitting in case of  $\alpha\text{-H}_2\text{CO}_3$  suggests that other types of dimers, oligomers or chainlike structures rather than well-separated monomers build  $\alpha\text{-H}_2\text{CO}_3$ . We also want to emphasize that we have interpreted the IR spectra to indicate the presence of two different conformational or H-bonded states of carbonic acid.<sup>[41]</sup> This assessment has been based on the observation of two intense IR band systems assignable to the asymmetric COH stretching modes, namely at  $1311/1327\text{ cm}^{-1}$  and  $1422/1447/1465/1479\text{ cm}^{-1}$ , respectively (Fig. 1, top). In the Raman spectra, only the latter band system,

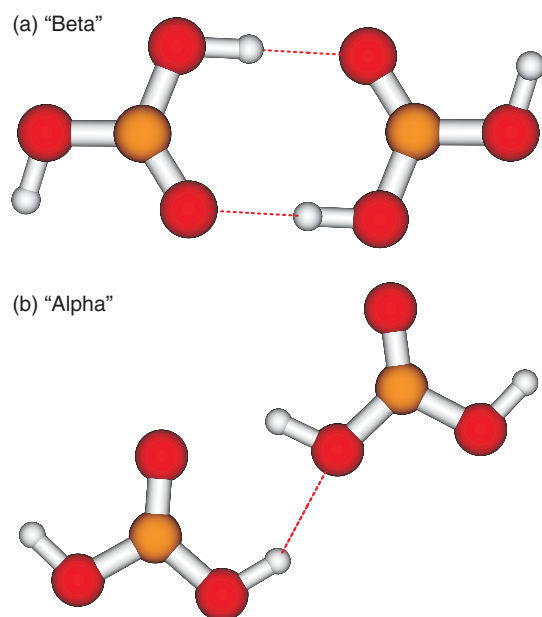


**Figure 4.** (a) Local structural motif suggested for  $\beta$ -H<sub>2</sub>CO<sub>3</sub> containing a center of inversion ( $C_{2h}$  point group). (b) Candidate local structural motif suggested for  $\alpha$ -H<sub>2</sub>CO<sub>3</sub> without a center of inversion ( $C_s$  point group symmetry).

but not the former, is observed. We explain this in terms of at least two carbonic acid entities in the primitive unit cell, and we assume that this is due to an element of symmetry in the unit cell other than a center of inversion. If we follow the picture of two catemer chains connected by weak interchain hydrogen bonds, then there are two different C(OH)<sub>2</sub> stretch vibrations in every chain: one with two hydrogen-bonded OH groups, and the other with one hydrogen-bonded OH group. We expect the completely interconnected C(OH)<sub>2</sub> group at lower wavenumbers and an increase of the full width at half-maximum due to the interaction, as observed in the FT-IR spectra. At the same time, we expect a stronger change of the symmetry for these groups. This might be the reason for its disappearance in the Raman spectra, in accordance with the symmetry selection rules.

Murillo *et al.*<sup>[68]</sup> have suggested a large number of different dimers, which might serve as the fundamental dimeric unit building such a catemer chain. We have selected among these some energetically rather low-lying dimers, which are capable of producing chainlike structures and which do not show a center of inversion. One candidate structure, which we regard as a good candidate building block of  $\alpha$ -H<sub>2</sub>CO<sub>3</sub> is depicted in Fig. 4(b). We wish to emphasize, though, that also other dimers not containing a center of inversion are possible as building blocks of  $\alpha$ -H<sub>2</sub>CO<sub>3</sub>. For instance, we also regard a crystal structure built from *cis-trans* carbonic acid monomers as consistent with the Raman spectroscopic results. These monomers could build linear chains via single (stronger) hydrogen bonds connecting one OH group from the first carbonic acid molecule with the C=O group of the second carbonic acid molecule. The second OH group in each carbonic acid molecule would link one linear chain of carbonic acid molecules with the other by forming (weaker) hydrogen bonds.

Recently, some candidate crystal structures have been predicted by Reddy *et al.*<sup>[69]</sup> and by us.<sup>[43]</sup> From the considerations mentioned above, the crystal structures shown in Figs. 1 and 5 in Ref. [69] and

in Fig. 5(b) and (c) in Ref. [43] are possible candidate structures for  $\beta$ -H<sub>2</sub>CO<sub>3</sub> but not for  $\alpha$ -H<sub>2</sub>CO<sub>3</sub>. By contrast, the crystal structures in Figs. 2–5 in Ref. [69] and in Fig. 5(a) and (d) in Ref. [43] are possible candidate structures for  $\alpha$ -H<sub>2</sub>CO<sub>3</sub> but not for  $\beta$ -H<sub>2</sub>CO<sub>3</sub>. In the absence of IR and Raman solid state spectra calculated from various candidate structures, the experimental IR and Raman data do not allow us to pick a specific crystal structure as the best candidate at present. However, they allow restricting which kind of structures are possible and which are not possible from symmetry considerations.

### Low wavenumber Raman spectra

It is well known that low wavenumber Raman spectra show highly characteristic patterns allowing easy discrimination between different crystals. This fingerprint information was recently employed to clearly distinguish between different solid nitric acid hydrates, including metastable polymorphs.<sup>[70,71]</sup> At  $<400\text{ cm}^{-1}$ ,  $\beta$ -H<sub>2</sub>CO<sub>3</sub> shows more Raman bands than  $\alpha$ -H<sub>2</sub>CO<sub>3</sub> (see Fig. 2). This is in contrast to the situation encountered at  $>400\text{ cm}^{-1}$  (see discussion above). While we explain the higher number of Raman bands at  $>400\text{ cm}^{-1}$  in  $\alpha$ -H<sub>2</sub>CO<sub>3</sub> in terms of missing local symmetry, the low number of Raman bands at  $<400\text{ cm}^{-1}$  hints at a rather simple unit cell for  $\alpha$ -H<sub>2</sub>CO<sub>3</sub>. By contrast, the unit cell in  $\beta$ -H<sub>2</sub>CO<sub>3</sub> could be more complex and contain more carbonic acid molecules. The lower limit for internal modes in a dicarboxylic acid is around  $250\text{ cm}^{-1}$ .<sup>[57]</sup> Whereas there are bands at  $250\text{--}500\text{ cm}^{-1}$  in case of  $\beta$ -H<sub>2</sub>CO<sub>3</sub>,<sup>[14]</sup> there is none in case of  $\alpha$ -H<sub>2</sub>CO<sub>3</sub>. There are only four bands at  $225, 149, 134$  and  $113\text{ cm}^{-1}$  detected at  $<400\text{ cm}^{-1}$  in  $\alpha$ -H<sub>2</sub>CO<sub>3</sub> (see Table 3). As mentioned above, the band at  $225\text{ cm}^{-1}$  (Fig. 2, bottom) can also arise from the translational band in condensed hexagonal ice. By contrast, at least ten bands appear in case of  $\beta$ -H<sub>2</sub>CO<sub>3</sub> in this region (see Fig. 2, top and Table 2). This includes the most intense Raman band appearing at  $192\text{ cm}^{-1}$ , which is missing in  $\alpha$ -H<sub>2</sub>CO<sub>3</sub>. A Raman band at  $194\text{ cm}^{-1}$  was recently detected in supersonic jet expansion studies of formic acid and attributed to the inter-monomer stretching mode in cyclic, centrosymmetric dimers of formic acid, i.e. the RC(OHO)<sub>2</sub>CR entity with R=H.<sup>[72]</sup> Also, in matrix isolation studies of gas-phase formic acid, an  $A_g$  band was found at  $196\text{ cm}^{-1}$ , which was attributed to this mode.<sup>[73]</sup> The cyclic centrosymmetric dimer of carbonic acid contains the same RC(OHO)<sub>2</sub>CR subunit with R=OH, and so this band might be attributed to the inter-monomer stretch in the cyclic dimer of  $C_{2h}$  symmetry (see Fig. 4(a)). Indeed, we calculate the Raman active inter-monomer normal mode of  $A_g$  type to be  $190 \pm 2\text{ cm}^{-1}$  at B3LYP and MP2 levels of theory using 6–31 + G(d) or aug-cc-pVDZ basis sets from the geometry shown in Fig. 4(a). We thus suggest the mode at  $192\text{ cm}^{-1}$  observed in  $\beta$ -H<sub>2</sub>CO<sub>3</sub> (Fig. 2, top) to be the inter-monomer stretching mode. Also, the intense modes observed at  $165$  and  $125\text{ cm}^{-1}$  agree very well with the predicted Raman modes at  $166 \pm 4$  and  $125 \pm 5\text{ cm}^{-1}$  (see Table 2). By contrast, the modes at  $176, 144$  or  $110\text{ cm}^{-1}$  are not predicted from this simplified gas-phase calculation and might necessitate consideration of larger clusters, inclusion of crystal symmetry and a proper description of the crystal field. The mode at  $144\text{ cm}^{-1}$ , for instance, appears in our calculation of the centrosymmetric carbonic acid tetramer (see Table 2). Calculation of vibrational spectra for all at least 200 different candidate crystal structures<sup>[43]</sup> are, however, not feasible.

The harmonic frequency calculations on the dimer depicted in Fig. 4(b) show two Raman active bands in the range

**Table 2.** Low wavenumber Raman modes ( $\text{cm}^{-1}$ ) of  $\beta\text{-H}_2\text{CO}_3$  obtained at  $\sim 80$  K

Experimental $\nu$ ( $\text{cm}^{-1}$ )	Raman intensity	Calculated (Fig. 4(a))	$\beta$ -Oxalic acid Ref. [76]
258	m, br		
192	vs	$190 \pm 2$ ( $A_g$ )	189 ( $A_g$ )
176	s		167/187 ( $B_g$ )
165	sh	$166 \pm 4$ ( $A_g$ )	159 ( $A_g$ )
144	s		
138	sh		
125	?	$121 \pm 2$ ( $B_g$ )	131 ( $B_g$ )
110	?		
92	?		

Note that experimental Raman intensities decay considerably at  $<150$   $\text{cm}^{-1}$  because of the use of a strong filter for the intense Rayleigh scattering (at  $0$   $\text{cm}^{-1}$ ). Calculated wavenumbers refer to gas-phase calculations in the harmonic approximation for the geometry depicted in Fig. 4(a). Error bars are given from a comparison of B3LYP and MP2 calculations and a comparison of different basis sets. Data at 300 K are from Ref. [76] and are corrected by  $+10$   $\text{cm}^{-1}$  in order to correct for the temperature change from 300 K to  $\sim 80$  K.

**Table 3.** Low wavenumber Raman modes ( $\text{cm}^{-1}$ ) of  $\alpha\text{-H}_2\text{CO}_3$  obtained at  $\sim 80$  K

Experimental $\nu$ ( $\text{cm}^{-1}$ )	Raman intensity	Calculated (Fig. 4(b))	$\alpha$ -Oxalic acid Ref. [76]
225	m, br	220 ( $A'$ )	
149	vs		161
134	s	135 ( $A'$ )	127/138
113	m		117

Note that experimental Raman intensities decay considerably at  $<150$   $\text{cm}^{-1}$  because of the use of a strong filter for the intense Rayleigh scattering (at  $0$   $\text{cm}^{-1}$ ). Calculated wavenumbers refer to gas-phase calculations in the harmonic approximation for the geometry. Most intense bands from Ref. [76] are given (90 K data).

$100\text{--}500$   $\text{cm}^{-1}$ , namely two  $A'$  modes at  $135$  and  $220$   $\text{cm}^{-1}$ . Most noteworthy, the mode at  $192$   $\text{cm}^{-1}$  is clearly absent in such type of dimer and, furthermore, the two predicted Raman bands can also be found in the measured spectrum of  $\alpha\text{-H}_2\text{CO}_3$  (Fig. 2, bottom and Table 3). We wish to emphasize that the observed mode at  $225$   $\text{cm}^{-1}$  might also arise from hexagonal ice condensed during sample transfer (see above). However, the broad, tailed nature of this band is also consistent with the presence of both hexagonal ice and carbonic acid dimer translational bands. In fact, band deconvolution is consistent with two weakly separated bands producing the band shape in Fig. 2, bottom. Of course, we have also considered other types of dimers, trimers and tetramers including the non-planar T-shaped dimer similar to the structures depicted in Fig. 4 in Ref. [68]. However, none of these can explain the vibrational features in the low wavenumber Raman spectrum of  $\beta\text{-H}_2\text{CO}_3$  and  $\alpha\text{-H}_2\text{CO}_3$  better than the structures depicted in Fig. 4(a) and (b), respectively.

The main finding of the absence of the Raman band at  $192$   $\text{cm}^{-1}$  in crystal structures based on non-centrosymmetric dimers is also found in the related case of oxalic acid. Just like in carbonic acid, there are also two polymorphs in oxalic acid.<sup>[74]</sup> And just like in carbonic acid, the crystal structure of the  $\beta$ -polymorph is based on

the centrosymmetric dimer, whereas the crystal structure of the  $\alpha$ -polymorph is not based on the centrosymmetric motif (see Fig. 1 in Ref. [75]). The Raman spectra of both polymorphs, including the low wavenumber region, were measured by DeVillepin and coworkers.<sup>[76]</sup> The most intense Raman modes in  $\alpha$ -oxalic acid were found at  $148$ ,  $130$ ,  $121$  and  $110$   $\text{cm}^{-1}$  at  $300$  K, which shifted by  $+7$  to  $+13$   $\text{cm}^{-1}$  when cooling the sample to  $90$  K. This compares very well with the Raman spectrum of  $\alpha$ -carbonic acid (Fig. 2, bottom). In case of  $\beta$ -oxalic acid, two  $A_g$  modes are observed at  $179$  and  $149$   $\text{cm}^{-1}$  at  $300$  K. The data at  $90$  K are not reported, but assuming a shift of  $+10$   $\text{cm}^{-1}$  these two modes would be at  $189$  and  $159$   $\text{cm}^{-1}$ , in excellent agreement with the observed spectrum of  $\beta$ -carbonic acid (Fig. 2, top). Also the three  $B_g$  modes observed in  $\beta$ -oxalic acid at  $121$ ,  $157$  and  $177$   $\text{cm}^{-1}$  are quite similar to the modes observed in  $\beta$ -carbonic acid (Fig. 2, top), most notably the  $B_g$  mode at  $121$   $\text{cm}^{-1}$ , which also appears in the gas-phase calculation of the cyclic dimer. We, thus, conclude that the observed low wavenumber Raman spectra are also consistent with the suggestion of the centrosymmetric dimer (Fig. 4(a)) as the local motif in  $\beta\text{-H}_2\text{CO}_3$  and a non-centrosymmetric dimer as the local motif in  $\alpha\text{-H}_2\text{CO}_3$  (Fig. 4(b)). Whether this local motif results in a sheet-like crystal structure or a chain-like catemer type one cannot be answered from the Raman data reported here and needs to be clarified in future work.

## Discussion/Conclusions

In summary, we report here the Raman spectra of  $\alpha\text{-H}_2\text{CO}_3$  including the low wavenumber range. In addition, we report new low wavenumber Raman data for  $\beta\text{-H}_2\text{CO}_3$ . While this type of Raman spectra has been reported between  $30$  and  $100$  years ago for other carboxylic or dicarboxylic acids such as formic acid,<sup>[77,78]</sup> oxalic acid,<sup>[76,79–81]</sup> malonic acid<sup>[57,79,82]</sup> or acetic acid,<sup>[67]</sup> the smallest organic acid, containing only one C atom, has eluded attempts of Raman characterization until 2009.<sup>[14]</sup> Because of the possible astrophysical relevance of carbonic acid<sup>[2–15]</sup> and the possibility of exploring astrophysical objects such as Mars using Raman spectroscopy,<sup>[83–88]</sup> the data are of importance in possibly identifying  $\alpha\text{-H}_2\text{CO}_3$  in outer space. For this purpose, the most intense band at  $928$   $\text{cm}^{-1}$  seems to be the best marker band. For comparison, the most intense band in  $\beta\text{-H}_2\text{CO}_3$  is located at  $1054$   $\text{cm}^{-1}$ , while there is no band close to  $928$   $\text{cm}^{-1}$ . Because of the separation of  $>100$   $\text{cm}^{-1}$  and the high intensity of the two bands, the  $\alpha$ - and  $\beta$ -polymorphs of carbonic acid can be easily discriminated by Raman spectroscopy. For comparison, the most intense Raman band in aqueous carbonic acid attributed to the C–OH stretching vibration is at  $1017$   $\text{cm}^{-1}$ .<sup>[26]</sup>

The interpretation of vibrational spectra provides valuable data, in particular concerning the local short-range ordering in these polymorphs. A comparison between IR and Raman spectra reveals that the principle of mutual exclusion only holds for  $\beta\text{-H}_2\text{CO}_3$  but not for  $\alpha\text{-H}_2\text{CO}_3$ . This suggests a local center of inversion in the former and the absence of such a center in the latter. Comparison of the observed Raman spectra with gas-phase calculations of simple carbonic acid dimers (*cf.* Fig. 4) is consistent with the idea of the centrosymmetric dimer shown in Fig. 4(a) building the  $\beta$ -polymorph and a non-centrosymmetric dimer similar to the one shown in Fig. 4(b) building the  $\alpha$ -polymorph. A similar situation of the cyclic, centrosymmetric  $\text{RC(OH)}_2\text{CR}$  motif is encountered in  $\beta$ -oxalic acid ( $\text{R}=\text{COOH}$ ),<sup>[76]</sup> and interestingly its low wavenumber Raman pattern observed resembles the one

observed here for  $\beta$ -carbonic acid ( $R=OH$ ). Most notably, the inter-monomer stretching mode is observed in both cases at approximately  $190\text{ cm}^{-1}$ . Similarly, the inter-monomer stretching mode in gas-phase formic acid ( $R=H$ ) is also observed at  $194\text{ cm}^{-1}$ , thus confirming the assignment of the intense Raman mode in  $\beta\text{-H}_2\text{CO}_3$  at  $192\text{ cm}^{-1}$ .<sup>[72]</sup> By contrast, this mode is missing in both  $\alpha$ -oxalic acid and  $\alpha$ -carbonic acid. Whereas it is known that the former has a sheet-like crystal structure built from oxalic acid dimers connected by hydrogen bonds at heads and tails, we infer from the present data that a similar situation is encountered in case of  $\alpha$ -carbonic acid. Whether  $\alpha$ -carbonic acid can be characterized on the long range by chain-like structures or by planar or wavy sheets and which monomer conformation is present cannot be answered from the present work. All of these possibilities can be found among the predicted candidate structures for carbonic acid,<sup>[43,69]</sup> and elucidation of the crystal structure will require future work. The Raman spectra presented here constitute an important guide for the process of determining the crystal structures of the two known polymorphs of carbonic acid, which is probably one of the last fundamental small molecules for which the crystal structure is unknown.

### Acknowledgements

We gratefully acknowledge discussions with Sarah L. Price and financial support by the Austrian Science Fund (project P18187) and the European Research Council (ERC Starting Grant SULIWA).

### References

- [1] T. Loerting, J. Bernard, *ChemPhysChem* **2010**, *11*, 2305.
- [2] J. S. Lewis, D. H. Grinspoon, *Science* **1990**, *249*, 1273.
- [3] N. DelloRusso, R. K. Khanna, M. H. Moore, *J. Geophys. Res. Planets* **1993**, *98*, 5505.
- [4] R. K. Khanna, J. A. Tossell, K. Fox, *Icarus* **1994**, *112*, 541.
- [5] W. Hage, A. Hallbrucker, E. Mayer, *J. Chem. Soc., Farad. Trans.* **1995**, *91*, 2823.
- [6] J. R. Brucato, A. C. Castorina, M. E. Palumbo, M. A. Satorre, G. Strazzulla, *Planet. Space Sci.* **1997**, *45*, 835.
- [7] G. Strazzulla, J. R. Brucato, G. Cimino, M. E. Palumbo, *Planet. Space Sci.* **1996**, *44*, 1447.
- [8] W. Hage, K. R. Liedl, A. Hallbrucker, E. Mayer, *Science* **1998**, *279*, 1332.
- [9] M. L. Delitsky, A. L. Lane, *J. Geophys. Res. [Planets]* **1998**, *103*, 31391.
- [10] R. L. Hudson, M. H. Moore, *J. Geophys. Res. [Planets]* **2001**, *106*, 33275.
- [11] M. H. Moore, R. L. Hudson, P. A. Gerakines, *Spectrochim. Acta* **2001**, *57A*, 843.
- [12] M. H. Moore, R. L. Hudson, R. F. Ferrante, *Earth, Moon, and Planets* **2003**, *92*, 291.
- [13] R. L. Hudson, *J. Chem. Educ.* **2006**, *83*, 1611.
- [14] I. Kohl, K. Winkel, M. Bauer, K. R. Liedl, T. Loerting, E. Mayer, *Angew. Chem., Int. Ed.* **2009**, *48*, 2690.
- [15] Z. Peeters, R. L. Hudson, M. H. Moore, A. Lewis, *Icarus* **2010**, *210*, 480.
- [16] A. Khanna, N. A. Kurtzman, *J. Nephrol.* **2006**, *19*, S86.
- [17] P. Swietach, R. D. Vaughan-Jones, A. L. Harris, *Cancer Metastasis Rev.* **2007**, *26*, 299.
- [18] R. D. Vaughan-Jones, K. W. Spitzer, P. Swietach, *J. Mol. Cell. Cardiol.* **2009**, *46*, 318.
- [19] G. Liamis, H. J. Milionis, M. Elisaf, *Drug Saf.* **2010**, *33*, 371.
- [20] C. L. Sabine, R. A. Feely, N. Gruber, R. M. Key, K. Lee, J. L. Bullister, R. Wanninkhof, C. S. Wong, D. W. R. Wallace, B. Tilbrook, F. J. Millero, T.-H. Peng, A. Kozyr, T. Ono, A. F. Rios, *Science* **2004**, *305*, 367.
- [21] R. A. Feely, C. L. Sabine, K. Lee, W. Berelson, J. Kleypas, V. J. Fabry, F. J. Millero, *Science* **2004**, *305*, 362.
- [22] J. C. Orr, V. J. Fabry, O. Aumont, L. Bopp, S. C. Doney, R. A. Feely, A. Gnanadesikan, N. Gruber, A. Ishida, F. Joos, R. M. Key, K. Lindsay, E. Maier-Reimer, R. Matear, P. Monfray, A. Mouchet, R. G. Najjar, G.-K. Plattner, K. B. Rodgers, C. L. Sabine, J. L. Sarmiento, R. Schlitzer, R. D. Slater, I. J. Totterdell, M.-F. Weirig, Y. Yamanaka, A. Yool, *Nature* **2005**, *437*, 681.
- [23] P. Glynn, *Rev. Mineral. Geochem.* **2000**, *40*, 481.
- [24] J. W. Morse, R. S. Arvidson, *Earth-Sci. Rev.* **2002**, *58*, 51.
- [25] R. Kruse, E. U. Franck, *Ber. Bunsenges. Phys. Chem.* **1982**, *86*, 1036.
- [26] H. Falcke, S. H. Eberle, *Water Res.* **1990**, *24*, 685.
- [27] K. Adamczyk, M. Premont-Schwarz, D. Pines, E. Pines, E. T. J. Nibbering, *Science* **2009**, *326*, 1690.
- [28] J. K. Terlouw, C. B. Lebrilla, H. Schwarz, *Angew. Chem., Int. Ed.* **1987**, *26*, 354.
- [29] T. Mori, K. Suma, Y. Sumiyoshi, Y. Endo, *J. Chem. Phys.* **2009**, *130*, 204308.
- [30] T. Mori, K. Suma, Y. Sumiyoshi, Y. Endo, *J. Chem. Phys.* **2011**, *134*, 044319.
- [31] J. Bernard, M. Seidl, I. Kohl, E. Mayer, K. R. Liedl, O. Galvez, H. Grothe, T. Loerting, *Angew. Chem. Int. Ed.* **2011**, *50*, 1939.
- [32] M. H. Moore, R. Khanna, B. Donn, *J. Geophys. Res. [Planets]* **1991**, *96*, 17541.
- [33] M. H. Moore, R. K. Khanna, *Spectrochim. Acta* **1991**, *47A*, 255.
- [34] J. R. Brucato, M. E. Palumbo, G. Strazzulla, *Icarus* **1997**, *125*, 135.
- [35] G. Strazzulla, G. Leto, F. Spinella, O. Gomis, *Astrobiology* **2005**, *5*, 612.
- [36] P. A. Gerakines, M. H. Moore, R. L. Hudson, *Astron. Astrophys.* **2000**, *357*, 793.
- [37] M. Garozzo, D. Fulvio, O. Gomis, M. E. Palumbo, G. Strazzulla, *Planet. Space Sci.* **2008**, *56*, 1300.
- [38] Y. Oba, N. Watanabe, A. Kouchi, T. Hama, V. Pirronello, *Astrophys. J.* **2010**, *722*, 1598.
- [39] W. Hage, A. Hallbrucker, E. Mayer, *J. Am. Chem. Soc.* **1993**, *115*, 8427.
- [40] W. Hage, A. Hallbrucker, E. Mayer, *J. Chem. Soc., Farad. Trans.* **1996**, *92*, 3197.
- [41] W. Hage, A. Hallbrucker, E. Mayer, *J. Chem. Soc., Farad. Trans.* **1996**, *92*, 3183.
- [42] W. Hage, A. Hallbrucker, E. Mayer, *J. Mol. Struct.* **1997**, *408*, 527.
- [43] K. Winkel, W. Hage, T. Loerting, S. L. Price, E. Mayer, *J. Am. Chem. Soc.* **2007**, *129*, 13863.
- [44] H. A. Al-Hosney, V. H. Grassian, *J. Am. Chem. Soc.* **2004**, *126*, 8068.
- [45] H. A. Al-Hosney, S. Carlos-Cuellar, J. Baltrusaitis, V. H. Grassian, *Phys. Chem. Chem. Phys.* **2005**, *7*, 3587.
- [46] H. A. Al-Hosney, V. H. Grassian, *Phys. Chem. Chem. Phys.* **2005**, *7*, 1266.
- [47] J. Baltrusaitis, J. D. Schuttlefield, E. Zeitler, J. H. Jensen, V. H. Grassian, *J. Phys. Chem. C* **2007**, *111*, 14870.
- [48] J. Baltrusaitis, V. H. Grassian, *J. Phys. Chem. A* **2010**, *114*, 2350.
- [49] J. A. Tossell, *Inorg. Chem.* **2006**, *45*, 5961.
- [50] T. Venkatarayudu, *J. Chem. Phys.* **1954**, *22*, 1269.
- [51] A. R. H. Cole, J. R. Durig, *J. Raman Spectrosc.* **1975**, *4*, 31.
- [52] R. Mendelsohn, E. U. Monse, *J. Chem. Educ.* **1981**, *58*, 582.
- [53] S. F. Parker, H. Herman, *Spectrochim. Acta* **1997**, *53A*, 119.
- [54] R. L. Frost, M. L. Weier, *J. Raman Spectrosc.* **2003**, *34*, 776.
- [55] I. Kohl, L. Bachmann, A. Hallbrucker, E. Mayer, T. Loerting, *Phys. Chem. Chem. Phys.* **2005**, *7*, 3210.
- [56] G. Strazzulla, G. A. Barratta, M. E. Palumbo, M. A. Satorre, *Nucl. Instrum. Methods Phys. Res. Sect. B* **2000**, *166–167*, 13.
- [57] D. Bougeard, J. De Villepin, A. Novak, *Spectrochim. Acta* **1988**, *44A*, 1281.
- [58] D. Lin-Vien, N. B. Colthup, W. G. Fateley, J. G. Grasselli, *The Handbook of Infrared and Raman Characteristic Frequencies of Organic Molecules*, Academic Press: New York, **1991**.
- [59] I. Wolfs, H. O. Desseyn, *Appl. Spectrosc.* **1996**, *50*, 1000.
- [60] P. T. T. Wong, E. Whalley, *J. Chem. Phys.* **1975**, *62*, 2418.
- [61] M. J. Taylor, E. Whalley, *J. Chem. Phys.* **1964**, *40*, 1660.
- [62] P. T. T. Wong, E. Whalley, *J. Chem. Phys.* **1976**, *65*, 829.
- [63] W. L. Qian, S. Krimm, *J. Phys. Chem.* **1996**, *100*, 14602.
- [64] W. L. Qian, S. Krimm, *J. Phys. Chem. A* **2002**, *106*, 11663.
- [65] P. Ballone, B. Montanari, R. O. Jones, *J. Chem. Phys.* **2000**, *112*, 6571.
- [66] N. B. Colthup, L. H. Daly, S. E. Wiberley, *Introduction to Infrared and Raman Spectroscopy*, Academic Press: New York, **1964**.
- [67] F. R. Dollish, W. G. Fateley, F. F. Bentley, *Characteristic Raman Frequencies of Organic Compounds*, Wiley: New York, **1974**, pp 105.
- [68] J. Murillo, J. David, A. Restrepo, *Phys. Chem. Chem. Phys.* **2010**, *12*, 10963.
- [69] S. K. Reddy, C. H. Kulkarni, S. Balasubramanian, *J. Chem. Phys.* **2011**, *134*, 124511.
- [70] H. Grothe, C. E. L. Myhre, C. J. Nielsen, *J. Phys. Chem. A* **2006**, *110*, 171.

- [71] R. M. Escribano, D. Fernandez-Torre, V. J. Herrero, B. Martin-Llorente, B. Mate, I. K. Ortega, H. Grothe, *Vib. Spectrosc.* **2007**, *43*, 254.
- [72] P. Zielke, M. A. Suhm, *Phys. Chem. Chem. Phys.* **2007**, *9*, 4528.
- [73] A. Olbert-Majkut, J. Ahokas, J. Lundell, M. Pettersson, *Chem. Phys. Lett.* **2009**, *468*, 176.
- [74] L. J. Bellamy, R. J. Pace, *Spectrochim. Acta* **1963**, *19*, 435.
- [75] I. Nobeli, S. L. Price, *J. Phys. Chem. A* **1999**, *103*, 6448.
- [76] J. De Villepin, A. Novak, D. Bougeard, *Chem. Phys.* **1982**, *73*, 291.
- [77] S. M. Blumenfeld, H. Fast, *Spectrochim. Acta* **1968**, *24*, 1449.
- [78] H. R. Zelsmann, Y. Marechal, A. Chosson, P. Faure, *J. Mol. Struct.* **1975**, *29*, 357.
- [79] D. Hadzi, N. Sheppard, *Proc. Roy. Soc. (London)* **1953**, *A216*, 247.
- [80] J. De Villepin, A. Novak, *Spectrochim. Acta* **1978**, *34A*, 1019.
- [81] J. De Villepin, A. Novak, *Spectrochim. Acta* **1978**, *34A*, 1009.
- [82] J. De Villepin, M. H. Limage, A. Novak, N. Toupry, M. Le Postollec, H. Poulet, S. Ganguly, C. N. R. Rao, *J. Raman Spectrosc.* **1984**, *15*, 41.
- [83] A. Wang, L. A. Haskin, A. L. Lane, T. J. Wdowiak, S. W. Squyres, R. J. Wilson, L. E. Hovland, K. S. Manatt, N. Raouf, C. D. Smith, *J. Geophys. Res., [Planets]* **2003**, *108*, 5005.
- [84] A. Ellery, D. Wynn-Williams, *Astrobiology* **2003**, *3*, 565.
- [85] J. L. Bishop, E. Murad, *J. Raman Spectrosc.* **2004**, *35*, 480.
- [86] J. Popp, M. Schmitt, N. Tarcea, W. Kiefer, M. Hilchenbach, T. Stuffer, S. Hofer, R. Hochleitner, A. Wuttig, R. Riesenberg, *Eur. Space Agency, [Spec. Publ.]* **2005**, *SP-588*, 385.
- [87] P. Sobron, F. Sobron, A. Sanz, F. Rull, *Appl. Spectrosc.* **2008**, *62*, 364.
- [88] J. Jehlicka, A. Culka, H. G. M. Edwards, *Planet. Space Sci.* **2010**, *58*, 875.

# 5 Polymorphism of Carbonic Acid

---

Polymorphism is of importance in fields such as pharmacology, solid-state chemistry and material science.<sup>[46]</sup> It describes the property that a single substance exists in different crystalline manifestations. While polymorphs of substances are built from the same molecules, they differ in structure, as well as physical and chemical characteristics. The different structures can be formed, among others, through pressure and/or temperature influences. For example calcium carbonate ( $\text{CaCO}_3$ ) appears in three different modifications: aragonite (orthorhombic), vaterite (hexagonal) and calcite (trigonal). Carbon – C – has the allotropic modifications graphite, diamond, fullerene and graphene. A molecule which is not too different from  $\text{H}_2\text{CO}_3$  (C1 diprotonic acid) is the C2 diprotonic acid, oxalic acid ( $\text{H}_2\text{C}_2\text{O}_4$ ). Oxalic acid forms two different anhydrous crystal structures as well as a dihydrate. In  $\beta$ -oxalic acid the molecules are connected in long chains by cyclic hydrogen bonds.<sup>[47]</sup> The  $\alpha$ -polymorph crystallizes in a form, in which the carbonyl and hydroxyl groups of a single COOH group are linked with other oxalic acid molecules to form a planar sheet structure.<sup>[47]</sup> The dihydrate's structure is similar to that of  $\beta$ -oxalic acid, but with two molecules of water in-between the carbonyl groups.<sup>[47]</sup>

Twenty years ago our group reported the first isolation of two polymorphs of carbonic acid,<sup>[1, 19-22]</sup> made by protonation of hydrogencarbonate ( $\text{HCO}_3^-$ ) using methanol or water as solvents at low temperature. By reaction of  $\text{HCO}_3^-$  with excess of HCl, both dissolved in  $\text{H}_2\text{O}$ , the  $\beta$ -polymorph of  $\text{H}_2\text{CO}_3$  is formed.<sup>[20]</sup> The  $\alpha$ -polymorph was obtained by reaction of  $\text{HCO}_3^-$  with excess of HCl, with methanol ( $\text{CH}_3\text{OH}$ ) as solvent.<sup>[19]</sup> The formation of  $\text{H}_2\text{CO}_3$  by proton or other high-energy irradiation of cryogenic  $\text{CO}_2:\text{H}_2\text{O}$  mixtures leads to the  $\beta$ -polymorph. Winkel et al. 2007<sup>[3]</sup> discussed the solvent effect on carbonic acid's polyamorphism and polymorphism. By protonation of  $\text{HCO}_3^-$  in methanol/water solution (56 wt% water) amorphous  $\alpha$ - $\text{H}_2\text{CO}_3$  forms, which does not crystallize.<sup>[19]</sup>  $\beta$ - $\text{H}_2\text{CO}_3$  could be transformed into amorphous  $\alpha$ - $\text{H}_2\text{CO}_3$  on treatment with methanol/HCl.<sup>[1]</sup> Weissbuch et al.<sup>[46, 48]</sup> showed the dramatic effect of the solvent on the crystallization of glycine. Glycine has three polymorphs –  $\alpha$ -glycine,  $\beta$ -glycine and  $\gamma$ -glycine. The order of thermodynamic stability at room temperature is  $\gamma > \alpha > \beta$ <sup>[46]</sup>. The addition of methanol and ethanol to aqueous solutions induces the crystallization of  $\beta$ -glycine, whereas  $\gamma$ - and  $\alpha$ -glycine precipitate from aqueous solution.<sup>[46, 48]</sup> Another example is tetrolic acid, which forms  $\alpha$ - or  $\beta$ -polymorph depending on the polarity of the solvents.<sup>[49]</sup>

To obtain other polymorphs of  $\text{H}_2\text{CO}_3$ , the idea was to change the solvents for  $\text{HCO}_3^-$  and HCl. The reaction of  $\text{HCO}_3^-$  and HCl dissolved in ethanol ( $\text{C}_2\text{H}_5\text{OH}$ ) or propanol ( $\text{C}_3\text{H}_7\text{OH}$ ), could lead to crystallization of unknown polymorphs. However,  $\text{KHCO}_3$  is

neither significantly soluble in ethanol nor in propanol. To come by this difficulty we tried to protonate  $\text{HCO}_3^-$ , dissolved in either  $\text{H}_2\text{O}$  or  $\text{CH}_3\text{OH}$  with excess of  $\text{HCl}$  dissolved in  $\text{C}_2\text{H}_5\text{OH}$ .

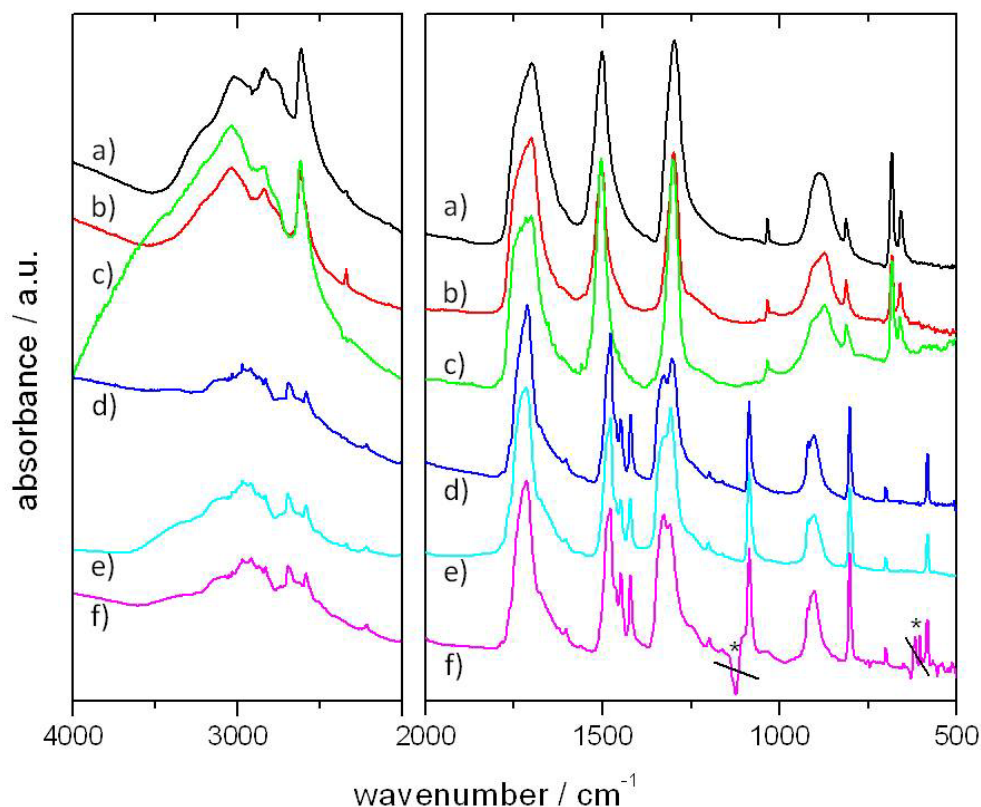


**Figure 5.1** a) – c) spectra of  $\beta\text{-H}_2\text{CO}_3$  by protonation of  $\text{KHCO}_3$  in  $\text{H}_2\text{O}$  with a)  $\text{HBr}$  in  $\text{H}_2\text{O}$  (recorded at  $T = 230\text{ K}$ ), b)  $\text{HCl}$  in  $\text{CH}_3\text{OH}$  ( $T = 230\text{ K}$ ) and c)  $\text{HCl}$  in  $\text{C}_2\text{H}_5\text{OH}$  ( $T = 220\text{ K}$ ). d) – f) spectra of  $\alpha\text{-H}_2\text{CO}_3$  by protonation of  $\text{KHCO}_3$  in  $\text{CH}_3\text{OH}$  with d)  $\text{HCl}$  in  $\text{CH}_3\text{OH}$  ( $T = 210\text{ K}$ ), e)  $\text{HCl}$  in  $\text{H}_2\text{O}$  ( $T = 200\text{ K}$ ) and f)  $\text{HCl}$  in  $\text{C}_2\text{H}_5\text{OH}$  ( $T = 200\text{ K}$ ). The absorbance of the spectra are scaled to have identical absorbance for the  $\nu(\text{CO})$  at about  $1700\text{ cm}^{-1}$ .

Studies of the protonation of  $0.4\text{ M KHCO}_3$  in  $\text{CH}_3\text{OH}$  with  $1.25\text{ M HCl}$  in  $\text{C}_2\text{H}_5\text{OH}$  at  $180\text{ K}$  result in the formation of the  $\text{H}_2\text{CO}_3$   $\alpha$ -polymorph (Figure 5.1f). Reaction of  $0.5\text{ M KHCO}_3$  in  $\text{H}_2\text{O}$  with  $1.25\text{ M HCl}$  in  $\text{C}_2\text{H}_5\text{OH}$  produced  $\beta\text{-H}_2\text{CO}_3$  (Figure 5.1c). In other experiments,  $0.4\text{ M KHCO}_3$  in  $\text{CH}_3\text{OH}$  was brought to reaction with  $2\text{ M HCl}$  in  $\text{H}_2\text{O}$ , forming  $\alpha\text{-H}_2\text{CO}_3$  (Figure 5.1e). The reaction of  $0.5\text{ M KHCO}_3$  in  $\text{H}_2\text{O}$  with  $1.5\text{ M HCl}$  in  $\text{CH}_3\text{OH}$  led to  $\beta\text{-H}_2\text{CO}_3$  (Figure 5.1b). Winkel et al. <sup>[3]</sup> reported that the main spectral features in the IR spectra of  $\alpha$ - and  $\beta\text{-H}_2\text{CO}_3$  are observable already in those of the two amorphous  $\text{H}_2\text{CO}_3$  forms. <sup>[3]</sup> This indicates that H-bond connectivity or conformational states in the two crystalline phases should already be developed in their amorphous forms. <sup>[3]</sup> The above mentioned results suggest that formation of different  $\text{H}_2\text{CO}_3$  polymorphs is dependent on the solvent used for dissolution of  $\text{HCO}_3^-$ . The different solvent molecules could be the cause of H-bond connectivity or the conformational state of the  $\text{HCO}_3^-$  anion. This means that a crystalline  $\text{CH}_3\text{OH}$  adduct or a hydrate could be precursors in forming  $\alpha$ - or  $\beta\text{-H}_2\text{CO}_3$ . <sup>[3]</sup>

## 5.1 Solid state / liquid state reaction

For more clarity about the formation of different  $\text{H}_2\text{CO}_3$  polymorphs, we investigated  $\text{KHCO}_3$  dissolved in different solutions. The solutions were deposited with a nebulizer (air brush pistol Harder & Steenbeck; model grafo or infinity) on a cryoplate at 80 K and then heated in vacuum to 290 K. This way the solvents evaporate, and only the hyperquenched solutes remain on the cryoplate. The solid compound ( $\text{KHCO}_{3(s)}$ ) was later protonated with HCl solutions (hyperquenching technique chapter 3).

### 5.1.1 Reaction of $\text{KHCO}_{3(s)}$ from $\text{H}_2\text{O}$ with HCl in $\text{CH}_3\text{OH}$

Figure 5.2a shows the IR spectrum of a solid residue isolated from a 2 M aqueous  $\text{KHCO}_3$  solution in vacuum at 290 K. It was produced by dissolving the salt in water (2 M solution). The solution was then deposited with a nebulizer on a cryoplate at 80 K and finally heated in vacuum to 290 K. During the heating the solution went from the glassy state to a freeze-concentrated state, where the glassy water crystallized to cubic ice. At about 210 K  $\text{H}_2\text{O}$  evaporated and the salt precipitated.

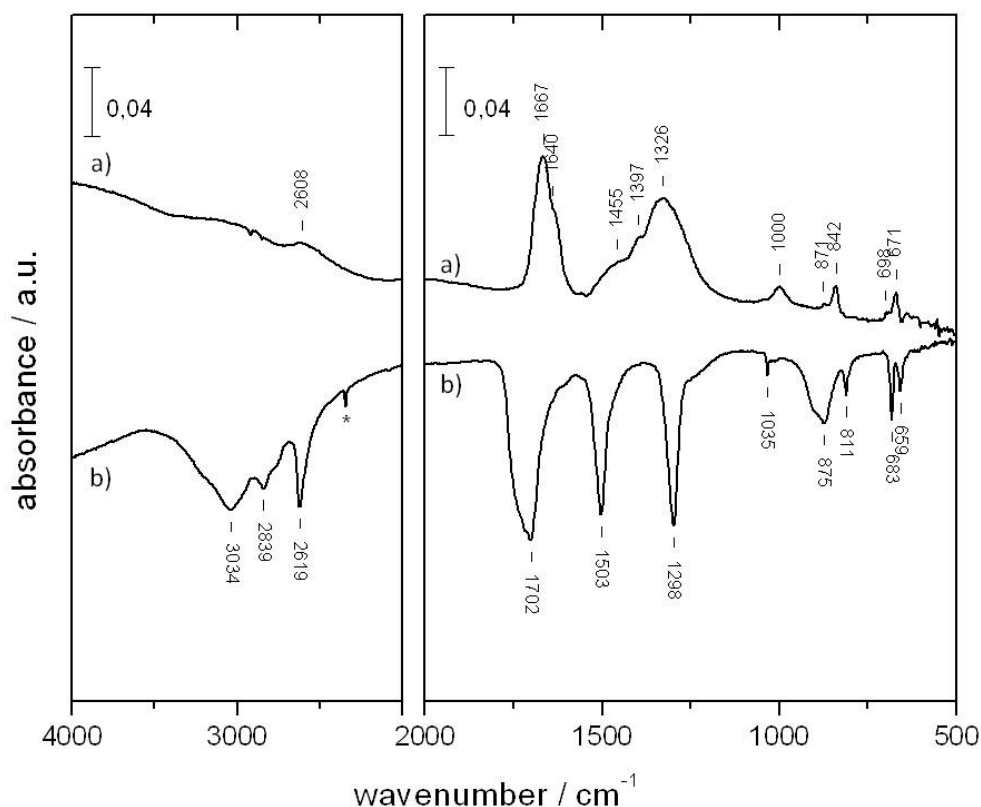


**Figure 5.2** a) IR spectrum of solid  $\text{KHCO}_3$  isolated from an aqueous solution in vacuum at 290 K. b) IR spectrum of crystalline  $\beta\text{-H}_2\text{CO}_3$  after protonation of the solid  $\text{KHCO}_3$  with HCl in  $\text{CH}_3\text{OH}$ , recorded at 230 K. The band marked with an asterisk belongs to  $\text{CO}_2$  which is trapped in the crystal. The negative absorbance arrives from a mathematical operation (multiplication with -1) facilitating the comparison between the different IR spectra.

It should show the IR-spectrum of solid  $\text{KHCO}_3$  isolated from  $\text{H}_2\text{O}$  measured at 290 K in vacuum. Nakamoto et al. were one of the first which measured the IR-spectrum of solid  $\text{KHCO}_3$ .<sup>[50]</sup> Between  $4000 - 500 \text{ cm}^{-1}$  they found the following bands: 2620(w), 1618(s), 1405(s), 1367(s), 1001(m), 830(m), 698(m) and  $655 \text{ cm}^{-1}$ .<sup>[50]</sup> The specifications in brackets indicate the intensity (w, weak; m, medium; s, strong). The comparison with our band positions only shows partial agreement. The most intensive peak is located at  $1667 \text{ cm}^{-1}$  and has a shoulder at about  $1640 \text{ cm}^{-1}$ . The second most intensive band is broad with a maximum at  $1326 \text{ cm}^{-1}$  and two shoulders at 1455 and  $1397 \text{ cm}^{-1}$ . The above bands are located at slightly higher wavenumbers than reported in Nakamoto et al.<sup>[50]</sup>. The peaks below  $1000 \text{ cm}^{-1}$  are at similar positions compared to the literature<sup>[50]</sup>. The bands are situated at 1000, 842 and  $671 \text{ cm}^{-1}$ . The deviation might be caused by the presence of amorphous  $\text{KHCO}_3$  instead of crystalline  $\text{KHCO}_3$ . In amorphous solids bands are broader and the positions agree nearly with the one in the crystal.  $\text{KHCO}_3$  grows as a monoclinic crystal, space group  $P21/a$  ( $a = 15.1725 \text{ \AA}$ ,  $b = 5.6283 \text{ \AA}$ ,  $c = 3.7110 \text{ \AA}$ ,  $\beta = 104.631^\circ$ ).<sup>[51-52]</sup>

**Table 5.1 Assignment of the IR frequencies of solid  $\text{KHCO}_3$  (all values in  $\text{cm}^{-1}$ ).**

$\text{KHCO}_3$		
lit. <sup>[50]</sup>	expt. (amorphous?)	Assign. <sup>[50]</sup>
2620 (w)	2608 (br)	$\nu(\text{O-H})$
1618 (s)	1667 (s) 1640 (sh)	$\nu(\text{C=O})$
1405 (s)	1455 (sh) 1397 (sh)	$\delta(\text{OHO})$
1367 (s)	1326 (s, br)	$\nu(\text{C-O}) + \nu(\text{C=O}) + \delta(\text{OHO})$
1001 (m)	1000 (m)	$\nu(\text{C-O}) + \nu(\text{C=O})$
988 (m)		$\pi(\text{OHO})$
830 (m)	842 (m)	$\pi(\text{CO}_3)$
698 (m)	698 (vw)	$\delta(\text{C=O}) + \nu(\text{O-H})$
655 (m)	671 (m)	$\delta(\text{CO}_3)$

***vw, very weak; w, weak; m, medium, s, strong; br, broad; sh, shoulder  
 $\nu$ , stretching;  $\delta$ , in-plane;  $\pi$ , out of plane bending***

The solid compound on the cryoplate was then cooled from 290 K to 180 K and HCl in  $\text{CH}_3\text{OH}$  was added to start the protonation reaction. Figure 5.2b shows the spectrum of solid  $\beta\text{-H}_2\text{CO}_3$  at 230 K after protonation of the above compound (reaction 1).



**reaction 1**

**Table 5.2 Assignment of the IR frequencies of solid  $\beta$ -H<sub>2</sub>CO<sub>3</sub> (all values in cm<sup>-1</sup>).**

lit. <sup>[20]</sup>	$\beta$ -H <sub>2</sub> CO <sub>3</sub>	
	expt.	Assign. <sup>[20]</sup>
3030		$\nu(\text{C=O}) + 2 \times \delta_{\text{ip}}(\text{CO}_3)$
2969	3034	$\nu(\text{C=O}) + \delta_{\text{ip}}(\text{COH})$ or $2 \times \nu_{\text{as}}[\text{C}(\text{OH})_2]$
2830	2839	$\nu_{\text{as}}[\text{C}(\text{OH})_2] + \delta_{\text{ip}}(\text{COH})$ or $2 \times \nu_{\text{as}}[\text{C}(\text{OH})_2] + 2 \times \delta_{\text{ip}}(\text{CO}_3)$
2613	2619	$2 \times \delta_{\text{ip}}(\text{COH})$
1698	1702	$\nu(\text{C=O})$
1504	1503	$\nu_{\text{as}}[\text{C}(\text{OH})_2]$
1302	1298	$\delta_{\text{ip}}(\text{COH})$
1038	1035	$\nu_{\text{s}}[\text{C}(\text{OH})_2]$
910		
881	875	$\delta_{\text{oop}}(\text{COH})$
813	811	$\delta_{\text{oop}}(\text{CO}_3)$
686	683	$\delta_{\text{ip}}(\text{CO}_3)$
664	659	$\delta_{\text{ip}}(\text{CO}_3)$

$\nu_{\text{s}}$  and  $\nu_{\text{as}}$ , symmetric and asymmetric stretching mode;  $\delta_{\text{ip}}$  and  $\delta_{\text{oop}}$ , in-plane and out-of-plane bending mode

The band positions correlate very well with the literature<sup>[3, 9, 20]</sup>. The band marked with an asterisk in Figure 5.2b belongs to CO<sub>2</sub> which is trapped in the crystal. The negative absorbance is a result of a mathematical operation (multiplication with -1), facilitating the comparison between the different IR spectra. The results and the assignments of the bands are reviewed in Table 5.1 and Table 5.2.

### 5.1.2 Reaction of $\text{KHCO}_{3(s)}$ from $\text{CH}_3\text{OH}$ with $\text{HCl}$ in $\text{H}_2\text{O}$

The same experiment was performed with different solvents.  $\text{KHCO}_{3(s)}$  was dissolved in  $\text{CH}_3\text{OH}$  to obtain a 0.4 M solution (stirring several hours at 48 °C). The solution was deposited through the hyperquenching method on a cryoplate and the solvent ( $\text{CH}_3\text{OH}$ ) was evaporated.

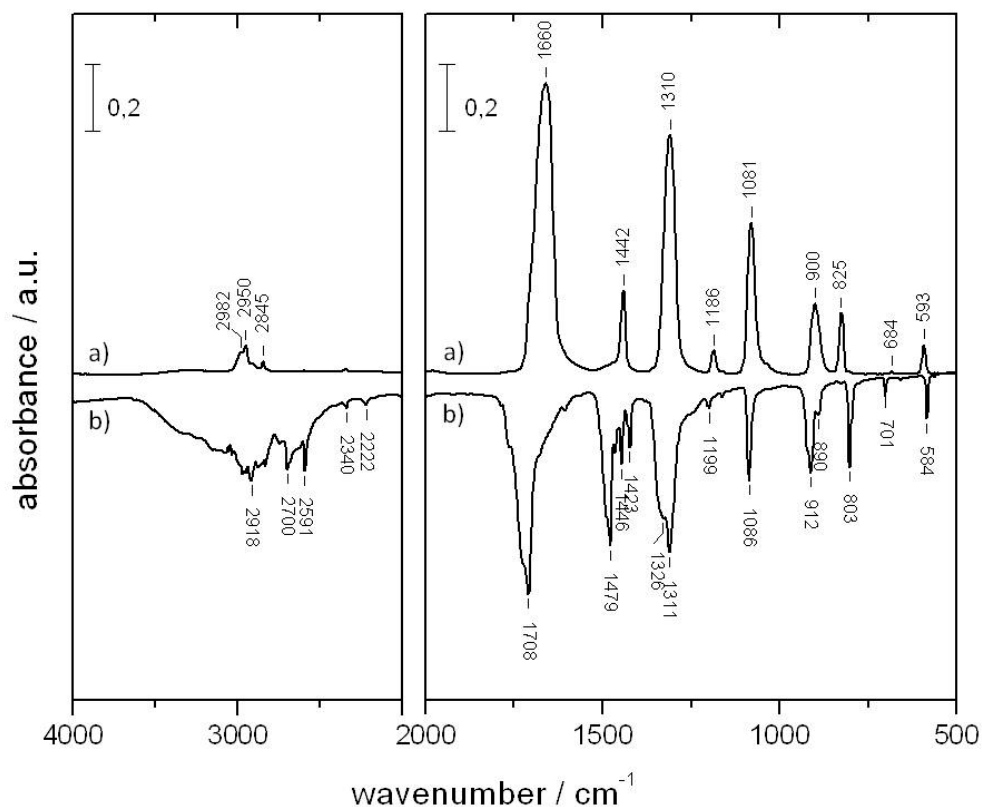


**Figure 5.3 a)** IR spectrum of solid  $\text{K}[\text{O}_2\text{COCH}_3]$  through reaction of methanolate ( $\text{CH}_3\text{O}^-$ ) with  $\text{KHCO}_3$ . The spectrum was recorded in vacuum at 290 K. **b)** IR spectrum of crystalline  $\alpha\text{-H}_2\text{CO}_3$  after protonation of solid  $\text{K}[\text{O}_2\text{COCH}_3]$  with  $\text{HCl}$  in  $\text{H}_2\text{O}$ , recorded at 80 K. The negative absorbance arrives from a mathematical operation (multiplication with -1), facilitating the comparison between the different IR spectra.

Figure 5.3a shows the IR spectrum of the solid residue, which was obtained after  $\text{CH}_3\text{OH}$  removal at 290 K. The comparison of the band positions of this spectrum with the spectrum Figure 5.2a as well as with the ones from literature <sup>[50]</sup> shows disagreement. Between 2000 – 500  $\text{cm}^{-1}$  Figure 5.3a shows nine bands. Bands at 1660, 1310 and 1081  $\text{cm}^{-1}$  are strong, bands at 1442, 900, 825  $\text{cm}^{-1}$  medium, at 1186 and 593  $\text{cm}^{-1}$  weak and at 684  $\text{cm}^{-1}$  very weak in intensity. Between 4000 – 2000  $\text{cm}^{-1}$  a band arises at 2950  $\text{cm}^{-1}$  with weak intensity and a shoulder at 2982  $\text{cm}^{-1}$ . Also a very weak band develops at 2845  $\text{cm}^{-1}$ .

In 1973 Behrendt et al. <sup>[53]</sup> have done investigations on hemiesters of carbonic acid. Monomethyl and monoethyl carbonates of potassium and other metals were formed by reaction of  $\text{CO}_2$  with alcoholates. The prepared salts were investigated by different

methods (IR, UV and  $^1\text{H-NMR}$ )<sup>[53]</sup>. Comparing the IR results of the potassium monomethyl carbonate ( $\text{K}[\text{O}_2\text{COCH}_3]$ )<sup>[53]</sup> with the spectrum from Figure 5.3a we find a good agreement. The results and the assignments of the peaks are shown in Table 5.3. Adam et al. 1994 have obtained  $\text{K}[\text{O}_2\text{COCH}_3]$  from reaction of dimethyl carbonate with hydroxide in methanol.  $\text{K}[\text{O}_2\text{COCH}_3]$  forms long, flattened and colorless needles, which are sensitive to moisture.<sup>[54]</sup> The crystal structure was determined as triclinic *P*-1, *Z* = 2,  $a = 3.809(2) \text{ \AA}$ ,  $b = 5.589(3) \text{ \AA}$ ,  $c = 9.853(3) \text{ \AA}$ ,  $\alpha = 100.71(2)^\circ$ ,  $\beta = 90.06(3)^\circ$ ,  $\gamma = 92.48(3)^\circ$ .<sup>[54]</sup>

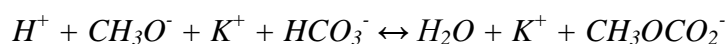
**Table 5.3 Assignment of the IR frequencies of solid  $\text{K}[\text{O}_2\text{COCH}_3]$  (all values in  $\text{cm}^{-1}$ ).**

<b><math>\text{K}[\text{O}_2\text{COCH}_3]</math></b>		
<b>lit.</b> <sup>[53]</sup>	<b>expt.</b>	<b>Assign.</b> <sup>[53]</sup>
3003 (w)	2982 (sh)	$\nu_{\text{as}}(\text{CH})$
2967 (w)	2950 (w)	
2857 (w)	2845 (vw)	$\nu_{\text{s}}(\text{CH})$
1689 (s)	1660 (s)	$\nu_{\text{as}}(\text{CO}_2)$
1475 (m)		$\delta_{\text{as}}(\text{CH}_3)$
1453 (s)	1442 (m)	
1435 (s)		
1305 (s)	1310 (s)	$\nu_{\text{s}}(\text{CO}_2)$
1282 (sh)		$\delta_{\text{s}}(\text{CH}_3)$
1185 (m)		$\nu(\text{CO})$
1163 (w)	1186 (w)	
1079 (s)	1081 (s)	$\nu(\text{CO})$
893 (s)	900 (m)	$\text{CH}_3\text{O}$
826 (s)	825 (m)	$\pi(\text{CO}_3)$
672 (w)	684 (vw)	$\delta_{\text{as}}(\text{CO}_2)$
589 (m)	593 (w)	$\delta_{\text{s}}(\text{CO}_2)$

*vw, very weak; w, weak; m, medium, s, strong; sh, shoulder*

*$\nu_{\text{s}}$  and  $\nu_{\text{as}}$ , symmetric and asymmetric stretching mode;  $\delta$ , in-plane;  $\pi$ , out of plane bending mode;*

The formation of  $\text{K}[\text{O}_2\text{COCH}_3]$  is described as follows:  $\text{KHCO}_3$  itself may be insoluble in  $\text{CH}_3\text{OH}$ . To obtain  $\text{KHCO}_3$  dissolved in  $\text{CH}_3\text{OH}$ , the  $\text{HCO}_3^-$  ions must react to a species, which is soluble in  $\text{CH}_3\text{OH}$ .  $\text{CH}_3\text{O}^-$  ions are generated by the autoprotolytic dissociation of methanol. The abundance of  $\text{CH}_3\text{O}^-$  is very low (equilibrium constant,  $K_{\text{dis}} = 10^{-16}$ )<sup>[55-56]</sup>.  $\text{CH}_3\text{O}^-$  ions react with the  $\text{HCO}_3^-$  through a  $\text{S}_{\text{N}}2$  nucleophilic reaction to  $\text{CH}_3\text{OCO}_2^-$  (reaction 2).



**reaction 2**

Behrent et al. reported that  $K[O_2COCH_3]$  is more easily soluble in  $CH_3OH$  compared to  $KHCO_3$ . Investigations of the compound which is obtained from a 0.1 M methanolic  $KHCO_3$  solution (stirring for 24 h at room temperature), or a methanolic  $K_2CO_3$  solution show the same IR spectra as in Figure 5.3a. The bands at 2950, 2982 and  $2845\text{ cm}^{-1}$  can be assigned to  $\nu(CH)$  and the band at  $1443\text{ cm}^{-1}$  to  $\delta(CH_3)$ . This corroborates the hypothesis, that in methanolic solution  $K[O_2COCH_3]$  is dissolved, and not  $KHCO_3$ .

**Table 5.4 Assignment of the IR frequencies of solid  $\alpha\text{-H}_2\text{CO}_3$  (all values in  $\text{cm}^{-1}$ ).**

lit. <sup>[19]</sup>	$\alpha\text{-H}_2\text{CO}_3$	
	expt.	Assign. <sup>[19]</sup>
	2972	
3024	2918	
	2833	
2694	2700	$\nu(OH)$
2585	2591	$\nu(OH)$
1715	1708	$\nu(C=O)$
1477	1479	$\nu_{as}[C(OH)_2]$
1457	1446	disordered $H_2CO_3?$
1420	1423	$\delta_{ip}(COH)$
1323	1326	
1304	1311	$\nu_{as}[C(OH)_2]$
1199	1199	disordered $H_2CO_3?$
1084	1086	$\nu_s[C(OH)_2]$
920	912	
	890	$\delta_{oop}(COH)$
801	803	$\delta_{oop}(CO_3)$
699	701	
583	584	$\delta_{ip}(CO_3)$

$\nu_s$  and  $\nu_{as}$ , symmetric and asymmetric stretching mode;  $\delta_{ip}$  and  $\delta_{oop}$ , in-plane and out-of-plane bending mode

By protonation of the above compound at 180 K with HCl in  $H_2O$ , the  $\alpha$ -polymorph of  $H_2CO_3$  was produced (Figure 5.3b). The band positions correlate very well with the literature <sup>[3, 19]</sup>. The negative absorbance is a result of a mathematical operation (multiplication with -1), which allows for more facile comparison of spectra.

$K[O_2COCH_3]$  has a different crystal structure compared to  $KHCO_3$ . For the protonation we use an excess of acid. By protonation of  $K[O_2COCH_3]$ , the excess of acid leads to the protonation of the  $CH_3OCO_2^-$  and to an acidic hydrolysis of the ester (Figure 5.4). This results in a small change in the crystal structure and  $\alpha\text{-H}_2\text{CO}_3$  is formed.

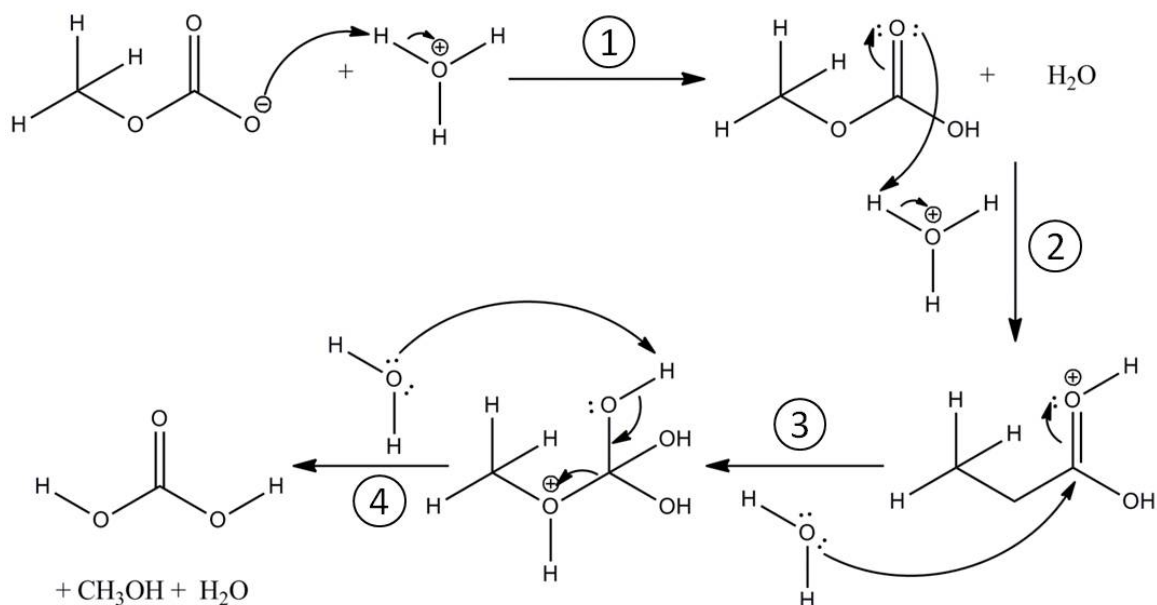


**Figure 5.4** Possible steps for the protonation and acidic hydrolysis of  $K[O_2COCH_3]$ . 1) protonation of  $CH_3OCO_2^-$ , 2) activation of the carbonyl group, 3) nucleophilic addition of  $H_2O$  and proton transfer to the  $CH_3O$  group, 4) elimination of the alcohol results in  $H_2CO_3$ .

The possible steps for the protonation and acidic hydrolysis of  $K[O_2COCH_3]$  can be described as:

- 1) protonation of  $CH_3OCO_2^-$ ,
- 2) activation of the carbonyl group,
- 3) nucleophilic addition of  $H_2O$  and proton transfer to the  $CH_3O$  group,
- 4) elimination of the alcohol results in  $H_2CO_3$ .

The high agreement in band positions for  $K[O_2COCH_3]$  between literature and our experiments shows obviously that  $\alpha$ - $H_2CO_3$  is formed through protonation of  $CH_3OCO_2^-$  ions instead of  $HCO_3^-$  ions. The results and the assignments of the bands are reviewed in Table 5.3 and Table 5.4.

### 5.1.3 Reaction of $\text{KHCO}_3(\text{s})$ from $\text{C}_2\text{H}_5\text{OH}$ with $\text{HCl}$ in $\text{C}_2\text{H}_5\text{OH}$

The new results from the solid/liquid reaction raise hope for the isolation of a new  $\text{H}_2\text{CO}_3$  polymorph by protonation in  $\text{C}_2\text{H}_5\text{OH}$  solution. We know that  $\text{KHCO}_3$  is not soluble in  $\text{C}_2\text{H}_5\text{OH}$ . However, what happens when a very small part is soluble, possibly by esterification. Which starting and protonation products do we obtain?

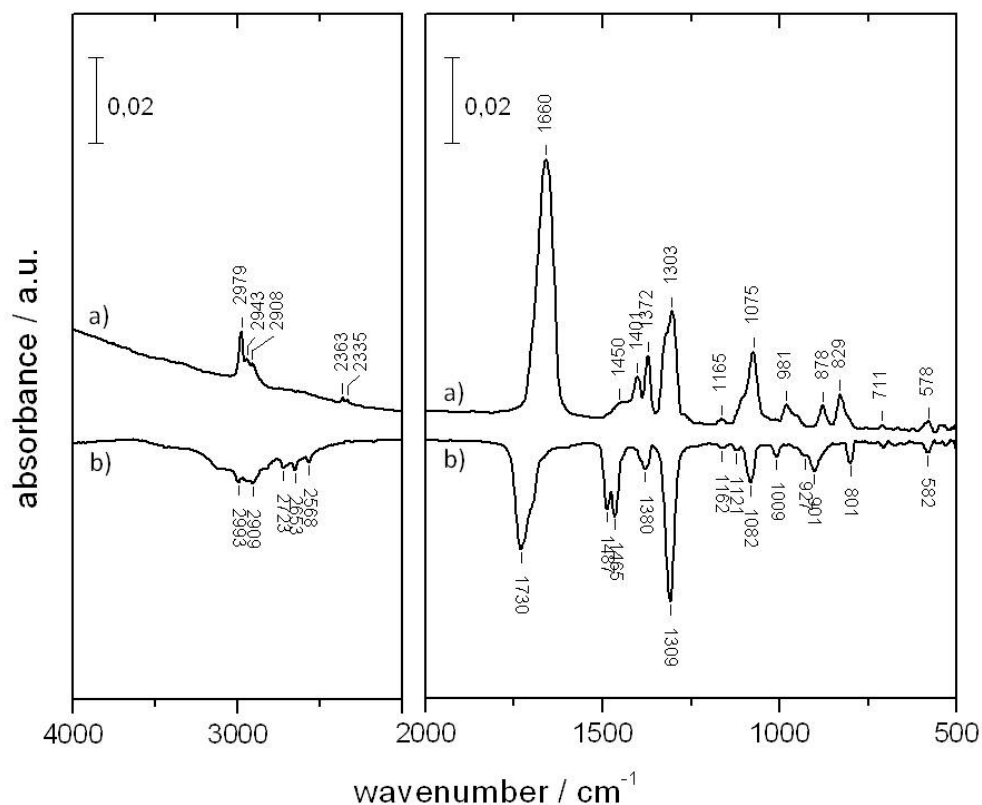
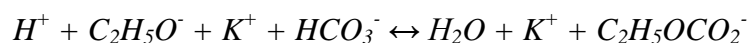


**Figure 5.5 a)** IR spectrum of solid ( $\text{K}[\text{O}_2\text{COC}_2\text{H}_5]$ ) from reaction of ethanolate ( $\text{C}_2\text{H}_5\text{O}^-$ ) with  $\text{KHCO}_3$ . The spectrum was recorded in vacuum at 290 K. **b)** IR subtraction spectrum of a crystalline species, which evaporates or decomposes at 210 K in vacuum. The new species is obtained after protonation of solid ( $\text{K}[\text{O}_2\text{COC}_2\text{H}_5]$ ) with  $\text{HCl}$  in  $\text{H}_2\text{O}$ . The new species is labeled  $\gamma\text{-H}_2\text{CO}_3$ .

For this experiment 0.25 g  $\text{KHCO}_3$  were suspended in 10 ml  $\text{C}_2\text{H}_5\text{OH}$ . The solution was stirred and heated to 48 °C for several hours. Subsequently, the suspended particles were sedimented and the solution was hyperquenched (chapter 3). At 200 K the solvent ( $\text{C}_2\text{H}_5\text{OH}$ ) evaporated and a solid residue remained on the sample holder. The IR spectrum of the residue is shown in Figure 5.5a. Compared to Figure 5.2a and Figure 5.3a, the spectrum in Figure 5.5a is different.

However, more likely the potassium monoethyl carbonate ( $\text{K}[\text{O}_2\text{COC}_2\text{H}_5]$ ) has been isolated. Comparison of the IR frequencies in our residue with the results from Behrendt et al. [53] (Table 5.5) again reveals a good resemblance. Bands at 2979, 2943 and 2908  $\text{cm}^{-1}$  can be assigned to  $\nu(\text{CH})$  and the bands at 1450, 1404 and 1372  $\text{cm}^{-1}$  to  $\delta(\text{CH})$ . We also find the  $\text{CH}_2$  wagging mode,  $\omega(\text{CH}_2)$ , at 878  $\text{cm}^{-1}$ .  $\text{KHCO}_3$  may in fact be insoluble in

C<sub>2</sub>H<sub>5</sub>OH, but to obtain dissolution in C<sub>2</sub>H<sub>5</sub>OH, KHCO<sub>3</sub> must react with C<sub>2</sub>H<sub>5</sub>O<sup>-</sup> ions, which show a very low abundance in pure anhydrous ethanol. The HCO<sub>3</sub><sup>-</sup> ions are transformed by a S<sub>N</sub>2 nucleophilic reaction to C<sub>2</sub>H<sub>5</sub>OCO<sub>2</sub><sup>-</sup> ions (reaction 3). Unlike KHCO<sub>3</sub>, the obtained K[O<sub>2</sub>COC<sub>2</sub>H<sub>5</sub>] is easily soluble in C<sub>2</sub>H<sub>5</sub>OH. The results and the assignments of the bands are shown in Table 5.5.



reaction 3

Table 5.5 Assignment of the IR frequencies of solid K[O<sub>2</sub>COC<sub>2</sub>H<sub>5</sub>] (all values in cm<sup>-1</sup>).

K[O <sub>2</sub> COC <sub>2</sub> H <sub>5</sub> ]		
lit. <sup>[53]</sup>	expt.	Assign. <sup>[53]</sup>
2967 (s)	2979 (m)	
2907 (m)	2943 (w)	v(CH)
	2908 (w)	
1689 (s)	1660 (vs)	v <sub>as</sub> (CO <sub>2</sub> )
1484 (w)	1450 (sh)	
1445 (w)	1401 (m)	δ(CH)
1389 (m)	1372 (m)	
1370 (s)		
1295 (s)	1303 (s)	v <sub>s</sub> (CO <sub>2</sub> )
1274 (m)		δ <sub>s</sub> (CH <sub>3</sub> )
1172 (w)		
1114 (m)	1165 (vw)	v(CO)
1075 (sh)		
1059 (s)	1075 (s)	v(CO)
966 (s)	981 (m)	CH <sub>3</sub> C
876 (s)	878 (m)	ω(CH <sub>2</sub> )
821 (s)	829 (m)	π(CO <sub>3</sub> )
812 (w)		
701 (w)	711 (vw)	δ <sub>as</sub> (CO <sub>2</sub> )
584 (w)	578 (w)	δ <sub>s</sub> (CO <sub>2</sub> )

*vw, very weak; w, weak; m, medium, s, strong; vs, very strong; sh, shoulder*  
*v<sub>s</sub> and v<sub>as</sub>, symmetric and asymmetric stretching mode; δ, in-plane; π, out of plane bending mode; ω, wagging mode;*

In Figure 5.5b the IR spectrum of a new species after protonation of the solid K[O<sub>2</sub>COC<sub>2</sub>H<sub>5</sub>] with HCl in H<sub>2</sub>O is shown. It shows the subtraction spectrum at different times and 210 K. The spectrum belongs to the species which evaporated or decomposed during this time at 210 K. This is of interest, since also α-H<sub>2</sub>CO<sub>3</sub> evaporates at 210 K in vacuum. The new species is labeled γ-H<sub>2</sub>CO<sub>3</sub>, and it is possibly a new polymorph of carbonic acid (reaction 4).



reaction 4

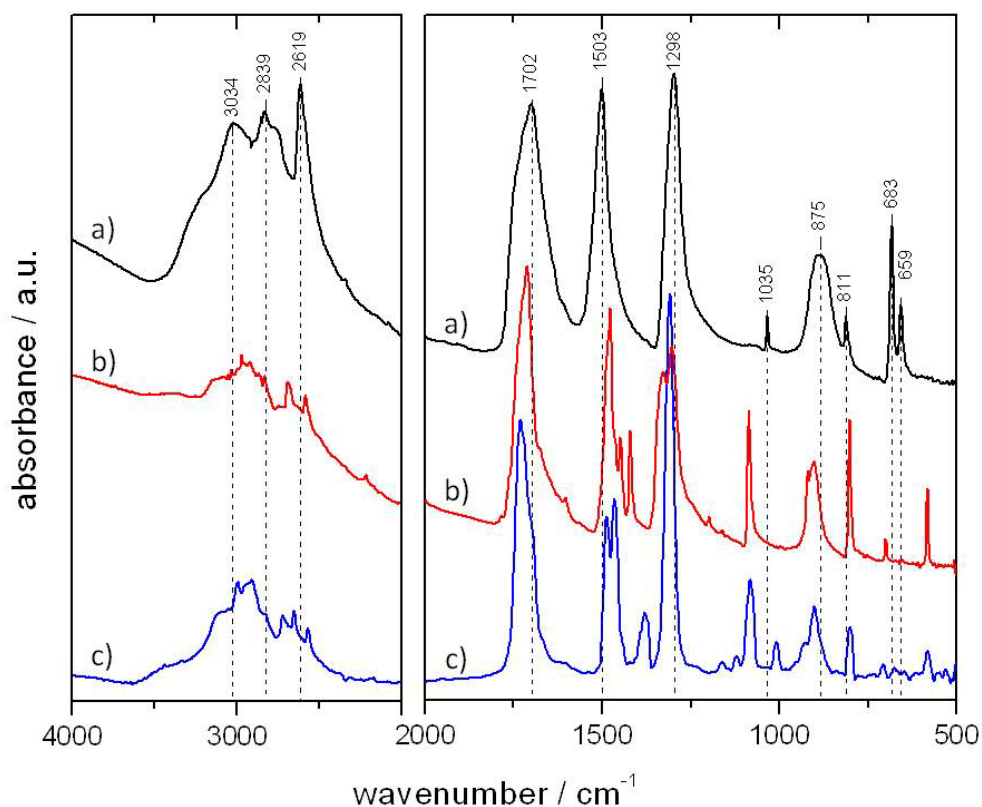
Comparing the IR spectrum of  $\alpha\text{-H}_2\text{CO}_3$  (Figure 5.3b) with  $\gamma\text{-H}_2\text{CO}_3$  (Figure 5.5b) reveals some disagreement. Between 2800 and 2500  $\text{cm}^{-1}$   $\alpha\text{-H}_2\text{CO}_3$  shows two bands at 2700 and 2591  $\text{cm}^{-1}$ . In contrast  $\gamma\text{-H}_2\text{CO}_3$  shows three bands at 2723, 2653 and 2568  $\text{cm}^{-1}$ . The  $\nu(\text{C}=\text{O})$  band of  $\gamma\text{-H}_2\text{CO}_3$  is shifted to higher wavenumbers compared to  $\alpha\text{-H}_2\text{CO}_3$ . Between 1500 and 1300  $\text{cm}^{-1}$  five bands arise for  $\alpha\text{-H}_2\text{CO}_3$ , with peaks at 1479, 1446, 1326 and 1311  $\text{cm}^{-1}$ . The IR frequencies at 1479, 1326 and 1311  $\text{cm}^{-1}$  were assigned to  $\nu_{\text{as}}[\text{C}(\text{OH})_2]$ , the band at 1423  $\text{cm}^{-1}$  to  $\delta_{\text{ip}}(\text{COH})$  and the one at 1446  $\text{cm}^{-1}$  to disordered  $\text{H}_2\text{CO}_3$ . In the case of  $\gamma\text{-H}_2\text{CO}_3$  four bands arise at 1487, 1465, 1380 and 1309  $\text{cm}^{-1}$ . The IR-frequencies of  $\alpha$ -,  $\beta$ - and  $\gamma\text{-H}_2\text{CO}_3$  are reviewed in Table 5.6.

Table 5.6 IR frequencies of the different  $\text{H}_2\text{CO}_3$  polymorphs.

$\beta\text{-H}_2\text{CO}_3$ lit. <sup>[20]</sup>	$\alpha\text{-H}_2\text{CO}_3$ lit. <sup>[19]</sup>	$\gamma\text{-H}_2\text{CO}_3$ expt.	Assign. $\beta\text{-H}_2\text{CO}_3$ <sup>[20]</sup>
3030		2993	$\nu(\text{C}=\text{O}) + 2 \times \delta_{\text{ip}}(\text{CO}_3)$
2969	3024	2909	$\nu(\text{C}=\text{O}) + \delta_{\text{ip}}(\text{COH})$ or $2 \times \nu_{\text{as}}[\text{C}(\text{OH})_2]$
		2723	$\nu_{\text{as}}[\text{C}(\text{OH})_2] + \delta_{\text{ip}}(\text{COH})$ or $2 \times \nu_{\text{as}}[\text{C}(\text{OH})_2] + 2 \times \delta_{\text{ip}}(\text{CO}_3)$
	2694	2653	
2613	2585	2568	$2 \times \delta_{\text{ip}}(\text{COH})$
1698	1715	1730	$\nu(\text{C}=\text{O})$
1504	1477	1487	$\nu_{\text{as}}[\text{C}(\text{OH})_2]$
	1457	1465	
1302	1420	1380	$\delta_{\text{ip}}(\text{COH})$
	1323	1309	
	1304		
	1199	1162	
		1121	
1038	1084	1082	$\nu_{\text{s}}[\text{C}(\text{OH})_2]$
		1009	
910		921	
881	920	901	$\delta_{\text{oop}}(\text{COH})$
813	801	801	$\delta_{\text{oop}}(\text{CO}_3)$
	699		
686		582	
664	583		$\delta_{\text{ip}}(\text{CO}_3)$

$\nu_{\text{s}}$  and  $\nu_{\text{as}}$ , symmetric and asymmetric stretching mode;  $\delta_{\text{ip}}$  and  $\delta_{\text{oop}}$ , in-plane and out-of-plane bending mode

The experiments show that, when using  $C_2H_5OH$  as solvent  $KHCO_3$  are transformed in  $C_2H_5OH$  to  $K[O_2COC_2H_5]$ . Protonation of  $K[O_2COC_2H_5]$  leads to a new species, we call  $\gamma-H_2CO_3$ . The reaction pathway is similar to the formation of  $\alpha-H_2CO_3$ . Here also, the starting compound defines which  $H_2CO_3$  polymorph is obtained after protonation. Figure 5.6 shows the IR-spectra of  $H_2CO_3$  polymorphs, namely  $\alpha$ -,  $\beta$ - and  $\gamma-H_2CO_3$ .



**Figure 5.6** IR-spectra of  $H_2CO_3$  polymorphs a)  $\beta-H_2CO_3$ , b)  $\alpha-H_2CO_3$  and c)  $\gamma-H_2CO_3$ . The absorbance of the spectra are scaled to have identical absorbance for the  $\nu(CO)$  at about  $1700\text{ cm}^{-1}$ . Vibrational modes which are assigned to  $\beta-H_2CO_3$  are shown with vertical dashed lines.

### 5.1.4 Reaction of $\text{KHCO}_3$ from $\text{CD}_3\text{OH}$ with $\text{HCl}$ in $\text{CH}_3\text{OH}$

To investigate further the polymorphs of  $\text{H}_2\text{CO}_3$  and their formation, experiments with isotope substituted solvents were made.  $\text{CD}_3\text{OH}$  was used to dissolve  $\text{KHCO}_3$  instead of  $\text{CH}_3\text{OH}$ . Figure 5.7a shows the IR spectrum of the solid residue which is obtained from a  $\text{CD}_3\text{OH}$  solution after evaporation of the solvent at 180 K in vacuum. It is evident that the band at  $1442\text{ cm}^{-1}$ , which was assigned to  $\delta_{\text{as}}(\text{CH}_3)$ , disappears and a new band at  $1107\text{ cm}^{-1}$  arises. New bands also arise at wavenumbers greater than  $2000\text{ cm}^{-1}$ , at  $2245$ ,  $2127$  and  $2077\text{ cm}^{-1}$ . The band at  $2339\text{ cm}^{-1}$  marked with an asterisk belongs to  $\text{CO}_2$ , the ones at  $2917$  and  $2850\text{ cm}^{-1}$  marked with a circle to impurities on the cryoplate.

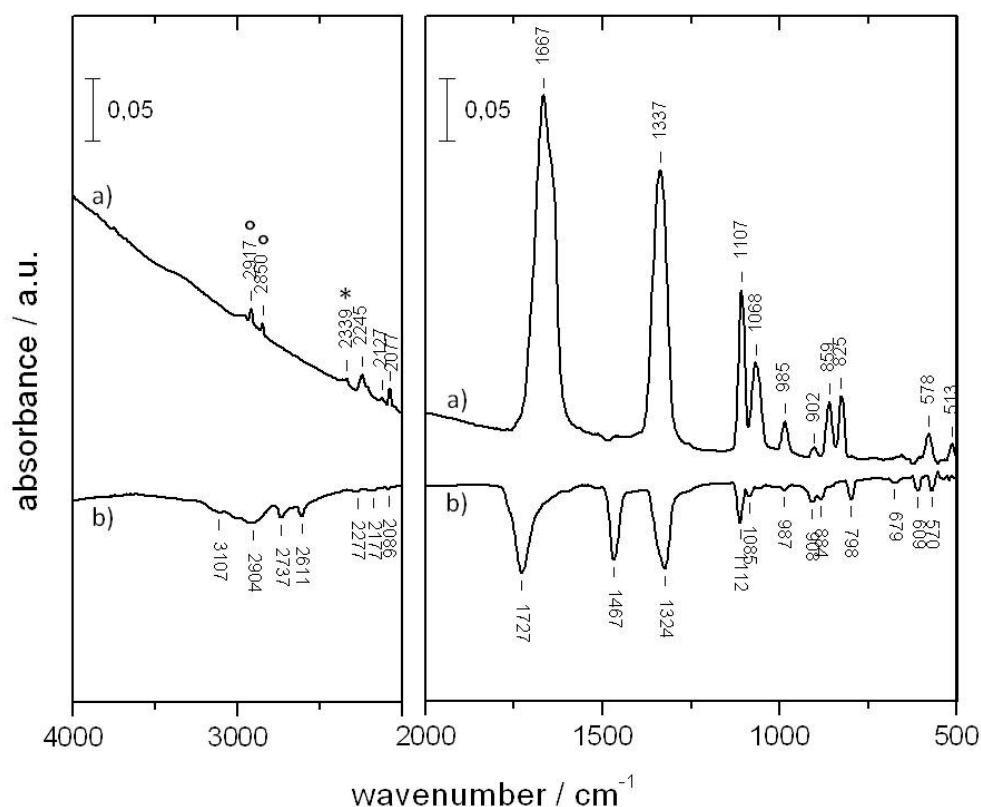
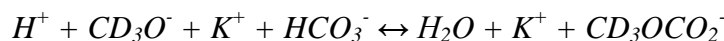


**Figure 5.7** a) IR spectrum of solid  $\text{K}[\text{O}_2\text{COCD}_3]$  by reaction of methanolate ( $\text{CD}_3\text{O}^-$ ) with  $\text{KHCO}_3$ . The spectrum was recorded in vacuum at 290 K. b) IR subtraction spectrum of a crystalline species, which evaporates or decomposes at 210 K in vacuum. The new species is obtained after protonation of solid  $\text{K}[\text{O}_2\text{COCD}_3]$  with  $\text{HCl}$  in  $\text{CH}_3\text{OH}$ . The new species is labeled  $\delta\text{-H}_2\text{CO}_3$ . The band marked with an asterisk belongs to  $\text{CO}_2$ , the one marked with a circle to impurities on the cryoplate.

If  $\text{K}[\text{O}_2\text{COCD}_3]$  has actually been isolated the  $\nu(\text{CD})$  and  $\delta_{\text{as}}(\text{CD}_3)$  should be shifted to lower frequencies compared to  $\nu(\text{CH})$  and  $\delta_{\text{as}}(\text{CH}_3)$  of  $\text{K}[\text{O}_2\text{COCH}_3]$ . When deuterium is used instead of hydrogen stretching modes shift by a factor of  $\approx \sqrt{2}$ . The vibration modes with deuterium shift to lower wavenumbers. Assigning the bands at  $2950$ ,  $2982$  and  $2845\text{ cm}^{-1}$  to  $\nu(\text{CH})$  and at  $1443\text{ cm}^{-1}$  to  $\delta(\text{CH}_3)$  for  $\text{K}[\text{O}_2\text{COCH}_3]$ , a shift by a factor of  $1.3 - 1.4$  to lower wavenumbers leads to an assignments of the peaks at  $2245$ ,  $2127$  and  $2077\text{ cm}^{-1}$  to  $\nu(\text{CD})$  and the signal at  $1107\text{ cm}^{-1}$  to  $\delta_{\text{as}}(\text{CD}_3)$ . Table 5.7 shows the assignments of

the frequencies to their respective mode. The results show evidently that in alcoholic solutions (ROH) the  $\text{KHCO}_3$  reacts with alcoholates ( $\text{RO}^-$ ) to the monoester of the carbonate ( $\text{RO}_2\text{CO}^-$ ). In this case reaction 5 takes place. The results and the assignments of the bands are reviewed in Table 5.7.



*reaction 5*

**Table 5.7 Assignment of the IR frequencies of solid  $\text{K}[\text{O}_2\text{COCH}_3]$  and  $\text{K}[\text{O}_2\text{COCD}_3]$  (all values in  $\text{cm}^{-1}$ ).**

$\text{K}[\text{O}_2\text{COCD}_3]$	$\text{K}[\text{O}_2\text{COCH}_3]$	H/D	
Expt.	expt.	isotope ratio	Assign. <sup>[53]</sup>
2245 (w)	2982 (sh)	1.33	$\nu_{\text{as}}(\text{CD})/\nu_{\text{as}}(\text{CH})$
2127 (vw)	2950 (w)	1.39	
2077 (w)	2845 (vw)	1.37	$\nu_{\text{s}}(\text{CD})/\nu_{\text{s}}(\text{CH})$
1667 (s)	1660 (s)	1.00	$\nu_{\text{as}}(\text{CO}_2)$
1107 (s)	1442 (m)	1.30	$\delta_{\text{as}}(\text{CD}_3)/\delta_{\text{as}}(\text{CH}_3)$
1337 (s)	1310 (s)	0.98	$\nu_{\text{s}}(\text{CO}_2)$
985 (m)			$\delta_{\text{s}}(\text{CD}_3)/\delta_{\text{s}}(\text{CH}_3)$
902 (w)	1186 (w)	1.31	$\nu(\text{CO});$ $\text{COCD}_3/\text{COCH}_3$
1068 (m)	1081 (s)	1.01	$\nu(\text{CO})$
578 (w)	900 (m)	1.56	$\text{CD}_3\text{O}/\text{CH}_3\text{O}$
825 (m)	825 (m)	1.00	$\pi(\text{CO}_3)$
	684 (vw)		$\delta_{\text{as}}(\text{CO}_2)$
	593 (w)		$\delta_{\text{s}}(\text{CO}_2)$

*vw, very weak; w, weak; m, medium, s, strong; sh, shoulder*

*$\nu_{\text{s}}$  and  $\nu_{\text{as}}$ , symmetric and asymmetric stretching mode;  $\delta$ , in-plane;  $\pi$ , out of plane bending mode;*

Now, this compound is used to be protonated. For the protonation HCl is dissolved in  $\text{CH}_3\text{OH}$ . Figure 5.7b shows the IR subtraction spectrum of a crystalline species, which evaporates or decomposes at 210 K in vacuum. The protonated species shows an IR spectrum similar to that of  $\alpha\text{-H}_2\text{CO}_3$ . The  $\nu(\text{C}=\text{O})$  mode shifts by  $\approx 10 \text{ cm}^{-1}$  to higher wavenumbers compared to  $\alpha\text{-H}_2\text{CO}_3$ . Between 1500 and 1400  $\text{cm}^{-1}$  only one broad band arises at 1467  $\text{cm}^{-1}$ , whereas in  $\alpha\text{-H}_2\text{CO}_3$  there are three sharp bands, at 1479, 1446 and 1423  $\text{cm}^{-1}$ . The bands situated at 2694 and 2585  $\text{cm}^{-1}$  for  $\alpha\text{-H}_2\text{CO}_3$  (curve 3, Figure 3 in ref.<sup>[3]</sup>) shift to higher wavenumbers at 2737 and 2611  $\text{cm}^{-1}$  for the new species. An absorbance at 1112  $\text{cm}^{-1}$  arises only for the new compound; in amorphous  $\alpha\text{-H}_2\text{CO}_3$  some band arises at 1136  $\text{cm}^{-1}$  (curve 1, Figure 3 in ref.<sup>[3]</sup>). The new species is labeled  $\delta\text{-H}_2\text{CO}_3$  and could be a new polymorph of carbonic acid.

## 5.2 Discussion

The results evidently point to the fact that for the formation of the different  $\text{H}_2\text{CO}_3$  polymorphs the starting compound is decisive. Changing the solvents for  $\text{KHCO}_3$  yields a new intermediate species which is then protonated. Comparison with literature shows that only in aqueous solution the  $\text{HCO}_3^-$  ions are present. In the case of organic solvents (e.g.  $\text{CH}_3\text{OH}$  and  $\text{C}_2\text{H}_5\text{OH}$ ) the  $\text{HCO}_3^-$  ions react with the  $\text{RO}^-$  ions to the monoalkylester of carbonate ( $\text{RO}_2\text{CO}^-$ ;  $\text{R} = \text{CH}_3, \text{C}_2\text{H}_5$ ). The mechanism of the reaction is likely a  $\text{S}_{\text{N}}2$  nucleophilic substitution.

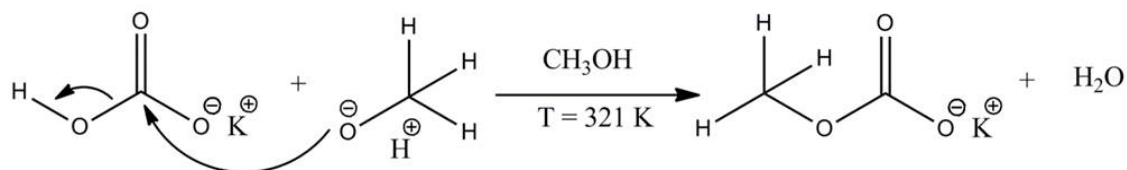


**Figure 5.8** Scheme of the  $\text{S}_{\text{N}}2$  nucleophilic substitution of  $\text{HCO}_3^-$  with  $\text{CH}_3\text{O}_2\text{CO}^-$  to  $\text{K[O}_2\text{COCH}_3]$ .

The presence of a  $\text{CH}_3$  group is obvious when the two different starting compounds in  $\text{CH}_3\text{OH}$  and  $\text{CD}_3\text{OH}$  solutions (Figure 5.8) are compared. As already mentioned in section 5.1.2 and Table 5.3, the stretching modes of  $\text{CH}_3 - \nu(\text{CH})$  – arise at frequencies of 2950, 2982 and 2845  $\text{cm}^{-1}$ . The bending mode of  $\text{CH}_3 - \delta_{\text{as}}(\text{CH}_3)$  – is situated at 1442  $\text{cm}^{-1}$ . When  $\text{CD}_3\text{OH}$  is used as solvent these four bands disappear. New bands arise at frequencies of 2245, 2127 and 2077  $\text{cm}^{-1}$ , as well as at 1107  $\text{cm}^{-1}$ . By using deuterium instead of hydrogen the vibration mode, where these atoms are involved, shift to lower wavenumbers. The ratio for deuterium and hydrogen modes is approximately  $\sqrt{2}$ . Also, the bands at 1186 and 900  $\text{cm}^{-1}$  in the spectrum of Figure 5.9a disappear in the spectrum of Figure 5.9b whereas new bands arise at 859 and 578  $\text{cm}^{-1}$ . The signals at 1186 and 859  $\text{cm}^{-1}$  are assigned to a  $\text{COCH}_3$  and  $\text{COCD}_3$  skeleton mode, whereas the ones at 900 and 578  $\text{cm}^{-1}$  to a  $\text{CH}_3\text{O}$  and  $\text{CD}_3\text{O}$  mode (Table 5.7).

The change of the crystal structures could be explained by trapping the solvent molecules in the crystal, or by the resemblance of the  $\text{H}_2\text{CO}_3$  crystal and the starting compound. Since the crystal structure of  $\text{KHCO}_3$  (monoclinic crystal space group  $P21/a$ ) is different from that of  $\text{K[O}_2\text{COCH}_3]$  (triclinic crystal, space group  $P-1$ ), a different polymorph of  $\text{H}_2\text{CO}_3$  is formed.

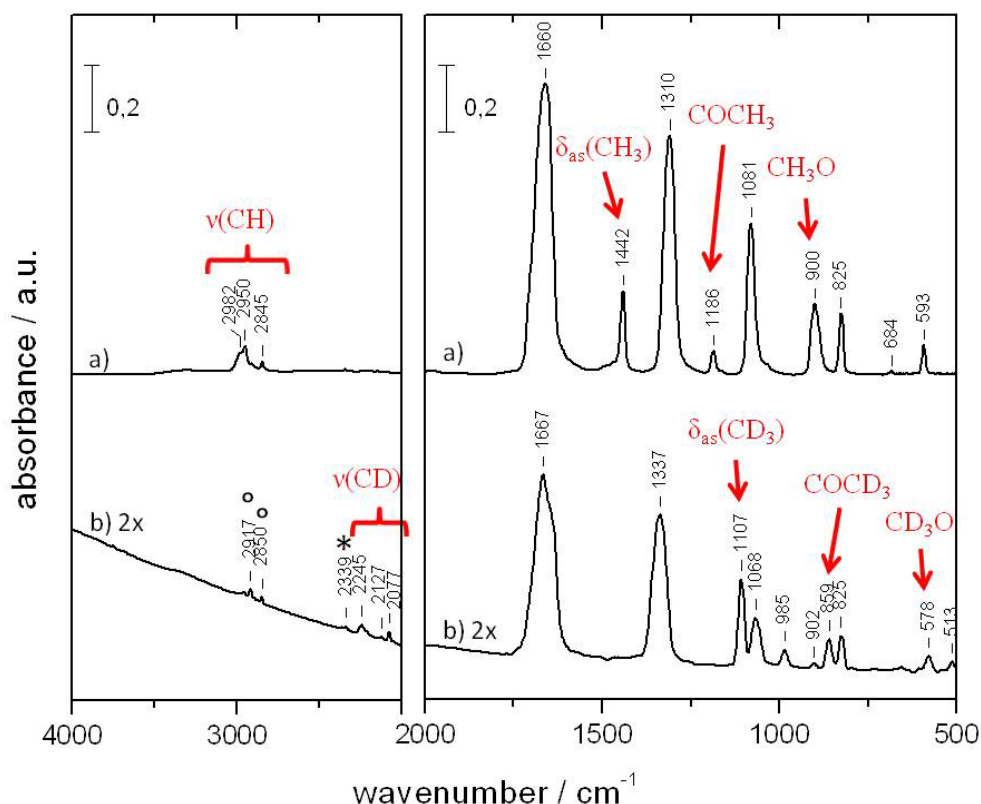
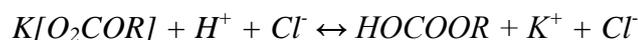


**Figure 5.9** a) IR spectrum of solid ( $K[O_2COCH_3]$ ) by reaction of methanolate ( $CH_3O^-$ ) with  $KHCO_3$ . The spectrum was recorded in vacuum at 290 K. b) IR spectrum of solid ( $K[O_2COCD_3]$ ) by reaction of  $d_3$ -methanolate ( $CD_3O^-$ ) with  $KHCO_3$ . The spectrum was recorded in vacuum at 290 K. The band marked with an asterisk belongs to  $CO_2$ , the one with a circle to impurities on the cryoplate. Vibrational modes which are assigned to the  $CH_3^-$  and  $CD_3^-$  group are shown in red.

An alternative explanation would be that it is not a polymorph of  $H_2CO_3$  that was isolated. The close resemblances of the IR spectra in Figure 5.3, Figure 5.5 and Figure 5.7 leads to the conclusion that possibly the monomethylester or monoethylester of carbonic acid ( $HOCOR$ ;  $R = CH_3, C_2H_5$ ) was formed (reaction 6) and not a polymorph of  $H_2CO_3$ , i.e., the hydrolysis step may not take place, which transforms the ester to  $H_2CO_3$ .



**reaction 6**

To further clarify the matter the spectra in Figure 5.3 and Figure 5.7 shall be discussed in more detail.  $K[O_2COCH_3]$  shows a band at  $1442\text{ cm}^{-1}$  (Figure 5.3a), which is assigned to  $\delta_{as}(CH_3)$  (Table 5.3). After protonation it shifts to  $1446\text{ cm}^{-1}$ . The band at  $1446\text{ cm}^{-1}$  in the IR spectrum of  $\alpha\text{-H}_2CO_3$  (Figure 5.3b) was assigned earlier to disordered  $H_2CO_3$  (Table 5.4).<sup>[19]</sup>  $K[O_2OCD_3]$  does not show the band at  $1442\text{ cm}^{-1}$  (Figure 5.7a), but a new one at  $1107\text{ cm}^{-1}$ , which is red shifted by a factor of 1.3 ( $\nu_2 \approx 1.41$ ). The signal at  $1107\text{ cm}^{-1}$  is assigned to  $\delta_{as}(CD_3)$ . After protonation it shifts weakly to  $1112\text{ cm}^{-1}$  (Figure 5.7b), but no band arises at  $1446\text{ cm}^{-1}$ .

Reaction of solid  $K[O_2COCH_3]$  with acid in methanol leads to the formation of  $\alpha\text{-H}_2\text{CO}_3$ . Solid  $K[O_2COCD_3]$  in the presence of acid in methanol results in  $\delta\text{-H}_2\text{CO}_3$ . Most likely the crystal structures of  $K[O_2COCH_3]$  and  $K[O_2COCD_3]$  are the same. If  $\alpha\text{-H}_2\text{CO}_3$  is a polymorph of carbonic acid,  $\alpha\text{-H}_2\text{CO}_3$  should also be formed after protonation and hydrolysis of  $K[O_2COCD_3]$  with acid in methanol. However, the IR spectra of  $\alpha\text{-H}_2\text{CO}_3$  (Figure 5.10b) and  $\delta\text{-H}_2\text{CO}_3$  (Figure 5.10a) are different. The presence of a band at  $1112\text{cm}^{-1}$  –  $\delta_{\text{as}}(\text{CD}_3)$  – and the absence of  $1446\text{cm}^{-1}$  –  $\delta_{\text{as}}(\text{CH}_3)$  – in  $\delta\text{-H}_2\text{CO}_3$  is an indicator, that the  $\text{CD}_3$  group is even present in the protonated form. Also, the weak bands at 2277, 2177 and  $2086\text{cm}^{-1}$ , that were assigned to  $\nu(\text{CD})$ , stress this suggestion. The frequencies at 2972, 2918 and  $2833\text{cm}^{-1}$  (Figure 5.3b) however, assigned to  $\nu(\text{CH})$ , disappear. Table 5.8 shows a possible assignment of the IR frequencies for  $\delta\text{-}$  and  $\alpha\text{-H}_2\text{CO}_3$ , based on a monomethylester of carbonic acid with either a  $\text{CD}_3\text{-}$  or  $\text{CH}_3\text{-}$  group. The values in red are the newly interpreted frequencies.

**Table 5.8 Assignment of the IR frequencies of solid  $\delta\text{-}$  and  $\alpha\text{-H}_2\text{CO}_3$  (all values in  $\text{cm}^{-1}$ ). The values in red are the newly interpreted frequencies.**

$\delta\text{-H}_2\text{CO}_3$ expt.	$\alpha\text{-H}_2\text{CO}_3$ expt.	$\alpha\text{-H}_2\text{CO}_3$ amorphous <sup>[3, 19]</sup>	Assign. <sup>[19]</sup>
2277	2972		
2177	2918	2963	$\nu_{\text{as}}(\text{CD})/\nu_{\text{as}}(\text{CH})$
2086	2833		
2737	2700		$\nu(\text{OH})$
2611	2591		$\nu(\text{OH})$
1727	1708	1717	$\nu(\text{C=O})$
1467	1479	1457	$\nu_{\text{as}}[\text{C}(\text{OH})]$
1112	1446	1136	$\delta_{\text{as}}(\text{CD}_3)/\delta_{\text{as}}(\text{CH}_3)$
	1423	1372	$\delta_{\text{ip}}(\text{COH})$
1324	1326 1311	1309	$\nu_{\text{as}}[\text{C}(\text{OH})]$
987			$\delta_{\text{s}}(\text{CD}_3)/\delta_{\text{s}}(\text{CH}_3)$
908	1199	1253	$\nu(\text{CO});$ $\text{COCD}_3/\text{COCH}_3$
1085	1086	1083	$\nu_{\text{s}}[\text{C}(\text{OH})_2]$
609	920	921	$\text{CD}_3\text{O}/\text{CH}_3\text{O}$
884	890		$\delta_{\text{oop}}(\text{COH})$
798	803	797	$\delta_{\text{oop}}(\text{CO}_3)$
	699	751	
570	584	584 561	$\delta_{\text{ip}}(\text{CO}_3)$

$\nu_{\text{s}}$  and  $\nu_{\text{as}}$ , symmetric and asymmetric stretching mode;  $\delta_{\text{ip}}$  and  $\delta_{\text{oop}}$ , in-plane and out-of-plane bending mode

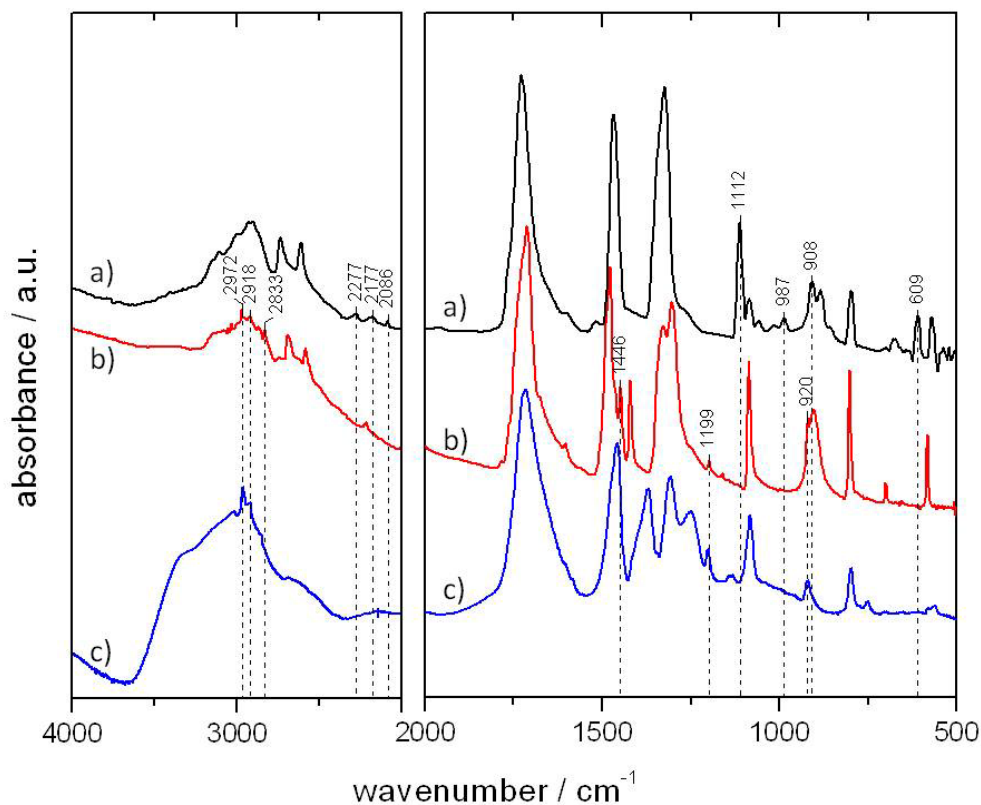


**Figure 5.10** IR-spectra of a)  $\delta$ - $\text{H}_2\text{CO}_3$ , b)  $\alpha$ - $\text{H}_2\text{CO}_3$  and c) amorphous  $\alpha$ - $\text{H}_2\text{CO}_3$  (spectrum (c) was taken from Figure 2 in Winkel et al. [3]). The absorbance of the spectra are scaled to have identical absorbance for the  $\nu(\text{CO})$  at about  $1700\text{ cm}^{-1}$ . Vibrational modes which are assigned to the  $\text{CH}_3^-$  and  $\text{CD}_3^-$  group are shown with vertical dashed lines.

Figure 5.11 shows the reaction pathway for the protonation of  $\text{K}[\text{O}_2\text{COCH}_3]$  with hydrochloric acid in methanol. The protonation takes place at 180 K, at 200 K methanol and water are pumped off and the monomethylester of carbonic acid ( $\text{HO}_2\text{COCH}_3$ ) crystallizes. The hydrolysis step may not take place, which transforms the ester to  $\text{H}_2\text{CO}_3$ .

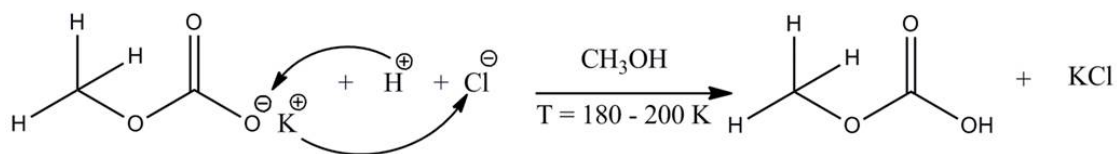


**Figure 5.11** Schema of the protonation of  $\text{K}[\text{O}_2\text{COCH}_3]$  with  $\text{HCl}$  in methanol.

Regarding the results, obtained by the reaction in ethanolic solution, nearly the same conclusions can be drawn (section 5.1.3). The bands at  $2979/2943/2908\text{ cm}^{-1}$  are assigned to the C-H stretching mode  $\nu(\text{CH})$  of  $\text{K}[\text{O}_2\text{COC}_2\text{H}_5]$ . The C-H bending mode  $\delta(\text{CH})$  can be found at  $1450/1401/1372\text{ cm}^{-1}$ , the  $\text{CH}_2$  wagging mode  $\omega(\text{CH}_2)$  at  $878\text{ cm}^{-1}$  and a  $\text{CH}_3\text{C}$  skeleton mode at  $981\text{ cm}^{-1}$  (Table 5.9, Figure 5.12). After protonation a broad band arises at  $1380\text{ cm}^{-1}$ , which can be assigned to  $\delta(\text{CH})$ . Also, the  $\nu(\text{CH})$  can be found at  $2993/2909\text{ cm}^{-1}$ . Due to the protonation, the band at  $878\text{ cm}^{-1}$   $\omega(\text{CH}_2)$  shifts to higher

wavenumbers at  $901\text{ cm}^{-1}$ , and the  $\text{CH}_3\text{C}$  mode at  $981\text{ cm}^{-1}$  is shifted to  $1009\text{ cm}^{-1}$ . These small changes in the IR spectrum of the protonated species (Figure 5.12b) suggest also the presence of the  $\text{C}_2\text{H}_5$  group and underline the theory of a formation of the carbonic acid monoalkylester. Table 5.9 shows a possible assignment of the IR frequencies for  $\gamma\text{-H}_2\text{CO}_3$ , based on a monoethylester of carbonic acid with either a  $\text{C}_2\text{H}_5\text{-}$  group. The values in red are the newly interpreted frequencies.

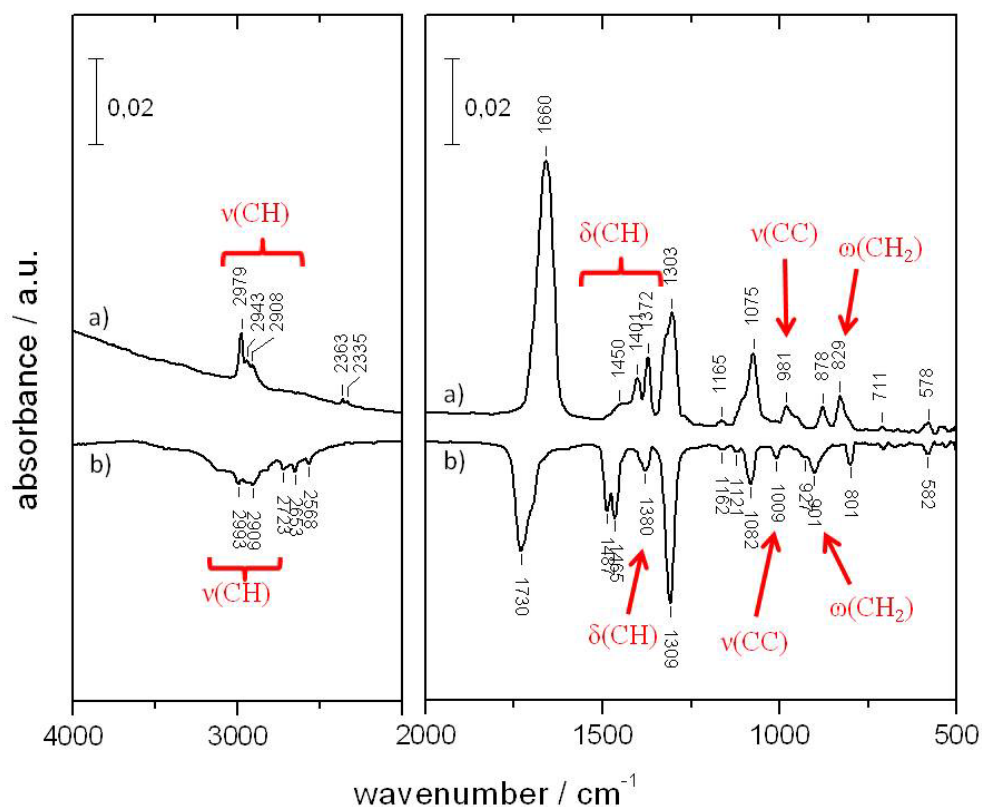


**Figure 5.12** a) IR spectrum of solid ( $\text{K}[\text{O}_2\text{COC}_2\text{H}_5]$ ) from reaction of ethanolate ( $\text{C}_2\text{H}_5\text{O}^-$ ) with  $\text{KHCO}_3$ . The spectrum was recorded in vacuum at 290 K. b) IR subtraction spectrum of a crystalline species, which evaporates or decomposes at 210 K in vacuum. The new species is obtained after protonation of solid ( $\text{K}[\text{O}_2\text{COC}_2\text{H}_5]$ ) with  $\text{HCl}$  in  $\text{H}_2\text{O}$ . The new species is labeled  $\gamma\text{-H}_2\text{CO}_3$ . Vibrational modes which are assigned to the  $\text{C}_2\text{H}_5\text{-}$  group are shown in red.

To shed further light on the nature of the different  $\text{H}_2\text{CO}_3$  polymorphs, more experiments need to be done. Mass spectrometry should be an important method for solving this puzzle. Also, matrix isolation studies of the new polymorphs should be helpful.

**Table 5.9 Assignment of the IR frequencies of solid  $\gamma$ -H<sub>2</sub>CO<sub>3</sub>, compared with the ones from K[O<sub>2</sub>COC<sub>2</sub>H<sub>5</sub>] (all values in cm<sup>-1</sup>). The values in red are the newly interpreted frequencies.**

K[O <sub>2</sub> COC <sub>2</sub> H <sub>5</sub> ]		$\gamma$ -H <sub>2</sub> CO <sub>3</sub>	K[O <sub>2</sub> COC <sub>2</sub> H <sub>5</sub> ]
lit. <sup>[53]</sup>	expt.		Assign. <sup>[53]</sup>
2967 (s)	2979 (m)	2993	v(CH)
2907 (m)	2943 (w)	2909	
	2908 (w)		
		2723	
		2653	
		2568	
1689 (s)	1660 (vs)	1730	v <sub>as</sub> (CO <sub>2</sub> )
		1487	
		1465	
1484 (w)	1450 (sh)		$\delta$ (CH)
1445 (w)	1401 (m)	1380	
1389 (m)	1372 (m)		
1370 (s)			
1295 (s)	1303 (s)	1309	v <sub>s</sub> (CO <sub>2</sub> )
1274 (m)			$\delta$ <sub>s</sub> (CH <sub>3</sub> )
1172 (w)		1162	v(CO)
1114 (m)	1165 (vw)	1121	
1075 (sh)			
1059 (s)	1075 (s)	1082	v(CC)
966 (s)	981 (m)	1009	
		921	
876 (s)	878 (m)	901	$\omega$ (CH <sub>2</sub> )
821 (s)		801	$\pi$ (CO <sub>3</sub> )
812 (w)	829 (m)		
701 (w)	711 (vw)		$\delta$ <sub>as</sub> (CO <sub>2</sub> )
584 (w)	578 (w)	582	$\delta$ <sub>s</sub> (CO <sub>2</sub> )

*vw, very weak; w, weak; m, medium, s, strong; vs, very strong; sh, shoulder*  
*v<sub>s</sub> and v<sub>as</sub>, symmetric and asymmetric stretching mode;  $\delta$ , in-plane;  $\pi$ , out of plane bending mode;  $\omega$ , wagging mode;*

## 6 Matrix Isolation: New Interpretation

---

I was successful in the isolation of  $\alpha$ -H<sub>2</sub>CO<sub>3</sub> in a solid matrix,<sup>[29]</sup> and later I also achieved the isolation of the  $\beta$ -polymorph ( $\beta$ -H<sub>2</sub>CO<sub>3</sub>) in a solid matrix. The analysis of the matrix spectra and the attempt of assigning bands prompts new questions, also about the two solid state H<sub>2</sub>CO<sub>3</sub> polymorphs.

Comparison of the band positions of the two carbonic acid monomers – symmetries C<sub>2v</sub> and C<sub>s</sub> – isolated from crystalline  $\beta$ -H<sub>2</sub>CO<sub>3</sub> (**Paper II**) and  $\alpha$ -H<sub>2</sub>CO<sub>3</sub> (**Paper I**) shows disagreement. If both matrix spectra contain the same two conformers, one would expect the band positions to be identical. However, the spectra show a blue shift between the monomers isolated from  $\beta$ - and  $\alpha$ -polymorph. The  $\nu$ (C=O) of the C<sub>2v</sub> monomer isolated from the  $\beta$ -polymorph arises in an Ar matrix at 1792/1788 cm<sup>-1</sup> and is blue shifted by about 12 cm<sup>-1</sup> compared to the one of  $\alpha$ -H<sub>2</sub>CO<sub>3</sub> arising at 1779/1776 cm<sup>-1</sup>.<sup>[29]</sup> The  $\nu$ (C=O) of the C<sub>s</sub> monomer is shifted from 1829/1826 cm<sup>-1</sup> ( $\alpha$ -H<sub>2</sub>CO<sub>3</sub>)<sup>[29]</sup> to 1833/1829 cm<sup>-1</sup> ( $\beta$ -H<sub>2</sub>CO<sub>3</sub>). The change in the  $\nu$ (C=O) mode suggests different environments for the two polymorphs. The shifts can result from the isolation of multimers instead of monomers. However, the very good correlation of the experiments for the  $\beta$ -H<sub>2</sub>CO<sub>3</sub>/Ar-matrix with the theory leads to the conclusion that only monomers are isolated. The small amount of starting compound and the saturation vapor pressure ( $p_s$ ) of  $4 \cdot 10^{-7}$  mbar – for the H<sub>2</sub>CO<sub>3</sub> monomer –<sup>[23]</sup> affirms this conclusion. The CO stretching mode observed for the  $\alpha$ -H<sub>2</sub>CO<sub>3</sub>/Ar-matrix correlates also with the theory. The disagreement might also be a result of the different (vibrational) temperatures associated with molecules isolated from the gas-phase above  $\alpha$ -H<sub>2</sub>CO<sub>3</sub> at > 210 K and above  $\beta$ -H<sub>2</sub>CO<sub>3</sub> at > 230 K. Based on this vibration mode it is difficult to make a final conclusion about the origin of the blue shift.

The region, where asymmetric and symmetric C-(OH) stretching and in-plane deformation modes overlap, also shows a change in the matrix spectra. For the  $\alpha$ -H<sub>2</sub>CO<sub>3</sub>/Ar-matrix the  $\nu_{as}$ (C(OH)<sub>2</sub>) of C<sub>2v</sub> arises at 1452 cm<sup>-1</sup> (see Figure 2 and Table 1 in ref.<sup>[29]</sup>). However, the  $\nu_{as}$ (C(OH)<sub>2</sub>) of C<sub>s</sub> does not appear. For the spectra of the other isotopologues also a disagreement between theory and experiments results, since many bands arise in this region. The  $\beta$ -H<sub>2</sub>CO<sub>3</sub>/Ar-matrix is easier to interpret: the band at 1446/1438 cm<sup>-1</sup> (matrix splitting) is assigned to  $\nu_{as}$ (C(OH)<sub>2</sub>) for the C<sub>2v</sub> monomer and the one at 1392/1385 cm<sup>-1</sup> (matrix splitting) to  $\nu_{as}$ (C(OH)<sub>2</sub>) for the C<sub>s</sub>. This shift is in good agreement with calculations carried out at the MP2/aug-cc-pVTZ level of theory by Mag. Roland G. Huber in Innsbruck. For the  $\alpha$ -H<sub>2</sub>CO<sub>3</sub>/Ar-matrix, bands arise with the same shift of 57 cm<sup>-1</sup> to lower wavenumbers, at 1383 cm<sup>-1</sup> C<sub>2v</sub> and 1326 cm<sup>-1</sup> C<sub>s</sub>. The shifts and the positions for the  $\beta$ -H<sub>2</sub>CO<sub>3</sub> vapor and other isotopologues agree much better with the theory, than for  $\alpha$ -H<sub>2</sub>CO<sub>3</sub>.

The  $\delta_{ip}(\text{COH})$  mode of  $\alpha\text{-H}_2\text{CO}_3$  monomer  $C_{2v}$  arises in Ar at 1182/1181  $\text{cm}^{-1}$  (see Figure 2 and Table 1 in ref. [29]). Comparison of the predicted band at 1166  $\text{cm}^{-1}$  reveals that the observed band is blue shifted by 15  $\text{cm}^{-1}$ . For the  $\beta\text{-H}_2\text{CO}_3/\text{Ar}$ , the one assigned to  $\delta_{ip}(\text{COH})$  arises at 1136  $\text{cm}^{-1}$  and is red shifted by 30  $\text{cm}^{-1}$  compared to the theory. Usually, the relationship between theory and experiment shows a deviation to lower wavenumbers (red shift) in the experiment.

There is conclusive evidence that in the  $\beta\text{-H}_2\text{CO}_3$  experiments the correct  $\text{H}_2\text{CO}_3$  monomers  $C_{2v}$  and  $C_s$  were isolated. However, the open questions and inconsistencies mentioned above prompt the question of what has been isolated in the first experiment of  $\alpha\text{-H}_2\text{CO}_3$  in Ar.

In the following I attempt to interpret the matrix spectra based on the assumption that a different species was in fact isolated. As candidate molecules I have investigated dicarbonic acid ( $\text{H}_2\text{C}_2\text{O}_5$ ), dimers, polymers, water complexes or the monomethyl ester of carbonic acid. As a best candidate species that allows to understand the matrix spectra isolated above  $\alpha\text{-H}_2\text{CO}_3$  I propose monomethyl carbonic acid. In order to answer the open question ultimately more experiments are required, in particular mass spectrometry and diffraction. Matrix isolation spectroscopy is an able technique to differentiate between the structures of evaporated molecules coming from these polymorphs and thus supplies valuable information in this ongoing puzzle of the carbonic acid.

## 6.1 The vapor molecules over $\alpha\text{-H}_2\text{CO}_3$

Here I propose a new hypothesis what the vapor molecules over  $\alpha\text{-H}_2\text{CO}_3$  might be. My investigations of  $\text{KHCO}_3$  in different organic solutions – methanol or ethanol – show the transformation of  $\text{HCO}_3^-$  to  $\text{ROCO}_2^-$  ( $R = \text{CH}_3, \text{C}_2\text{H}_5, \text{CD}_3$ ). The different carbonic acid polymorphs differ in the sublimation temperature, in the gas-phase stability as well as in the matrix-splitting. Hage et al. [1] have shown that only  $\beta\text{-H}_2\text{CO}_3$  can be transformed to amorphous  $\alpha\text{-H}_2\text{CO}_3$  by treatment with HCl in methanol [1, 21]. According to my hypothesis put forth in chapter 5 this transformation may actually be the result of an acidic esterification.

### 6.1.1 Monomethyl carbonic acid

The first synthesis of monomethyl carbonic acid ( $\text{HOCO}_2\text{CH}_3$ ) by Gattow and Behrendt was achieved by combining a suspension of  $\text{Na}[\text{OCO}_2\text{CH}_3]$  and  $\text{HCl}(\text{g})$  in dimethyl ether at  $-50\text{ }^\circ\text{C}$ . [57] The melting point is at  $-36 \pm 1\text{ }^\circ\text{C}$  and the dissociation constant in water at  $25\text{ }^\circ\text{C}$  was calculated to  $K_a = (2.44 \pm 0.03) \times 10^{-6}$ . [57-58] A solution of  $\text{HOCO}_2\text{CH}_3$  in diethyl ether shows IR absorbances at: [57-58]

3484 [s;  $\nu(\text{OH})$ ], 1779 [m;  $\nu_{as}(\text{CO})$ ], 1730 [s;  $\nu_{as}(\text{CO})$ ], 1277 and 1255 [s;  $\delta_s(\text{CH}_3)$ ], 823 [s;  $\pi(\text{CO}_3)$ ], 567 [w;  $\delta_s(\text{CO}_3)$ ]  $\text{cm}^{-1}$ . (s, strong; m, medium; w, weak)

Solid  $\text{HOCO}_2\text{CH}_3$  stands in decomposition equilibrium with  $\text{CO}_2$  and  $\text{CH}_3\text{OH}$ . The resulting decomposition enthalpy and entropy are  $\Delta H = 4.4 \pm 0.4$  kcal/mol and  $\Delta S = 23.6 \pm 0.8$  cal/mol degree. <sup>[57]</sup>

In 2006 Dibenedetto et al. characterized  $\text{HOCO}_2\text{CH}_3$  with  $^1\text{H}$  and  $^{13}\text{C}$  NMR spectroscopy. The monomethyl ester of carbonic acid has been prepared at 300 K by protonation of  $\text{Na}[\text{OCO}_2\text{CH}_3]$  with anhydrous HCl or water. <sup>[55]</sup> Theoretical studies on the gas-phase potential energy surface show that the global energy-minimum of the  $\text{HOCO}_2\text{CH}_3$  molecule corresponds to the cis-cis orientation of the  $\text{CH}_3$  and OH groups. Other conformations like cis-trans (1.3 kcal/mol) and trans-cis (3.2 kcal/mol) lie above the most stable isomer. <sup>[55]</sup> Also it was found that  $\text{HOCO}_2\text{CH}_3$  is slightly less acidic than  $\text{H}_2\text{CO}_3$ . <sup>[55]</sup> (Figure 6.1)

In 2009 Gohres et al. investigated the formation and dissociation of alkyl carbonic acid (ACA) in  $\text{CO}_2$ -expanded alcohols. With UV/vis spectroscopy the acid dissociation constant was obtained and it was found in agreement with the results by Gattow and Behrendt that methyl carbonic acid has a  $\text{p}K_a$  of 5.7. The experimental value for  $\text{p}K_a$  of  $\text{H}_2\text{CO}_3$  is  $3.45 \pm 0.15$ . <sup>[6]</sup>

In 2011 Vidal et al. investigated the formation and the properties of monoalkyl carbonates in aqueous medium. <sup>[59]</sup> With capillary electrophoresis they measured the effective mobility at different pH values of the monoalkyl carbonates to estimate the  $\text{p}K_a$  values. However, the results demonstrated that the  $\text{p}K_a$  values for alkyl carbonic acids are below 4.0. <sup>[59]</sup>

*Ab-initio* quantum mechanical calculations of alkyl carbonic acid in various isotope configurations were performed to obtain reference frequencies for annotating measured spectra. All calculations were performed using the Gaussian 09 package <sup>[36]</sup>. The different conformations shown in Figure 6.1 were employed for geometry optimization, where the cis-cis is the energetically most favorable conformation. <sup>[5, 37]</sup> Calculations were performed using second-order Møller-Plesset perturbation theory (MP2) with the augmented correlation consistent basis sets of Dunning and co-workers. <sup>[38-40]</sup> Initial optimization was done at the MP2/aug-cc-pVDZ level of theory requiring “verytight” convergence on displacement and forces. Starting from the resulting geometry, further optimization at the MP2/aug-cc-pVTZ level of theory using “verytight” convergence criteria yielded an energy minimum for frequency calculations. Subsequently, IR and Raman modes were determined at this minimum geometry using MP2/aug-cc-pVTZ. Isotope shifts were calculated by performing frequency calculations at the same minimum for either all  $^2\text{H}$  or  $^{13}\text{C}$ -labeled alkyl carbonic acid. Calculated frequencies and isotope shifts were then used to identify the various signals observed in the experimentally obtained spectra.

Calculations of four alkyl carbonic acid monomers were done. The monomer with cis-cis orientation of the  $\text{CH}_3$  and OH groups shown in Figure 6.1 is the global minimum. The

next lowest structure is the cis-trans conformer with an energy difference of 1.3 kcal/mol. The trans-cis monomer is a local minimum that is less stable by only 3.5 kcal/mol. The monomer with trans-trans orientation of CH<sub>3</sub> and OH lies above the most stable isomer by 10.6 kcal/mol.

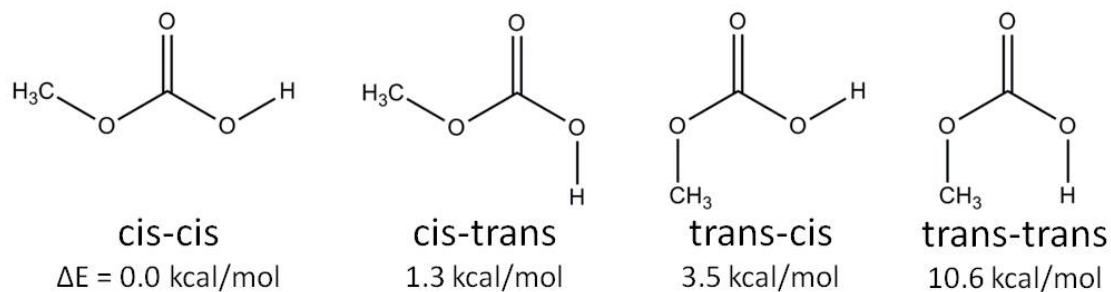


**Figure 6.1** The global energy-minimum for the monomethyl carbonic acid conformers.

The predicted IR frequencies for the cis-cis and cis-trans monomer are summarized in Table 6.1 and Table 6.2.

**Table 6.1 Predicted IR bands for the cis-cis HOCO<sub>2</sub>CH<sub>3</sub> monomer and isotopologues; wavenumbers in cm<sup>-1</sup> (theoretical intensities in % in parentheses). Level of theory: MP2/aug-cc-pVTZ**

<i>cis-cis monomer</i>			
HO <sup>12</sup> CO <sub>2</sub> CH <sub>3</sub>	HO <sup>13</sup> CO <sub>2</sub> CH <sub>3</sub>	DO <sup>12</sup> CO <sub>2</sub> CH <sub>3</sub>	Assignment
3800 (22)	3800 (23)	2765 (11)	ν(OH); ν(OD)
3225 (1)	3225 (1)	3225 (1)	ν <sub>as</sub> (CH <sub>3</sub> ); ν <sub>as</sub> (CD <sub>3</sub> )
3193 (2)	3193 (2)	3193 (2)	ν <sub>as</sub> (CH <sub>2</sub> ); ν <sub>as</sub> (CD <sub>2</sub> )
3095 (5)	3095 (5)	3098 (4)	ν <sub>s</sub> (CH <sub>3</sub> ); ν <sub>s</sub> (CD <sub>3</sub> )
1815 (82)	1768 (78)	1808 (72)	ν(C=O)
1521 (2)	1521 (2)	1521 (2)	σ(CH <sub>2</sub> )
1513 (2)	1513 (2)	1513 (1)	ω(CH <sub>3</sub> )
1495 (13)	1490 (7)	1493 (10)	ρ(CH <sub>3</sub> )
1409 (49)	1381 (41)	1364 (100)	δ <sub>ip</sub> (COH); δ <sub>ip</sub> (COD)
1228 (2)	1228 (5)	1228 (1)	ρ(CH <sub>3</sub> )
1219 (100)	1211 (100)	1031 (20)	δ <sub>ip</sub> (COH); δ <sub>ip</sub> (COD)
1192 (0)	1192 (1)	1192 (0)	τ(CH <sub>2</sub> )
1109 (1)	1106 (1)	1112 (4)	ν(O-(CH <sub>3</sub> ))
919 (4)	917 (4)	866 (3)	δ <sub>ip</sub> (CO <sub>3</sub> )
804 (6)	779 (6)	804 (4)	δ <sub>oop</sub> (CO <sub>3</sub> )

*ν<sub>s</sub> and ν<sub>as</sub>, symmetric and asymmetric stretching mode; δ<sub>ip</sub> and δ<sub>oop</sub>, in-plane and out-of-plane bending mode. For CH modes: σ, in plane bending mode ; ω, wagging mode; τ, twisting mode; ρ, rocking mode.*

**Table 6.2 Predicted IR bands for the cis-trans HOCO<sub>2</sub>CH<sub>3</sub> monomer and isotopologues; wavenumbers in cm<sup>-1</sup> (theoretical intensities in % in parentheses) Level of theory: MP2/aug-cc-pVTZ**

<i>cis-trans monomer</i>			
HO <sup>12</sup> CO <sub>2</sub> CH <sub>3</sub>	HO <sup>13</sup> CO <sub>2</sub> CH <sub>3</sub>	DO <sup>12</sup> CO <sub>2</sub> CH <sub>3</sub>	Assignment
3800 (15)	3800 (17)	2765 (50)	ν(OH); ν(OD)
3224 (1)	3223 (1)	3225 (1)	ν <sub>as</sub> (CH <sub>3</sub> ); ν <sub>as</sub> (CD <sub>3</sub> )
3196 (2)	3196 (2)	3193 (2)	ν <sub>as</sub> (CH <sub>2</sub> ); ν <sub>as</sub> (CD <sub>2</sub> )
3099 (4)	3099 (4)	3098 (3)	ν <sub>s</sub> (CH <sub>3</sub> ); ν <sub>s</sub> (CD <sub>3</sub> )
1862 (59)	1813 (60)	1854 (60)	ν(C=O)
1523 (2)	1522 (2)	1523 (1)	σ(CH <sub>2</sub> )
1512 (1)	1511 (2)	1512 (1)	ω(CH <sub>3</sub> )
1489 (7)	1487 (5)	1489 (4)	ρ(CH <sub>3</sub> )
1351 (100)	1330 (100)	1310 (100)	δ <sub>ip</sub> (COH); δ <sub>ip</sub> (COD)
1224 (2)	1224 (3)	1224 (2)	ρ(CH <sub>3</sub> )
1215 (13)	1202 (23)	981 (1)	δ <sub>ip</sub> (COH); δ <sub>ip</sub> (COD)
1192 (0)	1192 (0)	1192 (0)	τ(CH <sub>2</sub> )
1103 (5)	1100 (4)	1114 (5)	ν(O-(CH <sub>3</sub> ))
910 (10)	906 (11)	880 (11)	δ <sub>ip</sub> (CO <sub>3</sub> )
794 (3)	769 (3)	794 (3)	δ <sub>oop</sub> (CO <sub>3</sub> )

*ν<sub>s</sub> and ν<sub>as</sub>, symmetric and asymmetric stretching mode; δ<sub>ip</sub> and δ<sub>oop</sub>, in-plane and out-of-plane bending mode. For CH modes: σ, in plane bending mode; ω, wagging mode; τ, twisting mode; ρ, rocking mode.*

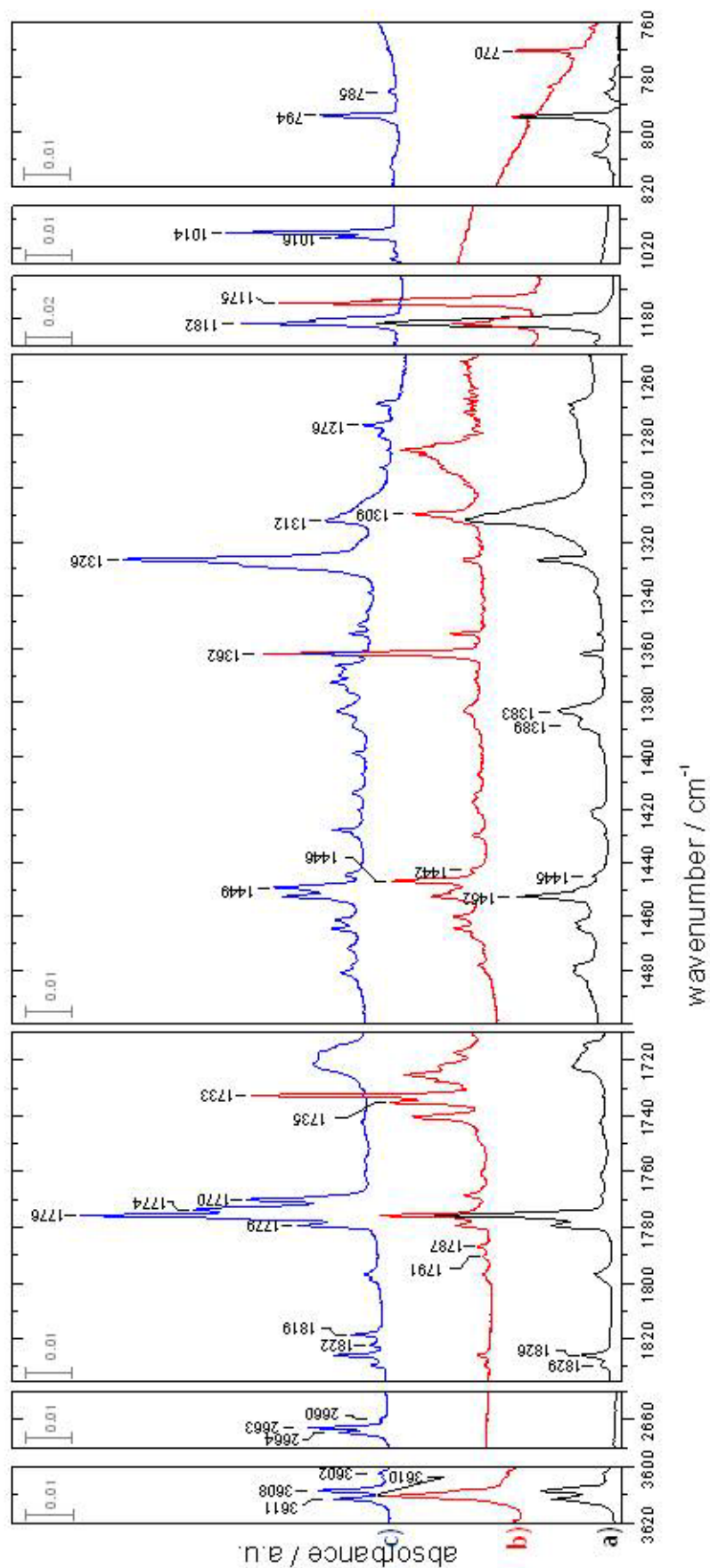


Figure 6.2 IR spectra of  $\alpha$ - $\text{H}_2\text{CO}_3$  and isotopologues vapour after sublimation of the crystal at 210 K and isolation in argon matrix at 6 K. a)  $\text{H}_2\text{CO}_3$ , b)  $\text{H}_2^{13}\text{CO}_3$  (65%), c)  $\text{D}_2\text{CO}_3$  (50%). Spectra are shifted for clarity. New assignment of the bands is given in Table 6.5 and Table 6.6.

### 6.1.2 New interpretation of the $\alpha$ -H<sub>2</sub>CO<sub>3</sub>/Ar-matrix

To obtain more information about the vapor molecules above  $\alpha$ -H<sub>2</sub>CO<sub>3</sub>, I tried to interpret the matrix spectra (Figure 6.2) based on MP2/aug-cc-pVTZ level of theory for dicarbonic acid, water complexes and carbonic acid ester. H<sub>2</sub>CO<sub>3</sub> polymers could be eliminated due to the sharp bands in the spectra (Figure 6.2). Bands with a FWHM (full width of half maximum) of about 2 cm<sup>-1</sup> are congruent with the presence of monomers. Dicarbonic acid (H<sub>2</sub>C<sub>2</sub>O<sub>5</sub>) could be excluded, since no evidence for the C-O-C stretch vibration calculated between 1170 – 1150 cm<sup>-1</sup> exists. Emanating from a production of crystalline  $\alpha$ -H<sub>2</sub>CO<sub>3</sub> free of H<sub>2</sub>O (reaction in methanolic solution), the non-formation of water complexes would be expected. A methanol adduct could be excluded due to the complete separation of excess methanol during the  $\alpha$ -H<sub>2</sub>CO<sub>3</sub> production, which is evident in the absence of the most intense methanol band at ca. 1029 cm<sup>-1</sup> [60] in the IR spectrum (Figure 5.3b).

The monomethyl carbonic acid ester is the best candidate to describe the absorbance in the spectra in Figure 6.2. In the region where the CO stretching vibration appears (region between 1840 – 1700 cm<sup>-1</sup>), the experimental results correlate with the theoretical calculations of the two H<sub>2</sub>CO<sub>3</sub> monomers as well as the HOCO<sub>2</sub>CH<sub>3</sub> species. The calculations show that  $\nu$ (CO) shifts to higher wavenumbers (blue shift of 20 cm<sup>-1</sup>) for the H<sub>2</sub>CO<sub>3</sub> monomers compared to the HOCO<sub>2</sub>CH<sub>3</sub> (Table 6.1 – Table 6.4). The experiment shows a shift of about 12 cm<sup>-1</sup> for  $\nu$ (CO) between the species isolated above  $\alpha$ -H<sub>2</sub>CO<sub>3</sub> and  $\beta$ -H<sub>2</sub>CO<sub>3</sub>. The change in the  $\nu$ (CO) mode suggests different environments for the two species. A CH<sub>3</sub>-group instead of an OH-group can be the origin of the blue shift reported above.

In the OH stretching mode  $\nu$ (OH) region the experimental results correlate also with the theoretical calculations of the two H<sub>2</sub>CO<sub>3</sub> monomers as well as the HOCO<sub>2</sub>CH<sub>3</sub> species. Based on the  $\nu$ (CO) and  $\nu$ (OH) vibration modes it is difficult to make a final conclusion about the isolated species.

Very interesting is the region between 1500 – 1250 cm<sup>-1</sup>. The spectra of  $\alpha$ -H<sub>2</sub>CO<sub>3</sub> in Ar show a lot of bands arising (Figure 6.2) in contrast to the ones of the  $\beta$ -H<sub>2</sub>CO<sub>3</sub>/Ar-matrix (see Figure 3 ref. [61]). Assignments of these bands are very hard. The calculations for the H<sub>2</sub>CO<sub>3</sub> monomers disagree here with the experiments. The asymmetric C(OH)<sub>2</sub> stretching vibration for the cis-cis H<sub>2</sub><sup>12</sup>CO<sub>3</sub> monomer is calculated to be at 1467 cm<sup>-1</sup>, for <sup>2</sup>H at 1399 cm<sup>-1</sup> (68 cm<sup>-1</sup> red shifted) and for <sup>13</sup>C at 1433 cm<sup>-1</sup> (34 cm<sup>-1</sup> red shifted; Table 6.3). Figure 6.2a shows a band arising at 1452 cm<sup>-1</sup> (<sup>12</sup>C), in Figure 6.2b a new band arises at 1447 cm<sup>-1</sup> (<sup>13</sup>C) and in the spectrum Figure 6.2c at 1449 cm<sup>-1</sup> (<sup>2</sup>H). The experimental shift between <sup>12</sup>C and <sup>13</sup>C isotopologues is 5 cm<sup>-1</sup>, and for <sup>12</sup>C and <sup>2</sup>H 3 cm<sup>-1</sup>. These shifts disagree with the calculations. However, calculations of the stable cis-cis HOCO<sub>2</sub>CH<sub>3</sub> monomer show a band at 1495 cm<sup>-1</sup> assigned to the CH<sub>3</sub> rocking mode  $\rho$ (CH<sub>3</sub>) of the <sup>12</sup>C

isotopologue. For the  $^{13}\text{C}$  this band shifts to lower wavenumbers of  $1490\text{ cm}^{-1}$  (red shift  $5\text{ cm}^{-1}$ ) which correlated with the experimental shift. The  $\text{CH}_3$  rocking mode of the  $^2\text{H}$  isotopologue is predicted at  $1493\text{ cm}^{-1}$  (red shift of  $2\text{ cm}^{-1}$ ), which agrees with the experimental shift of  $3\text{ cm}^{-1}$ . The cis-cis  $\text{HOCO}_2\text{CH}_3$  monomer better describes the bands around  $1450\text{ cm}^{-1}$  in Figure 6.2 than cis-cis  $\text{H}_2\text{CO}_3$ .

**Table 6.3 Predicted IR bands for the cis-cis  $\text{H}_2\text{CO}_3$  monomer and isotopologues; wavenumbers in  $\text{cm}^{-1}$  (theoretical intensities in % in parentheses). Level of theory: MP2/aug-cc-pVTZ**

<i>cis-cis monomer</i>			
$\text{H}_2\text{ }^{12}\text{CO}_3$	$\text{H}_2\text{ }^{13}\text{CO}_3$	$\text{D}_2\text{ }^{12}\text{CO}_3$	Assignment
3802 (3)	3802 (3)	2764 (25)	$\nu_s(\text{OH}); \nu_s(\text{OD})$
3801 (40)	3801 (42)	2769 (1)	$\nu_{as}(\text{OH}); \nu_{as}(\text{OD})$
1834 (100)	1788 (100)	1822 (100)	$\nu(\text{C}=\text{O})$
1467 (28)	1433 (21)	1399 (77)	$\nu(\text{C}(\text{OH})_2)$
1289 (5)	1289 (6)	1077 (10)	$\delta_{ip}(\text{COH})$
1166 (84)	1160 (91)	962 (27)	$\delta_{ip}(\text{COH})$
983 (4)	981 (4)	895 (0)	$\delta_{ip}(\text{CO}_3)$
802 (8)	777 (9)	801 (6)	$\delta_{oop}(\text{CO}_3)$

$\nu_s$  and  $\nu_{as}$ , symmetric and asymmetric stretching mode;  $\delta_{ip}$  and  $\delta_{oop}$ , in-plane and out-of-plane bending mode.

In the  $^2\text{H}$  spectrum (Figure 6.2c) an intensive band arises at  $1326\text{ cm}^{-1}$ . Comparison with the theoretical IR frequencies of the two  $\text{H}_2\text{CO}_3$  monomers (Table 6.3 and Table 6.4) reveal no analogy. So this band cannot be described with the  $\text{H}_2\text{CO}_3$  concept. Calculations of the cis-cis  $^2\text{HOCO}_2\text{CH}_3$  monomer (Table 6.1) show the most intense band at  $1364\text{ cm}^{-1}$  assigned to one of the COD in plane bending modes  $\delta_{ip}(\text{COD})$ . For the  $\text{HO}^{12}\text{CO}_2\text{CH}_3$  monomer the calculation predicts the  $\delta_{ip}(\text{COH})$  mode at  $1409\text{ cm}^{-1}$ , which results in a blue shift of  $45\text{ cm}^{-1}$ . In Figure 6.2a bands arise at  $1388/1383\text{ cm}^{-1}$  and show a shift of  $63/57\text{ cm}^{-1}$ . The  $\delta_{ip}(\text{COH})$  mode of the cis-cis  $^{13}\text{C}$  isotopologue is predicted at  $1381\text{ cm}^{-1}$  and is red shifted of about  $28\text{ cm}^{-1}$  to the  $^{12}\text{C}$  and blue shifted of about  $17\text{ cm}^{-1}$  to the  $^2\text{H}$  isotopologue. Figure 6.2b shows an intensive band at  $1362\text{ cm}^{-1}$ , which is red shifted of about  $27/21\text{ cm}^{-1}$  compared to the  $^{12}\text{C}$  but  $36\text{ cm}^{-1}$  blue shifted to the  $^2\text{H}$  isotopologue.

The calculation predicts the  $\delta_{ip}(\text{COH})$  mode of the cis-cis  $\text{H}_2\text{CO}_3$  monomer at  $1166\text{ cm}^{-1}$  (Table 6.3). In Figure 6.2a the more intense band arises at  $1182\text{ cm}^{-1}$  and is blue shifted to the theoretical prediction. The second  $\delta_{ip}(\text{COH})$  mode of the cis-cis  $\text{HOCO}_2\text{CH}_3$  monomer is calculated at  $1219\text{ cm}^{-1}$  and has the highest intensity (Table 6.1). The deviation between theory and experiment here results in a red shift. The calculation shows a red shift of  $8\text{ cm}^{-1}$  between  $^{12}\text{C}$  and  $^{13}\text{C}$  which correlates with the experimental

shift of 7 cm<sup>-1</sup>. The band at 1016/1014 cm<sup>-1</sup> was assigned to the second  $\delta_{ip}(\text{COD})$  mode for the cis-cis <sup>2</sup>HOCO<sub>2</sub>CH<sub>3</sub> monomer.

The cis-cis HOCO<sub>2</sub>CH<sub>3</sub> monomer describes certain intense bands in Figure 6.2 better than the H<sub>2</sub>CO<sub>3</sub> monomers. All theoretical predictions for the cis-cis and cis-trans H<sub>2</sub>CO<sub>3</sub> are summarized in Table 6.3 and Table 6.4.

**Table 6.4 Predicted IR bands for the cis-trans H<sub>2</sub>CO<sub>3</sub> monomer and isotopologues; wavenumbers in cm<sup>-1</sup> (theoretical intensities in % in parentheses). Level of theory: MP2/aug-cc-pVTZ**

<i>cis-trans monomer</i>			
H <sub>2</sub> <sup>12</sup> CO <sub>3</sub>	H <sub>2</sub> <sup>13</sup> CO <sub>3</sub>	D <sub>2</sub> <sup>12</sup> CO <sub>3</sub>	Assignment
3805 (23)	3805 (24)	2769 (12)	$\nu(\text{OH}_C)$ ; $\nu(\text{OD}_C)$
3797 (21)	3797 (23)	2763 (12)	$\nu(\text{OH}_T)$ ; $\nu(\text{OD}_T)$
1880 (100)	1832 (100)	1867 (100)	$\nu(\text{C}=\text{O})$
1409 (65)	1382 (62)	1343 (86)	$\nu(\text{C}(\text{OH})_2)$
1270 (25)	1270 (26)	1038 (17)	$\delta_{ip}(\text{COH})$
1152 (42)	1149 (48)	949 (12)	$\delta_{ip}(\text{COH})$
968 (10)	965 (11)	902 (3)	$\delta_{ip}(\text{CO}_3)$
790 (5)	767 (5)	789 (5)	$\delta_{oop}(\text{CO}_3)$

$\nu_s$  and  $\nu_{as}$  symmetric and asymmetric stretching mode;  $\delta_{ip}$  and  $\delta_{oop}$  in-plane and out-of-plane bending mode.

In Figure 6.2 a lot of bands cannot be interpreted. Some bands can be assigned to methanol, carbon dioxide and water (not shown). One of the most intense bands for the methanol monomer is the one at 1034 cm<sup>-1</sup> assigned to the CO stretching mode  $\nu(\text{CO})$ .<sup>[62]</sup> The decomposition of HOCO<sub>2</sub>CH<sub>3</sub> in methanol and carbon dioxide could be the source for the observed signals. The signal of water could come from traces of water, which condense during the transfer of the sample holder. To clarify the assignment of the bands in Figure 6.2 different methods of examination would have to be applied. UV-radiation of the matrix is a method suitable to gain this information. If one species appears or disappears in the curve of UV-radiation, a unique set of bands assignable to one substance can be identified.

### 6.1.3 UV irradiation

Figure 6.3 and Figure 6.4 show the difference spectra of  $\alpha$ -H<sub>2</sub>CO<sub>3</sub>/Ar and  $\alpha$ -H<sub>2</sub><sup>13</sup>CO<sub>3</sub>/Ar-matrix before and after irradiation of the matrix with UV light. Bands pointing upwards indicate an appearing species, bands pointing downwards a disappearing species. Comparison of the difference spectra with the predicted IR-absorbance of the two H<sub>2</sub>CO<sub>3</sub> monomers with symmetry C<sub>2v</sub> and C<sub>s</sub> shows a small variation, especially in the region where asymmetric and symmetric C-(OH) stretching and in-plane deformation modes overlap from 1500 – 1000 cm<sup>-1</sup>. The monomethyl carbonic acid – HOCO<sub>2</sub>CH<sub>3</sub> – with cis-cis and cis-trans orientation of the CH<sub>3</sub> and OH groups coincides better with the predicted IR-frequencies (Table 6.1 and Table 6.2). The appearing species is assigned to the cis-trans, the disappearing one to the cis-cis monomer of HOCO<sub>2</sub>CH<sub>3</sub> (Figure 6.1).

#### ***OH and OD stretching modes***

Between 3630 – 3590 cm<sup>-1</sup> one band arises and two bands decrease in Figure 6.3. The difference spectrum of the <sup>13</sup>C experiment (Figure 6.4) shows one arising and decreasing band. The assignment to  $\nu$ (OH) of the cis-cis monomer for HOCO<sub>2</sub>CH<sub>3</sub> and HO<sup>13</sup>CO<sub>2</sub>CH<sub>3</sub> is complicated. We interpret the bands at 3611 and 3608 cm<sup>-1</sup> (matrix splitting) as belonging to the  $\nu$ (OH) of the cis-cis monomer of HOCO<sub>2</sub>CH<sub>3</sub>, and the band at 3610 cm<sup>-1</sup> to  $\nu$ (OH) of the cis-cis monomer of HO<sup>13</sup>CO<sub>2</sub>CH<sub>3</sub>. The search for the respective  $\nu$ (OH) of the cis-trans monomer is rather difficult. However, the appearing bands located at 3602 cm<sup>-1</sup> in Figure 6.3 as well as Figure 6.4 may be assigned to the  $\nu$ (OH) of the trans OH-group. In the spectrum of <sup>2</sup>HOCO<sub>2</sub>CH<sub>3</sub> (Figure 6.2c) new bands arise at 2665/2663/2660 cm<sup>-1</sup> and show the same matrix splitting as in the one of HOCO<sub>2</sub>CH<sub>3</sub> (Figure 6.2a). The bands at 2665/2663 cm<sup>-1</sup> were assigned to  $\nu$ (OD) of the cis-cis monomer, the one at 2660 cm<sup>-1</sup> to the cis-trans monomer.

#### ***CO stretching mode***

The stretch vibration  $\nu$ (C=O) of the cis-cis monomer arises in an Ar matrix at 1779/1776 cm<sup>-1</sup> and is red shifted by about 50 cm<sup>-1</sup> compared to the one of the cis-trans monomer arising at 1829/1826 cm<sup>-1</sup>. The predicted  $\nu$ (C=O) stretch vibrations show a shift of 47 cm<sup>-1</sup> between the cis-cis at 1815 cm<sup>-1</sup> and the cis-trans monomer at 1862 cm<sup>-1</sup>. In the isotope substitution spectrum (Figure 6.4) bands disappear at 1735/1733 cm<sup>-1</sup> assigned to cis-cis, as one at 1791/1787 cm<sup>-1</sup> assigned to cis-trans appears. The predicted shift between the isotope substituted stable conformers – cis-cis – is about 47 cm<sup>-1</sup> and correlates excellently with the experimental shift of 43 cm<sup>-1</sup>. The less stable conformers show a predicted shift of 49 cm<sup>-1</sup>, as well as an experimental shift of 39 cm<sup>-1</sup> between the isotope substituted species. The stretch vibration  $\nu$ (C=O) of the deuterated form Figure 6.2a arises at 1774/1770 cm<sup>-1</sup> for the cis-cis and at 1822/1819 cm<sup>-1</sup> for the cis-trans. The predicted shift of 46 cm<sup>-1</sup> correlates excellently with the experimental shift of 48/49 cm<sup>-1</sup>.

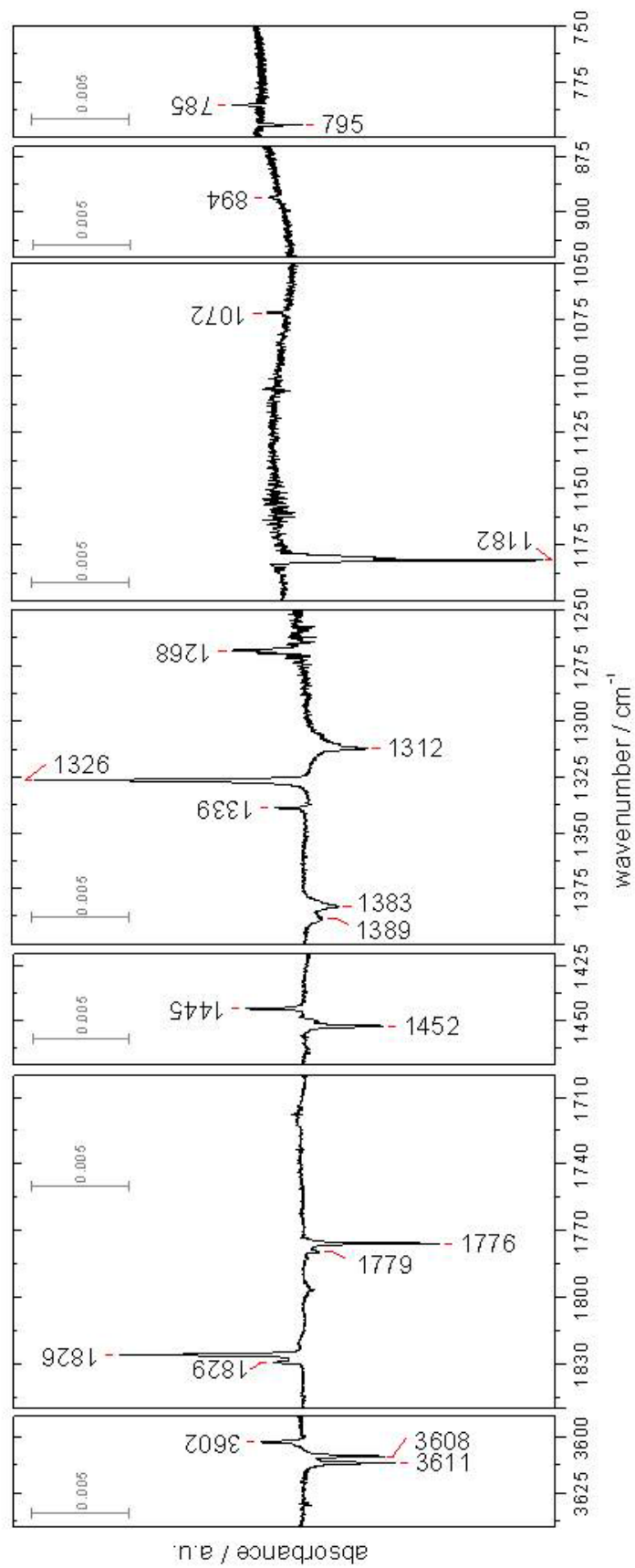


**Figure 6.3** Difference spectrum of  $\alpha$ -H<sub>2</sub>CO<sub>3</sub>/Ar-matrix before and after irradiation of the matrix with UV light (15 min;  $\nu = 250$  to 950 nm). Bands pointing upwards indicate an appearing species and bands pointing downwards a disappearing species.

In the  $\nu(\text{C}=\text{O})$  region theory and experiment are very close for the monomethyl carbonic acid and for the carbonic acid, and prevent a correct assignment.

### ***CH<sub>3</sub> rocking mode***

The calculated rocking vibration  $\rho(\text{CH}_3)$  of the cis-cis monomer at  $1495\text{ cm}^{-1}$  is blue shifted by about  $6\text{ cm}^{-1}$  to the one of the cis-trans monomer at  $1489\text{ cm}^{-1}$ . After UV irradiation the band at  $1452\text{ cm}^{-1}$  – assigned to the cis-cis monomer – decreases and the one, which was attributed to the cis-trans monomer, at  $1445\text{ cm}^{-1}$  increases. The experiment shows a  $7\text{ cm}^{-1}$  shift, which agrees very well with the theory. After isotope substitution  $\rho(\text{CH}_3)$  shifts weakly to lower wavenumbers for the cis-cis monomer to  $1446\text{ cm}^{-1}$  and for the cis-trans to  $1442\text{ cm}^{-1}$ . The theoretical shift of  $5\text{ cm}^{-1}$  (cis-cis) and  $4\text{ cm}^{-1}$  (cis-trans) between the species with different isotopes correlates with the experiment ( $6$  and  $3\text{ cm}^{-1}$ ). The  $\rho(\text{CH}_3)$  of the  $^2\text{HOCO}_2\text{CH}_3$  cis-cis at  $1449\text{ cm}^{-1}$  is red shifted by  $3\text{ cm}^{-1}$  to  $\text{HOCO}_2\text{CH}_3$  and agrees perfectly with the theory ( $5\text{ cm}^{-1}$ ). This mode is a very good indicator that a  $\text{CH}_3$  group is present in the isolated species. The absence of the methanol  $\nu(\text{CO})$  mode at  $1034\text{ cm}^{-1}$  in the UV-difference spectra (Figure 6.3 and Figure 6.4, not shown) corroborates the hypothesis that the  $\text{CH}_3$ -group does not appertain to the  $\text{CH}_3\text{OH}$  monomer, but to another species.

### ***COH and COD in plane bending modes***

The calculations show two in plane bending modes  $\delta_{\text{ip}}(\text{COH})$  at  $1409$  and  $1219\text{ cm}^{-1}$ . The in plane bending mode  $\delta_{\text{ip}}(\text{COH})$  calculated to be at  $1409\text{ cm}^{-1}$  for the cis-cis monomer shifts to lower wavenumber for the cis-trans at  $1351\text{ cm}^{-1}$ . It shows a displacement of  $58\text{ cm}^{-1}$ . Figure 6.3 shows in the region between  $1400 - 1250\text{ cm}^{-1}$  three bands pointing downwards and three others pointing upwards. The bands at  $1389/1383\text{ cm}^{-1}$  resulting from matrix splitting can be assigned to  $\delta_{\text{ip}}(\text{COH})$  for the cis-cis monomer. A red shift of  $57\text{ cm}^{-1}$  results in the band at  $1326\text{ cm}^{-1}$ , which can be assigned to  $\delta_{\text{ip}}(\text{COH})$  for cis-trans. Only for the arising bands at  $1339$  and  $1268\text{ cm}^{-1}$  as well as the decreasing one at  $1312\text{ cm}^{-1}$  no assignment can be found. In the  $^{13}\text{C}$  experiment the band at  $1362\text{ cm}^{-1}$  decreases and the one at  $1309\text{ cm}^{-1}$  increases. A predicted shift between  $^{12}\text{C}$  and  $^{13}\text{C}$  of  $28\text{ cm}^{-1}$  (cis-cis) and  $21\text{ cm}^{-1}$  (cis-trans) correlates with the experiment of  $21$  and  $17\text{ cm}^{-1}$ . In the  $^2\text{H}$  experiment, the band at  $1326\text{ cm}^{-1}$  is very intensive. The calculated  $\delta_{\text{ip}}(\text{COH})$  in  $^2\text{HOCO}_2\text{CH}_3$  at  $1364\text{ cm}^{-1}$  has the strongest IR intensity. The predicted shift between H and  $^2\text{H}$  of  $45\text{ cm}^{-1}$  coincides with the experiment of  $57\text{ cm}^{-1}$  (Table 6.5, Table 6.6).

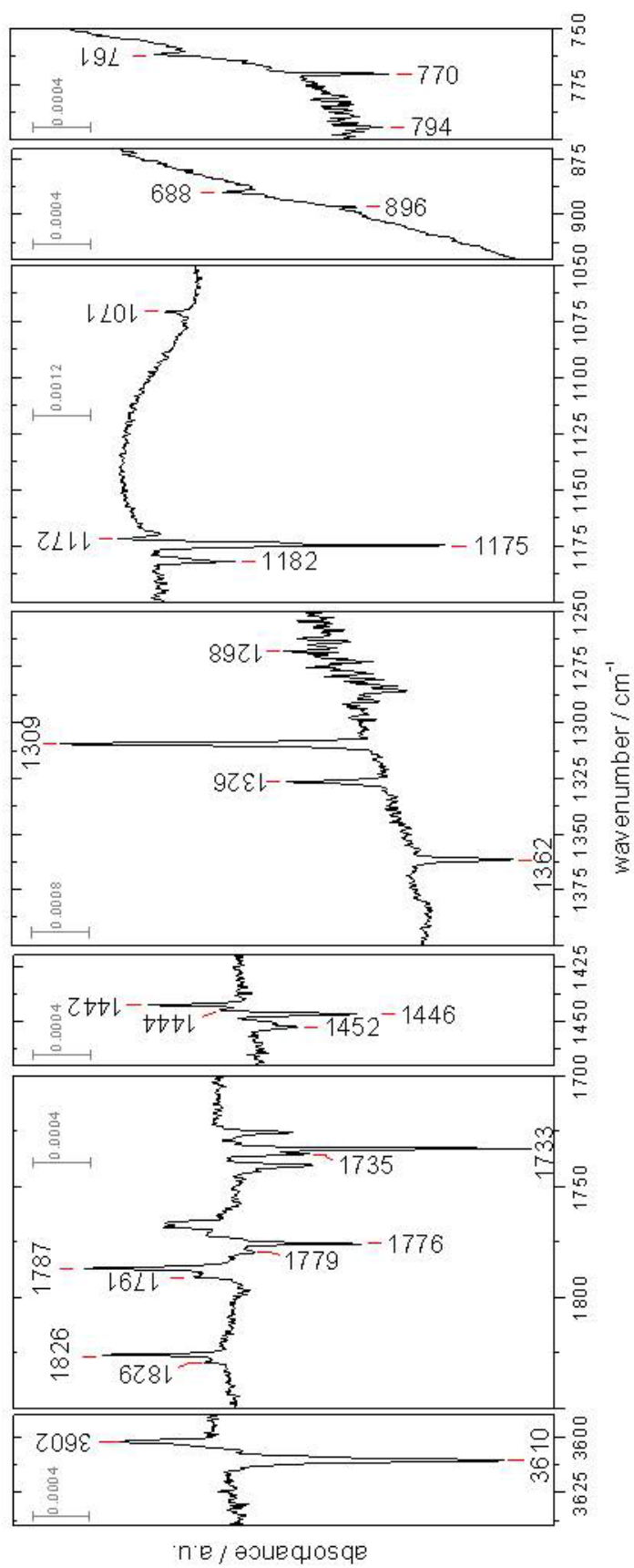


Figure 6.4 Difference spectrum of  $\alpha\text{-H}_2^{13}\text{CO}_2/\text{Ar}$ -matrix before and after irradiation of the matrix with UV light. Bands pointing upwards indicate an appearing species and bands pointing downwards a disappearing species. In the spectrum traces of the  $^{12}\text{C}$  species are obvious

The second  $\delta_{ip}(\text{COH})$  mode is the most intensive absorption in the predicted spectrum of the cis-cis  $\text{HOCO}_2\text{CH}_3$  monomer. The predicted peak at  $1219\text{ cm}^{-1}$  of the cis-cis shifts to  $1215\text{ cm}^{-1}$  (red shift of  $4\text{ cm}^{-1}$ ) for the cis-trans monomer. In the region of  $1200 - 1050\text{ cm}^{-1}$  the spectrum in Figure 6.3 shows a strong band located at  $1182\text{ cm}^{-1}$ , which disappears after UV irradiation. This peak is assigned to the  $\delta_{ip}(\text{COH})$  vibration for the more stable monomer. The predicted peak at  $1219\text{ cm}^{-1}$  for cis-cis of the  $^{12}\text{C}$ -species shifts to  $1211\text{ cm}^{-1}$  (red shift of  $8\text{ cm}^{-1}$ ) for cis-cis of the  $^{13}\text{C}$ -species. In the region of  $1200 - 1050\text{ cm}^{-1}$  the spectrum in Figure 6.4 shows a band located at  $1175\text{ cm}^{-1}$ . This peak is shifted to lower wavenumbers compared to the  $^{12}\text{C}$  experiment at  $1182\text{ cm}^{-1}$ . The shift of  $7\text{ cm}^{-1}$  is very close to the one predicted by theory and supports the interpretation. In the matrix spectrum of  $^2\text{HOCO}_2\text{CH}_3$  (Figure 6.2a) a new band arise at  $1016/1014\text{ cm}^{-1}$ . The predicted shift between  $\delta_{ip}(\text{COH})$  and  $\delta_{ip}(\text{COD})$  is  $188\text{ cm}^{-1}$ , the experiment shows a shift of around  $168\text{ cm}^{-1}$  which affirms the assignment. The bending vibration  $\delta_{ip}(\text{COH})$  for the cis-trans monomer could not be found. The predicted intensity for IR activity is very low compared to the one for the cis-cis, as well as the shift is small. This could be the reason that  $\delta_{ip}(\text{COH})$  of the cis-trans monomer could not be found.

#### ***OR stretching mode***

The  $\nu(\text{O}-(\text{CH}_3))$  stretching mode is more intensive for the cis-trans monomer and predicted to be at  $1103\text{ cm}^{-1}$ . The weak band located at  $1072\text{ cm}^{-1}$  in Figure 6.3 is assigned to  $\nu(\text{O}-(\text{CH}_3))$  of the less stable monomer. In the  $^{13}\text{C}$  experiment this band shifts to  $1071\text{ cm}^{-1}$  (red shift of  $1\text{ cm}^{-1}$ ) and agrees with the theoretical shift of  $3\text{ cm}^{-1}$  between  $1103$  and  $1100\text{ cm}^{-1}$ . The predicted  $\nu(\text{O}-(\text{CH}_3))$  for the cis-cis at  $1109\text{ cm}^{-1}$  is very low in IR activity and not visible in the spectrum.

#### ***CO<sub>3</sub> in plane bending mode***

The  $\text{CO}_3$  in plane bending mode  $\delta_{ip}(\text{CO}_3)$  predicted at  $919$  (cis-cis) and  $910\text{ cm}^{-1}$  (cis-trans) is low in IR activity. In Figure 6.3 only the mode for the cis-trans monomer located at  $894\text{ cm}^{-1}$  is obvious. In the  $^{13}\text{C}$  experiment this band shifts to  $889\text{ cm}^{-1}$  (red shift of  $5\text{ cm}^{-1}$ ). The predicted  $\delta_{ip}(\text{CO}_3)$  mode of the cis-trans monomer is located at  $910\text{ cm}^{-1}$  ( $^{12}\text{C}$ ) and at  $906\text{ cm}^{-1}$  ( $^{13}\text{C}$ ) and shows a red shift of  $4\text{ cm}^{-1}$ . In Figure 6.4 a blue shift of  $7\text{ cm}^{-1}$  leads to the decreasing band located at  $896\text{ cm}^{-1}$  (cis-cis), which also agrees with the theoretical shift of  $11\text{ cm}^{-1}$ . The experiment is very close to the theoretical prediction and supports the interpretation.

#### ***CO<sub>3</sub> out of plane bending mode***

The region at  $800 - 750\text{ cm}^{-1}$  shows the out of plane deformation mode of monomethyl carbonic acid, in which the band at  $795\text{ cm}^{-1}$  disappears and the one at  $785\text{ cm}^{-1}$  arises in the spectrum (Figure 6.3). The predicted  $\delta_{oop}(\text{CO}_3)$  of the cis-cis monomer is located at  $804\text{ cm}^{-1}$ , for the cis-trans monomer it can be found at  $794\text{ cm}^{-1}$  (red shift  $10\text{ cm}^{-1}$ ). The observed shift and position suggests the assignment of the band at  $795\text{ cm}^{-1}$  to  $\delta_{oop}(\text{CO}_3)$

of the cis-cis monomer and the one at 785 cm<sup>-1</sup> to the cis-trans monomer for the monomethyl carbonic acid. Confirmation of the assignment is provided by the spectrum of the other isotopologue. After <sup>13</sup>C substitution (Figure 6.4) the δ<sub>oop</sub>(CO<sub>3</sub>) of the cis-cis monomer shifts to lower wavenumbers at 770 cm<sup>-1</sup>. The predicted shift of about 25 cm<sup>-1</sup> between cis-cis of <sup>12</sup>C and <sup>13</sup>C correlates with the observed shift of 25 cm<sup>-1</sup> (Table 6.1). The cis-trans shifts from 785 cm<sup>-1</sup> (<sup>12</sup>C) to 761 cm<sup>-1</sup> (<sup>13</sup>C). The experimental shift of 24 cm<sup>-1</sup> correlates with the predicted shift of 25 cm<sup>-1</sup> and supports the above assignments.

After UV irradiation of the matrix the spectra show that the bands assigned to HOCO<sub>2</sub>CH<sub>3</sub> with cis-cis orientation of the CH<sub>3</sub> and OH groups disappear and the ones assigned to the cis-trans monomer arise. All the predicted band positions and assignments are summarized in Table 6.1 and Table 6.2. The experimental results are shown in Figure 6.2, Figure 6.3 and Figure 6.4 as well as in Table 6.5 and Table 6.6.

**Table 6.5 Band positions assigned to monomethyl carbonic acid monomers (all values in cm<sup>-1</sup>). Data taken from Figure 6.2, Figure 6.3, Figure 6.4 and Figure 6.5. Values in parentheses are calculated at MP2/aug-cc-pVTZ level of theory. Two distinct monomers, namely the cis-cis and cis-trans conformation are necessary to explain the spectra.**

HOCO <sub>2</sub> CH <sub>3</sub>		HO <sup>13</sup> CO <sub>2</sub> CH <sub>3</sub>	DOCO <sub>2</sub> CH <sub>3</sub>	HOCO <sub>2</sub> CD <sub>3</sub>		Assign.	conformers
Ar	(theor)	Ar	Ar	Ar			
3611/3608	(3800)	3610	2665/2663	3610		v(OH); v(OD)	cis-cis
3602	(3800)	3602	2660			v(OH); v(OD)	cis-trans
1829/1826	(1862)	1791/1787	1822/1819	1778/1774		v(CO)	cis-trans
1779/1776	(1815)	1735/1733	1774/1770			v(CO)	cis-cis
1452	(1495)	1446	1449	1115		ρ(CH <sub>3</sub> ); ρ(CD <sub>3</sub> )	cis-cis
1445	(1489)	1442				ρ(CH <sub>3</sub> ); ρ(CD <sub>3</sub> )	cis-trans
1389/1383	(1409)	1362	1326	1401		δ <sub>ip</sub> (COH); δ <sub>ip</sub> (COD)	cis-cis
1326	(1351)	1309	1276			δ <sub>ip</sub> (COH); δ <sub>ip</sub> (COD)	cis-trans
1182	(1219)	1175	1016/1014	1188		δ <sub>ip</sub> (COH); δ <sub>ip</sub> (COD)	cis-cis
	(1215)					δ <sub>ip</sub> (COH); δ <sub>ip</sub> (COD)	cis-trans
	(1109)					v(O-(CH <sub>3</sub> ))	cis-cis
1072	(1103)	1071				v(O-(CH <sub>3</sub> ))	cis-trans
900	(919)	896				δ <sub>ip</sub> (CO <sub>3</sub> )	cis-cis
894	(910)	889				δ <sub>ip</sub> (CO <sub>3</sub> )	cis-trans
795	(804)	770		792		δ <sub>oop</sub> (CO <sub>3</sub> )	cis-cis
785	(794)	761				δ <sub>oop</sub> (CO <sub>3</sub> )	cis-trans

*v*, stretching mode; *δ*<sub>ip</sub> and *δ*<sub>oop</sub>, in-plane and out-of-plane bending mode. For CH mode: *ρ*, rocking mode.

**Table 6.6 Isotope shift between monomethyl carbonic acid isotopologues, namely  $\text{HOCO}_2\text{CH}_3$ ,  $\text{HO}^{13}\text{CO}_2\text{CH}_3$ ,  $\text{DOCO}_2\text{CH}_3$  and  $\text{HOCO}_2\text{CD}_3$ .**

$\text{HOCO}_2\text{CH}_3$		$^{12}\text{C}/^{13}\text{C}$ – shift		H/D – shift (OH– group)		H/D – shift ( $\text{CH}_3$ – group)	
Ar	(theor)	Exp.	(theor.)	Exp.	(theor.)	Exp.	(theor.)
3611/3608	(3800)	1/-2	(0)	946/945	(1035)	1/-2	(0)
3602	(3800)	0	(0)	942	(1035)		
1829/1826	(1862)	36/39	(49)	7	(8)		
1779/1776	(1815)	44/43	(47)	5/6	(7)	1/2	(3)
1452	(1495)	6	(5)	3	(2)	337	(356)
1445	(1489)	3	(2)		( )		
1389/1383	(1409)	27/21	(28)	63/57	(45)	-12/-18	(-14)
1326	(1351)	17	(21)	50	(41)		
1182	(1219)	7	(8)	166/168	(188)	-6	(-3)
	(1215)		(13)				
	(1109)		(3)				
1072	(1103)	1	(3)				
900	(919)	4	(2)				
894	(910)	5	(4)				
795	(804)	25	(25)			3	(3)
785	(794)	24	(25)				

## 6.2 The vapour over the new species ( $\gamma$ - and $\delta$ -H<sub>2</sub>CO<sub>3</sub>)

The matrix isolation of  $\alpha$ -H<sub>2</sub>CO<sub>3</sub> and  $\beta$ -H<sub>2</sub>CO<sub>3</sub> was successful. In Figure 6.5 I show the Ar matrix isolation spectra of  $\gamma$ -H<sub>2</sub>CO<sub>3</sub>, product of the reaction of K[OCO<sub>2</sub>C<sub>2</sub>H<sub>5</sub>] with HCl and  $\delta$ -H<sub>2</sub>CO<sub>3</sub>, product of the reaction of K[OCO<sub>2</sub>CD<sub>3</sub>] with HCl. Due to the complexity of the spectra only the region of the stretch vibrations  $\nu$ (C=O) and  $\nu$ (OH) as well as the bending modes  $\delta_{ip}$ (COH),  $\delta_{ip}$ (CO<sub>3</sub>) and  $\delta_{oop}$ (CO<sub>3</sub>) shall be discussed here. These modes can be found also in the spectrum of H<sub>2</sub>CO<sub>3</sub>.

### ***OH stretching mode***

The OH stretching modes of  $\delta$ -H<sub>2</sub>CO<sub>3</sub> and  $\gamma$ -H<sub>2</sub>CO<sub>3</sub> are at similar positions compared to  $\alpha$ -H<sub>2</sub>CO<sub>3</sub> (3611/3608 cm<sup>-1</sup>; **Paper I**) and to  $\beta$ -H<sub>2</sub>CO<sub>3</sub> (3611/3607 cm<sup>-1</sup>; **Paper II**). The  $\delta$ -H<sub>2</sub>CO<sub>3</sub> shows a band at 3610 cm<sup>-1</sup> (Figure 6.5b). The  $\gamma$ -H<sub>2</sub>CO<sub>3</sub> however, exhibits band splitting at 3613/3611 cm<sup>-1</sup> (Figure 6.5a).

### ***CO stretching mode***

In carboxylic acids  $\nu$ (C=O) is located in the region of 1800 – 1700 cm<sup>-1</sup>. The  $\beta$ -polymorph shows  $\nu$ (C=O) at 1792/1788 cm<sup>-1</sup> and is blue shifted by about 13/12 cm<sup>-1</sup> compared to  $\nu$ (C=O) for  $\alpha$ -H<sub>2</sub>CO<sub>3</sub> (1779/1776 cm<sup>-1</sup>). In  $\delta$ -H<sub>2</sub>CO<sub>3</sub> there appears a doublet due to a splitting induced by different Ar matrix cages at 1778/1774 cm<sup>-1</sup> (Figure 6.5b). The  $\gamma$ -species shows a strong band at 1774 cm<sup>-1</sup> (Figure 6.5a). These modes are red shifted by about 2 cm<sup>-1</sup> in contrast to  $\alpha$ -H<sub>2</sub>CO<sub>3</sub> and 14 cm<sup>-1</sup> according to  $\beta$ -H<sub>2</sub>CO<sub>3</sub>. Similar to  $\alpha$ - and  $\beta$ -H<sub>2</sub>CO<sub>3</sub>, in  $\gamma$ - and  $\delta$ -H<sub>2</sub>CO<sub>3</sub> two different conformers can be found as well.  $\gamma$ -H<sub>2</sub>CO<sub>3</sub> shows a band blue shifted by 47 cm<sup>-1</sup> at 1821 cm<sup>-1</sup>, which can be assigned to another isolated conformer (Figure 6.5a). In  $\delta$ -H<sub>2</sub>CO<sub>3</sub> a weak band appears at 1824 cm<sup>-1</sup>. The new species absorb at similar wavenumbers as  $\alpha$ -H<sub>2</sub>CO<sub>3</sub>, and suggest a similar environment.

### ***COH in plane bending mode***

The  $\delta_{ip}$ (COH) mode of the new species are strong in intensity. In  $\gamma$ -H<sub>2</sub>CO<sub>3</sub> the  $\delta_{ip}$ (COH) mode appears as doublet – the splitting are induced by different Ar matrix cages – at 1181/1177 cm<sup>-1</sup>.  $\delta$ -H<sub>2</sub>CO<sub>3</sub> shows a strong band at 1188 cm<sup>-1</sup>. Compared to  $\alpha$ -H<sub>2</sub>CO<sub>3</sub> ( $\delta_{ip}$ (COH) at 1182 cm<sup>-1</sup>), the  $\delta_{ip}$ (COH) mode for  $\gamma$ -H<sub>2</sub>CO<sub>3</sub> is red shifted by about 1/5 cm<sup>-1</sup>. In the case of  $\delta$ -H<sub>2</sub>CO<sub>3</sub> it is blue shifted by 6 cm<sup>-1</sup>. In contrast, the shift between the  $\delta_{ip}$ (COH) mode for  $\gamma$ -H<sub>2</sub>CO<sub>3</sub> and  $\beta$ -H<sub>2</sub>CO<sub>3</sub> is about 45/49 cm<sup>-1</sup> (blue shift), between  $\delta$ - and  $\beta$ -H<sub>2</sub>CO<sub>3</sub> about 52 cm<sup>-1</sup> (blue shift). Also here, the new species absorb at wavenumbers similar to  $\alpha$ -H<sub>2</sub>CO<sub>3</sub>, and suggest a corresponding environment.

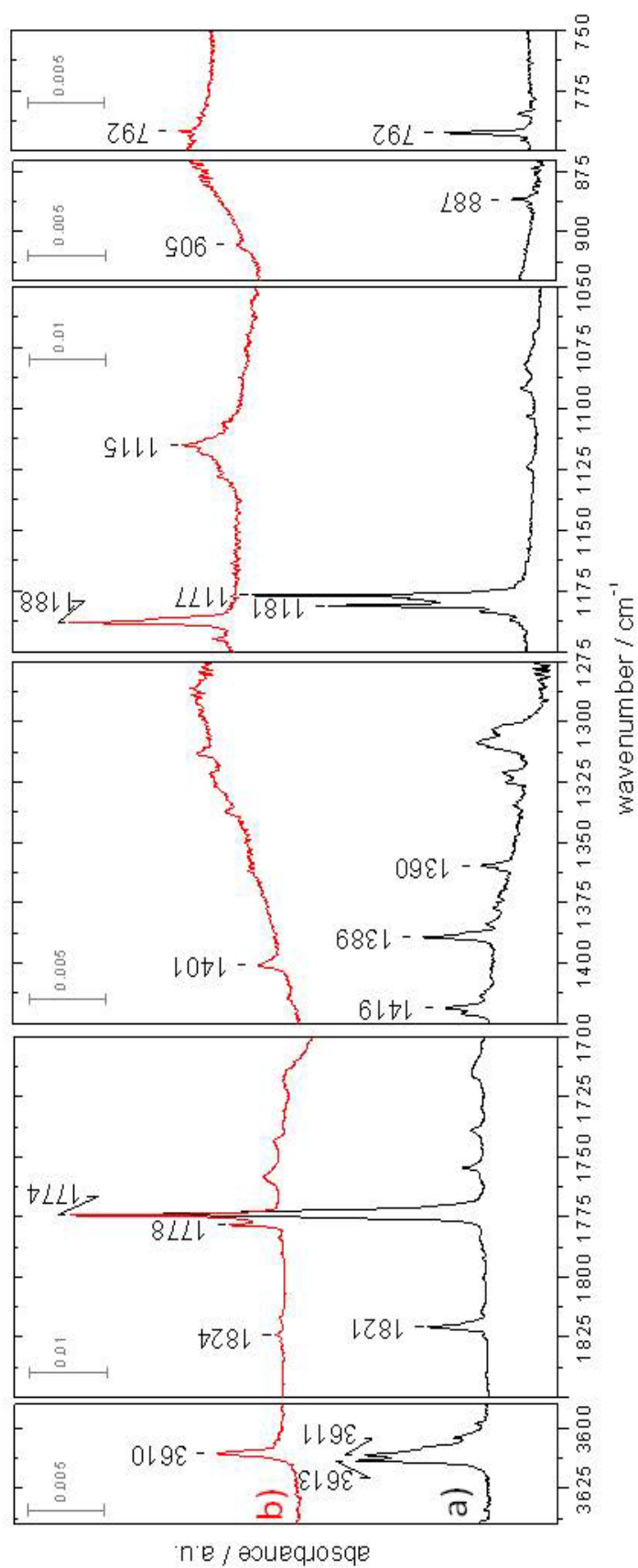


Figure 6.5 IR spectra of the new species vapour after sublimation of the crystal at 210 K and isolation in argon matrix at 6 K. a)  $\text{HOCO}_2\text{C}_2\text{H}_5$ , b)  $\text{HOCO}_2\text{CD}_3$ . Spectra are shifted for clarity. Assignment of the bands is given in Table 6.7.

### ***CO<sub>3</sub> in plane bending mode***

In the region between 920 – 870 cm<sup>-1</sup> one band arises for  $\gamma$ -H<sub>2</sub>CO<sub>3</sub> (Figure 6.5a) at 887 cm<sup>-1</sup>. The  $\delta$ -H<sub>2</sub>CO<sub>3</sub> shows a weak band at 905 cm<sup>-1</sup> (Figure 6.5b). The  $\delta_{ip}(\text{CO}_3)$  mode for  $\alpha$ -H<sub>2</sub>CO<sub>3</sub> appears at 900 cm<sup>-1</sup>. The  $\delta_{ip}(\text{CO}_3)$  mode for  $\beta$ -H<sub>2</sub>CO<sub>3</sub> could not be found in the matrix spectrum (***Paper II***).

### ***CO<sub>3</sub> out of plane bending mode***

The predicted  $\delta_{oop}(\text{CO}_3)$  mode for H<sub>2</sub>CO<sub>3</sub> is at 802 cm<sup>-1</sup> (C<sub>2v</sub> symmetry). In  $\alpha$ -H<sub>2</sub>CO<sub>3</sub> this mode appears at 795 cm<sup>-1</sup> and is blue shifted by 3 cm<sup>-1</sup> compared to  $\beta$ -H<sub>2</sub>CO<sub>3</sub> (792 cm<sup>-1</sup>; ***Paper II***).  $\gamma$ - and  $\delta$ -H<sub>2</sub>CO<sub>3</sub> show a band at 792 cm<sup>-1</sup>, which can be attributed to the  $\delta_{oop}(\text{CO}_3)$  mode.

Via these modes no exact distinction between the polymorphs can be done. All of them are found in the predicted spectra of H<sub>2</sub>CO<sub>3</sub> and HOCO<sub>2</sub>CH<sub>3</sub> at similar positions. The CO stretching and the COH in plane bending mode are different between the two species. The predicted  $\nu(\text{C}=\text{O})$  and  $\delta_{ip}(\text{COH})$  for H<sub>2</sub>CO<sub>3</sub> arise at 1834 and 1166 cm<sup>-1</sup>, the one for HOCO<sub>2</sub>CH<sub>3</sub> at 1815 and 1219 cm<sup>-1</sup>. The new theory presented here implies that  $\alpha$ -H<sub>2</sub>CO<sub>3</sub> is not a H<sub>2</sub>CO<sub>3</sub> polymorph but the monomethyl ester of carbonic acid. The  $\nu(\text{C}=\text{O})$  and  $\delta_{ip}(\text{COH})$  for  $\gamma$ - and  $\delta$ -H<sub>2</sub>CO<sub>3</sub> are at similar positions as in  $\alpha$ -H<sub>2</sub>CO<sub>3</sub>, in contrast to  $\beta$ -H<sub>2</sub>CO<sub>3</sub>. This suggests monoalkyl ester of carbonic acid for  $\gamma$ - and  $\delta$ -H<sub>2</sub>CO<sub>3</sub> too. For the bands at 1401 and 1115 cm<sup>-1</sup> (Figure 6.5b) as well as the ones at 1419, 1389 and 1360 cm<sup>-1</sup> (Figure 6.5a) no agreement with H<sub>2</sub>CO<sub>3</sub> can be found.

## 6.3 Discussion

The UV irradiation experiment conveniently allows to identify interrelated bands for the different species in the matrix. The assignment of the absorbances was difficult and could only be done by comparison with theoretical calculations and literature values of other carboxylic acids. The assignment given above is one way to interpret the matrix isolation spectra. Another assignment has been done in *Paper I*.

The matrix isolation gives more clarity about the different polymorphs of  $\text{H}_2\text{CO}_3$ . As already mentioned in *Paper II* the  $\text{H}_2\text{CO}_3$  monomers – symmetries of  $\text{C}_{2v}$  and  $\text{C}_s$  – isolated from  $\beta\text{-H}_2\text{CO}_3$ , show different IR absorbances compared to  $\alpha\text{-H}_2\text{CO}_3$ . Also, the matrix splitting as well as the sublimation temperature change between  $\beta\text{-H}_2\text{CO}_3$  and  $\alpha\text{-H}_2\text{CO}_3$  and underline the new hypothesis. However, the  $\nu(\text{C}=\text{O})$  of the new species –  $\gamma\text{-H}_2\text{CO}_3$  and  $\delta\text{-H}_2\text{CO}_3$  – isolated in a matrix are at similar positions like  $\alpha\text{-H}_2\text{CO}_3$ . The sublimation temperature is around 210 K and thus, nearly the same. The matrix spectra of  $\alpha$ -,  $\gamma$ -, and  $\delta\text{-H}_2\text{CO}_3$  are more complex compared to the one of  $\beta\text{-H}_2\text{CO}_3$ .

The fact, that the matrix isolation spectra of the  $\text{H}_2\text{CO}_3$  polymorphs are rather different suggests different species in the matrix. The solid  $\alpha$ - and  $\beta\text{-H}_2\text{CO}_3$  have been characterized in the 1990's. Some specific reasons were given by Hage et al. <sup>[19, 21]</sup> to eliminate the possibility of  $\alpha\text{-H}_2\text{CO}_3$  being monoalkyl ester or methanol adduct. The complete separation of excess methanol from  $\alpha\text{-H}_2\text{CO}_3$  as well as the absence of the methanol bands in the IR spectra excluded the methanol adduct. The absence of the  $\nu(\text{CH})$  stretching vibration in the spectra of solid  $\alpha\text{-H}_2\text{CO}_3$  after evaporation of the solvent (methanol) excluded the monoalkyl carbonic acid ester. <sup>[19]</sup>

However, in the past  $\text{KHCO}_3$  was believed to be protonated in methanol. The new results show that potassium monomethyl carbonate  $\text{K}[\text{OCO}_2\text{CH}_3]$  is the starting compound for producing  $\alpha\text{-H}_2\text{CO}_3$  (see chapter 5.1.2). Considering this, the formation of the monomethyl carbonic acid appears possible. In the spectra of Figure 6.3 and Figure 6.4 evidence for neither the stretching vibration  $\nu(\text{CH})$  nor the bending modes  $\sigma(\text{CH}_2)$  and  $\omega(\text{CH}_3)$  is apparent. However, the predicted  $\nu(\text{CH})$  modes for the cis-cis monomer at  $3225/3193/3095\text{ cm}^{-1}$  are slightly shifted to the cis-trans monomer at  $3224/3196/3099\text{ cm}^{-1}$ . The predicted IR intensity is very low compared to other vibrations. The bending modes  $\sigma(\text{CH}_2)/\omega(\text{CH}_3)$  for the cis-cis and for the cis-trans monomer are predicted to be at the same position at  $1521/1513\text{ cm}^{-1}$ . Also, here the theory predicts low IR activity. The very similar band positions and the low IR activity for the stretching vibration  $\nu(\text{CH})$  as well as the bending modes  $\sigma(\text{CH}_2)/\omega(\text{CH}_3)$  may be the reason that these modes are not visible in the spectra of Figure 6.3 and Figure 6.4.

In contrast, the predicted  $\rho(\text{CH}_3)$  at  $1495\text{ cm}^{-1}$  (cis-cis) and  $1489\text{ cm}^{-1}$  (cis-trans) could be found in the  $\alpha\text{-H}_2\text{CO}_3$  matrix spectrum at  $1452\text{ cm}^{-1}$  (cis-cis) as well as at  $1445\text{ cm}^{-1}$  (cis-trans), and in the solid spectrum (Figure 5.3b)  $\delta_{\text{as}}(\text{CH}_3)$  at  $1446\text{ cm}^{-1}$ . However, this is not

the case for of  $\beta$ - $\text{H}_2\text{CO}_3$ . The new species –  $\delta$ - $\text{H}_2\text{CO}_3$  – on the other hand does not show  $\delta_{\text{as}}(\text{CH}_3)$  in the solid spectrum (Figure 5.7b), but a band at  $1112\text{ cm}^{-1}$  which was assigned to  $\delta_{\text{as}}(\text{CD}_3)$ . The matrix isolation spectrum of  $\delta$ - $\text{H}_2\text{CO}_3$  shows  $\rho(\text{CD}_3)$  – red shifted by a factor of 1.3 – at  $1115\text{ cm}^{-1}$ , but not  $\rho(\text{CH}_3)$  at  $1452\text{ cm}^{-1}$  and suggests the presence of a  $\rho(\text{CD}_3)$ -group.

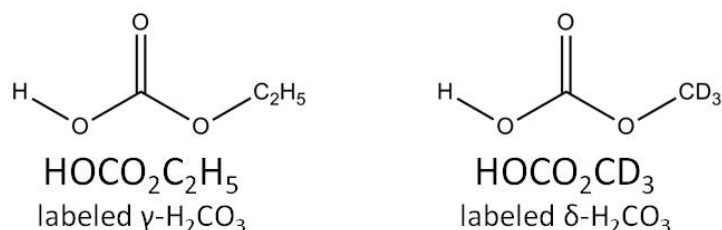


**Figure 6.6 Monomers of the new species.**

Table 6.7 gives some predicted bands for the most stable conformer of  $\text{HOCO}_2\text{CD}_3$  and  $\text{HOCO}_2\text{C}_2\text{H}_5$  and the assignment of the bands found in the spectra of Figure 6.5. Figure 6.6 shows the monomers of the new species, which are reported here.

**Table 6.7 Experimental and theoretical frequencies of  $\text{HOCO}_2\text{CD}_3$  and  $\text{HOCO}_2\text{C}_2\text{H}_5$  (all values in  $\text{cm}^{-1}$ ); Level of theory: MP2/aug-cc-pVTZ**

$\text{HOCO}_2\text{CD}_3$			$\text{HOCO}_2\text{C}_2\text{H}_5$		
Exp.	theor.	assignment	Exp.	theor.	assignment
3610	3800	$\nu(\text{OH})$	3613/3611	3798	$\nu(\text{OH})$
1778/1774	1812	$\nu(\text{C}=\text{O})$	1774	1811	$\nu(\text{C}=\text{O})$
1401	1425	$\delta_{\text{ip}}(\text{COH})$	1419	1448	$\omega(\text{CH}_2)$
1188	1222	$\delta_{\text{ip}}(\text{COH})$	1389	1422	$\delta_s(\text{CH}_3)$
1115	1149	$\rho(\text{CD}_3)$	1360	1385	$\omega(\text{CH}_2)$
905	923	$\tau(\text{CD}_2)$	1181/1177	1214	$\delta_{\text{ip}}(\text{COH})$
792	801	$\delta_{\text{oop}}(\text{CO}_3)$	887	890	$\delta_{\text{as}}(\text{CH}_3), \delta_{\text{ip}}(\text{COC})$
			792	801	$\delta_{\text{oop}}(\text{CO}_3)$

*$\nu$ , stretching mode;  $\delta_{\text{ip}}$  and  $\delta_{\text{oop}}$ , in-plane and out-of-plane bending mode;  $\delta_{\text{as}}$  and  $\delta_s$ , asymmetric and symmetric bending mode. For CH modes:  $\omega$ , wagging mode;  $\tau$ , twisting mode;  $\rho$ , rocking mode.*

These are indications for the presence of monoalkyl carbonic acid esters. The perception of different existing carbonic acid polymorphs has been agreed upon for more than twenty years. Hence, considering the new results I would like to present only a proposal explaining the different species – denoted as polymorphs of carbonic acid – as monoalkyl carbonic acid esters. To shed further light on the nature of the different

species, more experiments need to be done. Mass spectrometry should be an important method in solving this puzzle.

# 7 Carbonic Acid Hydrate

---

Acid hydrates, especially  $\text{HNO}_3$ -hydrates play an important role in polar stratospheric clouds (PSCs).<sup>[63]</sup> Nitric acid trihydrate (NAT) is believed to be the major compound of PSCs (type I).<sup>[63]</sup> Heterogeneous reactions on the surfaces of PSCs transform reservoir halogen compounds ( $\text{HCl}$ ,  $\text{ClONO}_2$ ) to active species ( $\text{Cl}_2$ ,  $\text{HOCl}$ ). Chlorine radicals ( $\text{Cl}\cdot$ ) cause a massive ozone depletion at the end of the polar night.<sup>[64]</sup>

Investigation of the  $\text{H}_2\text{SO}_4/\text{H}_2\text{O}$  binary system indicates that some hydrates of sulphuric acid may be formed and persist under the conditions of the high-latitude stratosphere.<sup>[65]</sup> Sulfuric acid aerosols are hygroscopic and may act as nuclei for the formation of polar stratospheric clouds (PSCs).<sup>[65-67]</sup>

In *Paper III* (chapter 4) we have shown the formation of bulk  $\text{H}_2\text{CO}_3$  by protonation of tropospheric calcite and its stability in a humid atmosphere. At 200 K aqueous/amorphous  $\text{H}_2\text{CO}_3$  is produced on a time scale of hours and crystallizes to  $\beta\text{-H}_2\text{CO}_3$  at higher temperatures under low humidity conditions. We demonstrate furthermore that  $\text{H}_2\text{CO}_3$  does not decompose readily even at 250 K in a humid atmosphere. This suggests the presence of  $\beta\text{-H}_2\text{CO}_3$  in our atmosphere, whereby the  $\text{H}_2\text{CO}_3/\text{H}_2\text{O}$  binary system has more significance.

## 7.1 Interaction of $\beta\text{-H}_2\text{CO}_3$ with water vapour

The study of  $\beta\text{-H}_2\text{CO}_3$  at high humidity conditions is shown in Figure 7.2. A thin film of crystalline  $\beta\text{-H}_2\text{CO}_3$  was exposed to a humid atmosphere, which leads to condensation of ice. The humidity was measured using a hygro-thermometer (Qhygo-Temp 80) sitting 20 cm above the cryo-sample holder. By measurement of the relative humidity at room temperature, the  $\text{H}_2\text{O}$  partial pressure in the chamber was calculated to be  $\approx 0.4$  mbar. The relative humidity with respect to ice ( $\text{RH}_{\text{ice}}$ ) near the sample holder was calculated via the vapour pressure curve of hexagonal ice  $I_h$  (Figure 7.1). Figure 7.1 shows the vapour pressure above water (black line) and above ice (red one).<sup>[68]</sup>

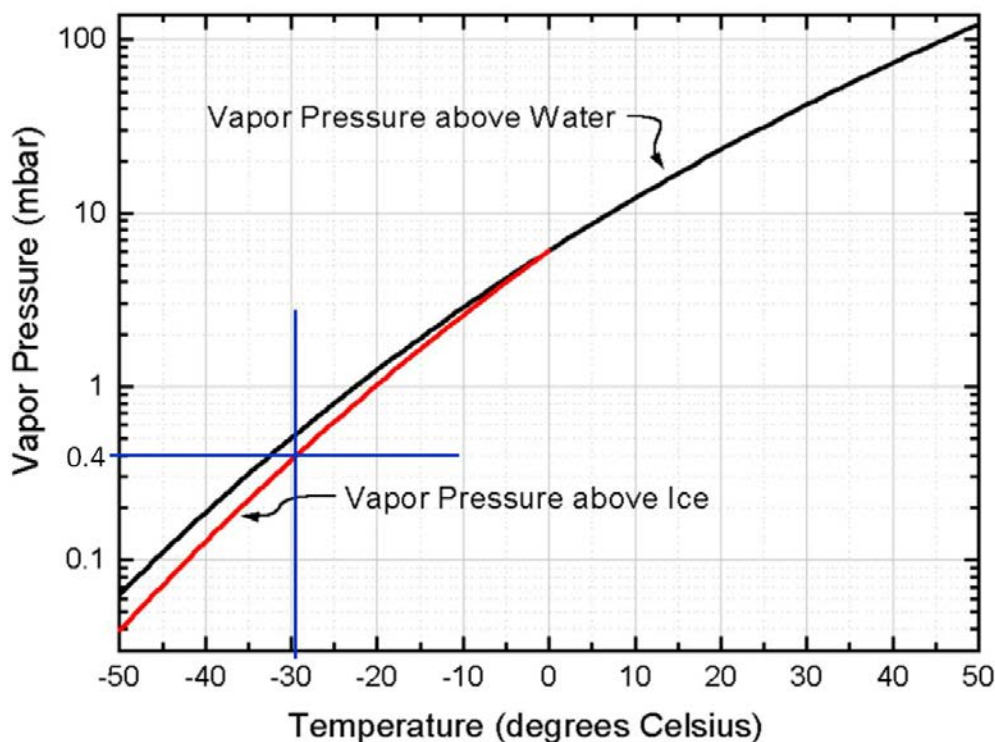
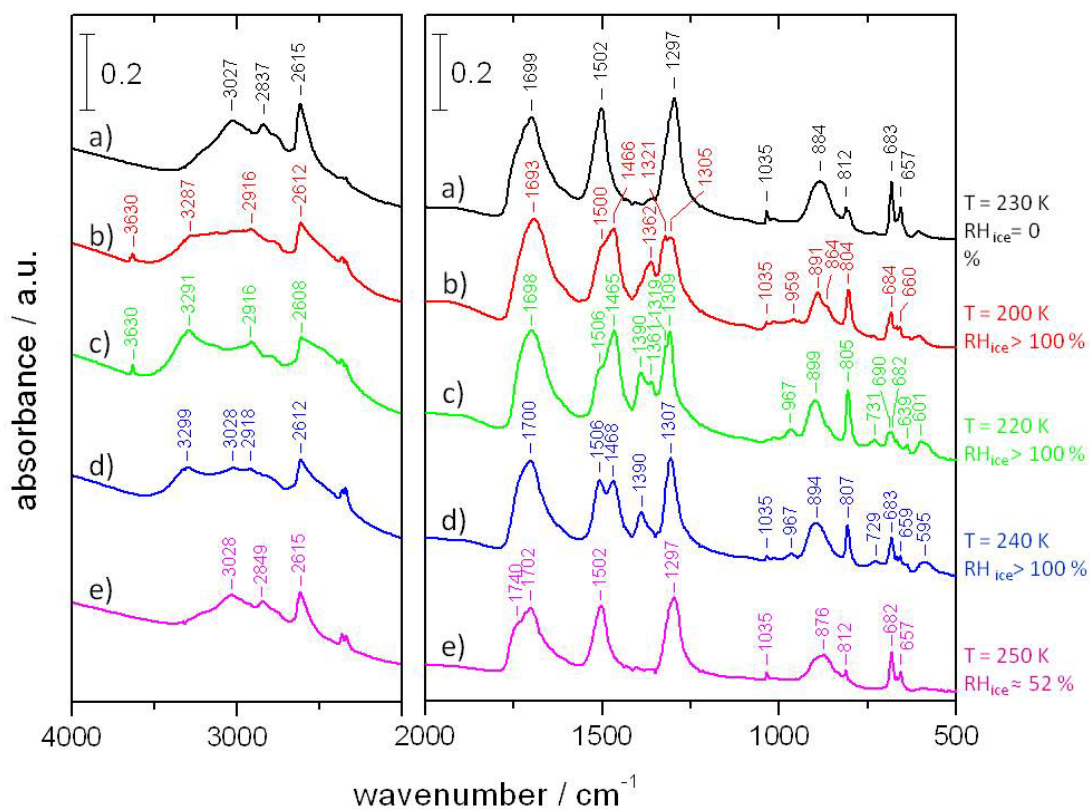


Figure 7.1 Vapor pressure curve of  $H_2O$  taken from B. J. Mason, *The Physics of Clouds* (Clarendon Press, 1971).<sup>[68]</sup> The black curve shows the vapor pressure above water and the red one above ice. In blue the vapor pressure during the experiment.

Figure 7.2 shows a phase transition induced by the interaction of  $\beta\text{-H}_2\text{CO}_3$  with  $H_2O$ -ice.  $\beta\text{-H}_2\text{CO}_3$  crystallizes at 230 K in *vacuo* (Figure 7.2a) by protonation of  $KHCO_3$  with  $HBr$ , both dissolved in  $H_2O$ . Exposing the crystalline phase at 200 K ( $t = 80$  min) to a 330 mbar He-atmosphere with 0.4 mbar water vapour pressure (more than 100 % relative humidity, suggesting the presence of condensing ice) leads to a change in the IR-spectrum (Figure 7.2b). New bands arise at 3630, 3287, 2916, 1466, 1362 and 959  $\text{cm}^{-1}$ , whereas some bands are shifted in the peak maximum, split or decrease. The band at 2615  $\text{cm}^{-1}$  (Figure 7.2a) assigned to the overtone of the  $\delta_{ip}(\text{COH})$ <sup>[20]</sup> shifts to 2612  $\text{cm}^{-1}$  (Figure 7.2b) and becomes broader. The  $\nu(\text{CO})$  mode shifts from 1699  $\text{cm}^{-1}$  (Figure 7.2a) to 1693  $\text{cm}^{-1}$  (Figure 7.2b). The  $\nu_{as}[\text{C}(\text{OH})_2]$  mode at 1502  $\text{cm}^{-1}$  (Figure 7.2a) decreases or shifts to 1466  $\text{cm}^{-1}$  (Figure 7.2b). The  $\delta_{ip}(\text{COH})$  at 1297  $\text{cm}^{-1}$  (Figure 7.2a) shifts to higher wavenumbers and splits into two bands at 1321 and 1305  $\text{cm}^{-1}$ . The sharp band at 1035  $\text{cm}^{-1}$  ( $\nu_s[\text{C}(\text{OH})_2]$ ), which is very intense in  $\beta\text{-H}_2\text{CO}_3$  and is an indication for the crystalline phase<sup>[3]</sup> decreases. The band at 891  $\text{cm}^{-1}$  with a shoulder at 864  $\text{cm}^{-1}$  (Figure 7.2b) develops from the broad band at 884  $\text{cm}^{-1}$  (Figure 7.2a) assigned to  $\delta_{oop}(\text{COH})$ <sup>[20]</sup>. The band at 812  $\text{cm}^{-1}$  (Figure 7.2a) assigned to  $\delta_{oop}(\text{CO}_3)$  shifts to 804  $\text{cm}^{-1}$  (Figure 7.2b) and becomes stronger, and the two  $\delta_{ip}(\text{CO}_3)$  modes at 683 and 657  $\text{cm}^{-1}$  decrease in intensity. The IR-spectrum (Figure 7.2b) looks like an aqueous/amorphous phase, but it is different from the IR-spectrum of amorphous  $H_2CO_3$  reported by Winkel et al. (Figure 1 in ref.<sup>[3]</sup>).



**Figure 7.2** IR-spectra of the interaction of  $\beta$ -H<sub>2</sub>CO<sub>3</sub> with H<sub>2</sub>O. **a)**  $\beta$ -H<sub>2</sub>CO<sub>3</sub> ( $T = 230$  K,  $p = 10^{-2}$  mbar); **b)**  $T = 200$  K,  $t = 80$  min,  $p_{\text{He}} = 330$  mbar and  $RH_{\text{ice}} > 100$  %; **c)**  $T = 220$  K,  $t = 30$  min,  $p_{\text{He}} = 350$  mbar and  $RH_{\text{ice}} > 100$  %; **d)**  $T = 240$  K,  $t = 30$  min,  $p_{\text{He}} = 440$  mbar and  $RH_{\text{ice}} > 100$  %; **e)**  $T = 250$  K,  $t = 0$  min,  $p_{\text{He}} = 470$  mbar and  $RH_{\text{ice}} \approx 52$  %.

After 30 minutes at 220 K with a 350 mbar He-atmosphere and 0.4 mbar water vapour pressure (relative humidity exceeding 100 %) the spectrum varies again (Figure 7.2c). Now, no evidence for the presence of crystalline  $\beta$ -H<sub>2</sub>CO<sub>3</sub> is observable. The band at 1035 cm<sup>-1</sup> disappears, whereas new broad bands arise below 800 cm<sup>-1</sup>, at 731, 639 and 601 cm<sup>-1</sup>. The band arising at 1362 cm<sup>-1</sup> (Figure 7.2b) shifts to 1390 cm<sup>-1</sup> (Figure 7.2c) and the one at 3287 cm<sup>-1</sup> (Figure 7.2b) becomes stronger and shifts to 3291 cm<sup>-1</sup> (Figure 7.2c).

By heating the sample to 240 K and staying there for 30 minutes with a 440 mbar He-atmosphere and 0.4 mbar water vapour pressure, the spectrum changes again (Figure 7.2d). Also here the relative humidity exceeds 100 %. Now the band at 3630 cm<sup>-1</sup> disappears and the one at 1035 cm<sup>-1</sup> increases. The bands at 1506 and 1468 cm<sup>-1</sup> are separated. The spectrum resembles more a crystalline phase.

By increasing the temperature to 250 K the relative humidity decreases from exceeding to 52 % (440 mbar He-atmosphere and 0.4 mbar water vapour pressure). The crystalline  $\beta$ -H<sub>2</sub>CO<sub>3</sub> is formed (Figure 7.2e). Figure 7.3 shows the IR-spectrum of hexagonal ice I<sub>h</sub> doped with KOH ( $c = 0.1$  M).

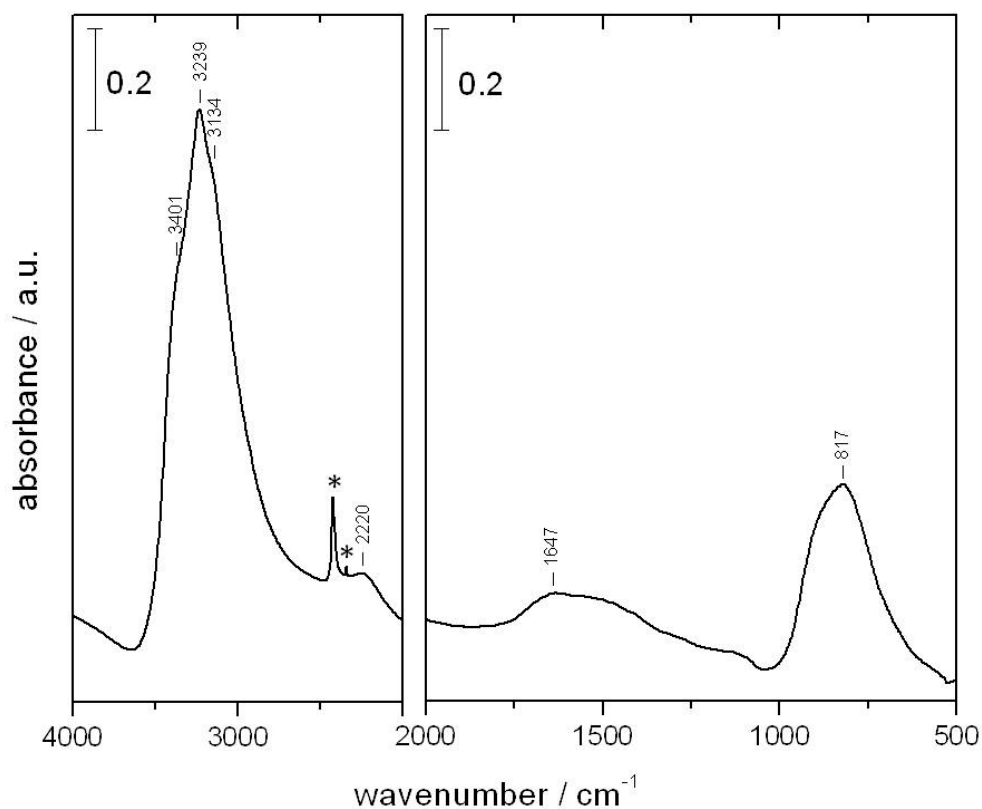


**Figure 7.3** IR-spectrum of hexagonal ice  $I_h$  doped with KOH ( $c = 0.1$  M) recorded at  $\approx 190$  K. The bands marked with asterisk belong to  $\text{CO}_2$  ( $^{12}\text{C}$  and  $^{13}\text{C}$ ).

That is, a new species appears if the  $\text{RH}_{\text{ice}}$  exceeds 100 %, which then disappears again once the  $\text{RH}_{\text{ice}}$  drops below 100 %. This new species is different from simple ice – IR bands in hexagonal ice are found at 3401 (sh), 3239 (s), 3134 (sh), 2220 (br, w), 1647 (br, w) and 817 (s)  $\text{cm}^{-1}$ , see Figure 7.3 (sh, shoulder; s, strong; br, broad; w, weak). Literature data of ice  $I_h$  at  $\approx 100$  K shows IR absorbance at 3380 (sh), 3220 (s), 3150 (s), 2266 (br, w), 1650 (br, w) and 840 (s)  $\text{cm}^{-1}$  [69] and agree with the one in Figure 7.3.

## 7.2 Reaction in concentrated solutions

Nearly the same results are received from reaction in concentrated aqueous solutions. By reaction of  $\text{KHCO}_3$  ( $c = 2$  M) and HBr ( $c = 4$  M), no evidence for amorphous  $\text{H}_2\text{CO}_3$  is found. The spectrum of amorphous  $\beta\text{-H}_2\text{CO}_3$  is shown in Figure 7.4a, taken from ref. [3]. By contrast to amorphous  $\beta\text{-H}_2\text{CO}_3$  obtained earlier for dilute solutions [3, 20] in concentrated solution a new species develops at 200 K.

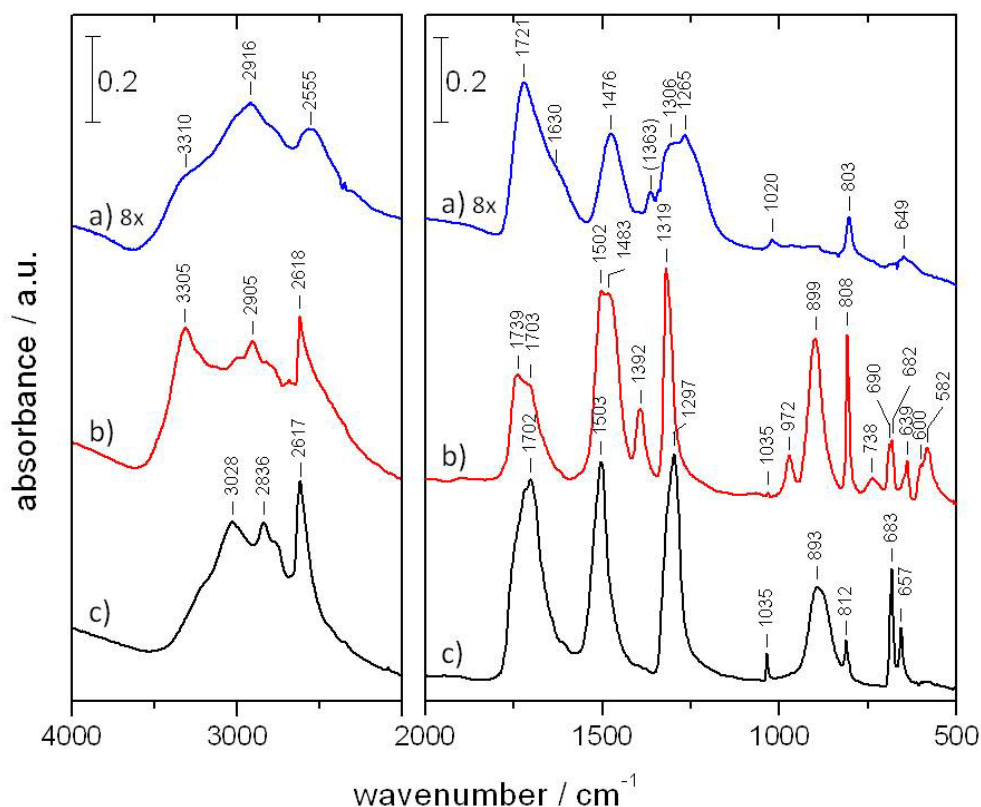


**Figure 7.4** IR-spectra of **a)** amorphous  $\text{H}_2\text{CO}_3$  (taken from Figure 1 in ref. <sup>[3]</sup>), **b)** unknown species ( $T=205$  K,  $p = 10^{-6}$  mbar) and **c)**  $\beta\text{-H}_2\text{CO}_3$  ( $T=230$  K,  $p = 10^{-6}$  mbar).

The spectrum of the new species is shown in Figure 7.4b, recorded at 205 K after 30 minutes and a pressure of  $10^{-6}$  mbar. Compared to crystalline  $\beta\text{-H}_2\text{CO}_3$  (Figure 7.4c) new bands arise at 3305, 2905, 1739, 1483, 1392, 972, 738, 600 (sh) and  $582\text{ cm}^{-1}$ . Other bands are shifted and changed in intensity. The  $\delta_{\text{ip}}(\text{COH})$  at  $1297\text{ cm}^{-1}$  (Figure 7.4c) shifts to higher wavenumbers at  $1319\text{ cm}^{-1}$  (Figure 7.4b). The  $\delta_{\text{oop}}(\text{COH})$  at  $893\text{ cm}^{-1}$  (Figure 7.4c) shifts to  $899\text{ cm}^{-1}$  and becomes sharper (Figure 7.4b). The band at  $812\text{ cm}^{-1}$  (Figure 7.4c) assigned to  $\delta_{\text{oop}}(\text{CO}_3)$  shifts to  $808\text{ cm}^{-1}$  (Figure 7.4b) and becomes stronger. The  $\delta_{\text{ip}}(\text{CO}_3)$  mode at  $683\text{ cm}^{-1}$  (Figure 7.4c) splits into two bands  $690/682\text{ cm}^{-1}$  (Figure 7.4b) and the one at  $657\text{ cm}^{-1}$  (Figure 7.4c) shifts to  $639\text{ cm}^{-1}$  (Figure 7.4b). The sharp band at  $1035\text{ cm}^{-1}$  ( $\nu_s[\text{C}(\text{OH})_2]$ ), which is very intense in  $\beta\text{-H}_2\text{CO}_3$  and is an indication for the crystalline phase <sup>[3]</sup> decreases. The spectrum of the new species in Figure 7.4b resembles the one of Figure 7.2d, and suggests the same species. The sharp bands in Figure 7.4b are indicative of a fully crystalline phase.

By heating the new species step by step to 230 K it transforms to  $\beta\text{-H}_2\text{CO}_3$  (Figure 7.4c). Figure 7.5 shows the phase transition from the new species to  $\beta\text{-H}_2\text{CO}_3$  by increasing the temperature. The blue curve was recorded at 205 K ( $t = 30$  min), the green one at 210 K ( $t = 30$  min), the red curve at 220 K ( $t = 23$  min) and the black one at 230 K ( $t = 5$  min). Bands marked with an arrow pointing downwards mark a decrease and the ones with the arrow pointing upwards an increase. Between  $4000 - 2000\text{ cm}^{-1}$  the bands at 3305

and  $2905\text{ cm}^{-1}$  decrease and the ones at  $3028$ ,  $2836$  and  $2617\text{ cm}^{-1}$  increase. Between  $2000 - 1000\text{ cm}^{-1}$  decreasing bands are located at  $1739$ ,  $1483$ ,  $1392$  and  $1319\text{ cm}^{-1}$  and the increasing one at  $1702$ ,  $1503$ ,  $1297$  and  $1035\text{ cm}^{-1}$ . Below  $1000\text{ cm}^{-1}$  the bands at  $972$ ,  $899$ ,  $808$ ,  $738$ ,  $639$  and  $582\text{ cm}^{-1}$  decrease and the ones located at  $683$  and  $657\text{ cm}^{-1}$  increase.

Figure 7.5 shows also several isosbestic points. At the specific wavelength of an isosbestic point the absorbance does not change during a chemical reaction or a physical change of the sample. The stoichiometry of the reaction remains unchanged and no secondary reactions occur. Appearance of isosbestic points are, therefore, indicative of the presence of two species, which can interconvert.

The nature of the unknown species, which converts upon heating to  $\beta\text{-H}_2\text{CO}_3$ , thus, needs to be determined. This unknown species appears in the presence of relative humidities with respect to ice ( $\text{RH}_{\text{ice}}$ ) in excess of 100 %. It also forms at  $\approx 200\text{ K}$  by reaction of  $\text{HCO}_3^-$  and  $\text{H}^+$  in concentrated aqueous solutions. By comparing the IR spectrum with the IR spectrum of amorphous  $\text{H}_2\text{CO}_3$ , the option of the unknown species being amorphous  $\text{H}_2\text{CO}_3$  can be excluded (Figure 7.4). In fact, the sharp bands clearly suggest a crystalline nature of the unknown species.

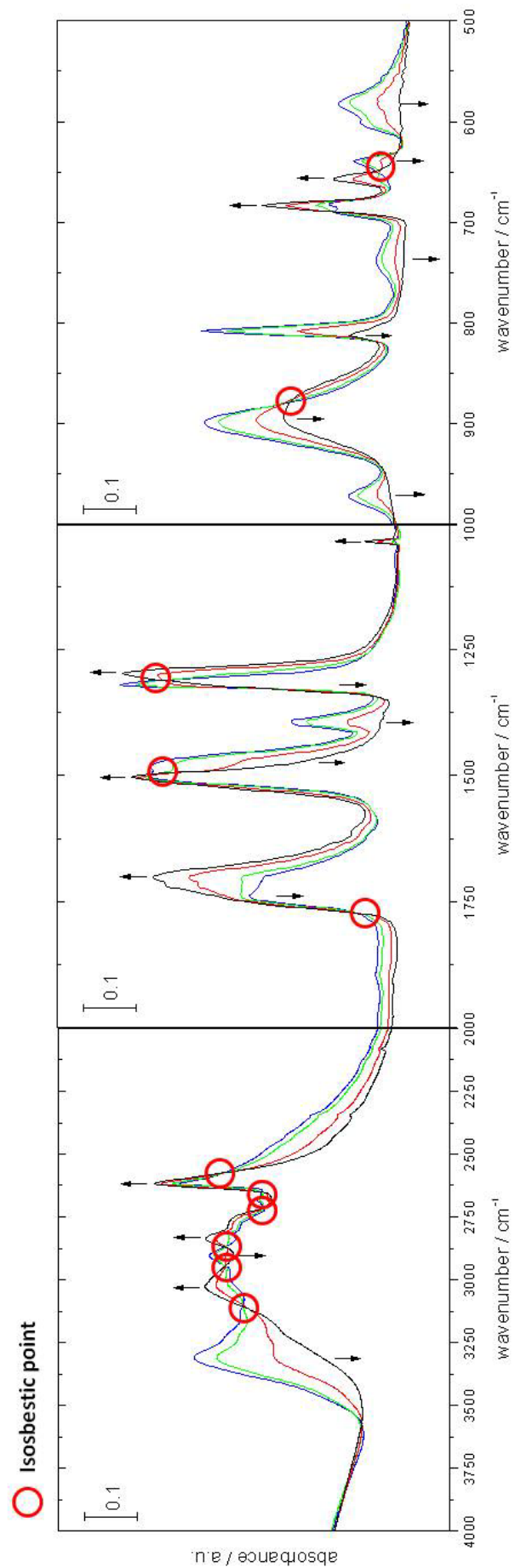
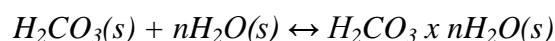


**Figure 7.5** Phase transition to  $\beta$ -H<sub>2</sub>CO<sub>3</sub> by increasing the temperature. The blue curve was recorded at 205 K (t = 30 min), the green one at 210 K (t = 30 min), the red curve at 220 K (t = 23 min) and the black one at 230 K (t = 5 min).

## 7.3 Discussion

The change in the IR-spectra (Figure 7.2) caused by  $RH_{ice} > 100\%$  and condensation of ice at different temperatures suggest reaction of carbonic acid with solid water. Condensation of ice is evident from the observed band at  $3630\text{ cm}^{-1}$  (Figure 7.2b & c), which is assigned to the dangling OH-mode of  $H_2O$ -ice, where the H-atom is not involved in a hydrogen bond. Ice clusters formed in  $He(g)$  at 80 K show the dangling OH-mode at  $3692\text{ cm}^{-1}$ .<sup>[66-67]</sup> Disappearance of the band at  $3630\text{ cm}^{-1}$  at 240 K at  $RH_{ice} > 100\%$  indicates a reaction of ice with  $H_2CO_3$ . One possibility would be the incorporation of water molecules into the crystal structure of  $H_2CO_3$ , thereby, forming a  $H_2CO_3$ -hydrate:



*reaction 7*

In this hydrate no surface water exists, since the dangling OH-mode cannot be detected.

In oxalic acid dihydrate the hydrogen atoms of the water molecules are bound by relatively weak hydrogen bonds, and  $\nu(OH)$  arises at  $3489/3431\text{ cm}^{-1}$ .<sup>[47, 70]</sup> The band at around  $3290\text{ cm}^{-1}$  ( $3287\text{ cm}^{-1}$  in Figure 7.2b,  $3291\text{ cm}^{-1}$  in Figure 7.2c and  $3299\text{ cm}^{-1}$  in Figure 7.2d) may arise from the  $\nu(OH)$  mode of  $H_2O$ , which has penetrated into the  $H_2CO_3$  crystal, by diffusion from the surface into the bulk. Here the hydrogen atoms of the water molecules may form stronger hydrogen bonds as in the one of oxalic acid dihydrate.

The change due to the presence of solid water leads to the hypothesis that a hydrate of carbonic acid is formed. In the presence of  $H_2O$ -ice,  $\beta$ - $H_2CO_3$  could be transformed to an amorphous hydrate, which crystallizes at higher temperature. After removal of  $H_2O$  a phase transition to  $\beta$ - $H_2CO_3$  takes place.

Very interesting is that by reaction in concentrated aqueous solutions ( $KHCO_3(aq)$   $c = 2\text{ M}$ ;  $HBr(aq)$   $c = 4\text{ M}$ ) at low temperature, the same new species is formed as in the case of  $\beta$ - $H_2CO_3$  interacting with solid water. In the case of water as solvent, protonation of  $HCO_3^-/CO_3^{2-}$  apparently occurs in the freeze-concentrated state. About 15 K above water's  $T_g \approx 136\text{ K}$  the layers crystallize to cubic ice and protonation to  $H_2CO_3$  occurs in a residual freeze-concentrated solution<sup>[2, 20]</sup>. It is conceivable that the cubic ice then also reacts with  $H_2CO_3$ , forming the hydrate  $H_2CO_3 \cdot nH_2O$ .

Here also, the arising band at  $3305\text{ cm}^{-1}$  in the spectrum (Figure 7.4b) can be assigned to  $\nu(OH)$  of  $H_2O$ , which has been incorporated into the  $H_2CO_3$  crystal. The absence of the dangling OH-mode at  $3630\text{ cm}^{-1}$  suggests absence of surface ice layers.

The shift and split of bands, e. g.  $\nu(CO)$  as well as  $\nu_{as}[C(OH)_2]$  in the spectrum (Figure 7.4b) may arise from a distortion of the crystal structure due to the interaction with the  $H_2O$  molecules.

The hydration reaction takes place only, if at low temperatures ice is deposited on  $\beta$ - $\text{H}_2\text{CO}_3$ . Depositing solid  $\text{H}_2\text{O}$  at 80 K in *vacuo* on the crystalline  $\beta$ - $\text{H}_2\text{CO}_3$  film and increasing the temperature to 200 K the hydrate is formed. The reverse reaction (dehydration) to  $\beta$ - $\text{H}_2\text{CO}_3$  proceeds slowly at 220 K, but fast at 230 K. In Table 7.1 an overview of the band positions for amorphous and crystalline  $\beta$ - $\text{H}_2\text{CO}_3$  as well as for the new species, the  $\text{H}_2\text{CO}_3$ -hydrate, is given. To shed further light on the nature of the different phases, also the assignment to  $\beta$ - $\text{H}_2\text{CO}_3$  is shown.

**Table 7.1 Overview of the band positions for amorphous and crystalline  $\beta$ - $\text{H}_2\text{CO}_3$  as well as for the  $\text{H}_2\text{CO}_3$ -hydrate (all values in  $\text{cm}^{-1}$ ). For more clarity the assignment to  $\beta$ - $\text{H}_2\text{CO}_3$  is shown.**

amorphous $\text{H}_2\text{CO}_3$ [3]	crystalline $\beta$ - $\text{H}_2\text{CO}_3$	hydrate of $\text{H}_2\text{CO}_3$	Assign. [20] $\beta$ - $\text{H}_2\text{CO}_3$
3310		3305	
	3028		$\nu(\text{C}=\text{O}) + 2 \times \delta_{\text{ip}}(\text{CO}_3)$ $\nu(\text{C}=\text{O}) + \delta_{\text{ip}}(\text{COH})$ or $2 \times \nu_{\text{as}}[\text{C}(\text{OH})_2]$
2619	2836	2905	$\nu_{\text{as}}[\text{C}(\text{OH})_2] + \delta_{\text{ip}}(\text{COH})$ or $2 \times \nu_{\text{as}}[\text{C}(\text{OH})_2] + 2 \times \delta_{\text{ip}}(\text{CO}_3)$
2555	2617	2618	$2 \times \delta_{\text{ip}}(\text{COH})$
1721	1702	1739	$\nu(\text{C}=\text{O})$
1630		1703	
1476	1503	1503 1483	$\nu_{\text{as}}[\text{C}(\text{OH})_2]$
(1363)		1392	
1306	1297	1319	$\delta_{\text{ip}}(\text{COH})$
1265			
1020	1035	1035	$\nu_{\text{s}}[\text{C}(\text{OH})_2]$
		972	
	893	899	$\delta_{\text{oop}}(\text{COH})$
803	812	808	
		738	$\delta_{\text{oop}}(\text{CO}_3)$
	683	690 682	
649	657	639	$\delta_{\text{ip}}(\text{CO}_3)$
		600	
		582	

$\nu_{\text{s}}$  and  $\nu_{\text{as}}$ , symmetric and asymmetric stretching mode;  $\delta_{\text{ip}}$  and  $\delta_{\text{oop}}$  in-plane and out-of-plane bending mode

For more clarity about the new species, e. g. about the hydration number  $n$ , the crystal structure, etc. more experiments are required. Especially isotope effects can be helpful for the interpretation of the IR-spectrum. Also DSC and powder X-ray diffraction should be important methods in solving this puzzle. Figure 7.6 shows local structure motif of

carbonic acid hydrate, by interaction of dimers containing a center of inversion ( $C_{2h}$  point group) with two  $H_2O$ -molecules, forming a dihydrate ( $H_2CO_3 \times 2 H_2O$ ).

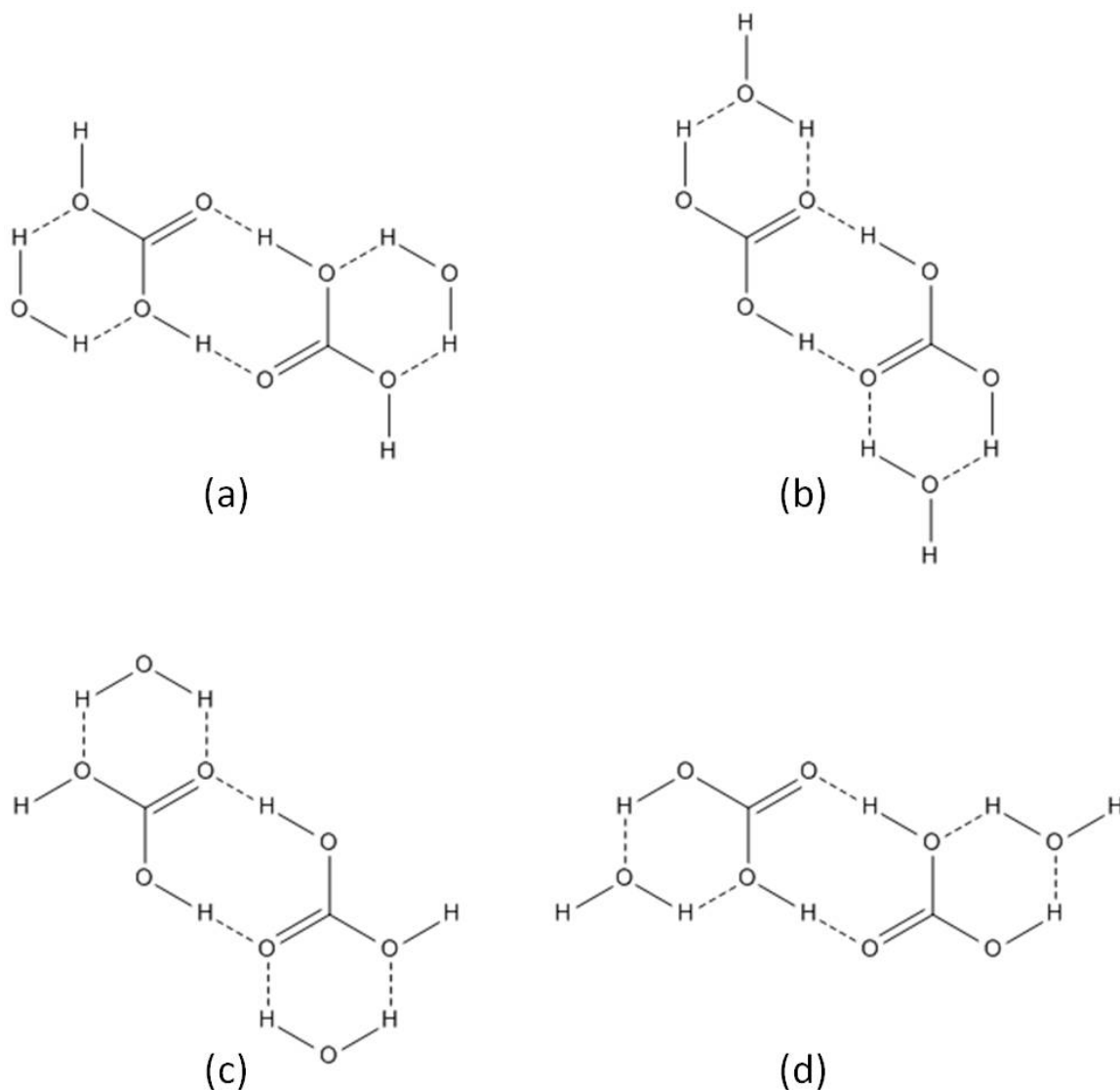


**Figure 7.6** Local structure motif of carbonic acid hydrate, by interaction of dimers containing a center of inversion ( $C_{2h}$  point group) with two  $H_2O$ -molecules, forming a dihydrate ( $H_2CO_3 \times 2 H_2O$ ). a) & b) dimer formed with cis-cis monomers and c) & d) with cis-trans monomers.

# 8 Appendix

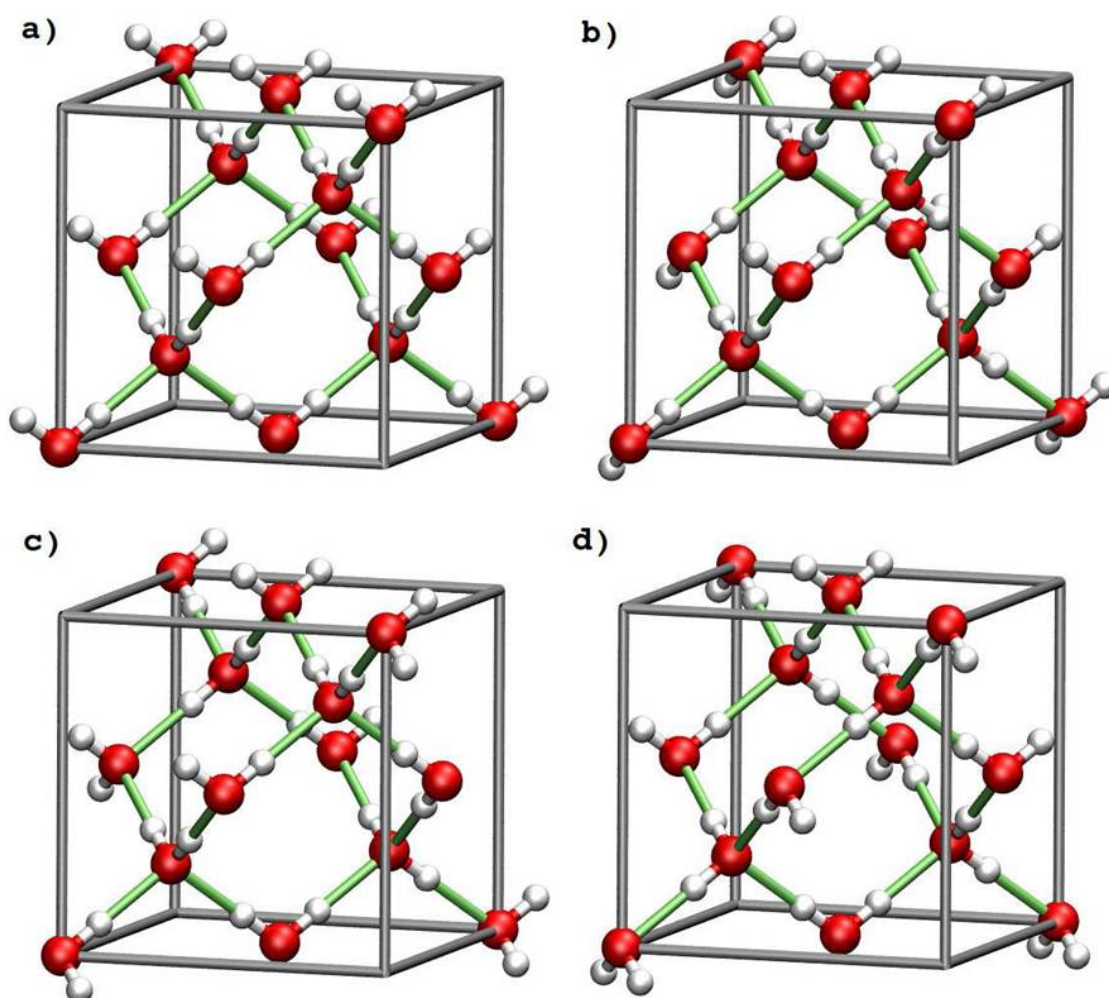
---

## 8.1 Submitted Publication

Philipp Geiger, Christoph Dellago, Markus Macher, Cesare Franchini, Georg Kresse, **Juergen Bernard**, Josef N. Stern and Thomas Loerting;

*“Proton ordering of cubic ice Ic: spectroscopy and computer simulations.”*

*J. Phys. Chem. Submitted 11.01.2014*



This document is confidential and is proprietary to the American Chemical Society and its authors. Do not copy or disclose without written permission. If you have received this item in error, notify the sender and delete all copies.

### Proton Ordering of Cubic Ice Ic: Spectroscopy and Computer Simulations

Journal:	<i>The Journal of Physical Chemistry</i>
Manuscript ID:	jp-2014-00324x
Manuscript Type:	Article
Date Submitted by the Author:	11-Jan-2014
Complete List of Authors:	Geiger, Philipp; University of Vienna, Faculty of Physics Dellago, Christoph; University of Vienna, Faculty of Physics Macher, Markus; University of Vienna, Faculty of Physics Franchini, Cesare; University of Vienna, Faculty of Physics Kresse, Georg; University of Vienna, Faculty of Physics Bernard, Jürgen; University of Innsbruck, Institute of Physical Chemistry Stern, Josef; University of Innsbruck, Institute of Physical Chemistry Loerting, Thomas; University of Innsbruck, Institute of Physical Chemistry

SCHOLARONE™  
Manuscripts

# Proton ordering of cubic ice Ic: spectroscopy and computer simulations

Philipp Geiger,<sup>†</sup> Christoph Dellago,<sup>\*,†</sup> Markus Macher,<sup>†</sup> Cesare Franchini,<sup>†</sup> Georg Kresse,<sup>†</sup> Jürgen Bernard,<sup>‡</sup> Josef N. Stern,<sup>‡</sup> and Thomas Loerting<sup>‡</sup>

*Faculty of Physics, University of Vienna, Boltzmannngasse 5, 1090 Vienna, Austria, and Institute of Physical Chemistry, University of Innsbruck, Innrain 52a, A-6020 Innsbruck, Austria*

E-mail: Christoph.Dellago@univie.ac.at

## Abstract

Several proton disordered crystalline ice structures are known to proton order at sufficiently low temperatures, provided the right preparation procedure is used. For cubic ice, ice Ic, however, no proton ordering has been observed so far. Here, we subject ice Ic to an experimental protocol similar to that used to proton order hexagonal ice. In situ FT-IR spectroscopy carried out during this procedure reveals that the librational band of the spectrum narrows and acquires a structure that is not observed in proton disordered ice Ic. Based on vibrational spectra we computed for ice Ic and various of its proton ordered variants using classical molecular dynamics and *ab initio* simulations, we interpret the features of our experimental spectra as arising from partial proton ordering. Among the four types of proton ordering considered in our simulations, a ferroelectric structure, which has the lowest energy, and a weakly ferroelectric structure with the second lowest energy best fit the experimental spectra.

---

\*To whom correspondence should be addressed

<sup>†</sup>Faculty of Physics, University of Vienna, Boltzmannngasse 5, 1090 Vienna, Austria

<sup>‡</sup>Institute of Physical Chemistry, University of Innsbruck, Innrain 52a, A-6020 Innsbruck, Austria

## Introduction

Despite its simple molecular structure, water has a remarkably complex phase diagram. Application of pressure produces a variety of different solid ice phases with densities considerably higher than that of ordinary hexagonal ice, ice Ih. To date, sixteen thermodynamically stable or metastable crystalline phases (labelled with Roman numerals as Ih, Ic, II, III, ..., XV)<sup>1-3</sup> and several amorphous phases<sup>4-6</sup> have been discovered. While in some crystalline ice structures, including ice Ih as well as cubic ice, ice Ic, only the oxygen atoms form a regular lattice and the protons are disordered, in other ice phases, such as ice II, also the protons are arranged in a regular way. Indeed, there exist pairs of ice structures, such as ice Ih and its protonically ordered counterpart ice XI, which have nearly identical oxygen sub-lattices but differ in their proton order. Recently, Salzmann and collaborators have identified experimentally<sup>2,3</sup> several previously unknown ice phases, completing the pairings V/XIII, XII/XIV and VI/XV, which differ only in proton ordering.

For all ice phases, in which water molecules remain intact and are tetrahedrally coordinated, the arrangement of protons in the protonically disordered structures is essentially governed by the so-called ice rules, or Bernal-Fowler rules.<sup>1,7</sup> These rules posit that (1) there are exactly two protons in proximity to each oxygen atom, to which they are covalently bonded, and (2) there is exactly one proton between two oxygen atoms, corresponding to a hydrogen bond between the neighboring molecules. According to the ice rules, all hydrogen configurations satisfying these two requirements are equally probable, implying that the interactions between non-neighboring molecules are not sufficient to stabilize a particular protonic arrangement. In this approximation, the ground state is thus strongly degenerate leading to the residual entropy of ice.<sup>1,8</sup> At very low temperatures, however, the difference in free energy between proton ordered and proton disordered configurations can lead to a phase transition to the proton ordered phase.

Experimentally, proton ordering transitions in crystalline ices are known to take place at low temperature and to be severely hampered by slow transformation kinetics. The highest ordering transition temperatures have been found for ice VII and ice III, which order below  $T \sim 270$  K at  $p > 2$  GPa to ice VIII<sup>9</sup> and below  $T \sim 170$  K at  $p \sim 0.3$  GPa to ice IX,<sup>10,11</sup> respectively. These

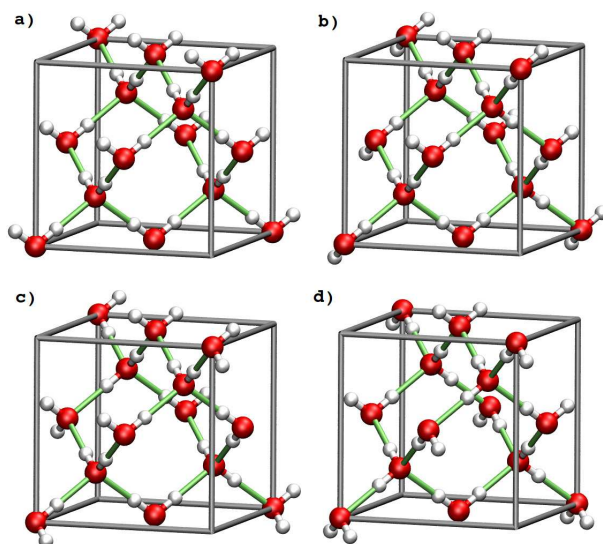


Figure 1: Four distinct proton arrangements in a unit cell of cubic ice containing 8 water molecules.<sup>27</sup> Green sticks denote hydrogen bonds and the boundaries of the unit cell are shown as grey lines. Each configuration is a representative of one of the four symmetry inequivalent proton arrangements with different Coulomb energies that exist in a unit cell of this size. According to the calculations of Lekner,<sup>27</sup> the fully ferroelectric configuration (a, space group  $I4_1md$ ) has the highest energy and the anti-ferroelectric configuration (d,  $P4_12_12$ ) the lowest energy. Configurations (b,  $Pna2_1$ ) and (c,  $P4_1$ ) are weakly ferroelectric and have intermediate electrostatic energies.

two hydrogen ordering transitions in ice are the only ones known to take place in the absence of a catalyst. Other ordering transitions in the intermediate pressure regime at  $p \sim 0.5\text{-}1.5$  GPa take place at about  $T = 100 - 150$  K, namely ice  $V \rightleftharpoons$  ice XIII,<sup>2</sup> ice  $VI \rightleftharpoons$  ice XV<sup>3</sup> and ice  $XII \rightleftharpoons$  ice XIV.<sup>2</sup> These three transitions take place at an observable rate by using HCl as a dopant, which increases the reorientation rates of individual water molecules in the ice lattice, presumably by producing rotational Bjerrum L-defects.<sup>1</sup> Ambient pressure hexagonal ice, ice Ih, shows the lowest experimentally found ordering transition temperature of  $T \sim 72$  K.<sup>12-19</sup> Such proton ordered ice XI is typically produced from ice Ih using hydroxide doping, *e.g.*, by freezing a 0.1 M KOH solution.

While several protonically ordered ice phases have been prepared and analyzed in the laboratory, the proton ordered counterpart of cubic ice Ic has not been observed to date. In ice Ic, which is metastable, the oxygen atoms are arranged on a diamond lattice corresponding to a ABCABC... stacking of the puckered layers of hexagonal rings orthogonal to the  $c$ -axis. (In hexagonal ice,

1  
2  
3 ice Ih, the stacking sequence is ABABAB... leading to a Wurtzite-like arrangement of the oxygen  
4 atoms.) The first coordination shell, however, is identical for both ice Ih and Ic such that one may  
5 expect ice Ih and ice Ic to proton order under similar conditions.  
6  
7  
8

9  
10 While large single crystals of hexagonal ice have been prepared in the laboratory, this has so  
11 far not been possible in the case of cubic ice. Depending on the route of preparation, cubic ice  
12 always contains more or less hexagonal stacking faults.<sup>20–24</sup> In order to minimize the number of  
13 hexagonal stacking faults in cubic ice we here use the hyperquenching technique of micron-sized  
14 droplets.<sup>25</sup> This technique was shown before to produce cubic ice of rather high cubicity (see Fig.  
15 1 in Ref. 26) as compared to cubic ice prepared e.g., by vapor-deposition or by a phase-transition  
16 from high-pressure ices upon heating at ambient pressure. We emphasize that hexagonal ice Bragg  
17 peaks, e.g., at  $2\theta = 34^\circ$  or  $40^\circ$  (Cu-K $\alpha$ ), are not detected at all. The observed (noise-level) intensity  
18 at  $2\theta = 34^\circ$  or  $40^\circ$  is lower by about a factor of 1000 compared to the most intense (111) Bragg  
19 peak of cubic ice at  $2\theta = 24^\circ$ . From this, we estimate that our cubic ice samples are contaminated  
20 with hexagonal ice levels of  $< 0.1\%$ . The possible ordering of the two-dimensional layers of  
21 hexagonal stacking faults that occur occasionally within the cubic stacking sequence certainly has  
22 a negligible effect on the IR band shape. The changes observed here by IR spectroscopy in Figs.  
23 7 and 8 are instead comparable in magnitude to the changes in IR spectra upon partial ordering of  
24 100% hexagonal ice to ice XI (see Ref. 66).  
25  
26  
27  
28  
29  
30  
31  
32  
33  
34  
35  
36  
37  
38  
39

40 To study the energetics of proton arrangements in ice Ic, Lekner computed the electrostatic en-  
41 ergies of all 90 proton configurations satisfying the ice rules in a periodically replicated unit cell of  
42 8 water molecules.<sup>27,28</sup> Due to the degeneracy of the Coulomb energy, there are only four classes  
43 of configurations with different energies, examples of which are shown in Fig. 1. Out of these, the  
44 perfectly ordered anti-ferroelectric proton configuration has the lowest electrostatic energy while  
45 the ferroelectric structure has the highest electrostatic energy. Weakly ferroelectric configurations  
46 have intermediate energies. This general trend is confirmed by calculations for larger unit cells  
47 such that, based on these results, thermodynamically one expects a transition to an anti-ferroelectric  
48 phase for ice Ic at sufficiently low temperatures. The purely electrostatic calculations of Lekner,  
49  
50  
51  
52  
53  
54  
55  
56  
57  
58  
59  
60

1  
2  
3 however, are contrasted by recent *ab initio* (density functional theory) calculations,<sup>29</sup> according to  
4 which the ferroelectrically ordered structure is the energetically most stable one. Similar differ-  
5 ences between *ab initio* results and calculations based on empirical force fields have been reported  
6 also for the energetic ordering of various proton ordered forms of hexagonal ice.<sup>30</sup> Most likely,  
7 such discrepancies are due to polarization effects,<sup>31</sup> which are fully taken into account in *ab initio*  
8 calculations but are almost entirely neglected by most empirical potentials. While the energetics  
9 of proton ordering plays an important role for the low temperature proton ordered phases of ice, it  
10 may be their kinetic accessibility that determines which structures are observed in the experiments.  
11  
12

13  
14  
15  
16  
17  
18  
19  
20 In this paper, we investigate the proton ordering of ice Ic using a combination of spectroscopic  
21 experiments and computer simulations. As discussed in detail below, the shape of the librational  
22 band of the IR-spectra measured in our work, interpreted on the basis of computed IR-spectra,  
23 indicates that hydroxide doped ice Ic partially proton orders following an experimental protocol  
24 similar to that used previously to proton order ice Ih. Interestingly, the combination of experiment  
25 and theory suggests that cubic ice indeed shows a tendency to ferroelectric proton order, however,  
26 kinetics may strongly influence the ordering transition.  
27  
28  
29  
30  
31  
32  
33

34  
35 The remainder of this article is organized as follows. In Sec. we explain the computational  
36 model and methods used to carry out the simulations and report their results. Experimental proce-  
37 dures and results are described in Sec. and discussed and interpreted in Sec. based on the spectra  
38 computed in our simulations.  
39  
40  
41  
42  
43  
44

## 45 Simulations

46  
47  
48 In order to detect proton ordered cubic ice in the laboratory it is important to be capable of distin-  
49 guishing the various degrees of protonic order that are consistent with the ice rules. One possible  
50 way to do that is *via* the signature of proton order on the vibrational spectrum obtained in infrared  
51 (IR) or Raman spectroscopy experiments, methods that have been employed before to study pro-  
52 ton order in ice.<sup>32-34</sup> In the present work, we used molecular dynamics simulations complemented  
53  
54  
55  
56  
57  
58  
59  
60

1  
2  
3  
4 with *ab initio* calculations to study the structural and dynamical properties of various proton or-  
5 dered ice Ic polymorphs. In particular, we determined radial distribution functions and IR spectra  
6 for different proton ordered cubic ice candidates and compared them to the ones for hexagonal  
7 ice Ih and its proton ordered counter part, ice XI. In doing so, we focused on translational and  
8 librational modes, as these modes carry the most information about proton ordering and provide  
9 the basis for the interpretation of the experimental IR-spectra presented in Sec. .  
10  
11  
12  
13  
14  
15  
16

## 17 **Model and Methods**

18  
19  
20 All our molecular dynamics simulations are performed using the TIP4P/ice model,<sup>35</sup> developed to  
21 reproduce the properties of the various ice phases and, specifically, the phase diagram of ice. In  
22 this model, each molecule is represented by four interaction sites rigidly connected with each other.  
23 These sites, placed at the oxygen atom, the two hydrogen atoms and on the bisector of the HOH-  
24 angle, interact solely through pair potentials. While the oxygen atoms interact with each other only  
25 *via* a Lennard-Jones potential, all other interaction sites carry charges that interact Coulombically.  
26 The TIP4P/ice model reproduces all ice phases consisting of intact water molecules and leads to a  
27 phase diagram with the correct topology and coexistence lines that are only slightly displaced with  
28 respect to the experimental phase diagram.<sup>36</sup> The model also yields an accurate prediction of the  
29 densities of the ice phases and the liquid phase. Since water molecules are rigid in the TIP4P/ice  
30 model, only motions that do not involve intramolecular vibrations can be studied such that our IR-  
31 spectra are limited to the low frequency bands corresponding to translational and librational modes.  
32 To investigate the higher frequency part of the spectrum a model with flexible water molecules  
33 would be required.<sup>37</sup>  
34  
35  
36  
37  
38  
39  
40  
41  
42  
43  
44  
45  
46  
47  
48

49 To follow the dynamics of the system, we integrated the equations of motion with a quaternion  
50 based integrator that maintains the rigid geometry of the water molecules. In particular, we carried  
51 out molecular dynamics simulations in the *NVT* and isotropic *NpT* ensembles using a slightly  
52 modified version of the Verlet-like integrator proposed by Kamberaj *et al.*,<sup>38</sup> based on the Trot-  
53 ter decomposition schemes applied by Miller *et al.*<sup>39</sup> and Martyna *et al.*<sup>40</sup> In this algorithm, the  
54  
55  
56  
57  
58  
59  
60

1  
2  
3 canonical and isothermal-isobaric molecular dynamics is implemented through thermostat chains  
4 based on the Nosé-Hoover<sup>41,42</sup> and the Andersen<sup>43</sup> approaches. Electrostatic interactions were  
5 treated with Ewald summation.<sup>44</sup>  
6  
7

8  
9 The initial configurations of the different proton ordered phases were generated by periodically  
10 replicating the unit cells given in Ref. 27 for cubic ice and Refs. 30 and 14 for ice XI, respectively.  
11 The proton disordered counterparts were set up following the procedure suggested by Rahman and  
12 Stillinger,<sup>45</sup> which starts from a hexagonal or cubic crystal with perfect proton order and protons  
13 located on the connecting lines between neighboring oxygens. The proton order is then disrupted  
14 by shifting protons from a position close to one oxygen to the position close to the neighboring  
15 oxygen originally accepting the hydrogen bond involving the shifted hydrogen. In order to keep  
16 the water molecules in the sample intact, this shifting operation has to be carried out along closed  
17 loops of hydrogen bonds. This sequence of basic steps is repeated until every water molecule has  
18 been touched several times and a vanishing total dipole moment is achieved. At the end of the  
19 procedure, the ideal water molecules, which have a geometry consistent with perfect tetrahedral  
20 coordination, are replaced by molecules with TIP4P geometry.  
21  
22  
23  
24  
25  
26  
27  
28  
29  
30  
31  
32  
33

34 To quantify the structural and dynamical diversity of various degrees of proton order, we have  
35 calculated energies, pair correlation functions as well as infrared absorption spectra. The pair  
36 correlation function  $g_{AB}(r)$  measures the conditional probability to find an atom of species B at  
37 distance  $r$  from an atom of species A relative to the same probability in a hypothetical ideal gas with  
38 the same density and composition. In the present case we consider the pair correlation functions  
39  $g_{OO}(r)$ ,  $g_{HH}(r)$ , and  $g_{OH}(r)$  between pairs of oxygen atoms, pairs of hydrogen atoms, and oxygen  
40 and hydrogen atoms, respectively. All of these functions can be extracted from data obtained in  
41 neutron diffraction experiments.<sup>46</sup>  
42  
43  
44  
45  
46  
47  
48  
49

50 Infrared absorption spectra are calculated in the classical approximation<sup>47,48</sup> as the Fourier  
51 transform of the time autocorrelation function  $\langle \mathbf{M}(0) \cdot \mathbf{M}(t) \rangle$  of the total dipole moment  $\mathbf{M}$ ,  
52  
53  
54

$$55 I(\omega) \propto \int_0^{\infty} dt \langle \mathbf{M}(0) \cdot \mathbf{M}(t) \rangle \cos \omega t, \quad (1)$$

56  
57  
58  
59  
60

1  
2  
3 where  $\omega$  is the vibrational frequency and angular brackets  $\langle \dots \rangle$  indicate a time or ensemble av-  
4 erage. The dipole-dipole correlation function can be written in terms of the dipole moments  $\mu_i$   
5 of individual water molecules, which are determined by the magnitude, sign and location of the  
6 charges on the TIP4P/ice molecules as well as by their orientation,  
7  
8  
9

$$\langle \mathbf{M}(0) \cdot \mathbf{M}(t) \rangle = \sum_{i,j} \langle \mu_i(0) \cdot \mu_j(t) \rangle. \quad (2)$$

10  
11  
12 Note that while the cross correlation terms  $\langle \mu_i(0) \cdot \mu_j(t) \rangle$ ,  $i \neq j$ , which quantify the correlations  
13 between the dipole moments of different water molecules, are negligible for high frequency modes  
14 associated with intramolecular stretching and bending motions, they play an important role for the  
15 form of the spectrum in the range characteristic for translations and librations involving collective  
16 motions of multiple molecules.<sup>49,50</sup>  
17

18 We complemented the results of our simulations based on the TIP4P/ice model with energies  
19 and spectra computed *ab initio* using the Vienna *ab initio* simulation package (VASP) and PAW<sup>51</sup>  
20 potentials in the implementation of Kresse and Joubert.<sup>52</sup> The outermost core radii for the O and H  
21 potentials are 1.52 and 1.1 a.u., respectively (corresponding to the standard potentials distributed  
22 with the VASP package). All calculations were performed using the Perdew-Burke-Ernzerhof  
23 (PBE) functional,<sup>53</sup> as well as using van der Waals density functional theory (vdW-DFT).<sup>54</sup> We  
24 specifically used the vdW-DFT of Klimeš *et al.* termed “optPBE” (optimized PBE).<sup>55,56</sup> The Brill-  
25 ouin zone was sampled at  $6 \times 6 \times 6$   $k$ -points. To determine the equilibrium volume of each  
26 structure, all internal parameters (including relative lattice parameters) were optimized at seven  
27 volumes around the equilibrium volume, and the energy vs. volume curve was fitted using an  
28 equation of state. The vibrational frequencies were evaluated using finite differences: all symme-  
29 try inequivalent atoms were displaced along symmetry inequivalent directions, and the interatomic  
30 force constant matrix was completed using symmetry considerations.<sup>57</sup> The vibrational frequen-  
31 cies were determined at the  $\Gamma$ -point by diagonalization of the force constant matrix. The dipole  
32 activity was calculated from Born effective charge tensors for oxygen and hydrogen, respectively.  
33  
34  
35  
36  
37  
38  
39  
40  
41  
42  
43  
44  
45  
46  
47  
48  
49  
50  
51  
52  
53  
54  
55  
56  
57  
58  
59  
60

Table 1: Average densities  $\langle\rho\rangle = m_{\text{H}_2\text{O}}N/\langle V\rangle$  and average potential energies per molecule  $\langle E_{\text{pot}}\rangle$  for the cubic and hexagonal ice phases at temperature  $T = 70$  K and  $T = 170$  K, respectively, and pressure  $p = 0.1$  bar. Also shown are the Coulomb energies  $E_{\text{Coul}}$  calculated by Lekner<sup>27,28</sup> and the cohesive energies per molecule computed using density functional theory ( $E_{\text{coh}}$ ) and exact exchange with the random phase approximation ( $E_{\text{RPA}}$ ) at  $T = 0$  and  $p = 0$ . All energies are stated with respect to the corresponding energy of the structure ice Ic (ord. d). For  $\langle E_{\text{pot}}\rangle_{70\text{K}}$  and  $\langle E_{\text{pot}}\rangle_{170\text{K}}$  the total average potential energy per molecule of the reference structure (d) at  $T = 70$  K is  $\langle E_{\text{pot}}\rangle_{70\text{K}} = -67.0872(2)$  kJ/mol and at  $T = 170$  K  $\langle E_{\text{pot}}\rangle_{170\text{K}} = -64.3298(3)$  kJ/mol. For  $E_{\text{coh}}$  the cohesive energy per molecule of the reference structure (d) with respect to infinitely separated water molecules is  $E_{\text{coh}} = -63.813$  kJ/mol. The statistical errors were calculated by block average analysis<sup>44</sup> and are given as single numbers in round brackets, which correspond to the error in the last digit.

ice phase	$\langle\rho\rangle_{70\text{K}}$ (kg/m <sup>3</sup> )	$\langle\rho\rangle_{170\text{K}}$ (kg/m <sup>3</sup> )	$\langle E_{\text{pot}}\rangle_{70\text{K}}$ (kJ/mol)	$\langle E_{\text{pot}}\rangle_{170\text{K}}$ (kJ/mol)	$E_{\text{Coul}}$ (kJ/mol)	$E_{\text{coh}}$ (kJ/mol)	$E_{\text{RPA}}$ (kJ/mol)
ice Ih	930.17(2)	919.00(3)	0.0098(2)	0.0169(5)			
ice XI (Cmc2 <sub>1</sub> )	930.31(3)	919.12(2)	0.0471(2)	0.0547(5)	0.750	-0.492	
ice XI (Pna2 <sub>1</sub> )	929.95(2)	919.25(3)	-0.0195(2)	-0.0250(5)	-0.032	-0.096	
ice Ic	932.11(2)	919.89(2)	0.0449(2)	0.0524(4)			
ice Ic (ord. a, I4 <sub>1</sub> md)	929.32(2)	918.39(2)	0.2319(2)	0.2299(5)	0.816	-0.531	-0.521
ice Ic (ord. b, Pna2 <sub>1</sub> )	932.29(2)	920.66(3)	0.0364(2)	0.0333(4)	0.408	-0.261	-0.212
ice Ic (ord. c, P4 <sub>1</sub> )	932.24(2)	920.51(2)	0.0277(1)	0.0261(5)	0.204	-0.106	-0.068
ice Ic (ord. d, P4 <sub>1</sub> 2 <sub>1</sub> 2)	932.57(3)	920.63(3)	0.0000	0.0000	0.000	0.000	0.000

For consistency with the molecular dynamics simulations and to account for thermal expansion, the vibrational frequencies were evaluated at the average densities computed in the MD simulations. The vdW-DFT equilibrium volumes (at  $T = 0$  K) are, however, only 3-4 % smaller than the average MD volumes.

## Simulation results

To investigate the structure of ice Ih and ice Ic, we calculated radial distribution functions using  $NpT$  molecular dynamics simulations of  $N = 1000$  (for the parental cubic ice) and  $N = 896$  (for the parental hexagonal ice) water molecules with orthogonal simulation boxes at temperature  $T = 170$  K and pressure  $p = 0.1$  bar. The proton ordered counterparts were calculated using the same simulation boxes, but are of lower space group symmetry, *e.g.*, orthorhombic symmetry in case of ice XI. Similarly, proton ordering of cubic ice Ic leads to configurations that are not cubic but display a lower symmetry. When we speak about cubic and hexagonal ordered structures in the

1  
2  
3 following, we always refer to the symmetry of the disordered parent structure. For the proton  
4 disordered configurations we also carried out simulations at  $T = 70$  K, the temperature to which  
5 ice Ic is cooled in the experiments. Note that at a temperature of  $T = 170$  K initially proton  
6 ordered configurations immediately disorder on the experimental time scale. In the simulations,  
7 however, no proton disordering is observed during the entire simulation because the simulation  
8 time is shorter than the time scale of proton disordering. In all simulations, a time step of 2 fs and  
9 a Lennard-Jones cutoff of  $3\sigma$  were used. The same cutoff was used for the real space part of the  
10 Ewald summation, where for the reciprocal space 1152  $k$ -vectors were employed. All simulations  
11 were performed for a hydrogen mass of  $m_{\text{H}} = 1$  and an oxygen mass of  $m_{\text{O}} = 16$ . The total length  
12 of the simulations was 5 ns in each case.  
13  
14  
15  
16  
17  
18  
19  
20  
21  
22  
23

24 Average densities and energies computed in these MD simulations are listed in Tab. 1 along-  
25 side with the electrostatic energies computed by Lekner<sup>27,28</sup> as well as the energies determined in  
26 our *ab initio* simulations. The electrostatic calculations for the idealized structures and the MD  
27 simulations carried out at  $T = 170$  K and at  $T = 70$  K agree in the energetic ordering of the various  
28 structures both finding that the anti-ferroelectric structure (d) has the lowest energy and the ferro-  
29 electric structure (a) has the highest energy while structures (b) and (c) have intermediate energies.  
30 The energies obtained using density functional theory, however, display the reverse energetic or-  
31 der but agree well with energies computed previously using DFT methods.<sup>29</sup> To double check the  
32 density functional theory data, we performed more accurate calculations using exact exchange and  
33 the random phase approximation (EXX-RPA) for the correlation energy.<sup>58,59</sup> These calculations  
34 were also extended to ice II, VIII, for which highly accurate diffusion Monte Carlo results are  
35 available.<sup>60</sup> In these cases (ice II, ice VIII, ice Ih), we found excellent agreement with the pub-  
36 lished diffusion Monte Carlo validating the EXX-RPA. The EXX-RPA results confirm the order  
37 of the cubic phases predicted by density functional theory: The ferroelectric structure (a) has the  
38 lowest energy, the anti-ferroelectric structure (d) has the highest energy, and the structures (b) and  
39 (c) have intermediate energies. This discrepancy, observed before for hexagonal ice,<sup>30</sup> is probably  
40 due to the neglect of polarization effects in the TIP4P/ice, which are expected to be particularly  
41  
42  
43  
44  
45  
46  
47  
48  
49  
50  
51  
52  
53  
54  
55  
56  
57  
58  
59  
60

pronounced in ferroelectric structures leading to a lowering of their energy. We would like to emphasize that predicting the correct energetic ordering is known to be difficult in case of proton ordered ices. Vega *et al.*<sup>61</sup> have shown that SPC/E, TIP4P and TIP5P predict a transformation from ice Ih to the anti-ferroelectric Pna21 structure<sup>62</sup> below 70 K. The ferroelectric Cmc21 structure, which is obtained in experiments, is predicted to be the lowest lying H-bond isomer only in the model by Nada and van der Eerden (NvdE).<sup>63</sup> The relative stability of different proton ordered configurations of hexagonal ice is also affected, if a cutoff for electrostatic interaction is used. While short-range interactions favor the anti-ferroelectric configuration, the ferroelectric configuration is stabilized by long-range contributions.<sup>64</sup> It is also worth noting that the free energetic ordering of different proton ordered configurations may also be significantly affected by higher order multipoles, which are not taken into account in our TIP4P/ice simulations.<sup>65</sup>

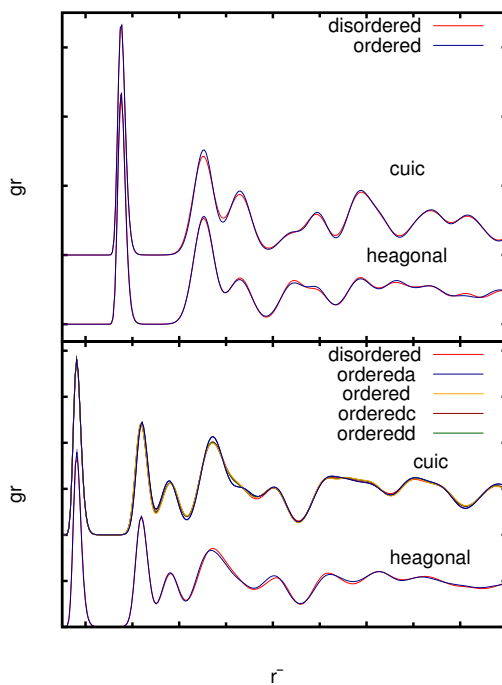


Figure 2: Partial radial distribution functions  $g_{OO}(r)$  and  $g_{OH}(r)$  for proton disordered hexagonal and cubic ice as well as their proton ordered counterparts at  $T = 170$  K. Both the oxygen-oxygen as well as the oxygen-hydrogen radial distribution functions are nearly identical in all cases including proton ordered and disordered configurations. The curves labeled a, b, c, and d correspond to the proton orderings shown in Fig. 1. Note that the peaks corresponding to the intramolecular OH-distances lie outside the range of the figure.

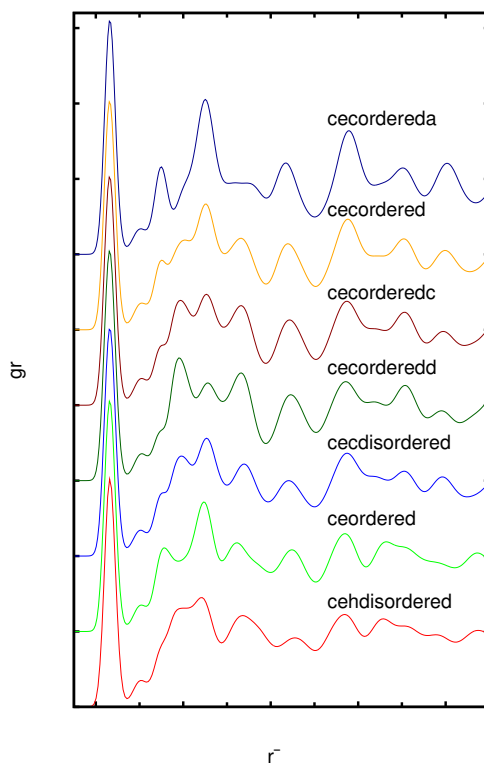


Figure 3: Partial radial distribution functions  $g_{\text{HH}}(r)$  for proton disordered hexagonal and cubic ice as well as their proton ordered counterparts at  $T = 170$  K. The labeling a, b, c, and d refers to the various proton ordering patterns shown in Fig. 1. Note that the peak corresponding to the intramolecular HH-distances lies outside the range of the figure.

The partial pair correlation functions of proton disordered hexagonal ice, ice Ih, and its proton ordered counterpart, ice XI, as well as disordered cubic ice, ice Ic, and its four proton ordered candidates are given in Figs. 2 and 3. As expected, the oxygen-oxygen pair correlation functions  $g_{\text{OO}}(r)$  feature no significant differences for all the order/disorder ice polymorph pairings. In addition, the oxygen-hydrogen pair correlation functions  $g_{\text{OH}}(r)$  show only minute deviations and only the hydrogen-hydrogen pair correlations  $g_{\text{HH}}(r)$  differ appreciably. However, these differences are small making it exceedingly difficult to distinguish between different variants of protonically ordered cubic ice based on the comparison of pair correlation functions determined experimentally from X-ray or neutron diffraction data.<sup>46</sup>

More detailed structural information on proton ordering is encoded in vibrational spectra. For the calculations of the IR-spectra using MD simulations we have set up cubic and hexagonal lattices

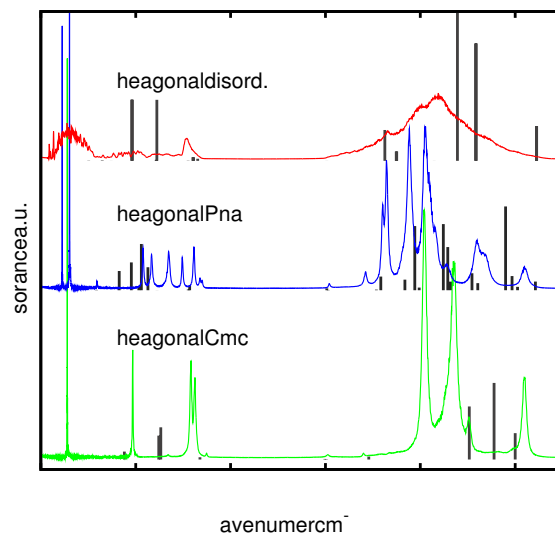


Figure 4: IR spectra obtained from molecular dynamics simulations for disordered hexagonal ice at  $T = 170$  K and two of its proton ordered forms at  $T = 70$  K. Vertical bars indicate the results of *ab initio* simulations at  $T = 0$ .

consisting of  $N = 1000$  and  $N = 896$  molecules, respectively. The time step was set to 2 fs, dipole-dipole time correlation functions were calculated for times up to 20 ps, and in total each system was propagated for 40 ns using a Nosé-Hoover  $NVT$  integrator. Here, the Lennard-Jones cutoff and the Ewald summation real space cutoff were chosen to be  $3\sigma$ . The densities for the different arrangements of hexagonal and cubic ice were set according to Table 1.

Figures 4 and 5 show the computed IR spectra for hexagonal and cubic ice, respectively. In general, the computed spectra are in reasonable agreement with experimental spectra. The broad librational band near  $850\text{ cm}^{-1}$  is in good agreement with experimental spectra of both cubic and hexagonal ice (see dashed line in Fig. 3 of Ref. 66). Also in the far-infrared ( $0\text{-}400\text{ cm}^{-1}$ ) the agreement is reasonable, even though there are some discrepancies especially regarding the band intensities. Hexagonal ice shows three broad bands in this area,<sup>67</sup> which are centered at 160, 230 and  $370\text{ cm}^{-1}$ . In our simulations there are three broad bands centered at 70, 195 and  $310\text{ cm}^{-1}$ . The absorption spectra of the proton disordered forms of hexagonal and cubic ice are clearly distinguishable from those of the various proton ordered phases, which split up in several bands, the number and position of which depend on the particular proton ordering pattern. Thus, these spectra

1  
2  
3  
4 provide a means of detecting the presence of proton order experimentally. IR spectra computed by  
5  
6 density functional theory for proton ordered cubic ice at  $T = 0$  are shown in Fig. 5 as vertical bars  
7  
8 and confirm this conclusion. The length of each bar shown in Fig. 5 corresponds to the dipole ac-  
9  
10 tivity of the corresponding mode. Since the spectra were determined using a harmonic approxima-  
11  
12 tion, finite temperature broadening of the individual peaks is entirely absent. The overall structure  
13  
14 of the *ab initio* spectra shares some important qualitative features with the spectra obtained from  
15  
16 the MD simulations, although in the density functional theory calculations the librational band  
17  
18 ( $550\text{-}1100\text{ cm}^{-1}$ ) is shifted by about  $100\text{ cm}^{-1}$  to higher frequencies. For instance, for structure  
19  
20 (a) a single librational band at  $930\text{ cm}^{-1}$  is predicted using density functional theory, whereas a  
21  
22  $20\text{ cm}^{-1}$  broad peak at  $856\text{ cm}^{-1}$  is observed in the molecular dynamics simulation. Likewise four  
23  
24 peaks are predicted for structure (b), which correspond well to the four peak structure observed in  
25  
26 the molecular dynamics simulations. A further noteworthy difference between the *ab initio* and the  
27  
28 MD results is that the average frequency calculated *ab initio* shifts significantly to the blue with  
29  
30 increasing ferroelectric ordering. We find average frequencies of  $930, 900, 880$  and  $850\text{ cm}^{-1}$  for  
31  
32 cubic ice with ordering (a) (ferroelectric), (b) (weakly ferroelectric), (c) (weakly ferroelectric) and  
33  
34 (d) (anti-ferroelectric), respectively. In the MD simulations the shift is smaller with frequencies of  
35  
36  $849, 833, 826$  and  $816\text{ cm}^{-1}$  for the four phases. The difference is most likely related again to the  
37  
38 neglect of polarization effects in the MD simulations using the TIP4P/ice model.  
39

40  
41 We have also investigated the possibility to probe proton order based on the OH-stretching  
42  
43 band using a recently developed computational method<sup>68,69</sup> that relates the OH-frequency with the  
44  
45 electric field acting on the proton. Such an analysis can therefore be carried out also for rigid water  
46  
47 molecules, in which the geometrical constraints prevent the OH-bond from vibrating. However, the  
48  
49 coupled OH-frequency is less suitable for probing proton ordering than the librational/translational  
50  
51 bands and the decoupled OH- or OD-stretching modes for slightly deuterated  $\text{H}_2\text{O}$  samples or  
52  
53 slightly hydrogenated  $\text{D}_2\text{O}$  samples.<sup>10,70</sup>  
54  
55  
56  
57  
58  
59  
60

## Experiments

As mentioned in Sec. , ice Ih and ice Ic differ in their layer stacking but have an identical local structure. One would therefore expect that ice Ic shows a similar proton ordering transition as ice Ih. The experimental protocol to proton order ice Ih involves bringing the sample to  $\sim 50$  K, which is thought to produce some ferroelectric ice XI seeds, and then waiting at  $\sim 55$ – $67$  K for several days or weeks, which allows the ice XI domains to grow.<sup>15–19</sup> Typically, about 50–60% of the hexagonal ice sample orders using this procedure. Since the local ordering is identical in cubic and hexagonal ice, we anticipate that a similar protocol might allow for hydrogen ordering in cubic ice. To investigate this possibility we have carried out experiments on cubic ice. As discussed in detail below, our observations indicate partial proton ordering detected by comparison of the measured IR-spectra with the results of our simulations.

To carry out our experiments, we prepared an aqueous 0.1 M KOH solution containing 2 mol% of D<sub>2</sub>O. The use of a small fraction of D<sub>2</sub>O allows for the observation of the decoupled OD-stretching mode in infrared spectra, in addition to the coupled OH-stretching mode. KOH introduces substitutional point defects in the ice lattice, which increase the proton mobility and hence reorientational dynamics drastically. We use 0.1 M KOH in order to reach a saturation level of these substitutional point defects. In principle, also lower concentrations such as 0.01 M KOH might be suitable for reaching this enhancement in the dynamics. Cubic ice was prepared by spraying droplets of this solution of about 3 micrometer in diameter into a vacuum-chamber containing a He-cryostated optical window, where the window was first kept at  $\sim 77$  K. This procedure is known to produce hyperquenched glassy water (HGW), which crystallizes to cubic ice upon heating to  $\sim 160$  K.<sup>26,71</sup> Cubic ice prepared in this way shows a comparably low number of hexagonal stacking faults and high cubicity index as judged from the intensity of the X-ray reflexes corresponding to the hexagonal faults.<sup>26</sup>

The crystallization from HGW to cubic ice was monitored by in situ FT-IR spectroscopy, and the librational band of cubic ice at  $\sim 160$  K is depicted as the blue curve in Fig. 6. Cubic ice was then cooled to  $\sim 60$  K for a few hours and then heated to 70 K for about 80 hours. The

1  
2  
3  
4 spectrum recorded after this procedure is depicted in red in Fig. 6. It can clearly be noted that  
5  
6 the half-width decreases for all observed bands. The librational band depicted in Fig. 6 shows a  
7  
8 decrease in FWHM from  $251\text{ cm}^{-1}$  to  $196\text{ cm}^{-1}$ , i.e, to about 80%. In addition to the narrowing  
9  
10 also some structuring of the band is apparent such that additional Gaussians are required to fit  
11  
12 the band. The band also loses intensity between  $500$  and  $600\text{ cm}^{-1}$ . From band decomposition  
13  
14 analysis two intense Gaussian components at  $837\text{ cm}^{-1}$  and approximately  $905\text{ cm}^{-1}$ , as well  
15  
16 as a less intense band at  $995\text{ cm}^{-1}$  are needed to explain the observed band shape. Note that a  
17  
18 similar band narrowing was observed in IR spectra of the partial ordering of hydrogen atoms in  
19  
20 ice Ih.<sup>66</sup> However, while there is no difference between cubic ice and hexagonal ice at 160 K,  
21  
22 shoulders emerge at different positions after partial hydrogen ordering, i.e., the hydrogen order  
23  
24 pattern differs between proton ordered cubic ice and ice XI.

25  
26 We now turn to the question whether the band changes seen in Fig. 6 are a result of a sim-  
27  
28 ple thermal effect or whether proton-ordering can be inferred from the data. Figure 7 shows the  
29  
30 evolution of the librational band in KOH-doped ice Ic when changing the temperature step by step  
31  
32 from 45 K to higher temperatures. The temperature-broadening of the band is best illustrated in the  
33  
34 magnified inset of Fig. 7. It is quite small when increasing the temperature in the range 45-70 K  
35  
36 ( $6\text{ cm}^{-1}$  per 25 K), but larger when changing the temperature from 70 K to 75 K ( $4\text{ cm}^{-1}$  per 5 K).  
37  
38 Above 75 K the temperature broadening is again quite small ( $5\text{ cm}^{-1}$  per 25 K). This shows that an  
39  
40 additional effect, besides thermal broadening, influences the change in half-width of the librational  
41  
42 band between 70 and 75 K, which we interpret to be proton-disordering of partially ordered cubic  
43  
44 ice. The occurrence of the proton disordering temperature between 70 and 75 K in cubic ice seen  
45  
46 in Fig. 7 compares to the known proton-disordering temperature of 72 K in hexagonal ice.<sup>12-19</sup>  
47  
48 This implies that the phase boundary between ordered and disordered cubic ice is located at almost  
49  
50 the same temperature as the phase boundary between ordered and disordered hexagonal ice. The  
51  
52 two thick lines in Fig. 7 compare two librational bands recorded for KOH-doped ice Ic, both de-  
53  
54 termined at 70 K after having kept the sample several hours at 70 K: the narrower band (blue line)  
55  
56 was obtained after several days of waiting at temperatures below 70 K and then heating to 70 K,  
57  
58  
59  
60

1  
2  
3  
4  
5  
6  
7  
8  
9  
10  
11  
12  
13  
14  
15  
16  
17  
18  
19  
20  
21  
22  
23  
24  
25  
26  
27  
28  
29  
30  
31  
32  
33  
34  
35  
36  
37  
38  
39  
40  
41  
42  
43  
44  
45  
46  
47  
48  
49  
50  
51  
52  
53  
54  
55  
56  
57  
58  
59  
60

whereas the broader band (black line) was obtained after cooling from 100 K to 70 K, without any waiting time at temperatures below 70 K. In case of the proton-ordering transition from hexagonal ice to ice XI it was shown that the proton-ordered phase grows much faster at 70 K if it was nucleated before at temperatures below 70 K, e.g., at 60 K,<sup>12-19</sup> whereas by cooling from 100 K to 70 K, without a prior nucleation step at lower temperature, the proton-ordering is much slower in case of KOH-doped hexagonal ice. We expect this to be similar in case of KOH-doped cubic ice. The difference in half-width at half-maximum of about  $6\text{ cm}^{-1}$  between the two spectra taken at 70 K seen in Fig. 7 clearly demonstrates that this expectation is really seen in the spectra. Indeed, an effect other than motional narrowing is operative, which we explain as proton-ordering when the proton-ordered phase was nucleated by keeping the sample for several days between 45 and 65 K. Note that also the peak-intensities and base-lines slightly shift from spectrum to spectrum, e.g., when comparing the thick black and blue lines in Fig. 7 or the black and red lines in Fig. 8. The error-bar on the changes in half-widths due to the ambiguities in half-height amount to at most  $\pm 0.5\text{ cm}^{-1}$ . The observed changes in half-width of 6 and  $10\text{ cm}^{-1}$  indicated in Figs. 7 and 8, respectively, are much larger than the error-bar of the method, and, thus, are real effects associated with changes within the sample itself.

Figure 8 shows a comparison of the two librational bands recorded at 70 K on KOH-doped cubic ice (black and blue traces, both taken from Fig. 7) and on undoped cubic ice (red trace), which was kept several days at 45-65 K before. Clearly, the librational band is narrower in the case of KOH-doped ice. In this case the difference in half-width is even about  $10\text{ cm}^{-1}$ . This shows that KOH-doping is required to achieve proton-ordering in cubic ice, that a smaller degree of proton-ordering is also reached when cooling directly from 100 K to 70 K, without the nucleation step at 45-65 K, whereas in the case of undoped cubic ice proton-ordering cannot be inferred from the data. Further systematic studies about the dependence of the half-width of the librational band on the thermal history using much longer waiting times (on the order of months) are necessary to find conditions that might allow for a higher degree of proton-ordering, or even to access the fully proton-ordered state of cubic ice. Also an investigation of the influence of other dopants (e.g.,

1  
2  
3  
4  
5  
6  
7  
8  
9  
10  
11  
12  
13  
14  
15  
16  
17  
18  
19  
20  
21  
22  
23  
24  
25  
26  
27  
28  
29  
30  
31  
32  
33  
34  
35  
36  
37  
38  
39  
40  
41  
42  
43  
44  
45  
46  
47  
48  
49  
50  
51  
52  
53  
54  
55  
56  
57  
58  
59  
60

NH<sub>3</sub>, HCl, etc.) is of interest in this context.

## Discussion

Assuming that the band structuring and narrowing that is observed in addition to the pure thermal narrowing in our spectra indeed arises from partial hydrogen ordering in cubic ice, we may now compare the observed band with the predicted spectra of Fig. 5. For protonically disordered cubic ice, the predicted librational band centered at  $\sim 800 \text{ cm}^{-1}$  coincides almost perfectly with the experimentally observed librational band both in position and width, which is about FWHM  $\sim 200 \text{ cm}^{-1}$ . Our MD simulations predict that depending on the particular type of proton ordering this band splits into up to 6 bands, all of which show a FWHM of about  $\sim 20 \text{ cm}^{-1}$ . That is, the FWHM of the ordered forms is about 10% of the FWHM in case of the disordered form. In the experiment, the FWHM in the possibly ordered form of cubic ice is reduced to about 80%, thus suggesting that the degree of hydrogen ordering achieved experimentally is no more than 20%.

Band deconvolution suggests that three bands contribute to the experimental band shape. The main peak at  $837 \text{ cm}^{-1}$  is most likely related to the predominant disordered cubic ice and shifts only little compared to the original disordered cubic ice phase ( $816 \text{ cm}^{-1}$ ). This small shift of  $20 \text{ cm}^{-1}$  might be related to the lower temperature of 70 K compared to 160 K. While usually there is a blue shift when lowering temperature, here we observe a red shift, which is probably related to the anomalous temperature dependence of ice<sup>1</sup> and may also result in positive Grüneisen parameters for several modes.<sup>72</sup> Furthermore, in the experiment a distinct shoulder at  $905 \text{ cm}^{-1}$  is observed accounting for about one third of the integrated intensity.

This band structure of the partially ordered phase seems to be consistent with a more pronounced ferroelectric order, which both in the DFT calculations as well as in the MD simulations leads to a pronounced blue shift compared to anti-ferroelectric order. In particular, for the ferroelectric structure (a) DFT predicts a strong single peak at  $930 \text{ cm}^{-1}$  while the vibrational band of the anti-ferroelectric order (d) is shifted to the red by about  $80 \text{ cm}^{-1}$  on the average. In the

1  
2  
3 TIP4P/ice simulations the dominant peak for cubic ice (a) as well as (b) is located at a lower  
4 frequency of  $856\text{ cm}^{-1}$ , a difference of  $70\text{ cm}^{-1}$ .  
5  
6

7 The experiment also shows a weak but clearly resolved shoulder at  $995\text{ cm}^{-1}$  approximately  
8  $90\text{ cm}^{-1}$  above the main peak arising as a result of the conjectured partial proton order. This side  
9 peak is not accounted for by the ferroelectrically ordered structure (a), which shows only one single  
10 peak. Such side peaks are, however, present both in the cubic ordered variants (b) and (c), with  
11 structure (b) showing very similar ratios between the main peak and the higher frequency shoulder  
12 as in the experiment. In fact, the magnitude of the two band splittings is about  $70\text{ cm}^{-1}$  and  $90$   
13  $\text{cm}^{-1}$  in the experiment, and thus quite similar to the splittings of  $90\text{ cm}^{-1}$  and  $90\text{ cm}^{-1}$  predicted  
14 for the ordered structure (b) (see Fig. 5). The other three ordered variants of cubic ice show quite  
15 different patterns and splittings. This might suggest that the transformation occurs into structural  
16 variant (b) and not the lowest energy structure ordered ice (a), so that the experimentally observed  
17 ordered form does not necessarily need to correspond to the thermodynamically most stable form,  
18 especially because kinetics is known to play an important role in the proton ordering transitions of  
19 ice, as for instance observed in ice XIV.<sup>73</sup> It is also possible that the experimental spectrum might  
20 develop into the spectrum of ordered ice (a) with increasing time and increasing proton ordering  
21 instead of developing the peak splittings predicted for structure (b).  
22  
23  
24  
25  
26  
27  
28  
29  
30  
31  
32  
33  
34  
35  
36  
37

38 Interestingly, the ordered variants of cubic ice also show shifts and/or splittings of the acoustic  
39 and optical modes at  $< 400\text{ cm}^{-1}$  compared to disordered cubic ice according to our simulations  
40 (see Fig. 5). That is, investigation of acoustic and optic modes in the future by means of IR or  
41 Raman seems to be a promising tool for critically testing the type of proton ordering obtained  
42 experimentally in cubic ice.  
43  
44  
45  
46  
47

48 The temperature dependence of the librational band shape and width suggest that the proton-  
49 order-disorder transition in cubic ice takes place at about  $70\text{--}75\text{ K}$ , which is very similar to the  
50 proton-order-disorder temperature of  $72\text{ K}$  observed in case of hexagonal ice. Furthermore, the  
51 degree of proton-ordering and narrowing of the bands at  $70\text{ K}$  is clearly enhanced when employing  
52 a "nucleation" step at temperatures of  $45\text{--}65\text{ K}$ . Whereas we observe in our experiments on KOH-  
53  
54  
55  
56  
57  
58  
59  
60

1  
2  
3 doped cubic ice at  $T < 75$  K a band narrowing in addition to the narrowing caused by motional  
4 narrowing, we do not observe such an additional narrowing in case of undoped, pure cubic ice on  
5  
6 the time scale of days.  
7  
8

9  
10 Finally, we compare our result presented here with the result obtained by Suga,<sup>74</sup> who was un-  
11 able to observe the onset of proton ordering in cubic ice prepared in the presence of a mole fraction  
12 of  $1.8 \times 10^{-3}$  KOH by measuring heat capacity and entropy (*i.e.*, the heat capacity divided by the  
13 temperature) in the temperature range 13-100 K. Suga suggests that his inability to observe proton  
14 ordering maybe related to his route of preparing cubic ice, namely by heating the high-pressure ice  
15 phase III/IX at ambient pressure to 160 K. In particular, the fact that "high-pressure forms of ice  
16 reject their ionic impurities from the specimen" is at the origin of the inability to produce proton-  
17 ordered cubic ice when going via high-pressure forms of ice. Suga hence concluded that "In order  
18 to realize the hypothetical ordered phase of Ic, the deposition method of atomized aerosol from  
19 a KOH aqueous solution will be worthy of trial". This is exactly what we have done here, and  
20 so Suga's expectation that proton-ordered cubic ice maybe accessible via a route, which does not  
21 involve high-pressure ice phases, has now turned out to be correct.  
22  
23  
24  
25  
26  
27  
28  
29  
30  
31  
32  
33

34 In summary, we have carried out FT-IR spectroscopy experiments combined with molecular  
35 dynamics and *ab initio* computer simulations to study the proton ordering transition of ice Ic. We  
36 find that the librational band of ice Ic displays some significant changes if the sample is subjected to  
37 an experimental protocol similar to that used before to proton order hexagonal ice. By comparison  
38 with theoretical IR-spectra computed with the TIP4P/ice model and using *ab initio* simulations we  
39 find that these changes are best explained by assuming that the ice Ic sample underwent a partial  
40 ordering transition. Based on a comparison of the computed and measured librational spectra  
41 no unique assignment of the type of protonic order is currently possible. While considering the  
42 intensity loss at low frequencies implies a partial ordering into a ferroelectric structure, the number  
43 and relative positions of the peaks obtained from deconvolution of the experimental data point to  
44 a weakly ferroelectric structure. Further experiments and simulations will be necessary to resolve  
45 this issue.  
46  
47  
48  
49  
50  
51  
52  
53  
54  
55  
56  
57  
58  
59  
60

## Acknowledgments

This work was supported by the European Research Council (ERC, Starting Grant SULIWA) and the Austrian Science Fund (FWF) within the SFB ViCoM (Grant F 41), the START award (Grant Y391), and Project P22087-N16. We thank Georg Menzl for useful discussions. All simulations were carried out on the Vienna Scientific Cluster (VSC).

## References

- (1) V. Petrenko and R. Whitworth, *Physics of ice* (Oxford University Press, USA, 1999).
- (2) C. G. Salzmann, P. G. Radaelli, A. Hallbrucker, E. Mayer, and J. L. Finney, *Science* **311**, 1758 (2006).
- (3) C. G. Salzmann, P. G. Radaelli, E. Mayer, and J. L. Finney, *Phys. Rev. Lett.* **103**, 105701 (2009).
- (4) T. Loerting and N. Giovambattista, *J. Phys.: Condens. Mat.* **18**, R919 (2006).
- (5) K. Winkel, M. S. Elsaesser, E. Mayer, and T. Loerting, *J. Chem. Phys.* **128**, 044510 (2008).
- (6) T. Loerting, K. Winkel, M. Seidl, M. Bauer, C. Mitterdorfer, P. H. Handle, C. G. Salzmann, E. Mayer, J. L. Finney, and D. T. Bowron, *Phys. Chem. Chem. Phys.* **13**, 8783 (2011).
- (7) J. D. Bernal and R. H. Fowler, *J. Chem. Phys.* **1**, 515 (1933).
- (8) L. Pauling, *J. Am. Chem. Soc.* **57**, 2680 (1935).
- (9) W. F. Kuhs, J. L. Finney, C. Vettier, and D. V. Bliss, *J. Chem. Phys.* **81**, 3612 (1984).
- (10) B. Minčeva-Šukarova, W. Shermann, and G. Wilkinson, *J. Mol. Struct.* **115**, 137 (1984).
- (11) J. D. Londono, W. F. Kuhs, and J. L. Finney, *J. Chem. Phys.* **98**, 4878 (1993).
- (12) H. Fukazawa, S. Ikeda, and S. Mae, *Chem. Phys. Lett.* **282**, 215 (1998).

- 1  
2  
3  
4 (13) A. J. Leadbetter, R. C. Ward, J. W. Clark, P. A. Tucker, T. Matsuo, and H. Suga, *J. Chem.*  
5 *Phys.* **82**, 424 (1985).  
6  
7  
8 (14) H. Fukazawa, A. Hoshikawa, H. Yamauchi, Y. Yamaguchi, and Y. Ishii, *J. Cryst. Growth* **282**,  
9 251 (2005).  
10  
11  
12 (15) Y. Tajima, T. Matsuo, and H. Suga, *J. Phys. Chem. Sol.* **45**, 1135 (1984).  
13  
14  
15 (16) O. Yamamuro, M. Oguni, T. Matsuo, and H. Suga, *J. Chem. Phys.* **86**, 5137 (1987).  
16  
17  
18 (17) R. Howe and R. W. Whitworth, *J. Chem. Phys.* **90**, 4450 (1989).  
19  
20  
21 (18) S. M. Jackson, V. M. Nield, R. W. Whitworth, M. Oguro, and C. C. Wilson, *J. Phys. Chem.*  
22 *B* **101**, 6142 (1997).  
23  
24  
25 (19) J.-C. Li, V. Nield, and S. Jackson, *Chem. Phys. Lett.* **241**, 290 (1995).  
26  
27  
28 (20) T. C. Hansen, M. M. Koza, and W. F. Kuhs, *J. Phys.: Condens. Matter* **20**, 285104 (2008).  
29  
30  
31 (21) T. C. Hansen, M. M. Koza, P. Lindner, and W. F. Kuhs, *J. Phys.: Condens. Matter* **20**, 285105  
32 (2008).  
33  
34  
35 (22) E. B. Moorea and V. Molinero, *Phys. Chem. Chem. Phys.* **13**, 20008 (2011).  
36  
37  
38 (23) W. Kuhs, Ch. Sippel, A. Falenty, and T. C. Hansen, *Proc. Natl. Acad. Sci. USA* **109**, 21259  
39 (2012).  
40  
41  
42 (24) T. L. Malkin, B. J. Murray, A. V. Brukhno, J. Anwar, and C. G. Salzmann *Proc. Natl. Acad.*  
43 *Sci. USA* **109**, 1041 (2012).  
44  
45  
46 (25) I. Kohl, L. Bachmann, A. Hallbrucker, E. Mayer, and T. Loerting, *Phys. Chem. Chem. Phys.*  
47 **7**, 3210 (2005).  
48  
49  
50 (26) I. Kohl, E. Mayer, and A. Hallbrucker, *Phys. Chem. Chem. Phys.* **2**, 1579 (2000).  
51  
52  
53 (27) J. Lekner, *Physica B: Cond. Matter* **240**, 263 (1997).  
54  
55  
56  
57  
58  
59  
60

- 1  
2  
3 (28) J. Lekner, *Physica B: Cond. Matter* **252**, 149 (1998).  
4  
5  
6 (29) Z. Raza, D. Alfe, C. G. Salzmann, J. Klimes, A. Michaelides, and B. Slater, *Phys. Chem.*  
7  
8 *Chem. Phys.* **13**, 19788 (2011).  
9  
10  
11 (30) T. K. Hirsch and L. Ojamäe, *J. Phys. Chem. B* **108**, 15856 (2004).  
12  
13  
14 (31) V. Buch, P. Sandler, and J. Sadlej, *J. Phys. Chem. B* **102**, 8642 (1998).  
15  
16  
17 (32) A. Garg, *Physica Status Solidi (a)* **110**, 467 (1988).  
18  
19  
20 (33) H. Itoh, K. Kawamura, T. Hondoh, and S. Mae, *J. Chem. Phys.* **109**, 4894 (1998).  
21  
22  
23 (34) K. Furic and V. Volovsek, *J. Mol. Structure* **976**, 174 (2010).  
24  
25  
26 (35) J. Abascal, E. Sanz, R. Fernandez, and C. Vega, *J. Chem. Phys.* **122**, 234511 (2005).  
27  
28  
29 (36) C. Vega and J. L. F. Abascal, *Phys. Chem. Chem. Phys.* **13**, 19663 (2011).  
30  
31  
32 (37) C. Lawrence and J. Skinner, *Chem. Phys. Lett.* **372**, 842 (2003).  
33  
34  
35 (38) H. Kamberaj, R. Low, and M. Neal, *J. Chem. Phys.* **122**, 224114 (2005).  
36  
37  
38 (39) T. Miller III, M. Eleftheriou, P. Pattnaik, A. Ndirango, D. Newns, and G. Martyna, *J. Chem.*  
39 *Phys.* **116**, 8649 (2002).  
40  
41  
42 (40) G. Martyna, M. Tuckerman, D. Tobias, and M. Klein, *Mol. Phys.* **87**, 1117 (1996).  
43  
44  
45 (41) S. Nosé, *J. Chem. Phys.* **81**, 511 (1984).  
46  
47  
48 (42) W. G. Hoover, *Phys. Rev. A* **31**, 1695 (1985).  
49  
50  
51 (43) H. C. Andersen, *J. Chem. Phys.* **72**, 2384 (1980).  
52  
53  
54 (44) D. Frenkel and B. Smit, *Understanding Molecular Simulation* (Academic Press, New York,  
55 2002).  
56  
57  
58  
59  
60

- 1  
2  
3  
4 (45) A. Rahman and F. Stillinger, *J. Chem. Phys.* **57**, 4009 (1972).  
5  
6  
7 (46) A. K. Soper, *Chem. Phys.* **258**, 121 (2000).  
8  
9  
10 (47) D. A. McQuarrie, *Statistical Mechanics* (Harper and Row, New York, 1976).  
11  
12 (48) R. Zwanzig, *Nonequilibrium Statistical Mechanics* (Oxford University Press, USA, 2001).  
13  
14  
15 (49) J. Martí, E. Guàrdia, and J. Padró, *J. Chem. Phys.* **101**, 10883 (1994).  
16  
17  
18 (50) J. Martí, J. Padró, and E. Guàrdia, *J. Mol. Liqu.* **62**, 17 (1994).  
19  
20  
21 (51) P. E. Blöchl, *Phys. Rev. B* **50**, 17953 (1994).  
22  
23  
24 (52) G. Kresse and D. Joubert, *Phys. Rev. B* **59**, 1758 (1999).  
25  
26  
27 (53) J. P. Perdew, K. Burke, and M. Ernzerhof, *Phys. Rev. Lett.* **77**, 3865 (1996).  
28  
29  
30 (54) M. Dion, H. Rydberg, E. Schröder, D. C. Langreth, and B. I. Lundqvist, *Phys. Rev. Lett.* **92**,  
31 246401 (2004).  
32  
33  
34 (55) J. Klimes, D. R. Bowler, and A. Michaelides, *J. Phys.: Cond. Mat.* **22**, 022201 (2010).  
35  
36  
37 (56) J. Klimes, D. R. Bowler, and A. Michaelides, *Phys. Rev. B* **83**, 195131 (2011).  
38  
39  
40 (57) G. Kresse, J. Furthmüller, and J. Hafner, *Europhys. Lett.* **32**, 729 (1995).  
41  
42  
43 (58) J. Harl and G. Kresse, *Phys. Rev. Lett.* **103**, 056401 (2009).  
44  
45  
46 (59) J. Harl, L. Schimka, and G. Kresse, *Phys. Rev. B* **81**, 115126 (2010).  
47  
48  
49 (60) B. Santra, J. c. v. Klimeš, D. Alfè, A. Tkatchenko, B. Slater, A. Michaelides, R. Car, and  
50 M. Scheffler, *Phys. Rev. Lett.* **107**, 185701 (2011).  
51  
52  
53 (61) C. Vega, C. McBride, E. Sanz, and J. L. F. Abascal, *Phys. Chem. Chem. Phys.* **7**, 1450 (2005).  
54  
55  
56 (62) E. R. Davidson and K. Morokuma, *J. Chem. Phys.* **81**, 3741 (1984).  
57  
58  
59  
60

- 1  
2  
3  
4 (63) S. J. Singer and C. Knight, *Adv. Chem. Phys.* **147**, 1 (2011).  
5  
6  
7 (64) S. Rick, *J. Chem. Phys.* **122**, 094504 (2005).  
8  
9  
10 (65) G. A. Tribello and B. Slater, *Chem. Phys. Lett.* **425**, 246 (2006).  
11  
12 (66) M. Arakawa, H. Kagi, and H. Fukazawa, *Astrophys. J. Suppl. Ser.* **184**, 361 (2009).  
13  
14  
15 (67) J. E. Bertie, H. J. Labbé, and E. Whalley, *J. Chem. Phys.* **50**, 4501 (1969).  
16  
17  
18 (68) J. Eaves, A. Tokmakoff, and P. Geissler, *J. Phys. Chem. A* **109**, 9424 (2005).  
19  
20  
21 (69) S. Corcelli and J. Skinner, *J. Phys. Chem. A* **109**, 6154 (2005).  
22  
23  
24 (70) A. Hallbrucker, J. L. Finney, and E. Mayer, *Phys. Chem. Chem. Phys.* **8**, 3088 (2006).  
25  
26  
27 (71) A. Hallbrucker, E. Mayer, and G. P. Johari, *Phil. Mag. B* **60**, 179 (1989).  
28  
29  
30 (72) B. Pamuk, J. M. Soler, R. Ramirez, C. P. Herrero, P. W. Stephens, P. B. Allen, and M.-V.  
31  
32 Fernandez-Serra, *Phys. Rev. Lett.* **108**, 193003 (2012)  
33  
34 (73) G. A. Tribello, B. Slater, and C. G. Salzmann, *J. Am. Chem. Soc.* **128**, 12594 (2006).  
35  
36  
37 (74) H. Suga, *Thermochim. Acta* **300**, 117 (1997).  
38  
39  
40  
41  
42  
43  
44  
45  
46  
47  
48  
49  
50  
51  
52  
53  
54  
55  
56  
57  
58  
59  
60

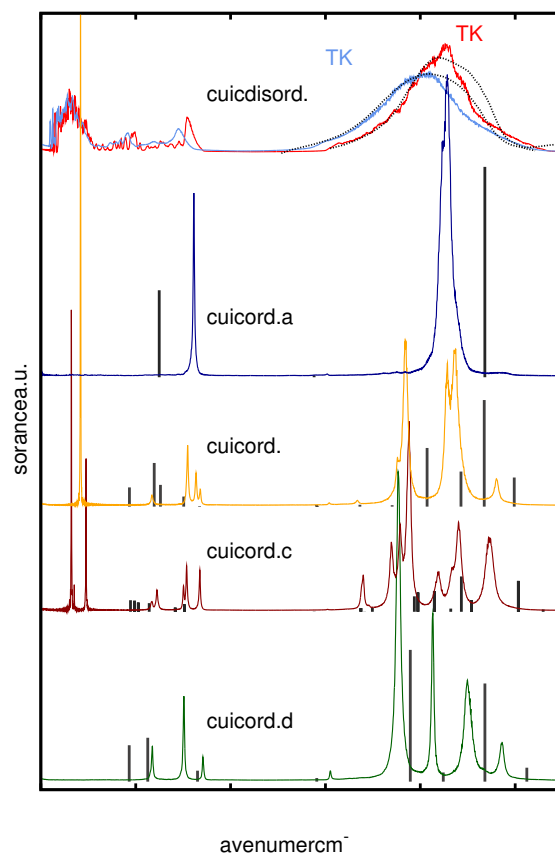


Figure 5: IR spectra for disordered cubic ice Ic and various of its proton ordered forms. Lines indicate results from the molecular dynamics simulations carried out at  $T = 70$  K and vertical bars indicate the results of *ab initio* simulations at  $T = 0$ . For the disordered variant of cubic ice also the spectrum obtained at  $T = 170$  K from MD simulations is shown. For better visibility, the spectra for disordered cubic ice are scaled by a factor of 2 vertically. The black dotted line lines shown at the top denote the experimental IR spectra of cubic ice at  $T = 160$  K and after the cooling procedure at  $T = 70$  K (same data as shown in Fig. 6). The labeling a, b, c, and d refers to the various proton arrangements shown in Fig. 1.

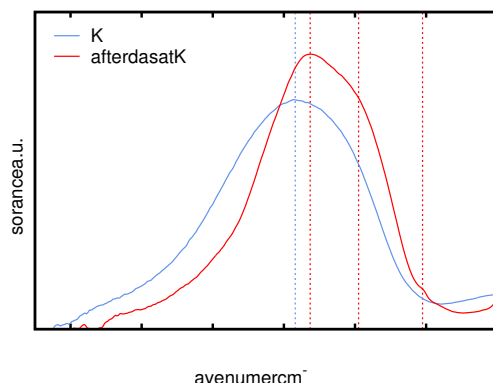


Figure 6: Librational band of the IR spectra of cubic ice determined experimentally at  $T = 160$  K (blue line) and after 80 hours at  $T = 70$  K (red line).

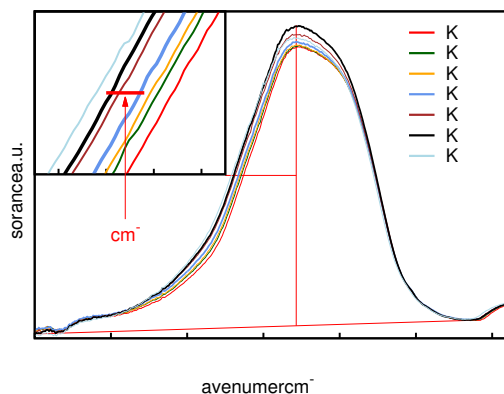


Figure 7: Libration mode of ice Ic doped with KOH at different temperatures, recorded after the following steps. Ice Ic doped with KOH was prepared by vitrification of the aqueous solution (200.2 g 0.1 M KOH(aq) + 4.9 g D<sub>2</sub>O) at 50 K using the technique of hyperquenching and subsequently crystallizing the amorphous deposit by bringing the sample holder for half an hour to 140 K. The following temperature protocol was then applied while continuously recording IR spectra: 14 h at 45K, 2 h at 50 K; 20.5 h at 60 K; 7.5 h at 65 K; 22 h at 70 K; 23 h at 75 K; 7 h at 80K; 2 h at 90 K and 2 h at 100 K. After these steps the temperature was decreased again to 70 K for 18.5 h. Selected spectra as marked are shown in the figure and magnified in the inset. The two thick lines show the librational mode after 22 h at 70 K (blue line), after the sample was kept at 45-65 K before, and after 18.5 h at 70 K (black line), after the sample was kept at 100 K before.

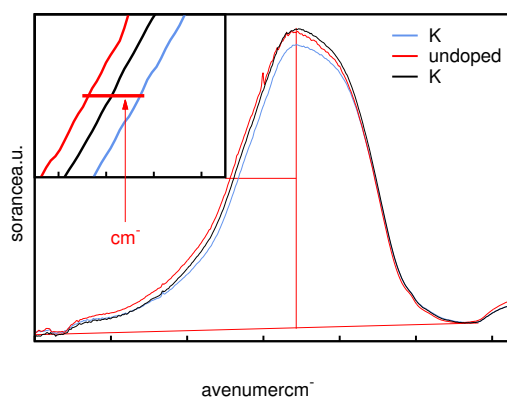


Figure 8: Libration mode of undoped ice Ic after very slow heating from 45 K to 70 K (red line) compared with KOH-doped ice Ic after cooling from 100 K to 70 K (black line, taken from Fig.7) and with KOH-doped ice Ic after very slow heating from 45 K to 70 K (blue line, taken from Fig.7). All spectra were recorded at 70 K after several hours at 70 K.

## 8.2 References

- [1] W. Hage, A. Hallbrucker, E. Mayer, *J. Chem. Soc., Farad. Trans.* **1995**, *91*, 2823.
- [2] W. Hage, A. Hallbrucker, E. Mayer, *J. Mol. Struct.* **1997**, *408*, 527.
- [3] K. Winkel, W. Hage, T. Loerting, S. L. Price, E. Mayer, *J. Am. Chem. Soc.* **2007**, *129*, 13863.
- [4] T. Loerting, C. Tautermann, R. T. Kroemer, I. Kohl, A. Hallbrucker, E. Mayer, K. R. Liedl, *Angew. Chem., Int. Edit.* **2000**, *39*, 892.
- [5] C. A. Wight, A. I. Boldyrev, *J. Phys. Chem.* **1995**, *99*, 12125.
- [6] K. Adamczyk, M. Premont-Schwarz, D. Pines, E. Pines, E. T. J. Nibbering, *Science* **2009**, *326*, 1690.
- [7] M. Eigen, K. Kustin, G. Maass, *Z. Physik. Chemie* **1961**, *30*, 130.
- [8] H. Falcke, S. H. Eberle, *Water Res.* **1990**, *24*, 685.
- [9] M. H. Moore, R. K. Khanna, *Spectrochim. Acta, Part A* **1991**, *47*, 255.
- [10] P. A. Gerakines, M. H. Moore, R. L. Hudson, *Astron. Astrophys.* **2000**, *357*, 793.
- [11] J. R. Brucato, M. E. Palumbo, G. Strazzulla, *Icarus* **1997**, *125*, 135.
- [12] M. Garozzo, D. Fulvio, O. Gomis, M. E. Palumbo, G. Strazzulla, *Planet. Space Sci.* **2008**, *56*, 1300.
- [13] D. C. B. Whittet, W. A. Schutte, A. Tielens, A. C. A. Boogert, T. deGraauw, P. Ehrenfreund, P. A. Gerakines, F. P. Helmich, T. Prusti, E. F. vanDishoeck, *Astron. Astrophys.* **1996**, *315*, L357.
- [14] J. Crovisier, *Farad. Discuss.* **1998**, *109*, 437.
- [15] R. W. Carlson, M. S. Anderson, R. E. Johnson, W. D. Smythe, A. R. Hendrix, C. A. Barth, L. A. Soderblom, G. B. Hansen, T. B. McCord, J. B. Dalton, R. N. Clark, J. H. Shirley, A. C. Ocampo, D. L. Matson, *Science* **1999**, *283*, 2062.
- [16] T. B. McCord, G. B. Hansen, R. N. Clark, P. D. Martin, C. A. Hibbitts, F. P. Fanale, J. C. Granahan, M. Segura, D. L. Matson, T. V. Johnson, R. W. Carlson, W. D. Smythe, G. E. Danielson, N. Team, *J. Geophys. Res.* **1998**, *103*, 8603.
- [17] K. C. Herr, G. C. Pimentel, *Science* **1969**, *166*, 496.
- [18] H. P. Larson, U. Fink, *Astrophys. J.* **1972**, *171*, L91.
- [19] W. Hage, A. Hallbrucker, E. Mayer, *J. Chem. Soc., Farad. Trans.* **1996**, *92*, 3183.
- [20] W. Hage, A. Hallbrucker, E. Mayer, *J. Chem. Soc., Farad. Trans.* **1996**, *92*, 3197.
- [21] W. Hage, A. Hallbrucker, E. Mayer, *J. Am. Chem. Soc.* **1993**, *115*, 8427.
- [22] W. Hage, A. Hallbrucker, E. Mayer, *Abstr. Pap. Am. Chem. Soc.* **1994**, *208*, 17.
- [23] W. Hage, K. R. Liedl, A. Hallbrucker, E. Mayer, *Science* **1998**, *279*, 1332.
- [24] Y. Oba, N. Watanabe, A. Kouchi, T. Hama, V. Pirronello, *Astrophys. J.* **2010**, *722*, 1598.
- [25] T. Mori, K. Suma, Y. Sumiyoshi, Y. Endo, *J. Chem. Phys.* **2009**, *130*.
- [26] T. Mori, K. Suma, Y. Sumiyoshi, Y. Endo, *J. Chem. Phys.* **2011**, *134*.
- [27] J. K. Terlouw, C. B. Lebrilla, H. Schwarz, *Angew. Chem., Int. Ed.* **1987**, *26*, 354.
- [28] T. Loerting, J. Bernard, *Chem. Phys. Chem.* **2010**, *11*, 2305.
- [29] J. Bernard, M. Seidl, I. Kohl, K. R. Liedl, E. Mayer, O. Galvez, H. Grothe, T. Loerting, *Angew. Chem., Int. Ed.* **2011**, *50*, 1939.
- [30] H. E. Hallam, *Vibrational Spectroscopy of Trapped Species* **1973**.
- [31] G. Tammann, *Z. Anorg. Allg. Chem.* **1926**, *157*, 321.
- [32] Z. Peeters, R. L. Hudson, M. H. Moore, A. Lewis, *Icarus* **2010**, *210*, 480.
- [33] E. Mayer, *J. Appl. Phys.* **1985**, *58*, 663.
- [34] E. Mayer, *Cryo-Letters* **1988**, *9*, 66.
- [35] W. Hage, A. Hallbrucker, E. Mayer, *J. Am. Chem. Soc.* **1993**, *115*, 8427.
- [36] M. J. Frisch, *Gaussian Inc., Wallingford CT* **2009**.
- [37] R. Janoschek, I. G. Csizmadia, *J. Mol. Struct.* **1993**, *300*, 637.
- [38] T. H. Dunning, *J. Chem. Phys.* **1989**, *90*, 1007.

- [39] R. A. Kendall, T. H. Dunning, R. J. Harrison, *J. Chem. Phys.* **1992**, *96*, 6796.
- [40] D. E. Woon, T. H. Dunning, *J. Chem. Phys.* **1995**, *103*, 4572.
- [41] S. E. Huber, S. Dalnodar, W. Kausch, S. Kimeswenger, M. Probst, *AIP Adv.* **2012**, *2*.
- [42] H. A. Al-Hosney, V. H. Grassian, *Phys. Chem. Chem. Phys.* **2005**, *7*, 1266.
- [43] H. A. Al-Hosney, V. H. Grassian, *J. Am. Chem. Soc.* **2004**, *126*, 8068.
- [44] A. L. Soli, R. H. Byrne, *Mar. Chem.* **2002**, *78*, 65.
- [45] C. Mitterdorfer, J. Bernard, F. Klauser, K. Winkel, I. Kohl, K. R. Liedl, H. Grothe, E. Mayer, T. Loerting, *J. Raman Spectrosc.* **2012**, *43*, 108.
- [46] I. Weissbuch, V. Y. Torbeev, L. Leiserowitz, M. Lahav, *Angew. Chem., Int. Edit.* **2005**, *44*, 3226.
- [47] L. J. Bellamy, R. J. Pace, *Spectrochim. Acta* **1963**, *19*, 435.
- [48] V. Y. Torbeev, E. Shavit, I. Weissbuch, L. Leiserowitz, M. Lahav, *Cryst. Growth Des.* **2005**, *5*, 2190.
- [49] R. J. Davey, G. Dent, R. K. Mughal, S. Parveen, *Cryst. Growth Des.* **2006**, *6*, 1788.
- [50] K. Nakamoto, Y. A. Sarma, H. Ogoshi, *J. Chem. Phys.* **1965**, *43*, 1177.
- [51] S. Abouelhassan, F. Salman, M. Elmansy, E. Sheha, *Surf. Rev. Lett.* **2004**, *11*, 83.
- [52] J. O. Thomas, R. Tellgren, I. Olovsson, *Acta Crystallogr. Sect. B* **1974**, *30*, 1155.
- [53] W. Behrendt, G. Gattow, M. Drager, *Z. Anorg. Allg. Chem.* **1973**, *397*, 237.
- [54] A. Adam, V. Cirpus, *Z. Anorg. Allg. Chem.* **1994**, *620*, 1702.
- [55] A. Dibenedetto, M. Aresta, P. Giannoccaro, C. Pastore, I. Papai, G. Schubert, *Eur. J. Inorg. Chem.* **2006**, 908.
- [56] P. Ballinger, F. A. Long, *J. Am. Chem. Soc.* **1960**, *82*, 795.
- [57] W. Behrendt, G. Gattow, *Z. Anorg. Allg. Chem.* **1973**, *398*, 198.
- [58] G. Gattow, W. Behrendt, *Angew. Chem., Int. Edit.* **1972**, *11*, 534.
- [59] D. T. R. Vidal, T. Nogueira, R. M. Saito, C. L. do Lago, *Electrophoresis* **2011**, *32*, 850.
- [60] M. Falk, E. Whalley, *J. Chem. Phys.* **1961**, *34*, 1554.
- [61] J. Bernard, R. G. Huber, K. R. Liedl, H. Grothe, T. Loerting, *J. Am. Chem. Soc.* **2013**, *135*, 7732.
- [62] A. J. Barnes, H. E. Hallam, *Trans. Faraday Soc.* **1970**, *66*, 1920.
- [63] S. Peil, S. Seisel, O. Schrems, *J. Mol. Struct.* **1995**, *348*, 449.
- [64] R. P. Turco, O. B. Toon, P. Hamill, *J. Geophys. Res.-Atmos.* **1989**, *94*, 16493.
- [65] R. Zhang, P. J. Wooldridge, J. P. D. Abbatt, M. J. Molina, *J. Phys. Chem.* **1993**, *97*, 7351.
- [66] B. Rowland, J. P. Devlin, *J. Chem. Phys.* **1991**, *94*, 812.
- [67] B. Rowland, M. Fisher, J. P. Devlin, *J. Chem. Phys.* **1991**, *95*, 1378.
- [68] B. J. Mason, *Clarendon Press* **1971**.
- [69] J. E. Bertie, E. Whalley, *J. Chem. Phys.* **1964**, *40*, 1637.
- [70] V. Mohacek-Grosev, J. Grdadolnik, J. Stare, D. Hadzi, *J. Raman Spectrosc.* **2009**, *40*, 1605.

## 8.3 List of Figure

Figure 1.1 The energy level and reaction schema for the formation of $\text{H}_2\text{CO}_3$ .....	3
Figure 1.2 Pathways to form $\text{H}_2\text{CO}_3$ . a) by high energy and proton irradiation of $\text{H}_2\text{O}/\text{CO}_2$ -ice, b) by acid base reaction at low temperature, c) by proton implantation in $\text{CO}_2$ -ice and d) by surface reactions of CO molecules with non-energetic hydroxyl radicals ( $\text{OH}\bullet$ ). .....	4
Figure 1.3 Two polymorphs of carbonic acid. By reaction in methanolic solutions the $\alpha$ -polymorph is obtained (the needles in the microscopic picture A). By reaction in aqueous solution and by proton irradiation the $\beta$ -polymorph of carbonic acid is obtained (the black area in the microscopic picture B).....	5
Figure 1.4 The two $\text{H}_2\text{CO}_3$ monomers, which were identified in experiment by Fourier-transform microwave spectroscopy. <sup>[25-26]</sup> .....	6
Figure 2.1 The concept of matrix isolation resembles a raisins cake, where the raisins represent the trapped molecules (our case $\text{H}_2\text{CO}_3$ ) and the cake mixture the inert solid (noble gas). (The picture of the raisins cake was taken from <a href="http://scientific-multimedia.com/index.php5?chap=5_1&amp;gid=581&amp;..">http://scientific-multimedia.com/index.php5?chap=5_1&amp;gid=581&amp;..</a> ).....	7
Figure 2.2 Difference between $\text{H}_2\text{O}$ gas phase (a) and $\text{H}_2\text{O}$ matrix isolation (b) spectrum. The gas phase spectrum depicts rotational vibrational transitions (Q-branch region with $\Delta J = 0$ ). The matrix spectrum shows the pure vibrational spectrum of the non-rotating $\text{H}_2\text{O}$ -molecule. The different bands in the matrix spectrum can be assigned to different species of $\text{H}_2\text{O}$ -molecule monomers, dimers and oligomers, which are isolated in the matrix. ....	8
Figure 2.3 Full width at half maximum (FWHM) of $\nu(\text{C}=\text{O})$ for $\text{H}_2\text{CO}_3$ in the crystalline solid state (red) and in matrix-isolation (black). .....	9
Figure 2.4 Sketch of the matrix isolation equipment. ....	11
Figure 2.5 Schema of the matrix isolation of $\text{H}_2\text{CO}_3$ .....	13
Figure 3.1 Hyperquenching setup. A solution is nebulized (droplets of $\approx 3 \mu\text{m}$ ) and introduced into a vacuum chamber ( $\approx 10^{-7}$ mbar) through an aperture. The solution droplets are immobilized almost instantaneously and form glassy layers at 78 K (cooling rates up to $10^7$ K/s) when they hit the IR transparent window. ....	14
Figure 3.2 Preparation and formation of crystalline $\text{H}_2\text{CO}_3$ upon heating the IR-windows.....	15
Figure 3.3 Protonation of $\text{HCO}_3^-/\text{CO}_3^{2-}$ apparently occurs in freeze-concentrated state, after crystallization of glassy water to cubic ice, when water is used as a solvent. ....	16
Figure 5.1 a) – c) spectra of $\beta$ - $\text{H}_2\text{CO}_3$ by protonation of $\text{KHCO}_3$ in $\text{H}_2\text{O}$ with a) HBr in $\text{H}_2\text{O}$ (recorded at $T = 230$ K), b) HCl in $\text{CH}_3\text{OH}$ ( $T = 230$ K) and c) HCl in $\text{C}_2\text{H}_5\text{OH}$ ( $T = 220$ K). d) – f) spectra of $\alpha$ - $\text{H}_2\text{CO}_3$ by protonation of $\text{KHCO}_3$ in $\text{CH}_3\text{OH}$ with d) HCl in $\text{CH}_3\text{OH}$ ( $T = 210$ K), e) HCl in	

H<sub>2</sub>O (T = 200 K) and f) HCl in C<sub>2</sub>H<sub>5</sub>OH (T = 200 K). The absorbance of the spectra are scaled to have identical absorbance for the  $\nu(\text{CO})$  at about 1700 cm<sup>-1</sup>. ..... 66

Figure 5.2 a) IR spectrum of solid KHCO<sub>3</sub> isolated from an aqueous solution in vacuum at 290 K. b) IR spectrum of crystalline  $\beta$ -H<sub>2</sub>CO<sub>3</sub> after protonation of the solid KHCO<sub>3</sub> with HCl in CH<sub>3</sub>OH, recorded at 230 K. The band marked with an asterisk belongs to CO<sub>2</sub> which is trapped in the crystal. The negative absorbance arrives from a mathematical operation (multiplication with -1) facilitating the comparison between the different IR spectra..... 67

Figure 5.3 a) IR spectrum of solid (K[O<sub>2</sub>COCH<sub>3</sub>]) through reaction of methanolate (CH<sub>3</sub>O<sup>-</sup>) with KHCO<sub>3</sub>.The spectrum was recorded in vacuum at 290 K. b) IR spectrum of crystalline  $\alpha$ -H<sub>2</sub>CO<sub>3</sub> after protonation of solid (K[O<sub>2</sub>COCH<sub>3</sub>]) with HCl in H<sub>2</sub>O, recorded at 80 K. The negative absorbance arrives from a mathematical operation (multiplication with -1), facilitating the comparison between the different IR spectra..... 70

Figure 5.4 Possible steps for the protonation and acidic hydrolysis of K[O<sub>2</sub>COCH<sub>3</sub>]. 1) protonation of CH<sub>3</sub>OCO<sub>2</sub><sup>-</sup>, 2) activation of the carbonyl group, 3) nucleophilic addition of H<sub>2</sub>O and proton transfer to the CH<sub>3</sub>O group, 4) elimination of the alcohol results in H<sub>2</sub>CO<sub>3</sub>. ..... 73

Figure 5.5 a) IR spectrum of solid (K[O<sub>2</sub>COC<sub>2</sub>H<sub>5</sub>]) from reaction of ethanolate (C<sub>2</sub>H<sub>5</sub>O<sup>-</sup>) with KHCO<sub>3</sub>.The spectrum was recorded in vacuum at 290 K. b) IR subtraction spectrum of a crystalline species, which evaporates or decomposes at 210 K in vacuum. The new species is obtained after protonation of solid (K[O<sub>2</sub>COC<sub>2</sub>H<sub>5</sub>]) with HCl in H<sub>2</sub>O. The new species is labeled  $\gamma$ -H<sub>2</sub>CO<sub>3</sub>. ..... 74

Figure 5.6 IR-spectra of H<sub>2</sub>CO<sub>3</sub> polymorphs a)  $\beta$ -H<sub>2</sub>CO<sub>3</sub>, b)  $\alpha$ -H<sub>2</sub>CO<sub>3</sub> and c)  $\gamma$ -H<sub>2</sub>CO<sub>3</sub>. The absorbance of the spectra are scaled to have identical absorbance for the  $\nu(\text{CO})$  at about 1700 cm<sup>-1</sup>. Vibrational modes which are assigned to  $\beta$ -H<sub>2</sub>CO<sub>3</sub> are shown with vertical dashed lines. .. 77

Figure 5.7 a) IR spectrum of solid (K[O<sub>2</sub>COCD<sub>3</sub>]) by reaction of methanolate (CD<sub>3</sub>O<sup>-</sup>) with KHCO<sub>3</sub>.The spectrum was recorded in vacuum at 290 K. b) IR subtraction spectrum of a crystalline species, which evaporates or decomposes at 210 K in vacuum. The new species is obtained after protonation of solid (K[O<sub>2</sub>COCD<sub>3</sub>]) with HCl in CH<sub>3</sub>OH. The new species is labeled  $\delta$ -H<sub>2</sub>CO<sub>3</sub>. The band marked with an asterisk belongs to CO<sub>2</sub>, the one marked with a circle to impurities on the cryoplate..... 78

Figure 5.8 Scheme of the S<sub>N</sub>2 nucleophilic substitution of HCO<sub>3</sub><sup>-</sup> with CH<sub>3</sub>O<sub>2</sub>CO<sup>-</sup> to K[O<sub>2</sub>COCH<sub>3</sub>]. 80

Figure 5.9 a) IR spectrum of solid (K[O<sub>2</sub>COCH<sub>3</sub>]) by reaction of methanolate (CH<sub>3</sub>O<sup>-</sup>) with KHCO<sub>3</sub>.The spectrum was recorded in vacuum at 290 K. b) IR spectrum of solid (K[O<sub>2</sub>COCD<sub>3</sub>]) by reaction of d<sub>3</sub>-methanolate (CD<sub>3</sub>O<sup>-</sup>) with KHCO<sub>3</sub>.The spectrum was recorded in vacuum at 290 K. The band marked with an asterisk belongs to CO<sub>2</sub>, the one with a circle to impurities on the cryoplate. Vibrational modes which are assigned to the CH<sub>3</sub>- and CD<sub>3</sub>- group are shown in red. 81

Figure 5.10 IR-spectra of a)  $\delta$ -H<sub>2</sub>CO<sub>3</sub>, b)  $\alpha$ -H<sub>2</sub>CO<sub>3</sub> and c) amorphous  $\alpha$ -H<sub>2</sub>CO<sub>3</sub> (spectrum (c) was taken from Figure 2 in Winkel et al. <sup>[3]</sup>). The absorbance of the spectra are scaled to have

identical absorbance for the $\nu(\text{CO})$ at about $1700\text{ cm}^{-1}$ . Vibrational modes which are assigned to the $\text{CH}_3^-$ and $\text{CD}_3^-$ group are shown with vertical dashed lines. ....	83
Figure 5.11 Schema of the protonation of $\text{K}[\text{O}_2\text{COCH}_3]$ with $\text{HCl}$ in methanol. ....	83
Figure 5.12 a) IR spectrum of solid $\text{K}[\text{O}_2\text{COC}_2\text{H}_5]$ from reaction of ethanolate ( $\text{C}_2\text{H}_5\text{O}^-$ ) with $\text{KHCO}_3$ . The spectrum was recorded in vacuum at 290 K. b) IR subtraction spectrum of a crystalline species, which evaporates or decomposes at 210 K in vacuum. The new species is obtained after protonation of solid $\text{K}[\text{O}_2\text{COC}_2\text{H}_5]$ with $\text{HCl}$ in $\text{H}_2\text{O}$ . The new species is labeled $\gamma\text{-H}_2\text{CO}_3$ . Vibrational modes which are assigned to the $\text{C}_2\text{H}_5^-$ group are shown in red. ....	84
Figure 6.1 The global energy-minimum for the monomethyl carbonic acid conformers. ....	89
Figure 6.2 IR spectra of $\alpha\text{-H}_2\text{CO}_3$ and isotopologues vapour after sublimation of the crystal at 210 K and isolation in argon matrix at 6 K. a) $\text{H}_2\text{CO}_3$ , b) $\text{H}_2^{13}\text{CO}_3$ (65%), c) $\text{D}_2\text{CO}_3$ (50%). Spectra are shifted for clarity. New assignment of the bands is given in Table 6.5 and Table 6.6. ....	92
Figure 6.3 Difference spectrum of $\alpha\text{-H}_2\text{CO}_3/\text{Ar}$ -matrix before and after irradiation of the matrix with UV light (15 min; $\nu = 250$ to $950\text{ nm}$ ). Bands pointing upwards indicate an appearing species and bands pointing downwards a disappearing species. ....	97
Figure 6.4 Difference spectrum of $\alpha\text{-H}_2^{13}\text{CO}_3/\text{Ar}$ -matrix before and after irradiation of the matrix with UV light. Bands pointing upwards indicate an appearing species and bands pointing downwards a disappearing species. In the spectrum traces of the $^{12}\text{C}$ species are obvious. ....	99
Figure 6.5 IR spectra of the new species vapour after sublimation of the crystal at 210 K and isolation in argon matrix at 6 K. a) $\text{HOCO}_2\text{C}_2\text{H}_5$ , b) $\text{HOCO}_2\text{CD}_3$ . Spectra are shifted for clarity. Assignment of the bands is given in Table 6.7. ....	104
Figure 6.6 Monomers of the new species. ....	107
Figure 7.1 Vapor pressure curve of $\text{H}_2\text{O}$ taken from B. J. Mason, The Physics of Clouds (Clarendon Press, 1971). <sup>[68]</sup> The black curve shows the vapor pressure above water and the red one above ice. In blue the vapor pressure during the experiment. ....	110
Figure 7.2 IR-spectra of the interaction of $\beta\text{-H}_2\text{CO}_3$ with $\text{H}_2\text{O}$ . a) $\beta\text{-H}_2\text{CO}_3$ ( $T = 230\text{ K}$ , $p = 10^{-2}\text{ mbar}$ ); b) $T = 200\text{ K}$ , $t = 80\text{ min}$ , $p_{\text{He}} = 330\text{ mbar}$ and $\text{RH}_{\text{ice}} > 100\%$ ; c) $T = 220\text{ K}$ , $t = 30\text{ min}$ , $p_{\text{He}} = 350\text{ mbar}$ and $\text{RH}_{\text{ice}} > 100\%$ ; d) $T = 240\text{ K}$ , $t = 30\text{ min}$ , $p_{\text{He}} = 440\text{ mbar}$ and $\text{RH}_{\text{ice}} > 100\%$ ; e) $T = 250\text{ K}$ , $t = 0\text{ min}$ , $p_{\text{He}} = 470\text{ mbar}$ and $\text{RH}_{\text{ice}} \approx 52\%$ . ....	111
Figure 7.3 IR-spectrum of hexagonal ice $I_h$ doped with $\text{KOH}$ ( $c = 0.1\text{ M}$ ) recorded at $\approx 190\text{ K}$ . The bands marked with asterisk belong to $\text{CO}_2$ ( $^{12}\text{C}$ and $^{13}\text{C}$ ). ....	112
Figure 7.4 IR-spectra of a) amorphous $\text{H}_2\text{CO}_3$ (taken from Figure 1 in ref. <sup>[3]</sup> ), b) unknown species ( $T = 205\text{ K}$ , $p = 10^{-6}\text{ mbar}$ ) and c) $\beta\text{-H}_2\text{CO}_3$ ( $T = 230\text{ K}$ , $p = 10^{-6}\text{ mbar}$ ). ....	113

Figure 7.5 Phase transition to  $\beta$ -H<sub>2</sub>CO<sub>3</sub> by increasing the temperature. The blue curve was recorded at 205 K (t = 30 min), the green one at 210 K (t = 30 min), the red curve at 220 K (t = 23 min) and the black one at 230 K (t = 5min)..... 115

Figure 7.6 Local structure motif of carbonic acid hydrate, by interaction of dimers containing a center of inversion (C<sub>2h</sub> point group) with two H<sub>2</sub>O-molecules, forming a dihydrate (H<sub>2</sub>CO<sub>3</sub> x 2 H<sub>2</sub>O). a) & b) dimer formed with cis-cis monomers and c) & d) with cis-trans monomers..... 118

## 8.4 List of Table

Table 2.1 Thermal properties of matrix materials according to H. E. Hallam (Hrsg.), <i>Vibrational Spectroscopy of Trapped Species</i> (1973). <sup>[30]</sup> .....	10
Table 5.1 Assignment of the IR frequencies of solid KHCO <sub>3</sub> (all values in cm <sup>-1</sup> ).....	68
Table 5.2 Assignment of the IR frequencies of solid β-H <sub>2</sub> CO <sub>3</sub> (all values in cm <sup>-1</sup> ). .....	69
Table 5.3 Assignment of the IR frequencies of solid K[O <sub>2</sub> COCH <sub>3</sub> ] (all values in cm <sup>-1</sup> ). .....	71
Table 5.4 Assignment of the IR frequencies of solid α-H <sub>2</sub> CO <sub>3</sub> (all values in cm <sup>-1</sup> ). .....	72
Table 5.5 Assignment of the IR frequencies of solid K[O <sub>2</sub> COC <sub>2</sub> H <sub>5</sub> ] (all values in cm <sup>-1</sup> ). .....	75
Table 5.6 IR frequencies of the different H <sub>2</sub> CO <sub>3</sub> polymorphs.....	76
Table 5.7 Assignment of the IR frequencies of solid K[O <sub>2</sub> COCH <sub>3</sub> ] and K[O <sub>2</sub> COCD <sub>3</sub> ] (all values in cm <sup>-1</sup> ). .....	79
Table 5.8 Assignment of the IR frequencies of solid δ- and α-H <sub>2</sub> CO <sub>3</sub> (all values in cm <sup>-1</sup> ). The values in red are the newly interpreted frequencies. ....	82
Table 5.9 Assignment of the IR frequencies of solid γ-H <sub>2</sub> CO <sub>3</sub> , compared with the ones from K[O <sub>2</sub> COC <sub>2</sub> H <sub>5</sub> ] (all values in cm <sup>-1</sup> ). The values in red are the newly interpreted frequencies.....	85
Table 6.1 Predicted IR bands for the cis-cis HOCO <sub>2</sub> CH <sub>3</sub> monomer and isotopologues; wavenumbers in cm <sup>-1</sup> (theoretical intensities in % in parentheses). Level of theory: MP2/aug-cc-pVTZ.....	90
Table 6.2 Predicted IR bands for the cis-trans HOCO <sub>2</sub> CH <sub>3</sub> monomer and isotopologues; wavenumbers in cm <sup>-1</sup> (theoretical intensities in % in parentheses) Level of theory: MP2/aug-cc-pVTZ.....	91
Table 6.3 Predicted IR bands for the cis-cis H <sub>2</sub> CO <sub>3</sub> monomer and isotopologues; wavenumbers in cm <sup>-1</sup> (theoretical intensities in % in parentheses). Level of theory: MP2/aug-cc-pVTZ .....	94
Table 6.4 Predicted IR bands for the cis-trans H <sub>2</sub> CO <sub>3</sub> monomer and isotopologues; wavenumbers in cm <sup>-1</sup> (theoretical intensities in % in parentheses). Level of theory: MP2/aug-cc-pVTZ .....	95
Table 6.5 Band positions assigned to monomethyl carbonic acid monomers (all values in cm <sup>-1</sup> ). Data taken from Figure 6.2, Figure 6.3, Figure 6.4 and Figure 6.5. Values in parentheses are calculated at MP2/aug-cc-pVTZ level of theory. Two distinct monomers, namely the cis-cis and cis-trans conformation are necessary to explain the spectra. ....	101
Table 6.6 Isotope shift between monomethyl carbonic acid isotopologues, namely HOCO <sub>2</sub> CH <sub>3</sub> , HO <sup>13</sup> CO <sub>2</sub> CH <sub>3</sub> , DO <sub>2</sub> CO <sub>2</sub> CH <sub>3</sub> and HOCO <sub>2</sub> CD <sub>3</sub> . .....	102

Table 6.7 Experimental and theoretical frequencies of  $\text{HOCO}_2\text{CD}_3$  and  $\text{HOCO}_2\text{C}_2\text{H}_5$  (all values in  $\text{cm}^{-1}$ ); Level of theory: MP2/aug-cc-pVTZ ..... 107

Table 7.1 Overview of the band positions for amorphous and crystalline  $\beta\text{-H}_2\text{CO}_3$  as well as for the  $\text{H}_2\text{CO}_3$ -hydrate (all values in  $\text{cm}^{-1}$ ). For more clarity the assignment to  $\beta\text{-H}_2\text{CO}_3$  is shown... 117

# 9 Curriculum Vitae

---



**Jürgen Bernard, Mag. rer. nat.**

\*06.03.1981

Email: Juergen.Bernard@uibk.ac.at

## **CAREER:**

Since 08/2009

**Scientific co-worker and PhD thesis** at the Institute of Physical Chemistry, University of Innsbruck, Austria (Supervisor: Assoc.-Prof. Dr. Thomas Loerting).

**Project:** Deeply supercooled liquid water

Since 16/12/2006

**Director** of the **S.E.P. – Service KG des Bernard Juergen & CO**, company for environmental technology and advice services in cooperation with Dr. Erich Bernard

01/05/2008 – 29/05/2009

**Diploma Thesis** at the Institute of Physical Chemistry, University of Innsbruck, Austria (Supervisor: Assoc.-Prof. Dr. Thomas Loerting).

**Project:** Poly(a)morphism of carbonic acid ( $H_2CO_3$ ).

06-09/2000-2005

**Assistant co-worker** at the **Ladurner GMBH company for environmental technology**. Function: landfill gas measurements and chemical analyses.

## **EDUCATION:**

since 10/2009

**Postgraduate Studies (Dr.rer.nat)** at the Leopold Franzens University Innsbruck, Austria.

01/10/2000 – 29/05/2009

**Diploma Studies Chemistry** at the Leopold Franzens University Innsbruck, Austria.

1995 – 2000

**Industry School „Johann Kravogl“**, special field electro technology, in Bozen, Italy.

## **TEACHING:**

01/03/2012 – 31/03/2013

**Lector** at the Institute of Physical Chemistry, University of Innsbruck, Austria.

**Practical course:** Physical Chemistry

01/10/2008 – 31/03/2009 **Tutor** at the Institute of Geology and Paleontology, University of Innsbruck, Austria.  
**Practical course:** General and Inorganic Chemistry

### ***SPECIALIZATION:***

2009 **Raman Workshop** for user

2007 – 2009 **Basic and Specialized Education in Radiation Protection** for medical / non-medical application

### ***AWARDS:***

2013 **Leopold-Franzens University Innsbruck (LFUI) Best Student Paper Award 2013.**

2011 **Dr. Otto Seibert Science-Advancement-Award 2011.**

2011 **Validation Award from the Jury of the LFUI-Best Student Paper Award 2011.**

2011 **IYC 2011 Fellowship of the Austrian Chemist Association.**

## ***PEER-REVIEWED PUBLICATIONS:***

### ***PAPERS:***

1. **J. Bernard**, R. G. Huber, K. R. Liedl, H. Grothe, T. Loerting;  
*"Matrix isolation studies of carbonic acid – the vapour phase above the  $\beta$ -polymorph."*  
*J. Am. Chem. Soc.* 135 (2013) 7732–7737
2. **J. Bernard**, M. Seidl, E. Mayer, T. Loerting;  
*"Formation and stability of bulk carbonic acid ( $H_2CO_3$ ) by protonation of tropospheric calcite."*  
*ChemPhysChem* 13 (2012) 3087–3091
3. C. Mitterdorfer, **J. Bernard**, F. Klauser, K. Winkel, I. Kohl, K. R. Liedl, H. Grothe, E. Mayer, T. Loerting;  
*"Local structural order in carbonic acid polymorphs: Raman and FT-IR spectroscopy."*  
*J. Raman Spectrosc.* 43 (2012) 108–115.
4. **J. Bernard**, M. Seidl, I. Kohl, K. R. Liedl, E. Mayer, Ó. Gálvez, H. Grothe, T. Loerting;  
*"Spectroscopic Observation of Matrix-Isolated Carbonic Acid Trapped from the Gas Phase."*  
*Angew. Chem. Int. Ed.* 50 (2011) 1939–1943; *Angewandte Chemie* 123 (2011) 1981–1985.

5. T. Loerting, **J. Bernard**;  
"Aqueous carbonic acid ( $H_2CO_3$ )."  
*ChemPhysChem* 11 (2010) 2305–2309.

### **ORAL PRESENTATIONS:**

1. **J. Bernard**, M. Seidl, I. Kohl, K.R. Liedl, E. Mayer, Ó. Gálvez, H. Grothe and T. Loerting  
"Spectroscopic Observation of Carbonic Acid Isolated from the Gas Phase in a Matrix"  
XIX International Conference on *Horizons in Hydrogen Bond Research* 2011 (Göttingen, Germany), 12- 17/09/2009
2. **J. Bernard**, M. Seidl, I. Kohl, K.R. Liedl, E. Mayer, Ó. Gálvez, H. Grothe and T. Loerting  
"Spectroscopic Observation of Carbonic Acid Isolated from the Gas Phase in a Matrix"  
Bunsentagung 2011 (Berlin, Germany), 02-04/06/2009
3. **J. Bernard**, I. Kohl, K. Winkel, M. Bauer, K. R. Liedl, T. Loerting, E. Mayer;  
„Kohlensäure ( $H_2CO_3$ ): Ramanspektroskopie am Mars?“  
9. Raman-Workshop für Anwender, Horiba Jobin Yvon GmbH (Bensheim, Germany), 10–11/03/2009

### **POSTER:**

1. **J. Bernard**, K. Winkel, M. Seidl, W. Hage, T. Loerting, S. L. Price, E. Mayer;  
"Retention of hydrogen-bond motif in solid  $H_2CO_3$ : Crystallization of two polymorphs from two amorphous forms."  
XVIII International Conference on *Horizons in Hydrogen Bond Research* (Paris, France), 14–18/09/2009.
2. T. Loerting, **J. Bernard**, M. Bauer, K. Winkel, I. Kohl, E. Mayer;  
"Spectroscopic characterization of solid carbonic acid ( $H_2CO_3$ )."  
Bunsentagung 2009 (Cologne, Germany), 21–23/05/2009.
3. **J. Bernard**, E. Mayer, T. Loerting;  
"Mass-spectrometry of carbonic acid in the gas-phase?"  
8. *Igler MS Tage: Perspectives in Mass Spectrometry* (Oberurgl, Austria), 22–25/02/2009

4. T. Loerting, **J. Bernard**, M. Bauer, K. Winkel, I. Kohl, E. Mayer;  
*"Spectroscopic characterization of solid carbonic acid (H<sub>2</sub>CO<sub>3</sub>)."*  
2. GÖCH-Symposium Physikalische Chemie (Innsbruck, Austria), 23–24/02/2009.
5. K. Winkel, **J. Bernard**, M. Seidl, W. Hage, T. Loerting, S. L. Price, E. Mayer;  
*"Crystallization of amorphous carbonic acid studied by FT-IR spectroscopy:  
Evidence for amorphous polymorphism."*  
58. Jahrestagung der Österreichischen Physikalischen Gesellschaft (Leoben,  
Austria), 22–26/09/2008.